

IL NUOVO CIMENTO

ORGANO DELLA SOCIETÀ ITALIANA DI FISICA

SOTTO GLI AUSPICI DEL CONSIGLIO NAZIONALE DELLE RICERCHE

VOL. XX, N. 5

Serie decima

1° Giugno 1961

Maximum Likelihood Determination of the Scattering Constant of an Emulsion Track in the Presence of Noise.

L. JÁNOSSY

Central Research Institute of Physics of the Hungarian Academy of Sciences

P. RÓZSA

Mathematical Institute of the Hungarian Academy of Sciences

(ricevuto il 5 Luglio 1960)

Summary. — Formulae are deduced for the determination of two parameters of an emulsion track with help of the maximum likelihood method. The parameters are the constant of the Coulomb scattering and the amplitude of background noise. Numerical expressions are obtained for the scatter of the measured values of these constants and it is shown, *e.g.* that in case of very fine subdivision of a track the statistical error of the constants thus obtained decreases proportionally to $N^{-\frac{1}{2}}$, where N is the number of sections. Formulae are obtained which are useful for the practical determination of the parameters and which give accuracies only slightly smaller than that obtained by the optimal maximum likelihood method. Graphs are provided to facilitate numerical computations.

Introduction.

The present paper deals with the determination of the scattering constant of high energy particles passing through an emulsion taking the background noise into account.

As recently several important results have been obtained relating to the same problems, it does not seem to be unnecessary to make a brief comparison between our results and some of those already published (*).

(*) The authors should like to thank Dr. DALLAPORTA and the Referee of this paper for drawing their attention to the papers quoted and for useful remarks.

An effort to apply the maximum likelihood method to the unbiased estimation of the scattering parameter can be found in the papers of several authors (¹⁻⁴). We should like to mention among these the excellent paper of N. SOLNTSEFF, whose paper contains in addition a short survey of the relevant literature. Writing down the likelihood equations (see (⁴) (2.10) and (2.11)) SOLNTSEFF, however, remarks: «... the differentiation... is unmanageable. Even if performed the resulting equations... would be extremely complicated so that an exact solution is impossible.»

Part I of our paper indeed gives the exact solution of the likelihood equations. For the relative standard deviations of the scattering parameters asymptotically exact explicit solutions are given in the case of a large number of measurements. The results are plotted in Fig. 1 as functions of the noise-

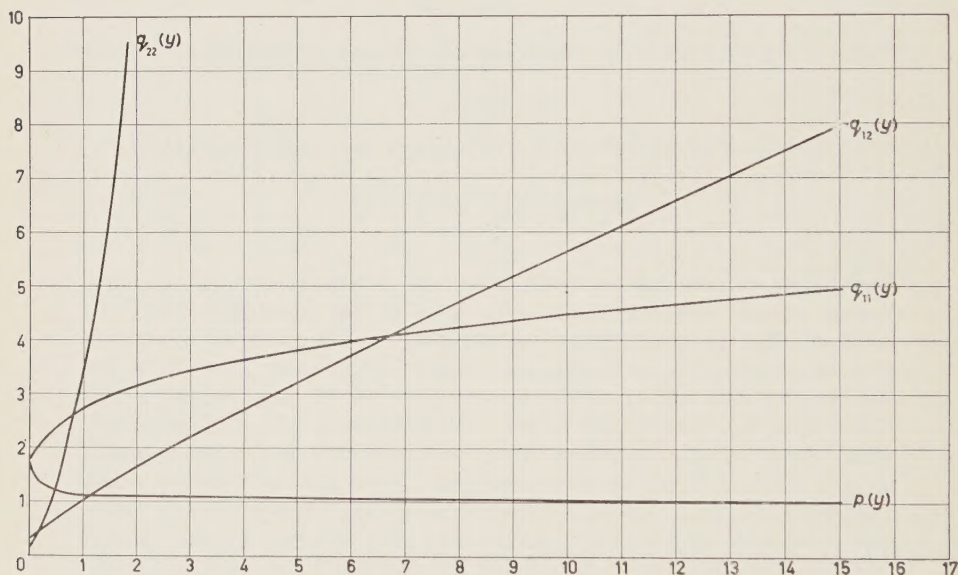


Fig. 1.

to-signal ratio. With help of these graphs it becomes possible to determine the theoretically optimal estimation of the scattering constant in the case of an arbitrary noise-to-signal ratio.

Our results resemble those of MOLIÈRE described in his paper (²) in so far as both discuss the matrix of the quadratic form for the estimation of the scattering constant (see eq. (4) for $\mathbf{C}^{(\sigma)}$ in the present paper and eq. (8.1) for Q

(¹) J. E. MOYAL: *Phil. Mag.*, **41**, 1058 (1950).

(²) G. MOLIÈRE: *Zeits. Naturforsch.*, **10 a**, 177 (1955).

(³) B. D'ESPAGNAT: *Compt. Rend.*, **232**, 800 (1951).

(⁴) N. SOLNTSEFF: *Nucl. Phys.*, **6**, 222 (1958).

in ⁽²⁾). MOLIÈRE in his paper ⁽²⁾ using an approximate method of inversion tabulates some elements of the matrix of the quadratic form for certain values of the noise-to-signal ratio. However, no reference can be found concerning the question: What is the best possible value of the relative standard deviation of the scattering parameter?

In the present paper we confine ourselves to writing down the matrix $\mathbf{C}^{(n)}$ in explicit form as function of the variances. However, the numerical application of the matrix proves to be extremely cumbersome and therefore it is not of interest for practical purposes, so that for practical purposes some approximate method has to be chosen. As the best possible estimation of the relative standard deviation of the scattering parameter is known from the maximum likelihood method, the loss of accuracy when using an approximate method can be determined, and thus the suitability of the approximation used can in every case be decided and improved upon if necessary.

In Part II of our paper a general theory of the application of approximate methods is worked out. For this purpose expressions containing arbitrary parameters are introduced to express the estimated values of the scattering constant; the best possible choice of the arbitrary parameters is then based on the maximum likelihood method.

Finally in Part III making use of the general principle developed in Part II a concrete method for the estimation of the scattering constant convenient for practical computation is proposed, the essence of which is the use of the quadratic sum and the sums of certain products of the sagittas for the estimation of the scattering constant.

This method is rather like the one proposed by MOLIÈRE and D'ESPAGNAT ^(2,3). However, these authors discuss only the simplest case, when only $\sum D_i^2$ and $\sum D_i D_{i+1}$ is made use of for the estimation of the scattering constant, while as is the case in our paper, taking into account $\sum D_i D_{i+2}$ and $\sum D_i D_{i+3}$ essentially improves the method. Furthermore, although we did not carry out the numerical computations, without difficulties our method could be extended so as to make use in an optimal way of sums up to $\sum D_i D_{i+l}$ for any desired value of l . Moreover—as was already mentioned—in the works quoted no information can be obtained as to the accuracy of the approximation used, while the method developed in the present paper renders a clear picture as to the degree to which the approximation used approaches the optimal case and therefore in the course of any particular computation it can be decided whether or not it is worth-while to improve the accuracy of the estimation by using a still higher approximation.

Our first approximation is identical with the result obtained by the method of Molière and d'Espagnat. (Compare the expressions for $\bar{\alpha}_1^{(1)}$ and $\bar{\alpha}_1^{(2)}$ on page 833 of the present paper with the formulae (2.36) of paper ⁽⁴⁾. Note that *e.g.* the scattering parameter $\bar{\alpha}_1^{(1)}$ corresponds to $\frac{1}{4}\sigma_s^2$ in the notation of paper ⁽⁴⁾.)

We should like to remark, that our considerations are not extended to differences of higher order, as these can always be expressed linearly with the help of the second differences. Some authors consider their use important from the point of view of the investigations of spurious scattering. The problems concerning spurious scattering as well as long-range distortion have not been dealt with in the present paper. We hope to return to their treatment at a later occasion.

I.

1. - The projection of a track on to the X - Y plane can be characterized by a number of points with co-ordinates $X_0, Y_0; X_1, Y_1; \dots; X_{N+1}, Y_{N+1}$. It is convenient to choose the system of co-ordinates so that the track lies as near as possible to the X -axis and to choose the X_v -values equidistant, *i.e.*

$$X_v = vs, \quad v = 0, 1, 2, \dots, N+1.$$

Instead of using the Y_v -values themselves it is convenient to introduce sagittas

$$D_v = Y_{v-1} - 2Y_v + Y_{v+1}.$$

The sagittas obey a multiple Gaussian distribution (see *e.g.* ref. (5)), we may write

$$(1) \quad P_2(\mathbf{D}) = (2\pi)^{-\frac{1}{2}N} (\det \mathbf{M})^{-\frac{1}{2}} \exp \left[-\frac{1}{2} \sum M_{v\mu}^* D_v D_\mu \right],$$

where the $M_{v\mu}^*$ are the elements of a matrix \mathbf{M}^{-1} . The elements of the matrix \mathbf{M} may be written

$$(2) \quad \mathbf{M} = \alpha^{(1)} \mathbf{A}^{(1)} + \alpha^{(2)} \mathbf{A}^{(2)},$$

where $\alpha^{(1)}$ and $\alpha^{(2)}$ are quantities proportional respectively to the parameters of Coulomb scattering and background noise. Using the notation of the previous paper (6), we may write

$$(3) \quad \alpha^{(1)} = as^3, \quad \alpha^{(2)} = \kappa_2^2 \quad \text{and} \quad a = \frac{1}{6} \langle \vartheta^2 \rangle,$$

(5) L. JÁNOSSY: *Acta Phys. Hung.*, **7**, 385 (1957).

(6) L. JÁNOSSY: *Acta Phys. Hung.*, **12**, 139 (1960).

where $\langle \vartheta^2 \rangle$ is the expected value of the square of the projection of the angle through which the particle is scattered along the unit path and κ_2^2 is the scatter of the measuring error of the individual Y_v -values.

The non-vanishing elements of the matrices $\mathbf{A}^{(1)}$ and $\mathbf{A}^{(2)}$ are collected in the Table I.

TABLE I.

$ v - \mu $		0	1	2
$A_{v\mu}^{(\sigma)}$	$\sigma = 1$	4	1	
	$\sigma = 2$	6	-4	1

The elements of the positive definite matrix \mathbf{M} are equal to the second order moments of the sagittas, *i.e.*

$$\langle D_v D_\mu \rangle = M_{v\mu}.$$

2. - According to the maximum likelihood method the measured values $\bar{\alpha}^{(1)}$ and $\bar{\alpha}^{(2)}$ of the constants $\alpha^{(1)}$ and $\alpha^{(2)}$ can be determined as the solutions of the following systems of equations:

$$\frac{\partial \ln P_2(\mathbf{D})}{\partial \alpha^{(\sigma)}} = 0 \quad \text{for} \quad \alpha^{(\sigma)} = \bar{\alpha}^{(\sigma)}, \quad \sigma = 1, 2.$$

Remembering (1) it is seen from these equations that the measured values $\bar{\alpha}^{(\sigma)}$ ($\sigma = 1, 2$) of the parameters $\alpha^{(\sigma)}$ are homogeneous quadratic forms in the sagittas. We may thus introduce quantities

$$(4) \quad \bar{\alpha}^{(\sigma)} = \sum_{v\mu} C_{v\mu}^{(\sigma)} D_v D_\mu, \quad \sigma = 1, 2,$$

where the $C_{v\mu}^{(\sigma)}$ form matrices $\mathbf{C}^{(\sigma)}$ ($\sigma = 1, 2$).

So as to ensure that

$$\langle \bar{\alpha}^{(\sigma)} \rangle = \alpha^{(\sigma)}, \quad \sigma = 1, 2,$$

the matrices $\mathbf{C}^{(\sigma)}$ have to satisfy

$$(5) \quad \text{Spur} (\mathbf{C}^{(\sigma)} \mathbf{A}^{(\tau)}) = \delta_{\sigma\tau}, \quad \sigma, \tau = 1, 2.$$

A short calculation gives for the scatters of the $\bar{\alpha}^{(\sigma)}$

$$(6) \quad \langle \delta \bar{\alpha}^{(\sigma)} \delta \bar{\alpha}^{(\tau)} \rangle = Q_{\sigma\tau} = 2 \text{ Spur} (\mathbf{C}^{(\sigma)} \mathbf{M} \mathbf{C}^{(\tau)} \mathbf{M}).$$

We have to choose the matrices $\mathbf{C}^{(\sigma)}$ so as to minimize the scatters $Q_{\sigma\sigma}$:

$$(7) \quad Q_{\sigma\sigma} = \text{minimum in } \mathbf{C}^{(\sigma)}. \quad (*)$$

The minimum condition (7) leads to the following system of equations

$$(8) \quad 4\mathbf{M}\mathbf{C}^{(\sigma)}\mathbf{M} - \sum_{\tau'=1}^2 L_{\sigma\tau'} \mathbf{A}^{(\tau')} = 0,$$

where the $L_{\sigma\tau}$ are the Lagrangian multipliers which have to be chosen so as to make the solutions of (8) satisfy the auxiliary conditions (5).

Multiplying (8) from the left-hand side by $\mathbf{C}^{(\tau)}$ and forming the spur, we find with help of (5) and (6)

$$(9) \quad L_{\sigma\tau} = 2Q_{\sigma\tau}, \quad \sigma, \tau = 1, 2.$$

Inserting (9) into the equation (8) and multiplying it from both sides by \mathbf{M}^{-1} , we get the matrices $\mathbf{C}^{(\sigma)}$ in the following form:

$$(10) \quad \mathbf{C}^{(\sigma)} = \frac{1}{2} \sum_{\tau'=1}^2 Q_{\sigma\tau'} \mathbf{M}^{-1} \mathbf{A}^{(\tau')} \mathbf{M}^{-1}.$$

The scatters $Q_{\sigma\tau}$ can be obtained from eq. (10): namely multiplying eq. (10) from the right-hand side by $\mathbf{A}^{(\tau)}$ and forming the spur, we get with help of (5)

$$(11) \quad \frac{1}{2} \text{Spur} \sum_{\tau'=1}^2 Q_{\sigma\tau'} \mathbf{M}^{-1} \mathbf{A}^{(\tau')} \mathbf{M}^{-1} \mathbf{A}^{(\tau)} = \delta_{\sigma\tau}.$$

Thus if the $Q_{\sigma\tau}^*$ ($\sigma, \tau = 1, 2$) denote the elements of the inverse of the matrix \mathbf{Q} with the elements $Q_{\sigma\tau}$ ($\sigma, \tau = 1, 2$) from (11) it turns out that

$$(12) \quad Q_{\sigma\tau}^* = \frac{1}{2} \text{Spur} (\mathbf{M}^{-1} \mathbf{A}^{(\sigma)} \mathbf{M}^{-1} \mathbf{A}^{(\tau)}).$$

Evaluation of (12) will lead to the scatters of the $\bar{\alpha}^{(\sigma)}$ defined in (6).

It follows from (2) and (12) that the $Q_{\sigma\tau}^*$ are homogeneous expressions in the $\alpha^{(1)}$ and $\alpha^{(2)}$. Introducing thus

$$(13) \quad y = \alpha^{(2)}/\alpha^{(1)} \quad \text{and} \quad \bar{y} = \bar{\alpha}^{(2)}/\bar{\alpha}^{(1)},$$

(*) Condition (7) can only be postulated for one value of the suffix σ . However, as it turns out the solution obtained for a fixed value of σ automatically satisfies (7) for both Q_{11} and Q_{22} .

we can introduce functions $q_{\sigma\tau}^*(y)$ so that

$$(14) \quad Q_{\sigma\tau}^* = N q_{\sigma\tau}^*(y) / 2\alpha^{(1)^2}.$$

With help of (2), (12) and (14) we find the following connections between the functions $q_{\sigma\tau}^*(y)$:

$$\begin{aligned} q_{\sigma\tau}^*(y) &= q_{\tau\sigma}^*(y), \\ q_{1\sigma}^*(y) + y q_{2\sigma}^*(y) &= \frac{1}{N} \text{Spur } (\mathbf{P}^{-1} \mathbf{A}^{(\sigma)}), \quad \sigma = 1, 2, \\ q_{11}^*(y) + 2y q_{12}^*(y) + y^2 q_{22}^*(y) &= 1, \end{aligned}$$

where we have written

$$(15) \quad \mathbf{M}/\alpha^{(1)} = \mathbf{A}^{(1)} + y \mathbf{A}^{(2)} = \mathbf{P}.$$

Instead of (12) we can write

$$(16) \quad q_{\sigma\tau}^*(y) = \frac{1}{N} \text{Spur } (\mathbf{P}^{-1} \mathbf{A}^{(\sigma)} \mathbf{P}^{-1} \mathbf{A}^{(\tau)}).$$

So as to evaluate (16) we introduce two matrices \mathbf{E} and \mathbf{F} with elements

$$E_{\nu\mu} = \delta_{\nu\mu}, \quad F_{\nu\mu} = \begin{cases} 2 & \text{for } |\nu - \mu| = 0, \\ -1 & \text{for } |\nu - \mu| = 1, \\ 0 & \text{for } |\nu - \mu| > 1. \end{cases}$$

The matrices $\mathbf{A}^{(1)}$ and $\mathbf{A}^{(2)}$ can be expressed in terms of \mathbf{E} and \mathbf{F} . One finds with help of the table for the $A_{\nu\mu}^{(\sigma)}$

$$(17) \quad \begin{cases} \mathbf{A}^{(1)} = 6\mathbf{E} - \mathbf{F}, \\ \mathbf{A}^{(2)} = \mathbf{F}^2 + \mathbf{F}_0, \end{cases}$$

where \mathbf{F}_0 is a matrix which has only two non-vanishing elements in the corners. It can be shown that neglecting \mathbf{F}_0 in the expression (17), thus supposing $\mathbf{A}^{(2)} = \mathbf{F}^2$, we commit errors only of the order of $1/N$ in the final result. Neglecting \mathbf{F}_0 we may write

$$\mathbf{P} = 6\mathbf{E} - \mathbf{F} + y\mathbf{F}^2.$$

To evaluate (16) numerically, we note that the spur of a matrix \mathbf{A} can also be written

$$\text{Spur } \mathbf{A} = \sum_{k=1}^N A_k,$$

where the A_k are the eigenvalues of \mathbf{A} . Introducing the notation

$$(18) \quad \mathbf{P}^{-1} \mathbf{A}^{(o)} \mathbf{P}^{-1} \mathbf{A}^{(\tau)} = \mathbf{R}^{(\sigma\tau)},$$

we have thus

$$q_{\sigma\tau}^*(y) = \frac{1}{N} \sum_{k=1}^N R_k^{(\sigma\tau)},$$

where the $R_k^{(\sigma\tau)}$ denote the eigenvalues of the matrix $\mathbf{R}^{(\sigma\tau)}$. Neglecting the matrix \mathbf{F}_0 , the matrices $\mathbf{A}^{(1)}$, $\mathbf{A}^{(2)}$ and \mathbf{P} are commutable and thus in the expression (18) the order of factors may be changed. Thus we may write e.g.

$$\mathbf{R}^{(11)} = (6\mathbf{E} - \mathbf{F})^2 / (6\mathbf{E} - \mathbf{F} + y\mathbf{F}^2)^2.$$

In general we can write

$$\mathbf{R}^{(\sigma\tau)} = f_{\sigma\tau}(\mathbf{F}).$$

The eigenvalues of $\mathbf{R}^{\sigma\tau}$ thus can be determined from the eigenvalues F_k of \mathbf{F} :

$$R_k^{(\sigma\tau)} = f_{\sigma\tau}(F_k).$$

It can be shown easily ⁽⁷⁾ that

$$F_k = 2 - 2 \cos \frac{k\pi}{N+1}, \quad k = 1, 2, \dots, N,$$

thus

$$(19) \quad q_{\sigma\tau}^*(y) = \frac{1}{N} \sum_{k=1}^N R_k^{(\sigma\tau)} = \frac{1}{N} \sum_{k=1}^N f \left(2 - 2 \cos \frac{k\pi}{N+1} \right).$$

If $N \gg 1$, only errors of the order of $1/N$ are committed if we replace the summation in (19) by integration. We thus obtain

$$q_{\sigma\tau}^*(y) = \frac{1}{\pi} \int_0^\pi f(2 - 2 \cos z) dz + o(1).$$

(7) See e.g. E. PASCAL: *I Determinanti* (Milano, 1897).

Carrying out the integration into z , one finds

$$q_{11}^*(y) = \frac{1}{\pi} \int_0^\pi \left(\frac{1 + \frac{1}{2} \cos z}{1 + y + (\frac{1}{2} - 2y) \cos z + y \cos^2 z} \right)^2 dz,$$

$$q_{12}^*(y) = \frac{1}{\pi} \int_0^\pi \frac{(1 + \frac{1}{2} \cos z)(1 - \cos z)^2}{(1 + y + (\frac{1}{2} - 2y) \cos z + y \cos^2 z)^2} dz,$$

$$q_{22}^*(y) = \frac{1}{\pi} \int_0^\pi \left(\frac{(1 - \cos z)^2}{1 + y + (\frac{1}{2} - 2y) \cos z + y \cos^2 z} \right)^2 dz.$$

For the second order central moments of the $\bar{\alpha}^{(\sigma)}$ one finds with the help of (6) and (14):

$$(20) \quad \langle \delta \bar{\alpha}^{(\sigma)} \delta \bar{\alpha}^{(\tau)} \rangle = 2\alpha^{(1)2} q_{\sigma\tau}(y)/N,$$

where $q_{\sigma\tau}(y)$ are the elements of the inverse of the matrix $q_{\sigma\tau}^*(y)$ ($\sigma, \tau = 1, 2$).

After evaluating the above integrals we get the following formulae for $q_{\sigma\tau}(y)$:

$$\begin{aligned} q_{11}(y) &= \frac{\frac{4}{3} \sqrt{6} \xi^3 \sqrt{(\xi + 2)^3} - 5\xi^4 - 15\xi^3 - 9\xi^2 + 9\xi + 12}{3\xi^4 + 9\xi^3 + 7\xi^2 + 9\xi + 12 - 2\sqrt{6} \xi(\xi + 1)^2 \sqrt{\xi + 2}}, \\ q_{12}(y) &= \frac{-(\xi^2 + 3\xi + 4)(\xi^2 - 3)^2}{24 \{ 3\xi^4 + 9\xi^3 + 7\xi^2 + 9\xi + 12 - 2\sqrt{6} \xi(\xi + 1)^2 \sqrt{\xi + 2} \}}, \\ q_{22}(y) &= \frac{(3\xi^4 + 9\xi^3 + 7\xi^2 + 9\xi + 12)(\xi^2 - 3)^2}{576 \{ 3\xi^4 + 9\xi^3 + 7\xi^2 + 9\xi + 12 - 2\sqrt{6} \xi(\xi + 1)^2 \sqrt{\xi + 2} \}}, \end{aligned}$$

where

$$\xi = \sqrt{3(1 + 8y)}.$$

The functions $q_{\sigma\tau}(y)$ are plotted in Fig. 1.

With help of (20) the relative scatters of the $\bar{\alpha}^{(\sigma)}$ can be obtained. One finds *e.g.* for $\sigma = \tau = 1$:

$$(21) \quad r_1 = \langle (\delta \bar{\alpha}^{(1)})^2 \rangle^{\frac{1}{2}} / \alpha^{(1)} = (2q_{11}(y)/N)^{\frac{1}{2}},$$

where

$$q_{11}(y) = q_{22}^*(y) / (q_{11}^*(y) q_{22}^*(y) - q_{12}^{*2}(y)).$$

In case of practical application, in the right-hand expressions of eq. (21) the unknown true values of $\alpha^{(\sigma)}$ or y must be replaced by their measured

values $\bar{\alpha}^{(s)}$ or \bar{y} so as to obtain a numerical estimate. In the following we shall replace the true values by their measured values in all those expressions where such an approximation is rendered necessary for the practical application of the formulae.

3. — The function $q_{11}(y)$ is plotted in Fig. 1. In the case when the background is known to be negligible, the relative scatter is given by the following expression:

$$(22) \quad \langle (\delta \bar{\alpha}^{(1)})^2 \rangle^{\frac{1}{2}} / \alpha^{(1)} = \left(\frac{2}{N} \right)^{\frac{1}{2}} \text{ if } \alpha^{(2)} = 0.$$

Comparing (21) with (22) it is seen that the function $q_{11}(y)$ is a measure of the loss of accuracy which is caused by the background noise.

Eq. (21) gives the relative scatter r_1 of $\bar{\alpha}^{(1)}$ in the case where both $\bar{\alpha}^{(1)}$ and $\bar{\alpha}^{(2)}$ are determined simultaneously from the sagittas **D** of the track.

If the background noise $\alpha^{(2)}$ can be estimated by independent measurements on other tracks, then the accuracy with which $\alpha^{(1)}$ can be determined is somewhat larger. Indeed, one finds

$$\varrho_1 = (2/N q_{11}^*(\bar{y}))^{\frac{1}{2}},$$

if $\alpha^{(2)}$ is determined by independent measurement.

If $\alpha^{(2)}$ is not known as the result of independent measurements, *i.e.* if $\alpha^{(1)}$ and $\alpha^{(2)}$ are both to be determined from the sagittas **D**, information on the loss of accuracy is given by

$$p(y) = q_{11}(y) q_{11}^*(y) = 1 / (1 - q_{12}^*(y) / q_{11}^*(y) q_{22}^*(y)).$$

We have plotted $p(y)$ in Fig. 1.

It is interesting that

$$p(0) = 1.7561 \dots,$$

thus the two-parameter method gives a smaller accuracy for $\alpha^{(1)}$ than the one-parameter method, even if the two-parameter method has led for the other parameter to the result

$$\bar{\alpha}^{(2)} \approx 0.$$

It turns out that even in this case, *i.e.* in the case where the existence of a background cannot be ascertained from the measured data in a significant manner, the uncertainty concerning the true value of $\alpha^{(2)}$ affects the accuracy of the value of $\alpha^{(1)}$.

4. — It is of interest to investigate the increase of accuracy which is obtained if the number N of co-ordinates measured on a given track is increased by subdividing the track into sections of smaller length.

Considering a track of length X , we have

$$s = X/N$$

and from (3) and (13) we find

$$y = \alpha^{(2)}/\alpha^{(1)} = N^3 \beta,$$

where

$$\beta = \kappa_2^2/aX^3.$$

We find from (21)

$$r_1 = (2q_{11}(N^3\beta)/N)^{\frac{1}{2}}.$$

The above equation can also be written

$$r_1 = \sqrt{2} \beta^{\frac{1}{2}} (r(z))^{\frac{1}{2}},$$

where

$$(23) \quad r(z) = q_{11}(z^3)/z \quad \text{with } z = N\beta^{\frac{1}{2}}.$$

In Fig. 2 we have plotted $r(z)$ as function of z . The function $r(z)$ is a decreasing

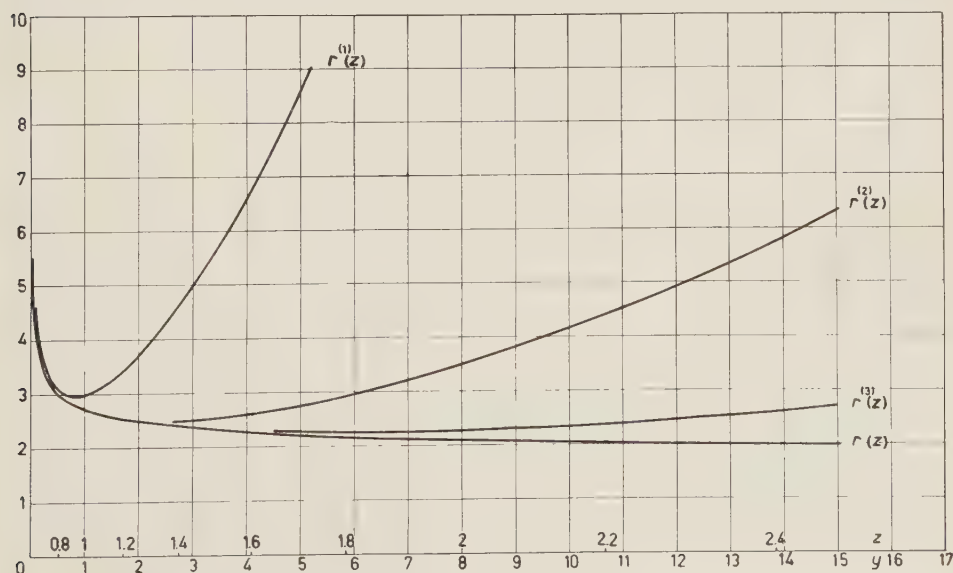


Fig. 2.

function of its argument; from this it follows that the scatter of $\mathbf{x}^{(1)}$ decreases monotonously with increasing N , *i.e.* with increasing subdivision of the track. The latter result is to be expected. Indeed, the more co-ordinates we measure, the more information we obtain about the track and consequently the more accurate measured parameter values can be obtained.

From the analytical form of $q_{11}(y)$ it follows that

$$(24) \quad q_{11}(y) \sim y^{\frac{1}{8}} \quad \text{if } y \gg 1,$$

thus from (23) and (24) follows

$$r_1 \sim N^{-\frac{1}{8}} \quad \text{if } N \text{ is large.}$$

We see thus that the accuracy of $\bar{\alpha}^{(1)}$ increases only proportional to the eighth root of the number of points measured. That means if the subdivision becomes very fine, that the increase is very slow and therefore it does not seem worth-while to use too fine a subdivision.

II.

5. — Although the eq. (4), (10), (12) in principle permit to determine the measured values $\bar{\alpha}^{(\sigma)}$ of the parameters $\mathbf{x}^{(\sigma)}$, the procedure is cumbersome and it appears useful to look for other expressions for measured values of $\mathbf{x}^{(\sigma)}$ which may be determined more conveniently than those defined by (4) and which at the same time have not much larger scatters than the former ones.

We may thus introduce quantities

$$(25) \quad \bar{\alpha}^{(\sigma)} = \sum_{\nu\mu} v_{\nu\mu}^{(\sigma)} D_{\nu} D_{\mu}, \quad \sigma = 1, 2,$$

where the $v_{\nu\mu}^{(\sigma)}$ are the elements of the matrices $\mathbf{V}^{(1)}$ and $\mathbf{V}^{(2)}$; we have to choose these matrices in such a way that the expected values of $\bar{\alpha}^{(\sigma)}$ ($\sigma = 1, 2$) are equal to the parameters $\alpha^{(\sigma)}$, the scatters of $\bar{\alpha}^{(\sigma)}$ should not much exceed the scatters of $\bar{\alpha}^{(\sigma)}$ and the numerical evaluation of the $\bar{\alpha}^{(\sigma)}$ should not be too complicated.

It is reasonable to express the elements of the matrices $\mathbf{V}^{(\sigma)}$ in terms of a small number of arbitrary parameters and then to determine these parameters so as to minimize the scatter. One obtains simple expressions if one chooses two sets of arbitrary parameters

$$\begin{aligned} & b_{01}, \quad b_{11}, \quad \dots, \quad b_{1l}, \\ & b_{02}, \quad b_{12}, \quad \dots, \quad b_{l2} \end{aligned}$$

and supposes the $\varphi_{\nu\mu}^{(\sigma)}$ to be linear functions of these parameters. Thus it is convenient to put

$$(26) \quad \mathbf{V}^{(\sigma)} = \sum_{\lambda=0}^l b_{\lambda\sigma} \mathbf{G}^{(\lambda)}, \quad \sigma = 1, 2,$$

where the matrices $\mathbf{G}^{(\lambda)}$ are arbitrary. So as to ensure that the expected values of the $\alpha^{(\sigma)}$ should indeed be equal to $\bar{\alpha}^{(\sigma)}$ we have to choose the coefficients $b_{\lambda\sigma}$ ($\lambda = 0, 1, 2, \dots, l$) so as to make the $\mathbf{V}^{(\sigma)}$ satisfy the conditions corresponding to (5):

$$(27) \quad \text{Spur}(\mathbf{V}^{(\sigma)} \mathbf{A}^{(\tau)}) = \delta_{\sigma\tau}, \quad \sigma, \tau = 1, 2,$$

and further so as to reduce the scatters $Q_{\sigma\sigma}$ to a minimum. Here

$$(28) \quad Q_{\sigma\tau} = \langle \delta \bar{\alpha}^{(\sigma)} \delta \bar{\alpha}^{(\tau)} \rangle = 2 \text{ Spur}(\mathbf{V}^{(\sigma)} \mathbf{M} \mathbf{V}^{(\tau)} \mathbf{M}).$$

Introducing (26) into (28) we may determine the $b_{\lambda\sigma}$ from the requirement

$$(29) \quad Q_{\sigma\sigma} = \text{minimum in } b_{\lambda 1}, b_{\lambda 2}.$$

The auxiliary conditions (27) can be written

$$(30) \quad \sum_{\lambda=0}^l b_{\sigma\lambda} T_{\lambda\tau} = \delta_{\sigma\tau}, \quad \sigma, \tau = 1, 2,$$

where

$$(31) \quad T_{\lambda\tau} = \text{Spur}(\mathbf{G}^{(\lambda)} \mathbf{A}^{(\tau)}).$$

The minimum condition (29) leads to the following system of equations:

$$(32) \quad 4 \sum_{\mu=0}^l \text{Spur}(\mathbf{G}^{(\lambda)} \mathbf{M} \mathbf{G}^{(\mu)} \mathbf{M}) b_{\mu\sigma} - \sum_{\tau=1}^2 T_{\lambda\tau} L_{\tau\sigma} = 0, \quad \sigma = 1, 2; \lambda = 0, 1, \dots, l,$$

where the $L_{\sigma\tau}$ are the Lagrangian multipliers.

6. — It is convenient for the further calculation to introduce the rectangular matrices \mathbf{T} and \mathbf{B} with elements $T_{\lambda\sigma}$ and $b_{\lambda\sigma}$, respectively ($\sigma = 1, 2; \lambda = 0, 1, \dots, l$). Further we introduce a square matrix \mathbf{S} with elements

$$(33) \quad S_{\lambda\mu} = \text{Spur}(\mathbf{G}^{(\lambda)} \mathbf{P} \mathbf{G}^{(\mu)} \mathbf{P}), \quad \lambda, \mu = 0, 1, 2, \dots, l$$

(see (15) for the definition of \mathbf{P}).

In the above notation the auxiliary condition (30) may be written

$$(34) \quad \tilde{\mathbf{B}}\mathbf{T} = \mathbf{E},$$

where $\tilde{\mathbf{B}}$ is the matrix transposed to \mathbf{B} and \mathbf{E} signifies the unit matrix of 2-nd order.

With help of (33) we may write instead of (28)

$$(35) \quad \mathbf{Q} = 2\alpha^{(1)2} \tilde{\mathbf{B}}\mathbf{S}\mathbf{B}.$$

The minimum condition (32) may be written

$$(36) \quad 4\alpha^{(1)2} \mathbf{S}\mathbf{B} - \mathbf{T}\mathbf{L} = 0,$$

where \mathbf{L} is the matrix with elements $L_{\sigma\tau}$. Multiplying (36) from the left by $\tilde{\mathbf{B}}$ we find with help of (34):

$$(37) \quad \mathbf{L} = 4\alpha^{(1)2} \tilde{\mathbf{B}}\mathbf{S}\mathbf{B}.$$

Inserting (37) into (36) results in

$$(38) \quad \mathbf{S}\mathbf{B} = \tilde{\mathbf{T}}\mathbf{B}\mathbf{S}.$$

Eq. (38) determines \mathbf{B} : namely, multiplying (38) from the left by \mathbf{S}^{-1} (the matrices $\mathbf{G}^{(2)}$ are to be chosen in such a way that the inverse of \mathbf{S} exists), we find

$$(39) \quad \mathbf{B} = \mathbf{S}^{-1} \tilde{\mathbf{T}}\mathbf{B}\mathbf{S}.$$

Multiplication of (39) by $\tilde{\mathbf{T}}$ (the matrix transposed to \mathbf{T}) again from the left leads with the use of (34) to

$$\mathbf{E} = (\tilde{\mathbf{T}}\mathbf{S}^{-1}\mathbf{T})(\tilde{\mathbf{B}}\mathbf{S}\mathbf{B}).$$

If the matrices $\mathbf{G}^{(2)}$ are chosen so that the columns of the matrix \mathbf{T} are linearly independent, the matrix $\tilde{\mathbf{T}}\mathbf{S}^{-1}\mathbf{T}$ of 2-nd order is invertible, so we have

$$(40) \quad \tilde{\mathbf{B}}\mathbf{S}\mathbf{B} = (\tilde{\mathbf{T}}\mathbf{S}^{-1}\mathbf{T})^{-1}.$$

Inserting (40) into (39) and (35) respectively, we find

$$(41) \quad \mathbf{B} = \mathbf{S}^{-1}\mathbf{T}(\tilde{\mathbf{T}}\mathbf{S}^{-1}\mathbf{T})^{-1},$$

$$(42) \quad \mathbf{Q} = 2\alpha^{(1)2}(\tilde{\mathbf{T}}\mathbf{S}^{-1}\mathbf{T})^{-1}.$$

Thus the scatter can be expressed in terms of the matrices **T** and **S** without explicit use of **B**.

III.

7. — We discuss presently how to choose the matrices $\mathbf{G}^{(1)}$ so as to obtain procedures which can be recommended for the practical determination of the parameters $\bar{\alpha}^{(\sigma)}$.

It seems to be reasonable to try to express the $\bar{\alpha}^{(\sigma)}$ as linear combinations of quadratic expressions in the sagittas, thus using expressions

$$(43) \quad d^{(\lambda)} = \frac{1}{N - \lambda} \sum_{\nu=1}^{N-\lambda} D_{\nu} D_{\nu+\lambda}.$$

Defining the matrices $\mathbf{G}^{(\lambda)}$ by supposing their elements to be given by

$$(44) \quad g_{\nu\mu}^{(\lambda)} = (\delta_{\nu,\mu+\lambda} + \delta_{\nu+\lambda,\mu})/2(N - \lambda); \quad \lambda = 0, 1, 2, \dots, l; \quad \nu, \mu = 1, 2, \dots, N$$

the expression (25) may be written

$$(45) \quad \bar{\alpha}^{(\sigma)} = \sum_{\lambda=0}^l b_{\lambda\sigma} d^{(\lambda)},$$

where the $d^{(\lambda)}$ are the quantities given in (43). Instead of (45) we may also write

$$(46) \quad \bar{\alpha}_l^{(\sigma)} = \sum_{\lambda=0}^l b_{\lambda\sigma}^{(l)} d^{(\lambda)},$$

where the suffix l refers to the number of parameters used in the procedure.

Introducing (44) into (33) we obtain the elements of the matrix **S** as function of $y = \alpha^{(2)}/\alpha^{(1)}$, similarly we obtain from (31) the elements of the rectangular matrix **T**. The latter quantities depend on l , the degree of approximation, but not upon y . Introducing the matrices **T** and **S** thus obtained into (42) we find the scatter of the coefficients as function of y and of the order l of the approximation.

8. — In particular, for the scatter of the measured value of the physically important parameter $\alpha^{(1)}$ we find an expression of the following type:

$$(47) \quad \langle (\delta \bar{\alpha}_l^{(\sigma)})^2 \rangle^{\frac{1}{2}} / \alpha^{(1)} \approx (2q_{11}^{(l)}(\bar{y})/N)^{\frac{1}{2}}.$$

The functions $q_{11}^{(l)}(y)$ have been computed in the way described above and are plotted in Fig. 3 together with the corresponding function $q_{11}(y)$.

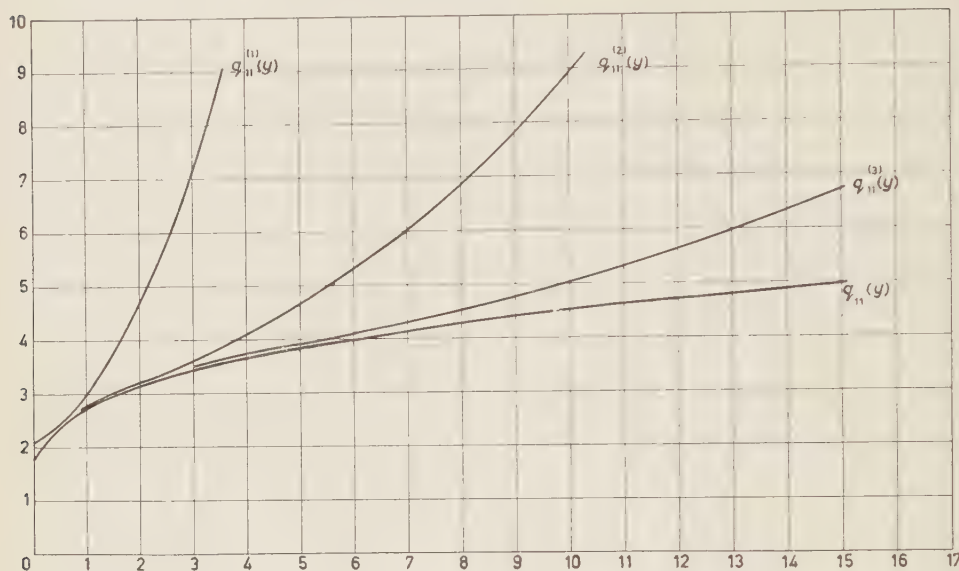


Fig. 3.

The functions $q_{11}^{(l)}(y)$ represent the loss of accuracy of the determination of $z^{(l)}$ because of the background noise together with the error incurred by using the expression (46) for the measured values instead of eq. (4) and (10) given by the maximum likelihood method.

As we see from Fig. 3, $q_{11}^{(l)}(y)$ decreases with increasing l and

$$q_{11}^{(l)}(y) > q_{11}(y)$$

holds for all values of y and l , as it must be, as the maximum likelihood method gives the smallest possible scatter.

As can be seen from Fig. 3 the loss of accuracy when using approximate methods is not very large, unless y is large, *i.e.* unless the background noise exceeds the Coulomb scattering.

9. - In Fig. 2 we have plotted $r(z) = q_{11}(z^3)/z$ together with the functions

$$r^{(l)}(z) = q_{11}^{(l)}(z^3)/z.$$

Unlike $r(z)$ which decreases monotonically with z the functions $r^{(l)}(z)$, $l=1, 2, 3$ show minima for certain values of z and rapidly increase for large values of z .

From this behaviour of the functions $r^{(l)}(z)$ we conclude that using the approximate determination (46) of the scattering parameters, a given track should not be subdivided into too small sections. The subdivision, where the signal-to-noise ratio y corresponds to that value of z for which $r^{(l)}(z)$ has its minimum, gives the best result. It is seen that already for $l=3$ the minimum of $r^{(3)}(z)$ is not very marked which means that it is not essential to use exactly the best subdivision.

10. – For the practical evaluation of a set of data we have thus to compute from the sagittas obtained from a track quantities

$$d^{(0)}, d^{(1)}, \dots, d^{(l)}$$

according to (43). Using these quadratic expressions we can compute measured values $\bar{x}_l^{(1)}$ and $\bar{x}_l^{(2)}$. The larger l , the better we approximate the maximum likelihood method and thus the smaller the scatter of the measured values thus obtained.

Since we have to determine two parameters, we have to use at least two quadratic expressions. In case of $l=1$, the coefficients $b_{\lambda\sigma}^{(1)}$ are uniquely determined already from the auxiliary conditions alone and we find thus

$$\bar{\alpha}_1^{(1)} = \frac{1}{22} (4d_0 + 6d_1),$$

$$\bar{\alpha}_1^{(2)} = \frac{1}{22} (d_0 - 4d_1).$$

The scatter of $\bar{\alpha}_1^{(1)}$ can be obtained with help of the function $q_{11}^{(1)}(y)$, where we may put

$$(48) \quad y \sim \bar{y} = \bar{\alpha}_1^{(2)} / \bar{\alpha}_1^{(1)}.$$

11. – Better approximations $\bar{\alpha}_2^{(\sigma)}, \alpha_3^{(\sigma)}, \dots$ can be obtained when using expres-

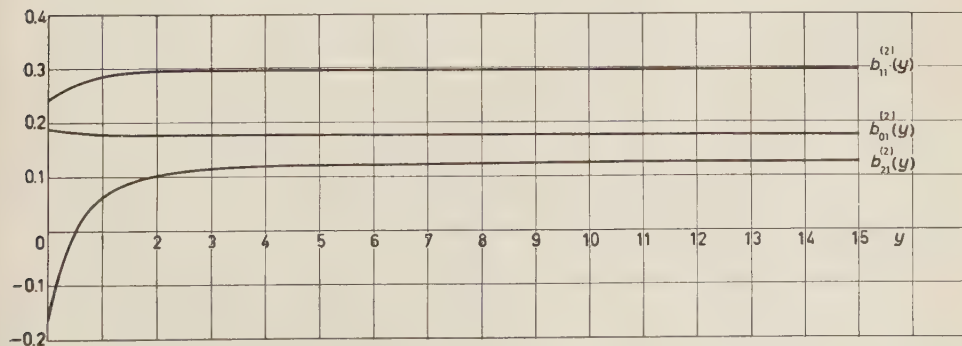


Fig. 4.

sion (46) for $l > 1$. The coefficients $b_{\lambda\sigma}^{(l)}$ can be determined numerically with help of (41) using the numerical values of the matrices **T** and **S** which, as

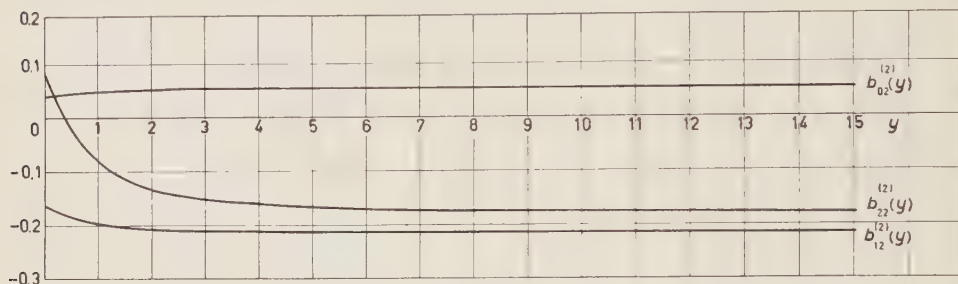


Fig. 5.

already mentioned above, can be determined numerically introducing (44) into (31) and (33). Since the elements of **S** depend on y , the coefficients $b_{\lambda\sigma}^{(l)}$ are

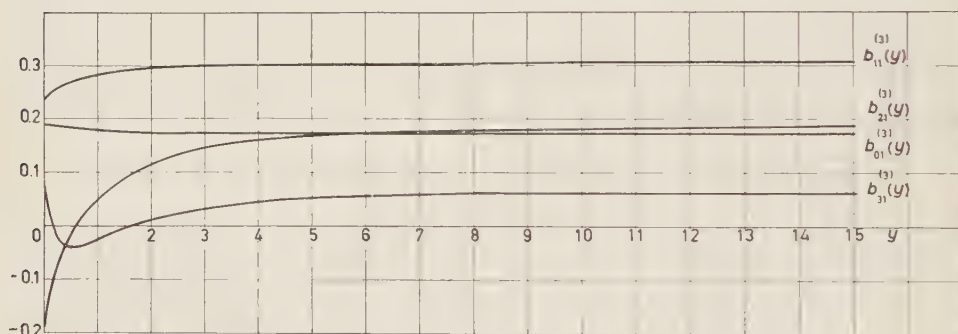


Fig. 6.

also functions of y . In Fig. 4-7 the coefficients $b_{\lambda\sigma}^{(l)}(y)$ as functions of y are plotted for $\lambda = 0, 1, \dots, l$; $l = 2, 3$; $\sigma = 1, 2$ (*).

The eq. (46) can be solved by a graphical procedure, *i.e.* the equation

$$(49) \quad \bar{\alpha}^{(2)}(y)/\bar{\alpha}^{(1)}(y) = y$$

has to be solved graphically. The solution of (49) can be taken to be y , the measured value of y . Inserting this value into (46) and (47) we determine the parameters $\bar{\alpha}^{(\sigma)}$ and their scatters.

(*) The original graphs were executed with sufficient accuracy so that the values taken from them can be used for practical work. We shall be pleased to send them on request to anybody interested.

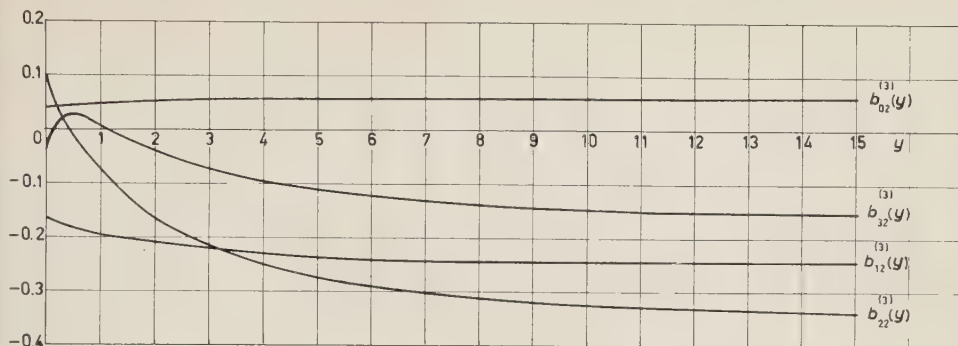


Fig. 7.

12. — Instead of evaluating the expressions (46) over a wide range of values of y , one may use the value obtained from (48) for \bar{y} as a first approximation. This can then be improved by solving (49) using Newton's method.

For this purpose we may write the eq. (49) in the form

$$(50) \quad y \bar{\alpha}_l^{(1)}(y) - \bar{\alpha}_l^{(2)}(y) = 0.$$

According to Newton's method we have the following recurrence formula for improving the approximations of the root of eq. (50):

$$y_{k+1} = y_k - \frac{y_k \bar{\alpha}_l^{(1)}(y_k) - \bar{\alpha}_l^{(2)}(y_k)}{\bar{\alpha}_l^{(1)}(y_k) + y_k \left(\frac{d}{dy} \bar{\alpha}_l^{(1)}(y) \right)_{y_k} - \left(\frac{d}{dy} \bar{\alpha}_l^{(2)}(y) \right)_{y_k}}.$$

RIASSUNTO (*)

Con l'aiuto del metodo della massima verosimiglianza, si deducono formule per la determinazione dei due parametri di una traccia in emulsione. I parametri sono la costante dello scattering coulombiano e l'ampiezza del rumore di fondo. Si ottengono espressioni numeriche per la diffusione dei valori misurati di queste costanti e si mostra che, per esempio, nel caso di una suddivisione molto minuta della traccia l'errore statistico nelle costanti così ottenute decresce proporzionalmente ad $N^{-\frac{1}{2}}$, in cui N è il numero di sezioni. Si ottengono formule che sono utili per la determinazione pratica dei parametri e che danno approssimazioni solo di poco inferiori a quelle ottenute col metodo ottimale della massima verosimiglianza. Si danno dei grafici per facilitare i calcoli numerici.

(*) Traduzione a cura della Redazione.

Résolution électronique analogique de problèmes statistiques d'accumulation poissonnienne.

G. BIZARD et J. SEGUINOT

Laboratoire de Physique Corpusculaire de la Faculté des Sciences - Caen

(ricevuto il 9 Dicembre 1960)

Summary. — In many a problem, we are driven to consider the sum of « small elementary effects ». The probability of obtaining the value x of an « elementary effect » obeys a statistic law $p(x)$. The law of accumulation of the « small effects » is a Poissonian distribution. Last, the law of « total effects » $\sum x$, is the only one which can be perceived directly. The analogic machine which is described in this article has been conceived in order to resolve such problems (Gallier's process, met in the multiple scattering of particles for example), in a wholly electronic way. The precision of this machine which practically depends upon the abundance in statistics only, can reach 3% when 10 000 values are examined.

1. — Introduction.

Dans de nombreux problèmes, on est amené à considérer la somme de petits « effets élémentaires ». La probabilité d'arrivée de la valeur x d'un « effet élémentaire » est régie par une loi statistique $p(x)$, la loi d'accumulation des « petits effets » est une distribution poissonnienne, enfin la loi des « effets totaux » $\sum x$ est la seule directement perceptible.

Ce processus de Gallier intervient par exemple en scattering ou l'on définit un angle de scattering subi par une particule traversant une épaisseur t de matière comme la somme d'angles de « scattering simple » $\varphi_1, \varphi_2, \dots, \varphi_n$, la loi poissonnienne d'accumulation étant une fonction de t , de la nature des particules de la cible.

2. - Principe théorique.

Mathématiquement, le processus est le suivant: (probabilité d'obtenir un effet final compris entre θ et $\theta + d\theta$ = (probabilité d'obtenir un effet élémentaire $\varphi = 0$) \times (probabilité pour qu'il n'y ait qu'une déviation) + (probabilité d'obtenir deux angles φ_1 et φ_2 , tels que $\varphi_1 + \varphi_2 = \theta$) \times (probabilité pour qu'il y ait deux déviations) + (probabilité pour qu'il y ait n effets élémentaires $\varphi_1, \varphi_2, \dots, \varphi_n$ tels que $\sum \varphi = \theta$) \times (probabilité pour qu'il y ait n déviations).

La loi de l'effet élémentaire étant $p(x)$, la probabilité pour que $\varphi_1 + \varphi_2 + \dots + \varphi_n = \theta$ est régie par

$$P_n(\theta) = \frac{1}{2\pi} \int_{-\infty}^{+\infty} [\varphi(y)]^n \exp[i\theta y] dy, \quad \text{où} \quad \varphi(y) = \int_{-\infty}^{+\infty} p(x) \exp[-ixy] dx.$$

On obtient donc

$$P(\theta) = \text{Prob.} \left(\sum_{\theta \neq 0} \varphi = \theta \right) = \frac{1}{2\pi} \sum_{n=1}^{\infty} \int_{-\infty}^{+\infty} [\varphi(y)]^n \frac{\exp[-k] k^n}{n!} \exp[i\theta y] dy,$$

$$P(\theta) = \frac{\exp[-k]}{2\pi} \int_{-\infty}^{+\infty} (\exp[k\varphi(y)] - 1) \exp[i\theta y] dy,$$

$$P(0) = \exp[-k] + \frac{\exp[-k]}{2\pi} \int_{-\infty}^{+\infty} (\exp[k\varphi(y)] - 1) dy,$$

k est le nombre moyen de la loi de Poisson.

Lorsque $p(x)$ a une forme analytique compliquée ou lorsqu'il n'est connu que par une courbe obtenue point par point, le calcul formel est souvent très ardu. Il peut donc être intéressant de réaliser une analogie du phénomène à l'aide d'une machine du type dit de « Monte-Carlo » de façon à obtenir expérimentalement une distribution statistique homologue de $P(\theta)$.

On sait que si l'on porte sur un système d'axes Oxy une courbe

$$x = \int_{-\infty}^y p(y) dy,$$

ou $p(y)$ est une loi de probabilité différentielle, la probabilité pour qu'un tirage effectué au hasard sur le segment $(0, 1)$ de l'axe des x , amène une valeur comprise entre y et $y + dy$, est proportionnelle à $p(y)$.

Supposons donc que $p(y)$ soit notre loi de « effets élémentaires », et que les tirages au hasard émanent d'une source poissonnienne de paramètre constant dans le temps. Il suffira de sommer les valeurs données pour chaque tirage pendant un intervalle de temps constant, et tel que le nombre moyen de tirages pendant cet intervalle de temps soit égal au nombre moyen du processus poissonnien d'accumulation de la loi cherchée (nombre moyen de scatterings simples, dans le cas du scattering), pour réaliser le problème homologue et déduire statistiquement la loi de probabilité finale.

3. - Principe expérimental.

La loi intégrale de probabilité élémentaire étant tracée sur l'écran d'un oscilloscope, le principe est d'en analyser l'amplitude à des intervalles de temps qui sont distribués suivant une loi de Poisson. Le balayage de l'oscilloscope étant réglé suivant l'axe des abscisses, une impulsion à temps de montée linéaire est envoyée sur les plaques verticales suivant cette loi. Il suffit de mesurer l'intervalle de temps entre le début de l'impulsion et l'instant où elle atteint la courbe tracée sur l'oscilloscope, pour avoir l'amplitude de la loi de probabilité élémentaire. Il est évidemment nécessaire que le temps de montée

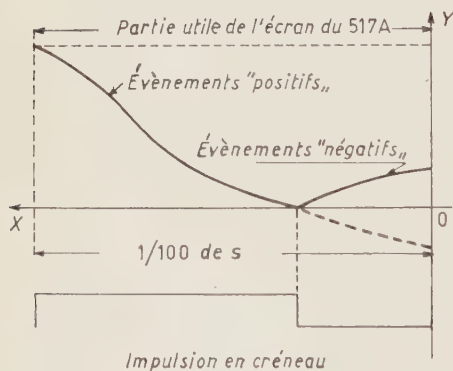


Fig. 1. - Centrage de l'impulsion en créneau.

en laissant la largeur totale constante. Cette impulsion ne servira que pour certains types de lois de probabilité ou il faudra distinguer entre événements positifs et événements négatifs: exemple le scattering, ou il peut se produire que deux angles de scattering simple soient d'amplitudes égales mais de signes opposés, ce qui conduit à un résultat global nul.

Pour traiter de tels problèmes, il suffira de centrer le point de basculement du créneau sur l'évènement 0 de la courbe de probabilité (Fig. 1).

maximum de l'impulsion ne dépasse pas une fraction acceptable de la vitesse de balayage.

La mesure de cet intervalle de temps est alors déterminée en modulant cette « porte » par un générateur d'impulsion à récurrence aussi élevée que possible.

On dispose d'une impulsion en créneau \square synchrone du balayage et de même durée (largeur totale 1/100 de seconde). On peut régler à volonté dans cette impulsion en créneau le rapport des durées des parties positives et négatives, tout

4. - Dispositif expérimental.

Le bloc diagramme très schématique de l'électronique est donné par la Fig. 2.

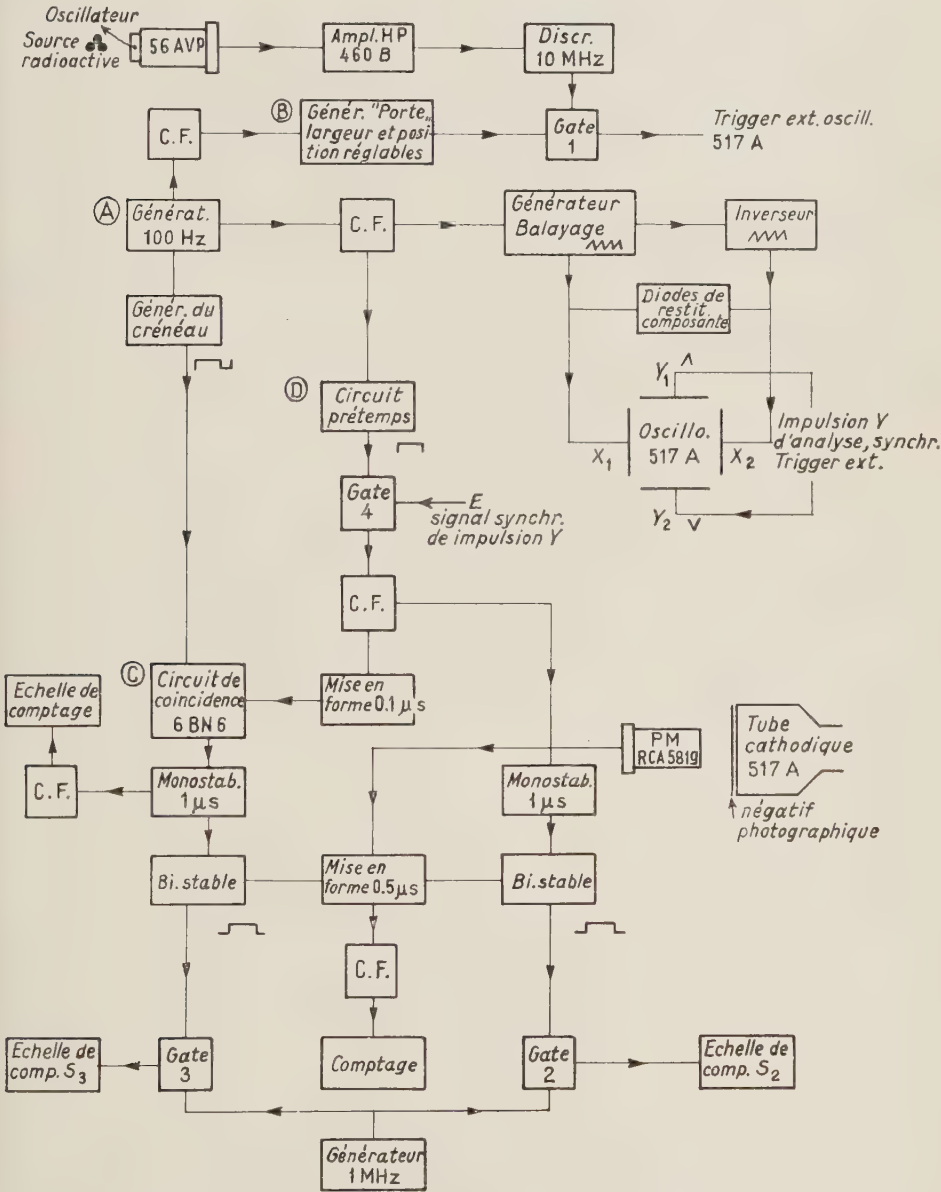


Fig. 2. - Bloc-diagramme de l'électronique.

Nous avons utilisé un oscilloscope Tektronix 517 A bien adapté à notre problème, car la rémanence de l'écran bleu est faible. Pour pouvoir utiliser la plus grande partie de l'écran, nous avons été amenés à choisir un rapport assez grand entre la durée de la dent de scie horizontale et celle de l'impulsion verticale, une correction étant néanmoins faite en traçant la loi de probabilité élémentaire en coordonnées obliques.

D'autre part, la durée de l'impulsion verticale devait être assez brève pour que le temps mort introduit n'amène pas de perturbations notables dans la loi de Poisson, et assez longue pour que la porte modulée par un générateur périodique donne une mesure suffisamment précise. Comme nous ne disposions pas de générateur périodique de fréquence supérieure à 1 MHz, cela nous a conduit à choisir une durée totale de 300 μ s pour l'impulsion verticale. Il fallait donc prévoir un balayage d'une durée voisine de 10 ms (défini par le générateur base de temps A), et comme le balayage le plus lent du Tektronix n'atteint qu'une durée totale de 300 μ s, nous avons dû construire un générateur externe, de balayage.

Ce générateur du type Boot-strap délivre deux dents de scie symétriques d'amplitude 350 V et de durée 10 ms, qui vont attaquer les plaques de déviation horizontales de l'oscilloscope.

Le balayage interne de l'oscilloscope qui délivre, par déclenchement extérieur, l'impulsion de mesure, a été transféré des plaques de déviation horizontales, aux plaques de déviation verticales. Nous avons dû pour tenir compte de la différence de sensibilité entre les deux couples de plaques de déviation, ne prélever qu'une partie de ce balayage et pour cela fractionner les charges des tubes de sortie des deux dents de scie symétriques (nous ne pouvions utiliser un pont diviseur compensé sous peine de perturber le fonctionnement des diodes de restitution de la composante continue, et d'introduire par conséquent une fluctuation importante sur l'ordonnée du départ sur l'écran de l'impulsion verticale).

Ces impulsions verticales sont déclenchées par la source poissonnienne. La source poissonnienne est constituée par un photomultiplicateur 56 AVP regardant un scintillateur plastique excité par une source γ . Les impulsions du 56 AVP sont ensuite amplifiées par un amplificateur Hewlett-Packard 460 B, puis mises en forme par un discriminateur 10 MHz. Nous avons en effet constaté qu'une électronique rapide permettait d'obtenir une répartition des impulsions plus proche de la loi de Poisson, lorsqu'il s'agit de fréquence moyenne faible.

Les impulsions poissonniennes sont alors envoyées sur le Trigger de l'oscilloscope à travers le gate 1. Ce gate est destiné, d'une part à empêcher les impulsions verticales d'arriver pendant le retour du balayage H , d'autre part à amputer les extrémités de ce balayage H de façon à ne conserver qu'une partie suffisamment linéaire de la montée de la dent de scie. Une impulsion

synchrone du départ de la dent de scie excite un univibrateur de retard dont la largeur est égale à la partie à éliminer au départ du balayage; on se sert ensuite de la retombée de l'impulsion carrée de cet univibrateur pour exciter un second univibrateur de retard dont l'impulsion carrée de durée égale à la partie linéaire utile de la dent de scie commande l'ouverture du gate 1 (circuit *B*).

L'écran du tube cathodique de l'oscilloscope est regardé par un photomultiplicateur RCA 5819, à travers un négatif photographique dont une bande transparente épouse la forme de la courbe à étudier, cette courbe doit évidemment être positionnée avec précision. Chaque fois qu'une impulsion poissonnienne arrive sur le Trigger de l'oscilloscope, une impulsion synchrone du départ du balayage vertical est envoyée pour ouverture, d'une part directement sur le gate 2, d'autre part sur le gate 3 après sélection par un système de coïncidence (circuit *C*) des impulsions tombant pendant la partie positive du signal créneau.

Les gates 2 et 3 reçoivent en permanence des impulsions périodiques de fréquence 1 MHz. Ces deux gates sont refermés par l'impulsion délivrée par le PM 5819 lorsque le spot passe devant la courbe. Les échelles 2 et 3 placées respectivement derrière les gates 2 et 3 enregistrent donc pour n impulsions poissonniennes:

— Pour l'échelle 2: la somme S_2 des amplitudes de la courbe aux abscisses d'arrivée des n impulsions.

— Pour l'échelle 3; la somme S_3 du comptage de l'échelle 3 se rapporte aux impulsions qui sont tombées dans la partie positive du signal en créneau.

D'autre part, le spot de l'impulsion ne démarrant pas exactement sur l'axe des abscisses de la courbe, mais en dessous, nous devons soustraire au comptage correspondant à une impulsion verticale un nombre constant « a » pour obtenir l'amplitude effective de la courbe au point d'arrivée de cette impulsion. Il faut donc compter:

— le nombre total n d'impulsions;

— le nombre p d'impulsions arrivant pendant la partie positive du créneau.

Le comptage $S_3 - pa$ donne alors le résultat intégré des événements élémentaires positifs, alors que le comptage $S_2 - n$ donne le résultat total sans distinction du signe des événements.

Le résultat exact compte tenu du signe des événements sera donc:

$$2 S_3 - S_2 - 2 pa + na .$$

Dans le cas où tous les événements sont nécessairement de même signe, le résultat de l'intégration sera donné directement par $S_2 - na$.

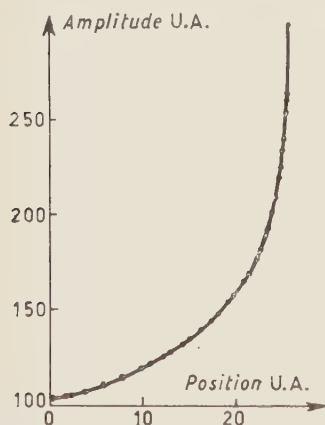
Enfin nous disposons d'un système de présélection (circuit *D*) qui permet :

— Soit de fonctionner en prétemps, en sélectionnant un temps de fonctionnement T multiple de la durée du balayage horizontal, le facteur de multiplicité étant compris entre 1 et 10 000. Il suffit alors de régler l'intensité de notre source poissonnienne de façon à ce que le nombre moyen d'événements arrivant pendant le temps T soit égal à la constante k du problème à étudier.

— Soit de fonctionner en précompte, en sélectionnant le nombre d'impulsions verticales sur lequel sera faite l'intégration.

5. — Tests préliminaires.

Nous avons testé la linéarité du balayage horizontal et de l'impulsion verticale: ces deux impulsions ont été trouvées linéaires à moins de 1% près.



Courbe 1. — Test préliminaire: comptage en fonction de la position d'une impulsion verticale d'exploration. Les points expérimentaux se répartissent pratiquement sur la courbe théorique.

Nous entendons par là que la valeur quadratique moyenne de l'angle de la montée de l'impulsion avec la direction moyenne de cette impulsion est inférieure à 0.01 radians. Nous avons enfin cherché à ausculter dans un test plus général les qualités globales de l'appareillage électronique, de façon à décompter les erreurs de mesure et de méthode. Nous avons pour cela exploré une courbe fixée sur l'écran de l'oscilloscope avec une impulsion verticale unique dont l'abscisse pouvait être réglée à volonté. La courbe résultante (nombre de coups filtrés par le gate en fonction de la position de l'impulsion verticale) s'est trouvée coïncider avec la courbe de départ, avec une précision inférieure à 1% (courbe 1).

6. — Tests de principe.

Nous avons testé l'appareil en lui soumettant la courbe $p(x) = \exp[-x]$. La courbe théorique attendue était alors

$$P(\theta) = 2\pi \exp[-\theta] \sqrt{\frac{k}{\theta}} I_1(2\sqrt{k\theta}),$$

I_1 étant la fonction de Bessel modifiée de première espèce, et k le nombre moyen de la loi de Poisson.

Nous avons choisi $k=9$, et tant pour éviter les fluctuations dues à la dérive dans le temps de la fréquence de notre générateur, que pour faciliter le dépouillement des résultats, nous avons opéré en précompte.

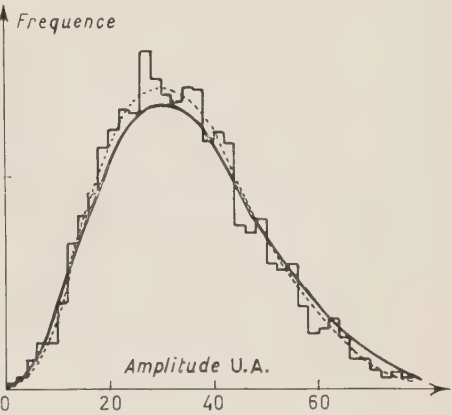
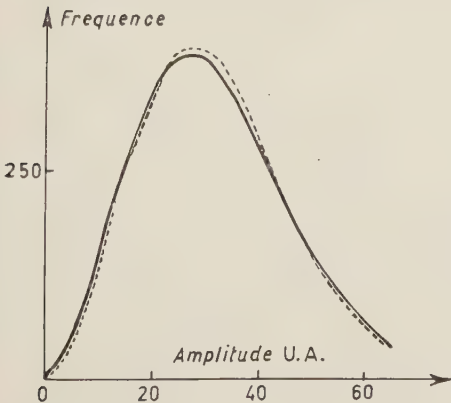
Nous avons calculé les fréquences théoriques d'arrivée de 1, 2, 3, n événements pour une loi de Poisson dont la constante est $k=9$, puis déclenchant notre système de prétemps, non plus avec des impulsions synchrones du balayage horizontal, mais par les impulsions verticales elles-mêmes, nous avons effectué pour chaque valeur 1, 2, 3, ..., n du précompte un nombre de relevés proportionnels aux fréquences calculées.

Nous avons relevé cinq histogrammes comprenant chacun 2 700 points distribués en 50 canaux.

Si nous définissons l'erreur avec laquelle une courbe approchée $y=f(x)$ s'écarte de sa représentation idéale $g(x)$ par

$$\frac{\int_{-\infty}^{+\infty} |f(x) - g(x)| dx}{\int_{-\infty}^{+\infty} |g(x)| dx} = \delta \% .$$

La courbe la mieux adaptée construite sur l'histogramme total groupant



Courbe 2. — Histogramme expérimental groupant 2700 tirages. On a représenté en pointillés, la courbe expérimentale la mieux adaptée, et en traits pleins, la courbe théorique.

tous nos résultats (soit 13 500 points) ne s'écarte pas plus de 3 % de la courbe théorique (courbe 3). Pour une courbe groupant 2 700 points, cette précision est de l'ordre de 7 % (courbe 2).

Courbe 3. — courbe expérimentale obtenue par lissage d'un histogramme groupant 13 500 valeurs. ——— courbe théorique.

Compte tenu du test global évoqué plus haut, les écarts constatés entre les courbes expérimentales et théoriques semblent donc devoir être attribués principalement aux erreurs statistiques.

* * *

Nous remercions Monsieur le Professeur SCHERER, Directeur du Laboratoire, pour son encouragement qui a rendu possible ce travail et pour l'intérêt qu'il y a apporté, et Monsieur le Professeur PHAM, pour les conseils qu'il nous a donnés, lors de la discussion mathématique du problème.

Nous tenons également à exprimer notre gratitude à Messieurs MILLIARD, PATRY, DUCHON, qui ont contribué à la réalisation des circuits électroniques, et nous ont aidé au dépouillement des résultats.

Ce travail a pu être effectué grâce aux moyens mis à notre disposition par le Centre National de la Recherche Scientifique.

RIASSUNTO (*)

In molti problemi siamo portati a considerare la somma di « piccoli effetti elementari ». La probabilità che si ottenga il valore x di un « effetto elementare », è regolata da una legge statistica $p(x)$. La legge di accumulazione dei « piccoli effetti » è una distribuzione poissoniana. Infine, la legge degli « effetti totali » $\sum x$ è la sola che può essere percepita direttamente. La calcolatrice analogica, descritta in questo articolo, è stata concepita allo scopo di risolvere problemi di questo tipo (per esempio, il processo di Galliher, che si incontra nello scattering multiplo di particelle) in maniera completamente elettronica. La precisione di questa calcolatrice, che in pratica dipende solo dall'abbondanza di dati statistici, può arrivare al 3%, quando si elaborano 10000 valori.

(*) Traduzione a cura della Redazione.

A Model of α -Decay Consistent with α -Reactions.

J. OSADA (*), D. R. DE OLIVEIRA, N. MARTINS and T. MIYAZIMA (**)

Instituto de Física Teórica - São Paulo

(ricevuto il 10 Gennaio 1961)

Summary. — A new model of α -decay is presented which is consistent with such α -reactions as (p, α) . Both the α -decay and the direct α -reaction suggest that with a certain probability α -particles exist in the nuclear surface. According to the current theories of α -decay the α formation probability turns out very small of the order of magnitude 10^{-4} while, from the analysis of (p, α) reactions the α probability is estimated to be of the order of magnitude of several times 0.1. Although there may be some difference in the physical meanings of the α probabilities in the two cases, there are enough reasons to believe they are of the same order of magnitude. In our model α -particles are assumed to be constantly formed within the nuclear matter and to go out into the nuclear surface where most of them are reflected back or destroyed and some of them go out into the outer space. Besides this specific mechanism, we have made use of as much experimental data as possible and we have succeeded to solve the above mentioned discrepancy and to explain some systematic tendencies in the α -decay isotopes on a unified basis.

1. — Introduction.

At first sight the α -decay might seem too old fashioned to find in it some important problem. The purpose of this paper is to point out that this is not always the case. Although, for instance, the shell theory of the nucleus has been so well developed that it has now become possible to treat and predict very detailed properties of excited nuclei, we have still very little knowledge concerning interparticle correlation or clustering in real nuclei. The

(*) On leave of absence from Tokyo Institute of Technology.

(**) On leave of absence from Tokyo University of Education.

nucleus is a system of many but finite number of particles, and, consequently, simple knowledge of shell structure may not exhaust all properties of nucleus. There do exist indications which point out for us the importance of correlation among nucleons. They are those phenomena as the α -decay and direct reactions in which clusters like α -particles take part. These phenomena are the main concern of this paper.

Since GAMOW⁽¹⁾, CONDON and GURNEY⁽²⁾ presented the first theory of the α -decay about thirty years ago, development in this field was rather slow. In their theory, they assumed a very simple model for the decaying system, and succeeded in explaining the Geiger and Nuttall law⁽³⁾, a relation between the decay constant and the energy of the emitted α -particle. Namely, they assumed continuous existence of one α -particle in the decaying nucleus, this α -particle being under the influence of a potential which implies a collective effect of all other nucleons. They divided the space into two regions by a « nuclear radius » R , outside of which the potential is assumed to be a pure Coulomb one and inside of which a square well. Under these assumptions, they calculated quantum-mechanically the penetrability of the α -particle through the Coulomb barrier and obtained the Geiger and Nuttall law.

In spite of this excellent success, their theory was not satisfactory in some points. They could adjust the « nuclear radius » R so that the theoretical expressions agreed with experimental values of the decay constant, but they could not explain the decay constant by relating it to the nuclear radius which is obtained from other experiments. Moreover, judging from recent knowledge of nuclear physics, the nuclear radius thus obtained seems to us somewhat too big compared with the values from other experiments, and we must sometimes use quite different values of nuclear radius for different nuclei. For example, we can obtain $R = 1.537 A^{1/3} f = 9.2 f$ for ^{214}Po . But, if we use this value for ^{210}Po , the calculated value of its decay constant turns out to be too big by a factor 10^7 compared to its experiment value. If we wanted to get good agreement, we must have used a smaller radius $R = 1.422 A^{1/3} f = 8.45 f$ in this case (*).

After the theory mentioned above, there appeared several theories⁽⁴⁾, but

(1) G. GAMOW: *Zeits. f. Phys.*, **51**, 24 (1928).

(2) E. U. CONDON and R. W. GURNEY: *Phys. Rev.*, **33**, 127 (1929).

(3) G. C. HANNA: *Experimental Nuclear Physics*, vol. **3**, part IX (1959); I. PERLMAN and J. O. RASMUSSEN: *Handb. d. Phys.*, **42**, 109 (1957).

(*) Slight fluctuations of the radius or shape may be expected due to difference in nuclear structure. The differences in R seem, however, to be too big to be explained only by this reason. ^{210}Po has the neutron closed shell 126. Cf. I. PERLMAN, A. GHIORSO and G. T. SEABORG: *Phys. Rev.*, **77**, 26 (1950).

(4) M. A. PRESTON: *Phys. Rev.*, **71**, 865 (1947); I. KAPLAN: *Phys. Rev.*, **81**, 962 (1951); J. J. DEVANEY: *Phys. Rev.*, **91**, 587 (1953).

they were concerned mainly in refinement of their calculation and extension to the decay of non-spherical nuclei.

Recently, TOLHOEK and BRUSSAARD ⁽⁵⁾ published very interesting discussions about the α -decay. The potential for the α -particle is not strictly square well, but it has a «tail» as known from scattering experiments. This may have a big effect on the penetrability. So they calculated the potential for the α -particle by using the experimental value of the nucleon density of the nucleus, the extension of the α -particle and the range of the two-body nuclear potential, and evaluated the penetration through this modified potential barrier. Thus, they could obtain an improved result, but the effect of the tail was so big in lowering the barrier that the penetrability became very big. In order to get the correct value of the decay constant, therefore, they were forced to assume that the α -particle does not exist continuously in the nucleus but it is formed with a very small probability $P_{\alpha} \simeq 10^{-4}$.

On the other hand, a probability of formation of α -particles can be inferred from medium energy scattering experiments. HODGSON ⁽⁶⁾ analysed an experiment in which protons of 45 MeV bombarded heavy nuclei in photographic emulsion and energy and angular distributions of α -particles were measured. From the fact that secondary protons were very often accompanied by α -particles and from the form of energy and angular distributions, he interpreted the reaction as knock-on by incident protons of those α -particles which were present in the nuclear surface with a probability P'_{α} . He assumed the same cross-section for proton- α scattering as that for free α -particles, and, by a classical calculation, he estimated the probability P'_{α} as about 0.4. We analysed this experiment quantum-mechanically by assuming relatively low angular momentum bound states for the α -particle, and showed that the main features of the angular distribution can be explained. The value we got for P'_{α} was nearly the same as Hodgson's ⁽⁷⁾. More recently, OSTROUMOV and FILOV ⁽⁸⁾ performed a similar experiment by using proton beams of somewhat higher energies between 100 and 660 MeV. In this case the mechanism of reaction becomes a little more complicated because of cascade multiplication ^(*) of nucleons within a nucleus, but they concluded that P'_{α} is an intrinsic quantity of a nucleus and is independent from the bombarding energies.

⁽⁵⁾ H. A. TOLHOEK and P. J. BRUSSAARD: *Physica*, **21**, 449 (1955).

⁽⁶⁾ P. E. HODGSON: *Nucl. Phys.*, **8**, 1 (1958).

⁽⁷⁾ T. MIYAZIMA *et al.*: *Informações entre Físicos*, **3**, 16 (1960), a mimeographed circular in Portuguese.

⁽⁸⁾ V. I. OSTROUMOV and R. A. FILOV: *Soviet Phys. JETP*, **37** (10), 459 (1960).

^(*) Proton beams of energies between 50 and 100 MeV seem to be most convenient for the study of this kind of direct reaction, because the cascade multiplication is not so important in this case and, at the same time, we can easily separate α -particles due to the direct reaction from those due to evaporation.

Now, P_α and P'_α are defined on different bases. While P_α is the probability of formation of α -particles which will later go out from the nucleus carrying a definite decay energy, P'_α is defined with a little looser condition. In both cases, however, we are considering α -particles which are limited within the nuclear surface. The state in which α -particles exist in the nuclear surface is not a pure stationary state but must be considered as a member of expansion of the nuclear wave function into resonant group states in the terminology of Wheeler. It seems thus quite reasonable to consider that P_α and P'_α should be of the same order of magnitude. As we have mentioned, experiments show, however, that P_α and P'_α differ from each other by the order of magnitude 10^3 .

The main purpose of the present work is to solve this contradiction. In the next section, we present a new model of the α -decay. In Section 3, we discuss the potential for the α -particle in detail. In Section 4, we calculate the penetrability in this model numerically. In Section 5, we discuss the consistency between the α -decay and the scattering experiments and an additional strong point of our model, *i.e.*, unnecessary of introduction of a too big fluctuation in the nuclear radius.

2. - A model of the α -decay.

We know from the electron-nucleus scattering experiments, etc., that the nucleon density in a nucleus has the form shown in Fig. 1. Let us divide the nucleus into two regions as shown in that figure and call them the inner and the surface region, respectively.

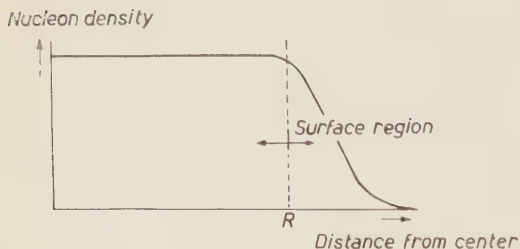


Fig. 1. - Nucleon density in a nucleus. We divide the nucleus into two parts, the inner and the surface region, at the point where the density becomes almost constant.

In the inner region, the binding energy per nucleon and the inter-nucleon distance are very similar to those of an α -particle. But, we do not know at all whether we may assume that the neighbouring two protons and two neutrons make an α -particle or not, since we have at present no precise mathematical definition of the clustering. Though an α -particle might be really formed in this region, it is very difficult for us to

recognize it as an α -particle, because it may be too similar to its surroundings. On the other hand, if an α -particle is in the surface region, we may recognize it very easily, because the nucleon density and the binding energy per nucleon may be very different in this region from those of an α -particle. We shall

therefore, consider the α -particle only in this surface region. We shall not pay any attention to its origin. It might come from the inner region or possibly be formed just outside of the inner region owing to a fluctuation of the «surface» of the inner region. Some α -particle might be formed in the outer part of the surface region, but this probability must be very small as shown by TOLHOEK and BRUSSAARD ⁽⁵⁾ in their calculation of the overlapping integral.

Now let us follow the behavior of the α -particle which has just come out of the inside to the surface region. It goes to the outer part of the surface region, where it may be mainly pushed back by the collective effect of the other nucleons and, entering back into the inner unrecognizable region, disappears from our attention, but sometimes it is dissociated into other smaller clusters or into four nucleons colliding with nucleons existing in this region and these four nucleons go back to the inner region ⁽⁹⁾. Very rarely, it may go out to infinity as a decay α -particle. The life time of the α -decay is very long compared to the period of the nuclear oscillation, so that the nucleus is considered to be almost stable. Therefore, we can consider that this kind of circulation in the nuclear surface always happens.

3. - Choice of the potential for an α -particle.

Following the usual way, we may express the collective influence of the nucleons in the daughter nucleus by a potential. A part of the influence which is responsible for the pushing back of α -particles is expressed by a real potential barrier like TOLHOEK and BRUSSAARD's, and the other part which causes the dissociation of the α -particle by an imaginary potential. Namely, we may take account of all effects by an appropriate complex potential.

A short while ago, IGO ⁽¹⁰⁾ obtained the following optical potential for an α -particle from his cumulative analysis of the scattering and reaction experiments of α -particles:

$$V(r) = -1100 \exp \left[-\frac{r - 1.17A^{\frac{1}{3}}}{0.574} \right] - i \cdot 45.7 \exp \left[-\frac{r - 1.40A^{\frac{1}{3}}}{0.578} \right].$$

This potential is valid in the region where the absolute value of the real part is smaller than 10 MeV. In the reaction experiments, however, the α -particle cannot penetrate deeply into the nucleus, that is, the wave function of the α -particle is damped away very rapidly in the nucleus. Thus, we cannot obtain any knowledge about the shape of the potential in the inner region.

⁽⁹⁾ G. H. WILSON: *Phys. Rev.*, **96**, 1032 (1954). We appreciate very much Dr. WINSLOW's remark that some of the basic points of our model are closely related to his model.

⁽¹⁰⁾ G. IGO: *Phys. Rev.*, **115**, 1665 (1959).

In the optical potential for a nucleon, we have an imaginary part even when the energy is sufficiently low and every inelastic channel is closed. This imaginary part comes from the averaging procedure of the cross-section. That is, the cross-section may oscillate with energy very rapidly, if we measure it by using a strictly monochromatic incident wave. In the usual experiments, however, the incident wave is not monochromatic, and only the cross-section which is smoothed out by averaging it over the energies is measured. In order to calculate this averaged value directly, we usually add a small imaginary part to the potential⁽¹¹⁾.

It may then be a little risky to use such an optical potential without any criticism for the α -decay in which the energy of the emitted α -particle seems to be well defined. In the case of the optical potential for α -particles, however, we have another origin of the imaginary part. The α -particle may be with some probability dissociated into four nucleons when it enters into a nucleus. Namely, real damping of the wave function of the α -particle occurs. In order to take account of this damping, we must also add some imaginary part to the potential.

The imaginary part in the Igo potential may be considered to come from these two origins. (Of course, in the case of higher incident energy, some of the imaginary part must come from the damping due to the inelastic and reaction processes in which the α -particle gives some part of its energy to other nucleons. But, this is not important in our case.)

Moreover, in the region where the effect of the optical potential is big, the energy of the α -particle is considered to be not so well defined, as discussed later.

Based on such reasons, we shall use Igo's optical potential itself without any modification for the outer part of our complex potential.

With respect to the inner part of our complex potential, we may make any assumptions, because no assumption contradicts with the scattering and reaction experiments. About the real part, we shall follow the discussion by TOLHOEK and BRUSSAARD. They considered an imaginary cycle of four nucleons: two protons and two neutrons go out from a nucleus, they form an α -particle in the outside of the nucleus, this α -particle enters back into the nucleus and is finally dissociated into four separate nucleons within the nucleus. Assuming that the binding energy of the α -particle in the nucleus is very near to that of a free α -particle, they obtained 167 MeV for the value of the potential at sufficiently inner points. Here we assume 147 MeV arbitrarily, because this value is not important for our purpose as will be seen from the calculation in the next section.

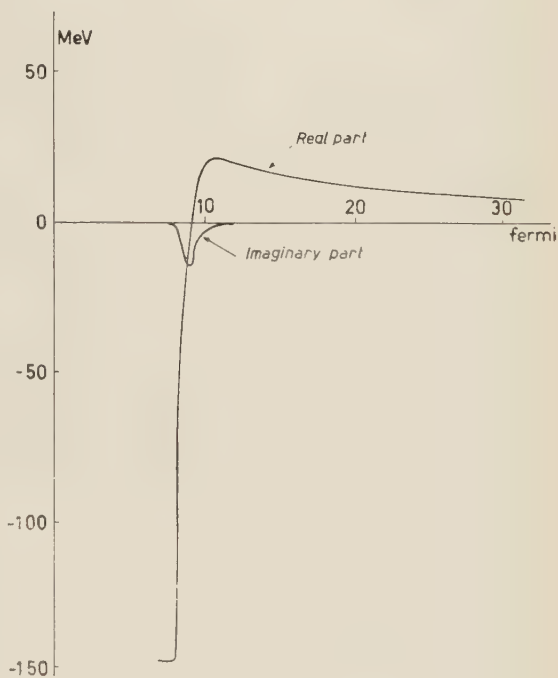
(11) H. FESHBACH, C. E. PORTER and V. F. WEISSKOPF: *Phys. Rev.*, **96**, 448 (1954).

About the imaginary part, we shall assume that it goes to zero at $r = 8f$. The reason is the following: in the central part of the nucleus, the nucleon density is so high that the α -particle cannot be dissociated because of the Pauli principle. Even if it were dissociated there, another one will be formed at once because it is the property of this part of the nucleus to be very similar to the α -particle. Then, the imaginary part may be rather small if it ever exists. The choice of $8f$ is not so meaningful. It is because, on one side, we can usually consider that the α -particle has reached the inner region when it came to $8f$ from the center of the nucleus, and on the other, this choice is not sensitive for the value of the penetrability.

Thus fixing the values of the potential at the inner part, we interpolate freely the complex potential from here to Igo's region.

In conclusion, we shall use the potential shown in Fig. 2.

Fig. 2. - Potential for the α -particle. This is the potential in case of the decay of ^{214}Po . The potentials are slightly different in case of the decays of other polonium isotopes, but very similar. We do not draw them here.



4. - Calculation of the decay constant.

In our model, the decay constant λ is given by

$$\lambda = S \exp[-2C],$$

where S denotes the number of α -particles per unit time which just appear at the surface region and are going toward the outer part, and $\exp[-2C]$ is the penetrability. In our case, C is given in WKB approximation by

$$C = \int [\{M^2(E - V_\alpha - V_c)^2 + M^2 W_\alpha^2\}^{\frac{1}{2}} - M(E - V_\alpha - V_c)]^{\frac{1}{2}} dr,$$

where V_λ and W_λ are the real and imaginary part of Igo's potential, respectively, and V_c is the Coulomb potential between the α -particle and the daughter nucleus, M is the reduced mass and E is the effective energy of the emitted α -particle.

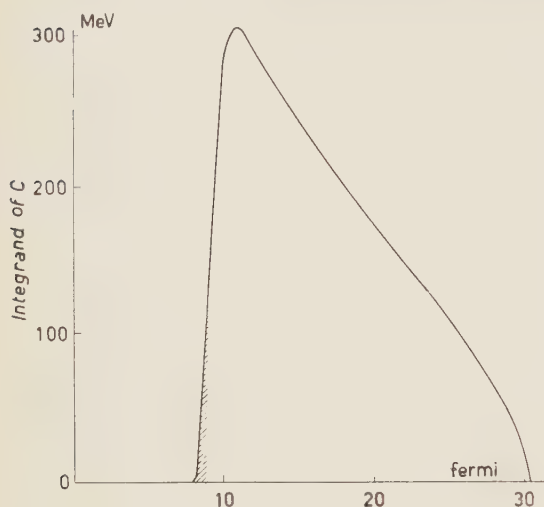


Fig. 3. — Integrand of C . If the shape of potential changes slightly in the inner part, this integrand changes slightly in the hatched part. This modifies only very little the total area of this graph.

We do not consider the effect of reflection. It must be very small, because there is no sudden change in the potential and it is absorptive.

The integral C is given by the area shown in Fig. 3. If the value of the potential changes slightly at a part near the inner region, the hatched part of the figure changes slightly. This change is not so important to the whole integral, because the main contribution comes from the outer part.

The results of the numerical calculations are shown in Table I. We have used $\delta^2 = 2\pi\hbar S$, the reduced width, for comparison with other works.

TABLE I. — Reduced widths for polonium isotopes.

Elements	$\lambda_{\text{exp}} (\text{s}^{-1})$	$\exp [-2C]$	$\delta^2 (\text{MeV})$
^{218}Po	$3.79 \cdot 10^{-3}$	$2.51 \cdot 10^{-23}$	0.623
^{216}Po	4.39	$3.29 \cdot 10^{-6}$	0.552
^{214}Po	$4.24 \cdot 10^3$	$3.61 \cdot 10^{-17}$	0.486
^{212}Po	$2.28 \cdot 10^6$	$3.24 \cdot 10^{-14}$	0.291
^{210}Po	$5.92 \cdot 10^{-8}$	$8.42 \cdot 10^{-17}$	0.029
^{208}Po	$7.50 \cdot 10^{-9}$	$8.76 \cdot 10^{-28}$	0.035
^{206}Po	$4.56 \cdot 10^{-8}$	$2.80 \cdot 10^{-27}$	0.067
^{204}Po	$5.67 \cdot 10^{-7}$	$1.63 \cdot 10^{-56}$	0.132
^{202}Po	$4.44 \cdot 10^{-6}$	$2.62 \cdot 10^{-25}$	0.070
^{200}Po	$1.05 \cdot 10^{-3}$	$4.07 \cdot 10^{-24}$	1.067

5. — Discussion.

In the old calculations, we used the potential barrier shown in Fig. 4. The bigger the hatched area of the figure, the smaller the penetrability. In TOLHOEK

and BRUSSAARD's work, they used a potential like that shown in Fig. 5. In this case, the hatched area became too small and consequently the penetrability became too big. Then they were forced to assume a very small formation probability of α -particles which contradicts completely the reaction experiments. But, in any way, we must use a modified potential like TOLHOEK and BRUSSAARD's because the existence of the potential tail is well established from the scattering experiments. The only way in which we can make both facts compatible with each other is to take account of the dissociation effect of the α -particle.

Now, S is considered to be composed of two factors as follows:

$$S = F \cdot N_{\alpha},$$

where F is the frequency of an α -particle in the nuclear surface, that is, the number of times in which an α -particle appears on the dividing sphere, and N_{α} is the average number of α -particles in the nuclear surface.

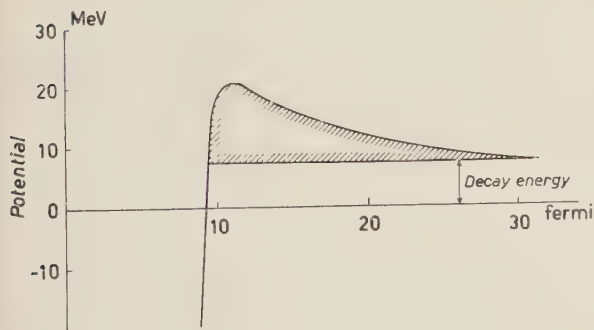


Fig. 5. - Potential in Tolhoek and Brussaard's theory. The barrier is rounded so much on account of the tail of the nuclear potential that the penetrability becomes too big.

reaction experiments. In Hodgson's analysis, he assumed that 60 nucleons make α -particles with the formation probability $P_{\alpha}=0.4$, so that the average number of α -particles is about 6. As we have discussed in Section 1, the two values of

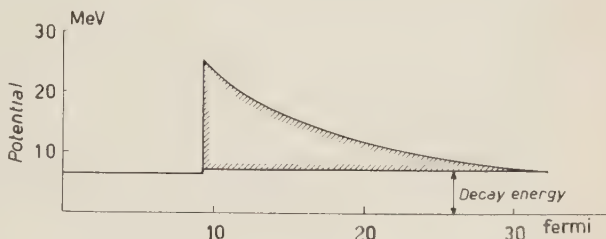


Fig. 4. - Potential barrier in Gamow's theory. The larger the hatched area, the smaller the penetrability.

We may consider that F is nearly equal to $D/2\pi\hbar$, according to DEVANEY ⁽⁴⁾ where D is the mean distance of the 0^+ energy levels of the nucleus, and of the order of 1 MeV. Then, the mean number N_{α} is considered to be approximately the non-dimensional value itself of the δ^2 measured in MeV as given in Table I. This is sufficiently big and compatible with the value obtained from the

N_α 's cannot be compared directly. In the case of the reaction experiments, the energy of the α -particles which are formed in the nuclear surface has a wide spread, while, in the case of the α -decay, it might be of a discrete level with a narrow width. The latter discussion, however, is not correct. The α -particle is not moving in a pure potential field; it is emitted from the inner region to a narrow surface region and reabsorbed into the former. According to the uncertainty principle, then these α -particles have a wide spread in energies comparable to that in reaction experiments. We have thus enough reason to assume that the mean number of α -particles in the theory of α -decays has the same order of magnitude with that in the reaction experiments.

Our model has another merit, that is, we need not introduce a big fluctuation in the nuclear radius. In the usual theory, we use a potential like Fig. 4. If the decay energy is low, the area becomes big. Consequently, the penetrability becomes small. But, the increase of this area is generally not big enough to make the penetrability sufficiently small, and we have to use a smaller nuclear radius for low energy decay elements (cf. Fig. 6, where we show the decay energies of ^{214}Po and ^{210}Po , as examples).

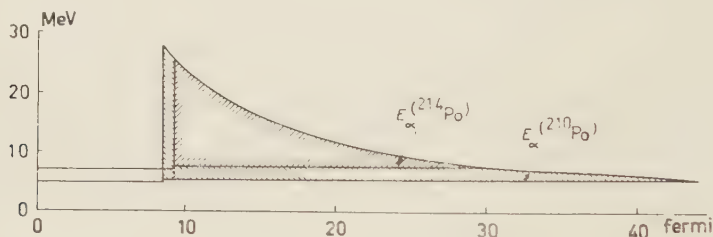


Fig. 6. — Penetrabilities in the decays of ^{214}Po and ^{210}Po in the usual model. In the case of pure Coulomb potential, the ratio of the areas is not sufficient if we do not use different radii for both decays.

In our case, however, the potential barrier is rounded by the tail of the nuclear potential. This area for ^{210}Po becomes sufficiently big compared to that for ^{214}Po , as seen in Fig. 7. Thus, we obtain reasonable values of the decay constant without using very different nuclear radii. Indeed, in the case of Gamow's theory, the reduced width for ^{210}Po is smaller by a factor 10^{-7} than that for ^{214}Po , if we use the same radius for ^{210}Po as that of ^{214}Po , while, in our case, the difference is only by a factor 17. Such a small difference may be explained by taking account of the difference in the configurations of nuclei, as discussed below.

This point was, however, discussed already by RASMUSSEN ⁽¹²⁾. He used

⁽¹²⁾ J. O. RASMUSSEN: *Phys. Rev.*, **113**, 1593 (1959).

only the real part of the Igo potential and calculated the reduced widths for many elements. But, as he did not take into account the dissociation effect of α -particles, he got rather small absolute values of reduced widths.

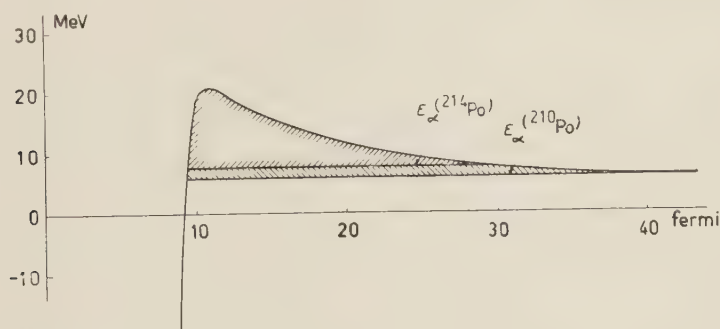


Fig. 7. — Penetrabilities in the decays of ^{214}Po and ^{210}Po in the present model. Since the top of the potential is rounded, the ratio of the areas is sufficiently big.

Recently, MANG⁽¹³⁾ developed a refined theory and obtained an expression for the reduced width. He calculated it assuming the shell model for the nucleus and showed that very good relative values of the reduced width are obtained. Unfortunately, the absolute values were very small, but we shall be able to obtain a good value by taking account of the effect of configuration mixing, as he suggested. In any way, taking into account the dissociation effect of α -particles in the nuclear surface, we have shown that our model of α -decay is consistent with the reaction experiments.

Generally speaking, nuclear reactions at medium energies (50 to 100 MeV) will give us a useful clue to clarify the nature of the nucleus. At these energies, direct scattering of nucleon clusters with the incident particle is the main mechanism giving composite particles in the final state. By observing angular distributions or correlations of the emitted composite particles, we shall be able to distinguish direct reactions from those through compound nuclei. Observation of direct reactions will be a sensitive method of obtaining information about clusters in the nucleus. It may be necessary to point out that, at these energies, the (p, α) reaction is not the reverse reaction to (α, p) , since (p, α) is actually $(p, p'\alpha)$ whose reverse reaction becomes a triple collision. We cannot, therefore, replace a (p, α) by an (α, p) experiment.

It is a very interesting question if a big probability of α -particle formation is compatible with the theory of nuclear matter by BRUECKNER or with the shell theory. Though it may be very hard to answer this question, the following

(13) H. J. MANG: *Zeits. f. Phys.*, **148**, 572 (1957); *Phys. Rev.*, **119**, 1069 (1960).

consideration may be of some use. Let us divide the nucleus into the inner and the surface regions. The total wave function Ψ may be expanded into products of cluster wave functions:

$$\Psi = \sum q_n \psi_n,$$

where q and ψ refer to the internal and surface regions respectively, and \sum indicates summation over different states n and various symmetrizations. For the ground state or very low excited states of the internal cluster, we may apply Brueckner's theory to q_n . Since the internal cluster states where there are many α clusters may have relatively low energies of excitation, those states may have rather big weights in the total wave function. In other words, even if Brueckner's theory gives the correct energy of nuclear matter, this does not mean that the total wave function of the nucleus is well approximated by Brueckner's wave function. Direct reactions may be a powerful method of investigating the true nuclear wave function.

* * *

The authors wish to express their thanks to the members of the Instituto de Física Teórica for many helpful discussions on this work. Two of us (J.O. and T.M.) would like to thank Dr. J. H. LEAL FERREIRA for the hospitality extended them at the Instituto de Física Teórica.

RIASSUNTO (*)

Presentiamo un nuovo modello del decadimento α che è coerente con le reazioni del tipo (p, α) . Sia il decadimento α che la reazione α diretta suggeriscono che, con una certa probabilità, sulla superficie nucleare esistono delle particelle α . Dalle teorie correnti sul decadimento α risulta che la probabilità di formazione delle particelle α è molto piccola, dell'ordine di grandezza di 10^{-4} , mentre, in base alle analisi delle reazioni (p, α) , si stima che la probabilità degli α è dell'ordine di grandezza di molte volte 0.1. Sebbene ci possa essere qualche diversità nei significati fisici delle probabilità α nei due casi, ci sono sufficienti motivi per ritenere che esse siano dello stesso ordine di grandezza. Nel nostro modello si suppone che le particelle α si formino continuamente nella materia nucleare ed emergano sulla superficie nucleare, dove la maggior parte viene respinta indietro o distrutta mentre alcune fuoriescono nello spazio esterno. Oltre che di questo meccanismo specifico, noi abbiamo fatto uso di tutti i dati sperimentali possibili e siamo riusciti a risolvere la suddetta discordanza ed a spiegare su una base unificata alcune tendenze sistematiche degli isotopi del decadimento α .

(*) Traduzione a cura della Redazione.

The Decay Modes and Lifetime of Negative K-Mesons.

B. BHOWMIK, P. C. JAIN and P. C. MATHUR

Department of Physics, University of Delhi - Delhi

(ricevuto il 25 Gennaio 1961)

Summary. — Two emulsion stacks, exposed to magnetically analysed enriched K^- -meson beam of average momentum 430 MeV/c and 440 MeV/c from Bevatron, have been used to estimate the relative abundance and lifetime of K^- -mesons. While following 103 m of track length, 48 decay-like events were observed. From the analysis of events with good geometry the following decay modes have been established: $K_{\mu 2}$, $K_{\pi 2}$, $K_{\mu 3}$, $K_{\pi 3}(\tau')$ and K_{β} . No example of τ -decay was found in the line scan sample, but the mode has been established from an area scan event. No knowledge of K^+ -decay modes, or of the mass of the primary particle was assumed in the analysis. The mean mass, obtained from the decay kinematics of $K_{\mu 2}$ and $K_{\pi 2}$ mode, is $(965.8^{+16.5}_{-21.5}) m_e$. The mass value from τ -decay mode is found to be $(964.45 \pm 2.91) m_e$. The percentages of various decay modes are as follows: $K_{\mu 2}$ (56.9 ± 12.8) , $K_{\pi 2}$ (33.4 ± 8.7) , $K_{\mu 3}$ (5.9 ± 3.1) , $K_{\pi 3}(\tau')$ (2.7 ± 2.8) , $K_{\beta 3}$ (2.9 ± 1.9) and τ^- (0.2 ± 0.1) . The mean lifetime has been determined after detailed considerations of the contamination due to decaylike clean interactions, and losses due to missing secondaries. The mean lifetime is $(1.27^{+0.36}_{-0.23}) \cdot 10^{-8}$ s.

1. — Introduction.

The lifetime and relative frequencies of various decay modes of positive K-mesons have been studied in detail by various authors. Unlike the positive K-mesons which decay at rest, the negative K-mesons produce capture stars, when brought to rest. The decay modes of K^- -mesons can be studied only by investigating decays in flight. Available information on K^- -decay modes⁽¹⁻⁴⁾

⁽¹⁾ S. NILSSON and Å. FRISK: *Ark. f. Fys.*, **14**, 293 (1958).

⁽²⁾ Y. EISENBERG, W. KOCH, E. LOHRMANN, M. NIKOLIĆ, M. SCHNEEBERGER and H. WINZELER: *Nuovo Cimento*, **8**, 663 (1958).

⁽³⁾ S. C. FREDEN, F. C. GILBERT and R. S. WHITE: *Phys. Rev.*, **148**, 564 (1960).

⁽⁴⁾ N. A. NICKOLS: *Thesis*, UCRL-8692 (1959).

is therefore limited. It is interesting to determine the relative abundance of K^- -decay modes, and compare it with that of K^+ -mesons. According to PCT invariance theorem, the lifetime and relative frequencies of K^- - and K^+ -decay modes are expected to be the same, if they are charge conjugate particles.

The various decay modes of an unstable particle, can be established by identifying the secondary particle and determining its energy. In case of decays in flight, the determination of the velocity of the primary and the space angle between the primary and the secondary is also necessary, so as to compute the kinetic energy of the secondary in the rest system (R.S.) of the primary, from the observed laboratory kinetic energy. When the secondary is emitted in the backward direction, and is quite slow, it could be easily identified when brought to rest by characteristic behaviour at the end or by ionization residual range measurements or by both. Particles going out of the stack can be identified by measuring the change of ionization with range, or by ionization — $p\beta$ measurements. Some of the fast secondaries can be identified by their characteristic interaction in flight. Having established the decay modes from the identified secondaries, it is possible to infer the decay mode where the identity of the secondary could not be established. Since the velocity of the secondary, having ionization greater than 1.1 times the minimum can be determined from accurate ionization measurements without any knowledge of its identity, the decay mode can be identified by comparing its R.S. velocity with the R.S. velocities of the already established decay modes. For flat secondary tracks, $p\beta$ could be determined with sufficient accuracy, and its energy in the rest frame can be calculated, attributing to it mass values corresponding to various possible decay modes. The mode can then be identified, if the R.S. energy of the secondary is found to be consistent with the R.S. energy of any one of the established decay modes. It may be remarked here that the analysis presented in Section 3 does not imply any knowledge of K^+ -decay modes or the mass of the primary particle. The only parameter involved is the velocity of the primary particle, which can be determined only from ionization measurements, since for a measured ionization, particles of all masses have the same velocity.

The question, whether various decay modes arise out of a single parent particle or different particles, is of great interest. In case of K^+ -mesons, the mass for different decay modes has been shown to be the same from momentum-range measurements. However, this cannot be done in case of K^- -mesons. The masses of K^- -mesons can be accurately calculated from the kinematics of a postulated two body decay mode. The mass spectrum of the primary particle has been calculated for $K_{\mu 2}$ and $K_{\pi 2}$ decay modes.

To determine the branching ratio of various decay modes and the lifetime of K^- -meson accurately, a correct estimation of the following two factors is necessary.

1) A certain fraction of K^- -interactions in flight may give rise to «clean» events with the emission of only one light particle, without any associated blob, recoil or electron at the point of interaction. Some of these interactions would be indistinguishable from true decay events, and their inclusion would result in an overestimation of the number of decays. This situation is unique in K^- -decay problem, and is not encountered in the investigation of K^+ lifetime.

2) In some cases, the light secondary may be missed due to poor development of the track, its steepness or proximity near glass or air surface of the emulsion. Such events are included amongst disappearances in flight, which arise due to charge exchange reactions and interaction of K^- -meson with free or bound proton, giving a Y^0 and a π^0 . This loss would lead to an underestimation of decay events.

Contributions from both these factors have been estimated, after detailed considerations, in Section 3'4 and 3'5, respectively.

2. - Experimental procedure.

2'1. *Exposure details.* - The present experiment was carried out with two emulsion stacks. First stack, (henceforth called K_1^-) consisting of 80, 8 in. \times 7 in. \times 600 μ m Ilford G-5 emulsion pellicles, was exposed to a magnetically analysed K^- -meson beam from the Bevatron. The average momentum at the point of entry is 430 MeV/c. Momentum dispersion across a plate is

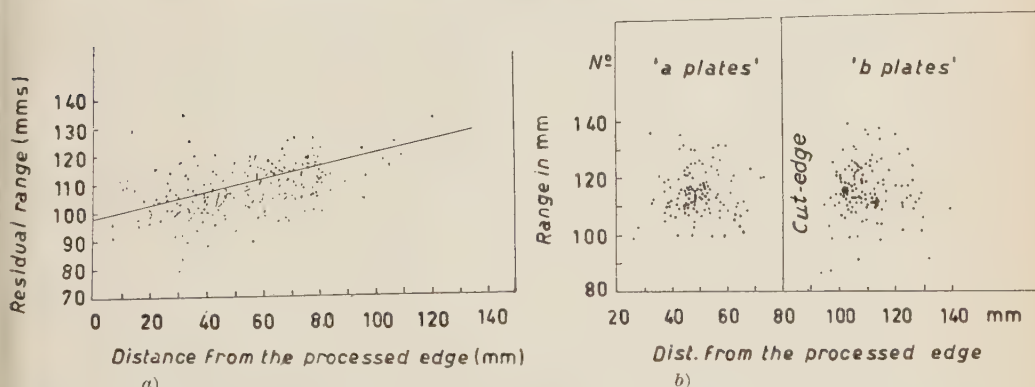


Fig. 1. - Range distribution for stopping tracks across a plate in stack K_1^- (Fig. 1a), and stack K_2^- (Fig. 1b).

displayed in Fig. 1a. The momentum is constant throughout the depth of the stack. A second stack, (henceforth called K_2^-) consisting of 60, 8 in. \times 6 in. \times 600 μ m Ilford G-5 and 40, 8 in. \times 6 in. \times 600 μ m Ilford K-5 emulsion sheets,

was exposed to an enriched beam of K^- -mesons from the Bevatron. In this stack, there was practically no momentum gradient across the plates, as displayed in Fig. 1b. The average momentum at the point of entry is 440 MeV/c. Both these stack were kept at low temperature during their transit to Bristol for processing after exposure. A high blob density (in stack K_1^- 21.1/100 μm and in stack K_2^- 24.9/100 μm) at minimum ionization was obtained as a result of this precaution (⁵).

2.2. Scanning procedure and identification of primary K^- -mesons. — Stack K_1^- : Tracks lying within 5° of the beam direction and having ionization expected for a K^- -meson corresponding to the mean beam momentum, were picked up 4 mm away from the entrance edge. These tracks were then followed to the end of their range or to a point where an interaction, decay or disappearance (stop) occurred. A total track length of 56.30 meters was followed.

Stack K_2^- : A different procedure was adopted in this stack and the total track length followed was 46.63 m. To get a larger time of flight per cm of the track length followed, K^- -meson tracks were picked up after they had considerably slowed down. Although available track length in the stack was about 11.5 cm, tracks were picked up at about 5 cm residual range.

In K_1^- -stack, stopping primaries were identified by usual blob count and residual range method. In case of events in flight (interactions, decays and stops) with observed track length less than 5 cm, the primary was identified by $b^* - p\beta$ measurements, while for events with track length more than 5 cm,

TABLE I. — *Scanning results.*

Type of event	Number of observed events	
	K_1^- -stack	K_2^- -stack
Capture stars at rest	349	854
Interactions in flight	199	140
« Stops » in flight	35	28
Decays in flight	19	29
Incomplete tracks	52 (*)	1
Total number of tracks	654	1052
Total track length	56.3 m	46.63 m
Total time of flight	$31.27 \cdot 10^{-8}$ s	$33.46 \cdot 10^{-8}$ s

(*) Mostly due to a broken plate.

(⁵) B. BHOWMIK, J. H. DAVIES, D. EVANS and D. J. PROWSE: *Nuovo Cimento*, **7**, 712 (1958).

identification was done by observing the change of blob density with range. Six short tracks, each having total track length less than 4 mm in the stack, could not be identified. Proton and pion contamination in this sample was estimated according to the statistics on the identified sample. No decaylike event was found amongst these events. In K_2^- -stack, stopping tracks were identified as usual by ionization-residual range method. For events in flight, the primary was identified by observing the change of blob density with range, and wherever necessary the primary was followed backwards.

Each individual track was identified in both the stacks. The scanning results are shown in Table I.

3. - Decay modes of K^- -mesons.

3'1. *Decay selection criteria.* - A sudden change of direction of a primary track, associated with a change of ionization, without any blob, recoil or electron at the point of deflection has been classified as a decay event. In most cases of decays in flight, the velocity of the secondary is higher than that of the primary, and the blob density shows a sharp decrease at the decay point. However, from kinematical considerations, it can be shown that for a given velocity of the primary, a secondary may appear with the same velocity as that of the primary, along some specific angle. Such events would simulate elastic scattering due to absence of any change of ionization on deflection. For certain space angles between the primary and the secondary, the latter may have a velocity even less than that of the former and the event would look like an inelastic scattering. In case of K^- -decays, the secondaries of these ambiguous events will be confined to a very narrow angular cone in the backward direction of the primary, and being slow can almost invariably be followed to rest and identified.

Out of 48 recorded decaylike events, only in two cases the ionization of the secondary was higher than that of the primary. One is identified as a μ -meson and the other as π -meson, by their characteristic behaviour, when brought to rest. In the remaining 46 cases, only one light secondary emerges at the point of deflection, without any associated blob, recoil or electron. Association of electron at the point of decaylike interaction may occur due to β -decay or γ -ray emission, following nuclear excitation. Auger electrons are not expected in case of interactions in flight, since the kinetic energy of the interacting particle, even at 1 mm residual range, is of the order of 10 MeV, whereas the energy involved in the cascade process of K^- -mesic atoms, is less than 1 MeV.

3'2. *Analysis of decay events.* - Only in 28 cases, the decay modes could be identified. We classify these analysed events into two broad groups.

a) Events with identified secondaries; the decay modes of these events have been uniquely established.

b) Events with unidentified secondaries, but with good geometry of the secondary to permit accurate $p\beta$ or ionization measurements.

In these cases, the decay modes have been inferred, by comparing the rest system energy of the secondary with the rest system energy of the secondaries of uniquely established decay modes, under category a). In few cases, the measurements on the secondaries are not accurate enough to permit a reliable estimation of the rest system energy, but the possible decay modes can be inferred from kinematical considerations. Analysis of 13 events with identified secondaries is shown in Table II-a; the method of their identification is indicated in the remarks column. The rest system energy ($T_{R.S.}$) of the secondaries, computed from observed laboratory energy, is shown in column 7. In case of stopping secondaries, the laboratory energy is obtained from the residual range, and for non-stopping cases, from the expected residual range, based on ionization measurements. The primary velocity is also estimated by ionization measurements, which does not involve any knowledge of its mass. Stopping power corrections for observed and expected ranges were applied, and the energies were computed using Barkas range-energy relation ⁽⁶⁾.

The rest system energy $T_{R.S.}$ of these 13 established decay events, with

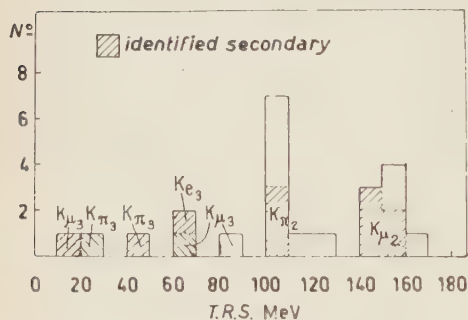


Fig. 2a. — Rest system kinetic energies of 23 analysed decay events.

identified secondaries, is shown as hatched events in Fig. 2a. In the remaining 10 events, secondaries could not be identified. Two peaks at $T_{R.S.} \simeq 150$ MeV and $T_{R.S.} \approx 110$ MeV corresponding to μ - and π -meson, secondaries, unambiguously establish the two-body decay modes $K_{\mu 2}$ and $K_{\pi 2}$. Pions and muons, having $T_{R.S.}$ values widely different from these line spectrum values, obviously arise from $K_{\pi 3}$ and $K_{\mu 3}$ modes respectively. The $K_{\beta 3}$ mode is also definitely established by event No. 11.

From the present analysis, we have therefore definitely established the following decay modes $K_{\mu 2}$, $K_{\pi 2}$, $K_{\mu 3}$, $K_{\pi 3}$, (τ') and $K_{\beta 3}$. No τ^- mode was found in our line scan sample. However, during the area scan of π - μ events for stopping power calibration, a slow positive pion was found to originate from

⁽⁶⁾ W. H. BARKAS: *Nuovo Cimento*, **8**, 201 (1958).

TABLE IIa. — Analysis of events, with identified secondaries.

Event no.	Velocity of the primary (β_K)	Space angle ($^\circ$)	Measurements on the secondary			$T_{R.S.}$ (MeV)	$\theta_{R.S.}$ ($^\circ$)	Decay mode	Remarks
			dip angle ($^\circ$)	ionization (b^*)	res. range (mm) or $p\beta$ (MeV/c)				
1	0.5454	127.8	2.6	—	61.181	$148.84^{+4.53}_{-4.90}$	153.2	$K_{\mu 2}$	0-prong star identified by $b^* - p\beta$; $m = 208.2 m_0$
2	0.6261	115.4	2.7	—	62.12)	$157.87^{+4.67}_{-5.60}$	149.9	$K_{\mu 2}$	β -decay at μ end
3	0.5140	111.8	7.7	1.589 ± 0.054	36.540	$109.92^{+4.70}_{-4.81}$	144.5	$K_{\pi 2}$	0-prong capture star
4	0.4652	69.5	15.3	—	5.856	$24.21^{+1.82}_{-1.89}$	129.2	$K_{\pi 3}$	3-prong capture star
5	0.3545	24.7	61.7	1.358 ± 0.058	34.049	$17.58^{+0.72}_{-0.80}$	43.9	$K_{\mu 3}$	β -decay at μ end
6	0.6132	118.5	59.0	—	6.108	$64.94^{+4.01}_{-4.32}$	154.9	$K_{\mu 3}$	β -decay at μ end
7	0.5021	135.7	26.7	1.296 ± 0.051 1.620 ± 0.087	$R = 23.000$	$145.71^{+11.03}_{-12.01}$	156.0	$K_{\mu 2}$	Identified by $b^* - R$
8	0.3939	65.6	2.5	0.998 ± 0.033	225 ± 18	$141.24^{+15.69}_{-15.97}$	100.8	$K_{\mu 2}$	Identified by $b^* - p\beta$
9	0.6049	63.9	5.0	1.014 ± 0.026	231 ± 19	$152.15^{+14.87}_{-16.50}$	106.8	$K_{\mu 2}$	—
10	0.3919	69.9	2.6	1.210 ± 0.038	173 ± 19	$102.41^{+12.85}_{-15.11}$	98.4	$K_{\pi 2}$	—
11	0.4878	147.2	11.2	1.118 ± 0.039	39 ± 7	$62.99^{+11.31}_{-11.31}$	160.5	$K_{\beta 3}$	—
12	0.4022	27.9	5.9	1.046 ± 0.052	266 ± 58	$106.45^{+29.79}_{-45.24}$	44.2	$K_{\pi 2}$	Interacts in flight
13	0.4227	16.1	7.7	1.186 ± 0.059	—	$41.99^{+10.85}_{-10.66}$	29.2	$K_{\pi 3}$	Large angle scattering $\approx 115^\circ$

a four-prong star. The analysis of this event is shown in Table II-b. The mass value (492.83 ± 1.49) MeV of the primary, obtained from decay kinematics and the coplanarity of the pions in the rest system, proves beyond doubt that the event is an example of τ^- -decay. The direction of the postulated primary was established by following it backward. All the known decay modes of the K^- -meson are therefore established in case of the K^- -meson, *ab initio*.

TABLE IIb. - Analysis of τ^- -decay (area scanned).

Secondary track no.	Identity of the secondary	Res. range (mm)	Kinetic energy (MeV)	Momentum p (MeV/c)	Space angle between the pions (degrees)		Mass (MeV)	Q (MeV)
					lab. system	rest system		
1	π^+ (π - μ -e)	0.43	3.825	32.906	$\theta_{12} = 139.5$	12.2	—	—
2	π^- (2-prong star)	78.94	82.435	172.674	$\theta_{23} = 104.0$	147.2	492.83 ± 1.49	73.94 ± 1.49
3	π^- (4-prong star)	1.56	7.961	47.818	$\theta_{31} = 29.8$	90.5	—	—
Total					357.9			

The results of analysis of ten events with unidentified secondaries are shown in Table II-c. The decay modes of events 14 and 15 are identified by computing the rest system velocity $\beta_{R.S.}$ (shown in the remarks column) from the laboratory velocity, obtained by ionization measurements. Comparing $\beta_{R.S.}$ with the unique velocities corresponding to the $K_{\mu 2}$ mode ($\beta_{R.S.} = 0.911$) and the $K_{\pi 2}$ mode ($\beta_{R.S.} = 0.828$) both these events are labelled as $K_{\pi 2}$, the corresponding $T_{R.S.}$ is shown in column 8. These modes are identified, without assuming the identity of the secondary.

For flat tracks (events 16 to 23), the extrapolated $p\beta$ shown in column 6, was computed after making scattering measurements at several distances from the decay point. In column 7 and 8, we display the rest system energy $T_{R.S.}$ assuming two alternative possible identity of the secondary, μ -meson and π -meson. The possible decay modes is inferred by comparing these values with the $T_{R.S.}$ values of established decay modes in Table II-a.

Two observations may be made regarding this group of events. Firstly none of these events could possibly simulate clean interactions due to the high value of the observed $p\beta$. In less than one per cent cases, pions from K^- -interactions can have such high $p\beta$ (> 286 MeV/c). Secondly, the resolution be-

TABLE IIc. — Analysis of events with unidentified secondaries.

Event no.	Velocity of the primary (β_K)	Space angle ($^\circ$)	Measurements on the secondary			$T_{R.S.}$ (MeV) assuming the secondary		$\theta_{R.S.}$ ($^\circ$)	Favoured decay mode	Remarks
			dip angle ($^\circ$)	ionization (b^*)	$p\beta$ (MeV/c)	μ	π			
14	0.3965	88.0	27.6	1.161 ± 0.032	—	—	$121.43^{+11.34}_{-11.75}$	116.1	$K_{\pi 2}$	$\beta_{R.S.}$ 0.8433
15	0.5209	56.1	13.6	1.100 ± 0.026	—	—	$109.38^{+15.04}_{-13.83}$	93.2	$K_{\pi 2}$	$\beta_{R.S.}$ 0.8283
16	0.5117	3.2	7.6	min.	413 ± 38	$151.02^{+19.22}_{-24.42}$	$131.63^{+18.24}_{-23.29}$	5.8	$K_{\mu 2}$	—
17	0.4937	52.0	5.0	1.025 ± 0.032	300 ± 62	$167.19^{+36.67}_{-59.53}$	$150.21^{+36.08}_{-45.72}$	82.1	$K_{\mu 2}$	—
18	0.4767	22.2	0.0	min.	363 ± 41	$160.08^{+21.93}_{-28.69}$	$133.47^{+20.00}_{-26.08}$	37.7	$K_{\mu 2}$	—
19	0.3956	16.5	6.3	min.	286 ± 27	$119.70^{+15.17}_{-20.62}$	$104.32^{+15.15}_{-17.01}$	26.3	$K_{\pi 2}$	—
20	0.4372	32.7	5.1	1.087 ± 0.036	279 ± 26	$122.88^{+15.34}_{-18.53}$	$109.57^{+14.31}_{-17.18}$	53.4	$K_{\pi 2}$	—
21	0.4227	21.7	7.6	min.	306 ± 25	$128.54^{+14.52}_{-17.08}$	$113.89^{+13.73}_{-16.19}$	35.5	$K_{\pi 2}$	—
22	0.5594	15.5	6.9	min.	357 ± 28	$118.69^{+12.99}_{-16.68}$	$101.86^{+12.58}_{-14.90}$	31.2	$K_{\pi 2}$	—
23	0.5902	19.4	8.2	1.011 ± 0.018	297 ± 20	$88.06^{+11.24}_{-12.80}$	$74.11^{+8.80}_{-10.69}$	40.0	$K_{\mu 3}$	—

tween the two decay modes, $K_{\mu 2}$ and $K_{\pi 2}$ is quite high in spite of the fact that the nature of the secondary is not known. It is evident from this table that the secondary giving $T_{R.S.}$ consistent with the $K_{\mu 2}$ mode, when considered as π -meson, would have the $T_{R.S.}$ value widely different from the $T_{R.S.}$ value of the $K_{\pi 2}$ mode. The situation is similar in case of a postulated $K_{\pi 2}$ mode, and with measurements of reasonable accuracy, there is hardly any chance of confusing a $K_{\mu 2}$ with a $K_{\pi 2}$ mode or vice-versa. The real difficulty arises out of the situation that unidentified secondaries, giving $T_{R.S.}$ values consistent with the $K_{\pi 3}$ mode, will always give $T_{R.S.}$ values consistent with the $K_{\mu 3}$ mode when the secondary is assumed to be a μ -meson. Also, high energy end of the $K_{\mu 3}$ spectrum is too close to the line spectrum of the $K_{\nu 2}$ mode, to allow adequate discrimination between the two.

Ionization measurements, on the secondary of five events, where the secondaries are emitted at such large space angle, that the difference between the expected ionizations for $K_{\mu 2}$ and $K_{\pi 2}$ modes is very large, are shown in Table II-d. Due to unfavourable geometry and steepness of the tracks, these measurements are of insufficient accuracy to permit a reliable estimate of $T_{R.S.}$. However, the $K_{\pi 2}$ mode can be completely excluded by comparing the expected and observed ionizations. All these events are therefore labelled as $K_{\mu 2}$. In case of the last event, $K_{\beta 3}$ cannot be excluded.

TABLE II-d. — Comparison of observed and expected ionization for $K_{\mu 2}$ and $K_{\pi 2}$ decay modes.

Event no.	Vel- ocity of the primary (β_K)	Space angle ($^\circ$)	Measurements on the secondary		Expected ionization considering the secondary		$\theta_{R.S.}$	Fa- voured decay mode	Remarks
			dip angle ($^\circ$)	observed ionization (b^*)					
					μ	π			
24	0.3887	69.9	30.6	0.98 ± 0.05	1.03	1.16	95.1	$K_{\mu 2}$	—
25	0.3788	69.2	12.6	1.00 ± 0.04	1.03	1.15	93.5	$K_{\mu 2}$	Becomes steep in next plate
26	0.5240	125.7	43.6	1.22 ± 0.07	1.24	1.79	153.1	$K_{\mu 2}$	—
27	0.3466	121.5	57.3	1.00 ± 0.07	1.05	1.44	138.6	$K_{\mu 2}$	—
28	0.3793	129.6	40.5	1.07 ± 0.07	1.13	1.53	146.7	$K_{\mu 2}$	$K_{\beta 3}$ not excluded

In Table II-c, measurements on the remaining 20 unanalysed events are shown. Most of these events are in the forward direction and are steep and near minimum. Although, these could not be classified in any single definite category of decay mode, the majority of them are likely to belong to either $K_{\nu 2}$ or $K_{\pi 2}$ mode. The expected ionization for $K_{\pi 3}$ and $K_{\beta 3}$ modes, practically rules out a large contamination of these events in this sample. The $K_{\mu 3}$ mode

cannot be excluded, but from the known abundance in the analysed sample, the percentage of $K_{\mu 3}$ events will also be very small.

TABLE IIe. — *Data on unanalysed decay events.*

Event no.	Velocity of the primary (β_K)	Space angle ($^\circ$)	Measurements on the secondary		Remarks
			dip angle ($^\circ$)	ionization (b^*)	
29	0.5554	24.4	20.8	1.002 ± 0.050	—
30	0.5930	38.6	17.9	0.962 ± 0.060	—
31	0.6202	27.4	19.1	1.086 ± 0.044	—
32	0.4992	6.5	11.0	1.002 ± 0.060	—
33	0.6066	19.1	15.3	1.008 ± 0.051	—
34	0.4892	12.5	17.0	1.008 ± 0.030	—
35	0.5826	41.3	11.0	1.023 ± 0.059	—
36	0.5597	38.4	26.2	1.040 ± 0.070	—
37	0.6172	41.7	46.8	1.007 ± 0.045	—
38	0.4511	41.4	42.5	1.002 ± 0.054	—
39	0.5790	28.8	22.4	1.040 ± 0.050	—
40	0.5597	24.8	24.8	1.003 ± 0.061	—
41	0.5609	6.0	11.2	1.005 ± 0.041	—
42	0.3785	31.2	24.4	1.011 ± 0.050	—
43	0.6228	108.3	36.6	1.250 ± 0.310	Could not be followed in the next plate.
44	0.6202	48.3	48.5	≈ 1.0	—
45	0.3928	53.9	49.1	≈ 1.0	—
46	0.4188	56.9	52.8	≈ 1.0	—
47	0.3674	64.8	61.7	—	—
48	0.4013	67.4	80.3	—	—

Each of the identified pion, and all unidentified secondaries, except those with very high laboratory energy ($T > 200$ MeV) in principle, could be a case of decay-like clean interaction of K^- -meson. The contamination of such events is estimated in Section 3'4.

3'3. *The mass spectrum of the primary particle.* — It has already been emphasized that the mass of a primary particle can be determined from

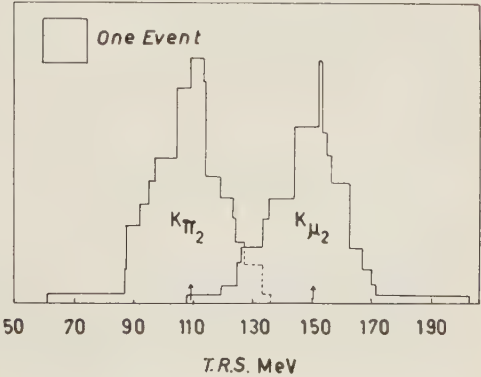


Fig. 2b. — Constant area histogram of rest system kinetic energies of $K_{\mu 2}$ and $K_{\pi 2}$ decay events.

the two-body decay modes, by determining the kinetic energy of the charged secondary in the rest system of the primary. The rest system energy for $K_{\mu 2}$ and $K_{\pi 2}$ modes is shown in the constant area histogram in Fig. 2b, giving due weight

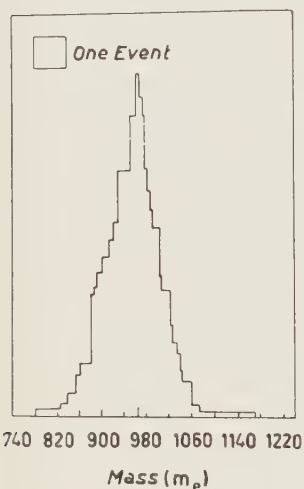


Fig. 3. - Mass spectrum of K^- -mesons, obtained from the decay kinematics of 17 analysed two-body decay events.

to statistical errors on individual events. The mean rest system kinetic energies for μ^- - and π^- -meson are $(151.10^{+6.57}_{-9.43})$ MeV and $(109.42^{+5.20}_{-6.83})$ MeV, respectively. We calculate the mass for the following two decay modes from 17 analysed two-body events:

$$K_{\mu 2}^- \rightarrow \mu^- + \bar{\nu} \quad (T_{\mu} = 151.10 \text{ MeV})$$

and

$$K_{\pi 2}^- \rightarrow \pi^- + \pi^0 \quad (T_{\pi} = 109.42 \text{ MeV}).$$

The mean mass for the $K_{\mu 2}$ mode is $(960.2^{+26.5}_{-34.6}) m_e$ and for $K_{\pi 2}$ is $(969.8^{+20.4}_{-26.4}) m_e$. These mass values are consistent with the assumption that both the modes arise out of a single parent particle. The mass spectrum of K^- -meson obtained from decay kinematics of all these events is shown in Fig. 3. The mean mass $(965.8^{+16.5}_{-21.5}) m_e$ obtained from the two-body decay modes can be compared with the mass for the τ^- -mode. Since all the decay products are charged particles in

τ^- -decay, the determination of the τ^- -mass, $(964.45 \pm 2.91) m_e$ does not require any knowledge of the velocity of the primary particle. The mass value obtained from the decay kinematics, is in excellent agreement with other mass estimations of the K^- -meson, such as the direct estimation by momentum $(7,8)$ residual range on the primary, or by the absorption process $(9,10)$ $K^- + p \rightarrow \Sigma + \pi$ by a free proton.

3.4. *Estimation of decaylike «clean» interactions.* - As mentioned earlier, some of the observed decaylike events could be «clean» interactions. To estimate the upper limit of these events, we consider the angular distribution

(7) J. HORNOSTEL and E. O. SALANT: *Phys. Rev.*, **99**, 338 (1955).

(8) F. H. WEBB, W. W. CHUPP, G. GOLDBABER and S. GOLDBABER: *Phys. Rev.*, **101**, 1212 (1956).

(9) W. F. FRY, J. SCHNEPS, G. A. SNOW, M. S. SWAMI and D. C. WOLD: *Phys. Rev.*, **104**, 270 (1956).

(10) W. H. BARKAS, W. F. DUDZIAK, P. C. GILES, H. H. HECKMAN, F. W. INMAN, C. J. MASON, N. A. NICKOLS and F. M. SMITH: *Phys. Rev.*, **105**, 1417 (1957).

of 48 decaylike events in Fig. 4, which shows only 10 events in the backward direction as against 38 in the forward direction. Out of these 10 events, there are 4 identified μ -mesons and one electron. If we consider all the remaining 5 to be interactions, the total number of clean interactions in the entire sample will be 10 because the angular distribution of interactions in the laboratory frame is isotropic. This is displayed in Fig. 5 (unpublished Dehli data). We therefore conclude that the upper limit of decaylike interactions in our sample is 21 %.

We now make a positive estimate of clean interactions amongst various decay modes. From the established K_{π^2} and K_{π^3} decay modes, it is evident that the energy of the secondary pions in the rest system of the primary would be confined between $(0 \div 55)$ MeV and $(90 \div 130)$ MeV, respectively. This large spread in the K_{π^2} line spectrum takes account of the experimental uncertainties.

Pions having R.S. energy between $(55 \div 90)$ MeV and greater than 130 MeV therefore originate from decaylike clean interactions. Since the identification of pions, having R.S. energy above 130 MeV, is not free from ambiguity, let us

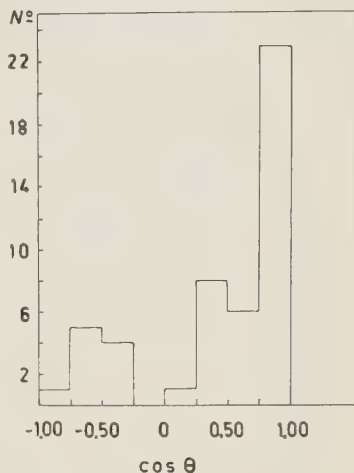


Fig. 4. — Angular distribution of 48 decaylike events in the laboratory system.

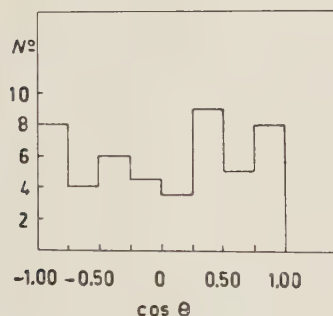


Fig. 5. — Angular distribution of 52 pions from K^- -interactions in flight (with associated prongs), in the laboratory system.

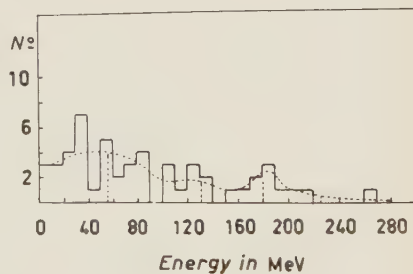


Fig. 6. — Energy spectrum of pions from K^- -interactions in flight (with associated prongs), in the rest system of the primary.

consider only the lower energy interval between 55 and 90 MeV. Amongst the 115 analysed events (28 Dehli, 17 Uppsala ⁽¹⁾, 22 Berne ⁽²⁾, and 48 Berkeley ⁽⁴⁾) there are six identified pions having R.S. energy between 55 and 90 MeV. These six cases are therefore definite cases of clean interactions. To estimate the

total number of clean interactions, we display in Fig. 6, the R.S. energy of 52 pions from K^- -stars in flight with visible prongs (unpublished Delhi data). It is found that 23.4 % of the pions have R.S. energy in this interval. The total number of clean interactions amongst 115 analysed events, having all possible R.S. energy, would therefore be 25.7. Hence the contamination of clean interactions is 22.3 %.

TABLE III. — *Clean interactions in decaylike events.*

Serial no.	R.S. energy interval (MeV)	% of pions from K^- -stars in flight	Expected no. of interactions amongst 28 events	Observed no. of events	Contribution to clean interactions
1	0 ÷ 55	37.0	2.31	2 ($K_{\pi 3}$)	0.60
2	55 ÷ 90	23.4	1.46	1 ($K_{\mu 3}$)	0.00
3	90 ÷ 130	13.5	0.84	9 ($K_{\pi 2}$)	0.84
4	130 ÷ 170	9.4	0.59	3 ($K_{\mu 2}$) (*)	0.00
5	170 ÷ 230	14.9	0.93 }	5 $K_{\mu 2}$ (**)	1.04
6	> 230	1.8	0.11 }		
					2.48

(*) Unidentified secondary-scattering group $p\beta > 286$ MeV/c.

(**) Unidentified secondary-ionisation group.

In Table III, the clean interactions are estimated among various decay modes. The six pion R.S. energy intervals correspond to:

- 1) (0 ÷ 55) MeV pions from clean interactions, simulating the $K_{\pi 3}$ decay mode.
- 2) (55 ÷ 90) MeV unambiguous interactions.
- 3) (90 ÷ 130) MeV simulating the $K_{\pi 2}$ decay mode.
- 4) (130 ÷ 170) MeV simulating the $K_{\mu 2}$ decay mode—scattering group. (When the energy of the light particle is determined by scattering measurements, the unidentified π -mesons having R.S. energy between 130 and 170 MeV, when assumed to be μ -mesons, will have energy corresponding to $K_{\mu 2}$ mode).
- 5) (170 ÷ 230) MeV simulating $K_{\mu 2}$ mode—ionisation group. (For a given ionization, unidentified pion having R.S. energy between 170 and 230 MeV, when assumed to be a μ -meson, will have the same velocity but their energy would correspond to about (130 ÷ 175) MeV.
- 6) Unambiguous interaction $\left\{ \begin{array}{l} \text{above 225 MeV - ionisation group,} \\ \text{above 170 MeV - scattering group.} \end{array} \right.$

We expect 6.24 clean interactions in 28 analysed events. The distribution of these events amongst various energy intervals is shown in column 4 of Table III. The actual number of observed events is shown in column 5. Seven events with identified μ -meson secondaries and one with electron secondary, have been excluded. In the first interval, there are two $K_{\pi 3}$ events against 2.32 expected interactions. Both of them therefore could be clean interactions. However, on probability analysis of individuals events ⁽⁴⁾, we expect 1.4 $K_{\pi 3}$ events. It may be remarked, that the $K_{\pi 3}$ decay mode is indistinguishable from a clean interaction unless an associated π^0 is found to decay in the Dalitz mode, giving rise to an electron pair in the vicinity of the decay point. One such event has been observed by for K^- -decay by FREDEN *et al.* ⁽¹¹⁾.

In group three, there are 9 $K_{\pi 2}$ events, whereas the expected number of clean interactions simulating the $K_{\pi 2}$ mode is 0.84. Finally, 5 $K_{\mu 2}$ events have only been partially analysed by ionisation measurements of limited accuracy. These may belong to either fifth or sixth group. We include 1.04 interactions in the last column as contributions from these two groups. In the analysed sample, therefore, there are 2.48 interactions. Amongst 20 unanalysed events, we expect 4.46 interactions. In the entire sample of 48 decaylike events, we therefore have a total of 6.94 interactions.

It may be pointed out, that in the above analysis it has been tacitly assumed that the pion energy spectrum from K^- -stars with prongs is same as the pion spectrum from clean interactions. The energy spectrum of six definite cases of clean interactions is consistent with this assumption.

3.5. *Estimation of loss factor in decay events.* — Decay events where the secondary is missed from observation are included in disappearance in flight.

To estimate this loss, we compare the depth distribution of decay events and disappearances (stops) in Fig. 7, for K_1^- - and K_2^- -stacks. In stack K_1^- both for decays and stops, distributions are uniform in the upper half of the emulsion. However, in the lower part of the emulsion, particularly near the glass, a heavy loss of decays is clearly indicated. Since any loss of decay events due to missing secondaries, would result in a corresponding gain in the number of stops, the

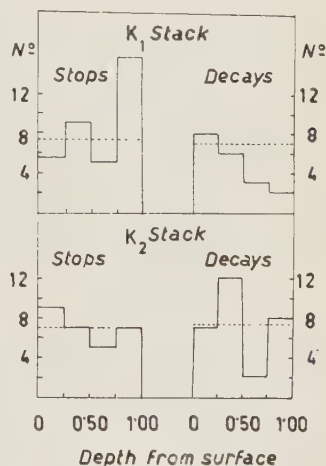


Fig. 7. — Depth distribution of decay events and « stops » in K_1^- - and K_2^- -stacks.

⁽¹¹⁾ S. C. FREDEN, F. C. GILBERT and R. S. WHITE: *Phys. Rev. Lett.*, **1**, 217 (1958).

two histograms are expected to be complementary. Indeed, the histograms for stops shows a rapid rise near glass. Let S and D denote the true number of stops and decays respectively, and ΔS and ΔD denote their gain and loss. It is clear from the above discussion, that $\Delta S = \Delta D$. From the constancy of the two histograms near surface, it may reasonably be assumed that the loss of decay events between .1 to .5 of the emulsion thickness is negligible. Therefore the ratio of the observed number of stops to decays in this region, represents the true ratio S/D , which is equal to 13.5/13. The total observed number of stops and decays are $(S + \Delta D) = 35$ and $(D - \Delta D) = 19$, respectively. From these two relations, we get $\Delta D = 7.49 \pm 5.45$. For K_2^- -stack, a very small loss is indicated by the histogram, and on similar considerations, we get $\Delta D = 2.45 \pm 6.17$. This large difference in the loss factor arises because of difference in the degree of development of the two stacks.

3'6. *Dependence of loss factor on the degree of development.* — To determine the dependence of visibility of a light track on the degree of development, we estimate the percentage loss of electrons in $\pi - \mu \rightarrow e$ events, by scrutinizing 112 events in K_1^- -stack, and 51 events in K_2^- -stack. The respective losses are

$(17.9 \pm 3.6)\%$ and $(5.9 \pm 3.3)\%$. In Fig. 8, we illustrate these two losses as circles, plotted against blob density per $100 \mu m$ of the track. The relative density ($b^* = b/(b_0)K_1^-$), expressed in terms of minimum blob density in K_1^- -stack, is also indicated in the diagram. Loss of decay secondaries is expected to be higher since most of the secondaries have near minimum ionization, whereas electrons in $\pi - \mu \rightarrow e$ events are in the plateau. The mean ionization of missing secondaries is estimated in the following manner.

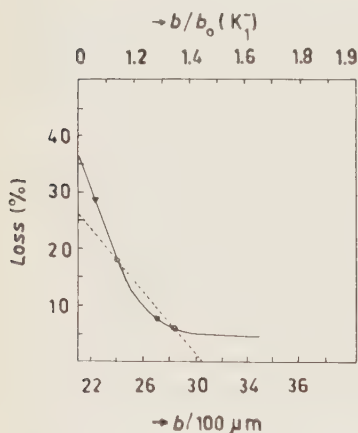


Fig. 8. — Variation of per cent loss of secondaries, with degree of development.

We divide the secondaries in groups of eight equal solid angle intervals in the rest system, and calculate their expected laboratory energy for the mean primary velocity $\beta = 0.49$ in K_1^- -stack, and find out corresponding ionization. As a first approxi-

mation, we draw a dotted line passing through the two fixed points, corresponding to electron losses, and estimate the percentage loss of decay secondaries in various solid angle intervals. The weighted mean ionization of missing μ -meson secondaries in the $K_{\mu 2}$ -decay mode is 1.041, and for pions secondaries in the $K_{\pi 2}$ -mode is 1.071. Neglecting the losses of other modes and considering the ratio of $K_{\mu 2}/K_{\pi 2}$ as 2 the mean ionization of missing secondaries is

found to be 1.051. A second successive approximation changes this value to 1.058. In the K_2^- -stack, the mean primary velocity (β) is 0.41 and the mean ionization of missing secondaries, after the second successive approximation, is found to be 1.091. This ionization relative to the K_1^- -minimum is 1.288. We plot the overall loss of K^- -secondaries (28.30 % and 7.8 % in the K_1^- - and K_2^- -stacks, respectively) estimated in Section 3'4, as triangles against the corresponding mean ionization of the missing secondaries. The solid line passing through all the four points, therefore, indicates the dependence of loss factor on blob density. It is evident from the above discussion and the loss factor curve, that the estimation of percentage loss of decay secondaries from a direct comparison with the loss of electrons, would lead to an underestimation of the loss factor, particularly when the stack is poorly developed. This difference, in case of a well developed stack like the K_2^- -stack, is negligible. In an exceptionally well developed stack, specially when the development gradient near glass is avoided, the actual loss may tend to zero. It may be remarked here, that the loss factor depends primarily on the degree of development and its uniformity, the proximity of the track near the glass or surface, or its steepness play only a secondary role.

The ratio of the number of missing μ and π secondaries can be found by using the solid line in Fig. 8, and reading their losses at various ionizations, corresponding to eight equal solid angle intervals. Considering the branching ratio $K_{\mu 2}/K_{\pi 2}$ to be 2, we find this ratio to be 2.906 and 2.962 in the K_1^- - and K_2^- -stacks respectively.

4. - Relative abundance of the decay modes of K^- -mesons.

The frequency of decay modes, obtained from the analysed sample, does not represent the relative abundance of decays in a normal population. The sample is biased because of the deficiency of events with fast secondaries. This missing fraction consists mainly of $K_{\mu 2}$ and $K_{\pi 2}$ events, which have been labelled as «stops». One must therefore not only take account of these missing events, but also estimate their branching ratio. Furthermore, the contamination due to clean interaction amongst various decay modes has also to be eliminated.

The relative abundance of various modes in the analysed sample is shown in column 2 of Table IV. Column 3 represents the number of events after elimination of the contamination from interactions, as estimated in Table III. In column 4, 5.46 stops estimated to be missing events in the analysed sample, are distributed amongst the $K_{\mu 2}$ and $K_{\pi 2}$ modes, in a manner explained below.

In K_1^- -stack, 52.6 % of the missing events have been restored to the analysed sample. The ratio of missing $K_{\mu 2}$ to $K_{\pi 2}$ events being 2.906 (as discussed in Sec-

TABLE IV. — *Relative abundance.*

Decay mode	No. of decay events		Contribution from « stops »	Corrected number of events in unanalysed sample	Contribution from unanalysed events	Total corrected number of events	Relative abundance (%)
	observed	corrected for clean interactions					
$K_{\mu 2}$	13	11.96	4.07	16.03	12.55	28.58	56.0 ± 12.8
$K_{\pi 2}$	9	8.16	1.39	9.55	7.47	17.02	33.4 ± 8.7
$K_{\mu 3}$	3	3.00	—	3.00	—	3.00	5.9 ± 3.2
$K_{\pi 3} \begin{cases} \tau \\ \tau' \end{cases}$	0	0.00	—	0.00	—	0.00	0.00
	2	1.40	—	1.40	—	1.40	2.8 ± 3.8
$K_{\beta 3}$	1	1.00	—	1.00	—	1.00	2.0 ± 1.9
Total	28	25.52	5.46	30.98	20.02	51.00	—

tion 3'6), 2.93 events will belong to the $K_{\mu 2}$ and 1.01 to the $K_{\pi 2}$ -mode. Similarly in the K_2^- -stack, in which 62.0% of the events have been analysed, from similar considerations it can be shown that 1.14 events belong to the $K_{\mu 2}$ and 0.38 to the $K_{\pi 2}$ -mode.

This brings the total number of $K_{\mu 2}$ and $K_{\pi 2}$ events in the sample to 16.03 and 9.55, respectively, as shown in column 5. It can be reasonably assumed, that the ratio $16.03/9.55 = 1.68$, approximates the correct ratio of $K_{\mu 2}$ $K_{\pi 2}$ decay modes in a normal sample.

From the unanalysed 20 decay events, we remove 4.46 interactions. Restoring 4.48 « stops », the total number of decays become 20.02. Events in this group have fast and steep secondaries, and consist mainly of $K_{\mu 2}$, $K_{\pi 2}$ events. Since this sample has been normalized by restoring missing events and removing pseudodecays, we can divide 20.02 events amongst $K_{\mu 2}$ and $K_{\pi 2}$ decay modes in the ratio 1.68:1. This gives us 12.55 and 7.47 events in the respective modes, as shown in column 6. The total number of corrected events amongst various decays modes is shown in column 7, and the relative abundance in column 8. The errors shown are statistical, and take account of the uncertainty in the estimation of the loss factor and clean interactions.

We compare the relative abundance of the K^+ -decay modes determined by BIRGE *et al.* ⁽¹²⁾ and ALEXANDER *et al.* ⁽¹³⁾ with our results in Table V. Our results are in good agreement with these estimations and other estimations of

⁽¹²⁾ R. W. BIRGE, D. H. PERKINS, J. R. PETERSON, D. H. STORK and M. N. WHITEHEAD: *Nuovo Cimento*, **4**, 834 (1956).

⁽¹³⁾ G. ALEXANDER, R. H. W. JOHNSTON and C. O'CEALLAIGH: *Nuovo Cimento*, **6**, 478 (1957).

the relative abundance of K^+ -mesons ($^{14-18}$), which is expected for charge conjugate particles.

TABLE V.

Decay mode	K^+ relative abundance		K^- relative abundance	
	BIRGE <i>et al.</i>	ALEXANDER <i>et al.</i>	NICKOLS	BHOWMIK <i>et al.</i>
$K_{\mu 2}$	58.5 ± 3.0	57.0 ± 2.6	56.5 ± 7.3	56.0 ± 12.8
$K_{\pi 2}$	27.7 ± 2.7	23.2 ± 2.2	26.3 ± 6.6	33.4 ± 8.7
$K_{\mu 3}$	2.8 ± 0.95	5.9 ± 1.3	9.5 ± 4.3	5.9 ± 3.1
$K_{\pi 3} \left\{ \begin{array}{l} \tau \\ \tau' \end{array} \right.$	5.56 ± 0.44	6.77 ± 0.45	0.0 ± 2.1	0.0 ± 2.0
	2.15 ± 0.47	2.15 ± 0.45	2.8 ± 2.4	2.7 ± 2.8
$K_{\beta 3}$	2.23 ± 1.30	5.1 ± 1.3	4.9 ± 3.2	2.0 ± 1.9

The present results, are also in good agreement with the K^- relative abundance, determined by NICKOLS (14) (shown in column 4) and other authors ($^{1-3}$).

5. - The lifetime of K^- -mesons.

We have observed (48 ± 6.93) decaylike events, which includes 6.94 ± 2.40 interactions. Amongst the stops, we have estimated 9.94 ± 0.23 decays. The total number of true decay events therefore is 51.01 ± 11.24 . The proper time of flight for stopping tracks has been calculated using Barkas range-energy relation, after correcting the ranges for stopping power. For non-stopping tracks, the time of flight has been calculated by taking the difference between the average time of flight for stopping tracks, and the time of flight for the expected residual range of the event. The total proper time for the two stacks is $64.73 \cdot 10^{-8}$ s. Therefore the lifetime is $1.27^{+0.36}_{-0.23} \cdot 10^{-8}$ s. Statistical errors include uncertainty in the estimation of clean interactions, and losses due to missing secondaries. This value of lifetime is in good agreement with the

(14) G-STACK COLLABORATION: *Nuovo Cimento*, **2**, 1063 (1955).

(15) J. CRUSSARD, V. FOUCHÉ, J. HENNESSY, G. KAYAS, L. LEPRINCE-RINGUET, D. MORELLET and F. RENARD: *Nuovo Cimento*, **3**, 731 (1956).

(16) D. M. RITSON, A. PEVSNER, S. C. FUNG, M. WIDGOFF, G. T. ZORN, S. GOLDBERGER and G. GOLDBERGER: *Phys. Rev.*, **101**, 1085 (1956).

(17) H. H. HECKMAN, F. M. SMITH and W. H. BARKAS: *Nuovo Cimento*, **3**, 85 (1956).

(18) T. F. HOANG, M. F. KAPLON and G. YEKUTIELI: *Phys. Rev.*, **102**, 1185 (1956).

life-time of K^+ -meson, obtained by various authors (¹⁹⁻²³), showing that K^- - and K^+ -mesons are charge conjugate particles.

The value of life-time obtained by us is also in agreement with the other estimations (^{1-4,24-26}) of the life-time of K^- -mesons.

* * *

We are very grateful to Prof. E. J. LOFGREN of the Radiation Laboratory for exposure facilities at the Bevatron. We would like to thank Prof. D. J. PROWSE for making the actual exposures, and Dr. D. EVANS for processing the stack at Bristol. Without their co-operation this work would not have been possible. We gratefully acknowledge the use of a grid printing machine, made available by Prof. G. GOLDBABER.

We would like to take this opportunity to express our indebtedness to Prof. C. F. POWELL for his kind hospitality during the processing of the stack, and for his helpful suggestions.

We express our gratitude to Prof. D. S. KOTHARI for providing all laboratory facilities. We have great pleasure in thanking Mr. D. P. GOEL for helping us in measurements and in some calculations. Our further thanks are due to Mrs. J. BHOWMIK for her painstaking scanning and for taking some measurements, and Miss M. GHOSH and Miss S. GUPTA for their efficient scanning work.

This work is an outcome of a research project, financially supported by the Department of Atomic Energy, Government of India. Our indebtedness to the Department is gratefully acknowledged.

(¹⁹) E. L. ILOFF, W. W. CHUPP, G. GOLDBABER, S. GOLDBABER, J. E. LANNUTTI, A. PEVSNER and D. RITSON: *Phys. Rev.*, **99**, 1617 (1955).

(²⁰) W. ALVAREZ and S. GOLDBABER: *Nuovo Cimento*, **2**, 344 (1955).

(²¹) B. BHOWMIK, D. EVANS, S. NILSSON, F. ANDERSON, D. KEEFE, A. KERNAN, D. J. PROWSE, N. N. BISWAS, M. CECCARELLI, P. WALOSCHEK, J. E. HOOPER, M. GRILLI and L. GUERRIERO: *Nuovo Cimento*, **5**, 994 (1957).

(²²) L. W. ALVAREZ, F. S. CRAWFORD, M. L. GOOD and M. L. STEVENSON: *Phys. Rev.*, **101**, 563 (1956).

(²³) V. FITCH and R. MOTLEY: *Phys. Rev.*, **105**, 265 (1957).

(²⁴) J. HORNOSTEL and G. T. ZORN: *Phys. Rev.*, **109**, 165 (1958).

(²⁵) F. H. WEBB, E. L. ILOFF, F. H. FEATHERSTON, W. W. CHUPP, G. GOLDBABER and S. GOLDBABER: *Nuovo Cimento*, **8**, 899 (1958).

(²⁶) B. CORK, G. R. LAMBERTSON, O. PICCIONI and W. WENZEL: *Phys. Rev.*, **106**, 167 (1957).

RIASSUNTO (*)

Abbiamo adoperato due pile di emulsioni, esposte ad un fascio arricchito di mesoni K^- , analizzato magneticamente, di momento medio 430 MeV/c e 440 MeV/c, provenienti dal Bevatrone, per stimare l'abbondanza relativa e la vita media dei mesoni K. Nel seguire 103 m di lunghezza di traccia abbiamo osservato 48 eventi apparenti come decadimenti. Dall'analisi degli eventi con buona geometria abbiamo accertato i seguenti modi di decadimenti: $K_{\mu 2}$, $K_{\pi 2}$, $K_{\mu 3}$, $K_{\pi 3}(\tau')$ e $K_{\beta 3}$. Non abbiamo trovato alcun esempio di decadimento τ^- nel campione di scanning lungo linee, ma questo modo è stato accertato da un evento a mezzo di scanning di superficie. Nell'eseguire l'analisi non si è presupposta alcuna conoscenza dei modi di decadimento dei K^+ o della massa della particella primaria. La massa media, dedotta dalla cinematica di decadimento dei modi $K_{\mu 2}$ e $K_{\pi 2}$, è $(965.8^{+16.5}_{-21.5}) m_e$. Il valore della massa trovato in base al modo di decadimento τ^- è $(964.45 \pm 2.91) m_e$. Le percentuali dei vari modi di decadimento sono le seguenti: $K_{\mu 2}$ (56.0 ± 12.8) , $K_{\pi 2}$ (33.4 ± 8.7) , $K_{\mu 3}$ (5.9 ± 3.1) , $K_{\pi 3}(\tau')$ (2.7 ± 2.8) , $K_{\beta 3}$ (2.9 ± 1.9) e τ^- (0 ± 2.0) . La vita media è stata determinata tenendo accuratamente conto della contaminazione dovuta a interazioni pulite simili a decadimenti e delle perdite dovute a secondari dispersi. La vita media è $(1.27^{+0.36}_{-0.23}) \cdot 10^{-8}$ s.

(*) Traduzione a cura della Redazione.

On the Phenomenological Analysis of the S -Matrix in Multiple Production.

D. ITO (*), A. H. ZIMERMAN, S. RAGUSA and T. MIYAZIMA (**)

Instituto de Física Teórica - São Paulo

(ricevuto il 28 Gennaio 1961)

Summary. — An attempt is made to analyse the structure of S -matrix elements for multiple production by phenomenological considerations based upon the two center model. We start from two assumptions: 1) the momentum distributions of pions emitted in the for- and backward cones are isotropic in each center-of-mass system (the fire ball rest system) and the average values ε_0 of the pion energies in this system do not depend on the details of collisions; 2) the mean value of the momentum transfer Δ is always of the order of the nucleon mass M . From these assumptions the following results are derived in Sect. 2: 1) the multiplicity is given by $n \simeq \xi \sqrt{2E_0 |\Delta|} / \varepsilon_0$, where ξ is the ratio $\mathcal{M} / \mathcal{M}_{\max}$ of the fire ball mass \mathcal{M} and its maximum value \mathcal{M}_{\max} . Experimentally, $\xi \simeq 0.5$ at 10^{13} eV; 2) the lower limit of the inelasticity K is given by $K \geq \xi^2$. At 10^{13} eV we have $K \geq \xi^2 \simeq 0.2$ which is consistent with experiments. The relation between multiplicity and inelasticity is discussed; 3) in the center-of-mass system of the fire ball and the recoil nucleon (« isobar system » IBS), the ratio $|\bar{\mathbf{p}}| / \mathcal{M}$ of the momentum of the nucleon $\bar{\mathbf{p}}$ and the fire ball mass \mathcal{M} is also expressed by the parameter ξ as $|\bar{\mathbf{p}}| / \mathcal{M} = (1 - \xi^2) / 2\xi$. At 10^{13} eV we have $|\bar{\mathbf{p}}| / \mathcal{M} \simeq 1$. This means that an equipartition of energy is approximately valid for the three possible degrees of freedom: the motion of the recoil nucleon, the translational and internal motion of the fire ball. $|\bar{\mathbf{p}}| \ll \mathcal{M}$ is excluded, unless K is unity, contrary to experiments; 4) when the equipartition holds, the mean value of the transverse momentum is constant and its value is of the order of ε_0 . In Sect. 3, the \mathcal{M} and n -dependence of the S -matrix is discussed. And by using the corresponding results we estimate the asymmetry in numbers of particles n_1 and n_2 emitted in the for- and backward cones. The parameter $[\langle (n_1 - n_2)^2 \rangle / \langle (n_1 + n_2)^2 \rangle]^{1/2}$, a measure of the asymmetry, becomes $\frac{1}{2}$ due to statistical fluctuation alone. It becomes larger if the energy transfer Δ_0 is not zero. Discussion is also made of the condition by

(*) On leave of absence from Hokkaido University, Sapporo.

(**) On leave of absence from Tokyo University of Education, Tokyo.

which the average value ε_0 of the pion energy in the fire ball is constant. The properties of the fire ball seem to be independent from the mechanism of its production. Extending this point of view, the similarity between the multiple production in $N^{\circ}\text{-}N^{\circ}$ collisions and $N^{\circ}\text{-}\bar{N}^{\circ}$ annihilation is discussed in Sect. 4. Conclusions are given in Sect. 5.

1. - Introduction.

As early as 1936, the importance of multiple production of particles was pointed out by HEISENBERG ⁽¹⁾ in connection with discussions on the limits of validity of the present quantum field theory. The well known difficulties of ultra-violet divergences appearing in the quantum field theory was considered to be due to unlimited extrapolation of the interaction laws, which were deduced only from low energy experiments. HEISENBERG anticipated a possible change in the interaction law in extremely high energy regions. According to him the equations describing fields would be non-linear. This change in the law was supposed to eliminate the divergence difficulties on one hand, and would cause multiple production of particles on the other hand. Another way of overcoming the difficulties is the non-local theory, which was proposed by WATAGHIN ⁽²⁾ who discussed possible effects due to non-locality in connection with multiple production. In this way, the theory of multiple production was developed in intimate connection with fundamental problems of the theory of elementary particles.

On the other hand, OPPENHEIMER *et al.* ⁽³⁾ pointed out the possibility of multiple production even in the present formalism of the meson theory. After long discussions of the multiple or plural ⁽⁴⁾ production, unambiguous verification for existence of multiple production of pions was given by accelerator experiments ⁽⁵⁾. Recently, many important features of extremely high energy events were clarified by experiments on high energy jets, penetrating showers, extensive air-showers and so on. On account of the very complicated nature of the processes, statistical or kinematical methods of analysis were applied and many important conclusions were derived, such as the angular distribution

⁽¹⁾ W. HEISENBERG: *Zeits. f. Phys.*, **101**, 533 (1936); **110**, 251 (1938); **113**, 61 (1936).

⁽²⁾ G. WATAGHIN: *Zeits. f. Phys.*, **88**, 92 (1934); *Suppl. Nuovo Cimento*, **8**, 792 (1958).

⁽³⁾ H. W. LEWIS, R. J. OPPENHEIMER and S. A. WOUTHUYSEN: *Phys. Rev.*, **73**, 127 (1948).

⁽⁴⁾ W. HEITLER and L. JÁNOSSY: *Proc. Phys. Soc. London*, **62**, 669 (1949).

⁽⁵⁾ W. B. FOWLER, R. P. SHUTT, A. M. THORNDIKE and W. L. WHITTEMORE: *Phys. Rev.*, **95**, 1026 (1954).

of emitted pions, constancy of the transverse momentum ⁽⁶⁾, average behaviors of the multiplicity and the inelasticity, etc.

In order to understand these main features, several models were proposed by many authors, *e.g.*, WATAGHIN ⁽⁷⁾ Fermi's ⁽⁸⁾ statistical model, Landau's ⁽⁹⁾ hydrodynamical model, two center models, etc. Among the two center models we have that one introduced by TAKAGI ⁽¹⁰⁾ and developed further by KRAUSHAAR-MARKS. In this so called *isobar model*, we have after the collision the formation of two excited nucleons which then decay emitting mesons. This model was successful in giving the characteristic double-cone angular distribution, but one of the main difficulties is that it gives a very high inelasticity.

Recently, CIOK *et al.*, COCCONI and NIU ⁽¹¹⁾ proposed the *fire ball model*. This is also a two center model which assumes the inelastic scattering of the two nucleons with the formation of two independent meson clouds, the so called *fire balls*. According to the analysis made by the above authors, the final nucleons travel in C.M. system with a much higher velocity than the fire balls and in this way we can get a small value for the inelasticity. However, during the last few years accuracy of measurements has been much improved, so that as WATAGHIN pointed out, it does not seem premature to attack the problem starting from first principles.

As a preliminary towards this direction, we shall make here an attempt to determine the structure and the semi-quantitative properties of sub-structure of the *S*-matrix by using information obtained by kinematical analysis of the experimental results. In order to carry out this program, we shall analyse in Section 2 the experimental results in *N*-*N* collisions by using a kinematics based upon the fire ball model and we shall introduce several parameters which are useful to determine the structure and properties of the *S*-matrix. In Section 3, an attempt is made to determine properties of *S*-matrix parts by using knowledge obtained by a kinematical analysis.

This kind of approach is a generalization of the method used in the investigation of scattering problems, in which parameters characterizing the *S*-matrix,

⁽⁶⁾ The constancy of transverse momentum was discovered by J. NISHIMURA in 1956 (*Soryushiroky Kenkyu*, **12**, 24 (1954)).

⁽⁷⁾ G. WATAGHIN: *Phys. Rev.*, **74**, 975 (1948).

⁽⁸⁾ E. FERMI: *Progr. Theor. Phys.*, **5**, 570 (1950); *Phys. Rev.*, **81**, 689 (1951); W. HEISENBERG: *Zeits. f. Phys.*, **126**, 569 (1949).

⁽⁹⁾ L. D. LANDAU: *Dokl. Akad. Nauk (USSR)*, **17**, 51 (1953).

⁽¹⁰⁾ S. TAKAGI: *Progr. Theor. Phys.*, **7**, 123 (1952); W. L. KRAUSHAAR and L. J. MARKS: *Phys. Rev.*, **93**, 326 (1954).

⁽¹¹⁾ P. CIOK, T. COGHEN, J. GIERULA, R. HOLYŃSKI, A. JURAK, M. MIĘSOWICZ, T. SANIEWSKA, O. STANISZ and J. PERNEGR: *Nuovo Cimento*, **8**, 166 (1958); G. COCCONI: *Phys. Rev.*, **111**, 1699 (1958); P. CIOK, T. COGHEN, J. GIERULA, R. HOLYŃSKI, A. JURAK, M. MIĘSOWICZ, T. SANIEWSKA and J. PERNEGR: *Nuovo Cimento*, **10**, 741 (1958); K. NIU: *Nuovo Cimento*, **10**, 994 (1958).

the phase shifts, are determined by scattering experiments. The importance of this kind of approach may be clear if we remember the importance of phase shift analysis or of the characterization of S -matrix elements by using dispersion relations. The attempt which we have done here is neither complete nor final, nevertheless the knowledge obtained on the properties of the S -matrix substructure provides us with many important suggestions on the mechanism of multiple production. For example, the deduced dependence of S -matrix elements on n , the number of emitted pions, seems to suggest that fire balls are produced as if they were elementary particles, independent of the details of their formation. The same situation appears in the fire ball formation in $N-\bar{N}$ annihilation, which will be discussed in Section 4.

2. - Kinematical properties of high energy jets.

In this section we shall show that the main features of high energy jets can be derived from two simple assumptions.

The most general mechanism of the multiple pion production in high energy nucleon-nucleon collision may be illustrated in the center-of-mass system C.M.S. by the graphical representation in Fig. 1, where (*) $\Delta_\mu = (\Delta, \Delta_0)$ is the total energy-momentum transfer between nucleons, $p_{0\mu}^{(1)} = (\mathbf{p}_0, E_0)$, $p_\mu^{(1)} = (\mathbf{p}_1, E_1)$ and $k_{\mu i}^{(1)} = (\mathbf{k}_i, \varepsilon_i)$ are the energy-momenta of incident and recoil nucleons, and emitted pions in « branch » 1 and $p_{0\mu}^{(2)} = (-\mathbf{p}_0, E_0)$, $p_\mu^{(2)} = (-\mathbf{p}_1, E_1)$ and $k_{\mu i}^{(2)} = (-\mathbf{k}'_i, \varepsilon'_i)$ are the corresponding quantities in « branch » 2.

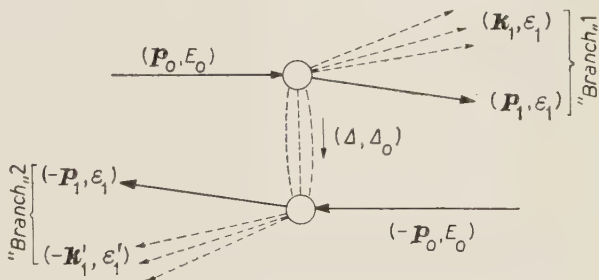


Fig. 1. - Inelastic collision of two nucleons in C.M.S. with formation of two fire balls. For simplicity we assume that recoiling nucleons have equal and opposite momenta.

We call the group of pions emitted from each nucleon a *fire ball* and we define momentum, energy and mass of each fire ball by the expressions

$$(2.1) \quad \sum_i \mathbf{k}_i = \mathbf{Q}_1, \quad \sum_i \varepsilon_i = Q_{10}, \quad -\mathcal{M}_1^2 = Q_1^2 - Q_{10}^2,$$

for branch (1) and similar expressions for branch (2).

(*) We use the natural units $\hbar=c=1$.

Let us now consider a system of reference in which

$$\sum_i \mathbf{k}_i = \mathbf{Q}_1 \rightarrow 0, \quad \sum \varepsilon_i = Q_{10} \rightarrow \mathcal{M}_1.$$

We shall refer to this system as « fire ball system » FBS and the quantities referring to it will be denoted by *.

2.1. Assumptions.

Assumption 1. — The angular distribution of pion momenta \mathbf{k}_i^* in FBS is isotropic, and the average values $\langle k_i^{*2} \rangle^{\frac{1}{2}} = k_0$, $\langle \varepsilon_i^* \rangle = \varepsilon_0$ are constant for all collisions, that is,

$$(2.2) \quad \mathcal{M}_1 = \sum_{i=1}^{n_1} \varepsilon_i^* = n_1 \varepsilon_0.$$

The isotropy of the angular distribution of mesons in each fire ball was verified with a reasonable accuracy ⁽¹⁾ and the constancy of the mean energy of mesons is based upon the constancy of transverse momentum and the fact that the measured average values of transverse and longitudinal momenta of pions are practically the same in FBS.

Assumption 2. — On the momentum transfer.

Let us assume that the magnitude of energy-momentum transfer $|\Delta^2 - A_0^2|$ is not so large and in average

$$(2.3) \quad \langle |\Delta^2 - A_0^2| \rangle \simeq M^2 \quad (M = \text{nucleon mass}).$$

This assumption is based on Niu's analysis ⁽¹⁾ and perhaps it is in intimate connection with the structure of the nucleon or with the properties of the nuclear forces. The physical meaning of this assumption is still not quite clear, but many important results are derived from it.

Now let us derive several kinematical conclusions from these assumptions.

2.2. Results from energy momentum conservations. — Energy momentum conservation for « branches » (1) and (2) are

$$(2.4) \quad \begin{cases} p_{0\mu}^{(1)} - A_\mu = p_\mu^{(1)} + Q_\mu^{(1)} & \text{for « branch » (1),} \\ p_{0\mu}^{(2)} + A_\mu = p_\mu^{(2)} + Q_\mu^{(2)} & \text{for « branch » (2),} \end{cases}$$

or in C.M.S. (see Fig. 1)

$$(2.5) \quad \begin{cases} E_0 - A_0 = E_1 + Q_{10}, & \mathbf{p}_0 - \Delta = \mathbf{p}_1 + \mathbf{Q}_1 & \text{« branch » (1),} \\ E_0 + A_0 = E_2 + Q_{20}, & -\mathbf{p}_0 + \Delta = \mathbf{p}_2 + \mathbf{Q}_2 & \text{« branch » (2).} \end{cases}$$

Now let us derive many conclusions from these conservation laws and the assumptions made above.

Result 1. — The energy-momentum transfer Δ_μ must be a spacelike vector. In fact as p_μ and Q_μ are time-like vectors pointing to the future, $p_\mu^{(1)} + Q_\mu^{(1)} = p_{0\mu}^{(1)} - \Delta_\mu$, must also be time-like. Therefore

$$(2.6) \quad -(p_{0\mu}^{(1)} - \Delta_\mu)^2 = 2(\mathbf{p}_0 \cdot \Delta - E_0 \Delta_0) + M^2 - (\Delta^2 - \Delta_0^2) \geq 0.$$

In high energy collisions, $E_0 \gg M$, then $(\mathbf{p}_0 \cdot \Delta - E_0 \Delta_0) \geq 0$ must hold by assumption 2. Therefore we get

$$(2.7) \quad |\Delta| - \Delta_0 \geq \frac{|\mathbf{p}_0|}{E_0} \Delta_\parallel - \Delta_0 \geq 0,$$

where Δ_\parallel is the projection of Δ in the \mathbf{p}_0 direction. By using this result the assumption 2 can be written as

$$(2.8) \quad M \geq \langle |\Delta| \rangle - \langle \Delta_0 \rangle.$$

Result 2. — Δ_\parallel must be always positive ⁽¹²⁾, that is,

$$0 \leq \angle \mathbf{p}_0, \Delta \leq 90^\circ.$$

Result 3. — On the upper limit of the fire-ball mass: \mathcal{M}_{\max} .

Let us consider a system of reference in which

$$(2.9) \quad \mathbf{p}_1 + \mathbf{Q}_1 = \mathbf{p}_0 - \Delta \rightarrow 0.$$

For simplicity we shall refer to this system as « isobar system » ⁽¹³⁾ (IBS); the quantities referring to this system will be denominated by « bars ».

In this system, momentum-energy conservation will be

$$(2.10) \quad \begin{cases} -\bar{\mathbf{p}}_1 = \bar{\mathbf{Q}}_1 = \bar{\mathbf{p}}, \\ \bar{E}_0 - \bar{A}_0 = \bar{E}_1 + \bar{Q}_{10} = \sqrt{\bar{\mathbf{p}}^2 + M^2} + \sqrt{\bar{\mathbf{p}}^2 + \mathcal{M}_1^2}. \end{cases}$$

⁽¹²⁾ When Δ_0 is negative for « branch (1) », then it is positive for « branch (2) ». Therefore, we can assume $\Delta_0 \geq 0$ without violating generality.

⁽¹³⁾ If we suppose a hypothetical excited nucleon (Isobar) in intermediate states, then I.B.S. is the rest system of this isobar.

The mass of the fire ball will be maximum when $\bar{\mathbf{p}} = 0$. Therefore,

$$(2.11) \quad \bar{E}_0 - \bar{\Delta}_0 = M + \mathcal{M}_{1\max}.$$

Now, the left hand side of the above equation is nothing but the square root of the invariant quantity $-(p_0^{(1)} - \Delta)^2$ in this special system of reference. In the original C.M.S. we have

$$(2.12) \quad M + \mathcal{M}_{\max} = \sqrt{2(\mathbf{p}_0 \cdot \Delta \pm E_0 \Delta_0) + M^2 - (\Delta^2 - \Delta_0^2)}.$$

Therefore, the maximum of the fire ball mass will be approximately given by

$$(2.13) \quad \begin{cases} \mathcal{M}_{1\max} \simeq \sqrt{2E_0(\Delta_{\parallel} - \Delta_0)}, \\ \mathcal{M}_{2\max} \simeq \sqrt{2E_0(\Delta_{\parallel} + \Delta_0)}. \end{cases}$$

2'3. *Multiplicity and its asymmetry.* - From (2.2) and (2.13), the number of particles emitted in each fire ball is given by

$$(2.14) \quad \begin{cases} n_1 = \frac{\mathcal{M}_1}{\varepsilon_0} = \frac{\mathcal{M}_1}{\mathcal{M}_{1\max}} \cdot \frac{\mathcal{M}_{1\max}}{\varepsilon_0} \simeq \xi_1 \frac{\sqrt{2E_0(\Delta_{\parallel} - \Delta_0)}}{\varepsilon_0}, \\ n_2 = \frac{\mathcal{M}_2}{\varepsilon_0} = \frac{\mathcal{M}_2}{\mathcal{M}_{2\max}} \cdot \frac{\mathcal{M}_{2\max}}{\varepsilon_0} \simeq \xi_2 \frac{\sqrt{2E_0(\Delta_{\parallel} + \Delta_0)}}{\varepsilon_0}. \end{cases}$$

According to Niu's analysis the mass of each fire ball is proportional to both $E_0^{\frac{1}{2}}$ and $\Delta_{\parallel}^{\frac{1}{2}}$. As ε_0 is a constant independent of the incident energy, it follows that ξ_1 and ξ_2 should be constant with respect to E_0 and Δ_{\parallel} .

When $\Delta_0 = 0$ and $\xi_1 = \xi_2$, the number of particles emitted in forward and backward cones in C.M.S. will be the same. For such symmetric productions, the

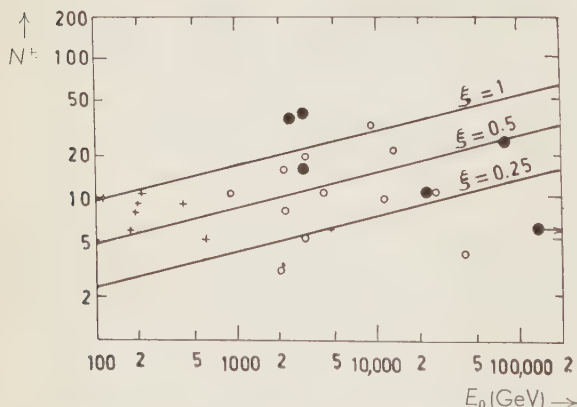


Fig. 2. - Experimental distribution of the multiplicity N^{\pm} of charged particles as function of energy of one of the incident nucleons in C.M.S.; from EDWARDS *et al.* ⁽¹⁵⁾. The straight

lines correspond to different values of the parameter ξ . \circ primary proton jets ($N_h \leq 2$); \bullet primary α -particle jets ($N_h \leq 2$); $+$ secondary jets ($N_h \leq 2$).

number of charged particles is given by

$$(2.15) \quad N^{\pm} = \frac{4}{3} n = \frac{4\sqrt{2}}{3} \xi \frac{M}{\varepsilon_0} \sqrt{\frac{E_0}{M}} \simeq 3.06 \xi E_{\text{Lab}}^{\frac{1}{2}}.$$

For $\varepsilon_0 = 3.6 \mu$ (*), $\Delta \simeq 1 M$ and E_{Lab} expressed in GeV. In Fig. 2, N^{\pm} is plotted as a function of the energy for several values of ξ . By comparing with experiments we find that the value of $\langle \xi \rangle$ is of the order of 0.5. Theoretically $\langle \xi \rangle$ is calculated by

$$(2.16) \quad \langle \xi \rangle = \int_0^{\mathcal{M}_{\max}} \frac{\mathcal{M}}{\mathcal{M}_{\max}} \varrho(\mathcal{M}^2) d\mathcal{M}^2 / \int_0^{\mathcal{M}_{\max}} \varrho(\mathcal{M}^2) d\mathcal{M}^2,$$

when the mass spectrum $\varrho(\mathcal{M}^2)$ of the fire ball is known. We shall discuss this point in Section 3.

When $\Delta_0 \neq 0$ the maxima of the fire ball masses $\mathcal{M}_{1 \max}$ and $\mathcal{M}_{2 \max}$ will be different and in general ξ_1 and ξ_2 may also be different. Then asymmetry appears. Recently considerable asymmetry of this kind was observed experimentally (¹⁴). By simple calculations, it is easily shown that the measure of this asymmetry $\langle (n_1 - n_2)^2 \rangle / \langle (n_1 + n_2)^2 \rangle$ is given by

$$(2.17) \quad \frac{\langle (n_1 - n_2)^2 \rangle}{\langle (n_1 + n_2)^2 \rangle} \simeq \frac{\langle (\xi_1 - \xi_2)^2 \rangle}{4 \langle \xi^2 \rangle} + \frac{\langle (\mathcal{M}_{1 \max} - \mathcal{M}_{2 \max})^2 \rangle}{4 \langle \mathcal{M}_{\max}^2 \rangle}.$$

When Δ_0^2 is small, we have

$$\frac{\langle (n_1 - n_2)^2 \rangle}{\langle (n_1 + n_2)^2 \rangle} \simeq \frac{\langle \xi^2 \rangle - \langle \xi \rangle^2}{2 \langle \xi^2 \rangle} + \frac{\langle \Delta_0^2 \rangle}{4 \langle \Delta_0^2 \rangle}.$$

Consequently, the parameter $\langle (n_1 - n_2)^2 \rangle / \langle (n_1 + n_2)^2 \rangle$ gives upper limits for $\langle \xi^2 \rangle / \langle \xi \rangle^2$ and $\langle \Delta_0^2 \rangle / \langle \Delta^2 \rangle$. Unfortunately no experimental values of this parameter are yet available. But even for such a very large value as

$$\frac{\langle (n_1 - n_2)^2 \rangle}{\langle (n_1 + n_2)^2 \rangle} = \frac{1}{3}, \quad 0.9 \leq \frac{\langle \xi^2 \rangle^{\frac{1}{2}}}{\langle \xi \rangle} \leq 1.1,$$

holds. Therefore $\langle \xi^2 \rangle^{\frac{1}{2}}$ is practically equal to $\langle \xi \rangle$. This means that the second moment $(\int \mathcal{M}^2 \varrho(\mathcal{M}^2) d\mathcal{M}^2)^{\frac{1}{2}}$ of the mass spectrum is of the same order of magnitude as the first one.

(*) μ = pion mass.

(¹⁴) Informed by Prof. G. WATAGHIN. Calorimetric exp.

2'4. *Inelasticity*. — In the symmetric case the inelasticity is defined by

$$(2.18) \quad K = \frac{Q_{10}}{E_0 - M} = \frac{Q_{10}}{E_1 + Q_{10} \pm A_0 - M} \simeq \frac{Q_{10}}{E_1 + Q_{10}}.$$

By Lorentz transformation we have

$$(2.19) \quad \begin{cases} E_1 = \gamma(\sqrt{\bar{\mathbf{p}}^2 + M^2} - \mathbf{V} \cdot \bar{\mathbf{p}}) \\ Q_{10} = \gamma(\sqrt{\bar{\mathbf{p}}^2 + M^2} + \mathbf{V} \cdot \bar{\mathbf{p}}) \end{cases} \quad \mathbf{V} = \frac{\mathbf{p}_0 - \Delta}{E_0 - A_0}.$$

K is expressed by quantities in IBS:

$$(2.20) \quad K = \frac{\sqrt{\bar{\mathbf{p}}^2 + M^2} - \mathbf{V} \cdot \bar{\mathbf{p}}}{\sqrt{\bar{\mathbf{p}}^2 + M^2} + \sqrt{\bar{\mathbf{p}}^2 + M^2}} \simeq \frac{\sqrt{1 + M^2/\bar{\mathbf{p}}^2} - \cos \theta}{\sqrt{1 + M^2/\bar{\mathbf{p}}^2} + 1} = \frac{\sqrt{1 + M^2/\bar{\mathbf{p}}^2} - 1}{\sqrt{1 + M^2/\bar{\mathbf{p}}^2} + 1}$$

By using energy-momentum conservation (2.10) in this system, the ratio $|\bar{\mathbf{p}}|/M$ is expressed by the parameter ξ :

$$(2.21) \quad \frac{|\bar{\mathbf{p}}|}{M} = \frac{1 - \xi^2}{2\xi}.$$

Then (2.20) turns out to be

$$(2.22) \quad K \geq \xi^2.$$

According to the Bristol group ⁽¹⁵⁾ the lower limit of K at 10^{13} eV is about 0.2 (see Fig. 3).

Then ξ will be $\simeq 0.45$ which

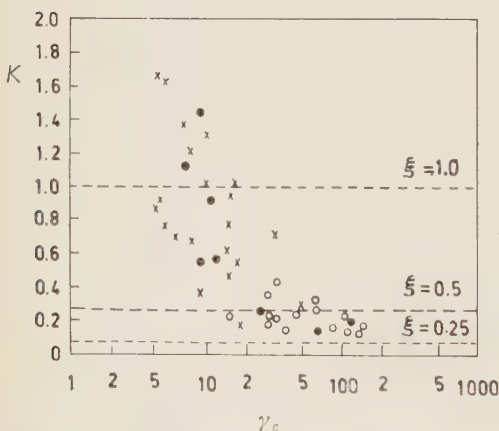


Fig. 3. Experimental distribution of the inelasticity K as function of the Lorentz factor γ_c of the C.M.S. of the two colliding nucleons, according to EDWARDS *et al.* ⁽¹⁵⁾; \times secondary jets (charged); \bullet secondary jets (neutral); \circ primary jets. We see that at high energies $0.1 < K < 0.4$ the straight lines represent the lower limits of K for the three values of ξ considered in Fig. 2.

⁽¹⁵⁾ B. EDWARDS, J. LOSTY, D. H. PERKINS, K. PINKAU and J. REYNOLDS: *Phil. Mag.*, **3**, 237 (1958).

is in agreement with the value estimated from multiplicity. From Fig. 2, ξ seems to be a decreasing function of energy. For $\xi \simeq 0.5$ the ratio $|\bar{\mathbf{p}}|/\mathcal{M}$ will be $\simeq 1$. Then the ratio of the energy of the recoil nucleon, to the translation and internal energies of the fire ball in IBS will be

$$\sqrt{\mathbf{p}^2 + \mathcal{M}^2} : (\sqrt{\mathbf{p}^2 + \mathcal{M}^2} - \mathcal{M}) : \mathcal{M} \simeq 1 : 0.4 : 1.$$

This means that approximate equipartition of energies holds for the three possible degrees of freedom.

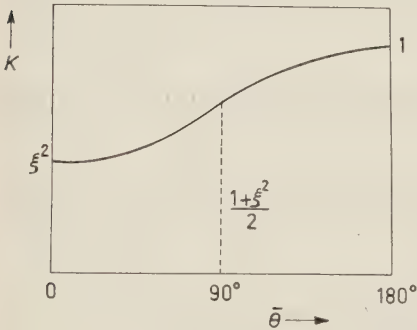


Fig. 4. - Angular distribution of the inelasticity K , as function of the angle of emission of the fire ball in I.B.S.

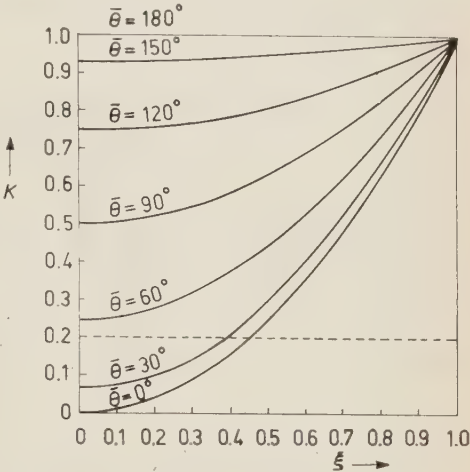


Fig. 5. - Variation of the inelasticity K , with the parameter ξ for several values of $\bar{\theta}$, the angle of emission of the fire ball in I.B.S.

K depends on the angle of emission of the fire ball:

(2.23)
$$K = \frac{1 + \xi^2}{2} - \frac{1 - \xi^2}{2} \cos \bar{\theta}.$$

The fluctuation of K comes from that of ξ and $\bar{\theta}$. It is calculated as

(2.24)
$$\Delta K = K_{\max} - K_{\min} \simeq \frac{1 + \langle \cos \bar{\theta} \rangle}{2} \Delta \xi^2 + \frac{1 - \langle \xi^2 \rangle}{2} (1 - \cos \bar{\theta}_{\max}).$$

This gives upper limits for the fluctuations of ξ^2 and $\bar{\theta}$. For example ΔK seems to be ~ 0.2 at 10^{13} eV. Then $1 - \cos \bar{\theta}_{\max} \lesssim \frac{1}{2}$ and $\bar{\theta}_{\max} \lesssim 60^\circ$. This result shows that $\bar{\theta}_{\max}$ is not necessarily small as usually supposed ⁽¹¹⁾.

2.5. *Transverse momentum and angular distribution of fire balls.* - Let us denote by \mathbf{e}_0 and \mathbf{e} the unit vectors parallel to \mathbf{p}_0 and \mathbf{Q}_1 respectively and by \mathbf{k}^* the momentum of a pion in FBS.

In C.M.S. the momentum of the pion will be given by

$$(2.25) \quad \mathbf{k} = \mathbf{k}^* + \mathbf{e}[(\mathbf{e} \cdot \mathbf{k}^*)(\gamma_B - 1) + \gamma_B V_B \varepsilon^*],$$

where V_B is the velocity of the fire ball in C.M.S. and γ_B is the corresponding Lorentz factor.

The average value of the transverse momentum $\mathbf{k}_T^2 = (\mathbf{k} \times \mathbf{e}_0)^2$ will be given by

$$(2.26) \quad \langle \mathbf{k}_T^2 \rangle = \frac{2}{3} \langle \mathbf{k}^{*2} \rangle + (\mathbf{e} \times \mathbf{e}_0)^2 \left[(\gamma_B^2 - 1) \frac{\langle \mathbf{k}^{*2} \rangle}{3} + \gamma_B^2 v_B^2 \langle \varepsilon^{*2} \rangle \right],$$

using assumption 1.

For very high energy, \mathbf{p}_0 and $\mathbf{p}_0 - \Delta$, because of assumption 2, are practically parallel and so we can write

$$(2.27) \quad \langle \mathbf{k}_T^2 \rangle = \frac{2}{3} k_0^2 + \left(\frac{\bar{\mathbf{p}}}{\mathcal{M}} \right)^2 \sin^2 \bar{\theta} \left(\frac{k_0^2}{3} + \varepsilon_0^2 \right),$$

where $\bar{\theta}$ denotes the angle of emission of the fire ball in IBS.

If $\bar{\theta} = 0$, $\langle \mathbf{k}_T^2 \rangle \simeq k_0^2$ which is consistent with experiments ⁽¹¹⁾.

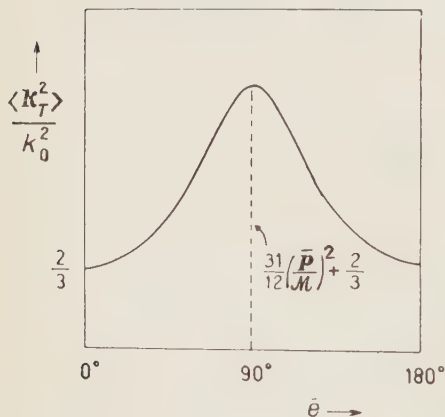


Fig. 6. - Angular distribution of the relative average value of the (square) transverse momentum. θ is the angle of emission of the fire ball in I.B.S.

However we have shown that $\bar{\theta} \lesssim 60^\circ$ and so $\bar{\theta} \neq 0$ is also possible and in fact it has been observed recently in a jet of $\sim 10^{13}$ eV that the angle between the direction of motion of the two fire balls is $\sim 7^\circ$ in laboratory system ⁽¹⁶⁾.

In this case in order to have $\langle \mathbf{k}_T^2 \rangle \simeq k_0^2$ we must exclude the possibility that $|\bar{\mathbf{p}}| \gg \mathcal{M}$. Now $|\bar{\mathbf{p}}| \ll \mathcal{M}$ gives a very high inelasticity by (2.20) and so in order to obtain the correct values for inelasticity, transverse momentum and multiplicity, $|\bar{\mathbf{p}}| \sim \mathcal{M}$ seems to be very probable.

In Fig. 6 we give the angular dependence of $\langle \mathbf{k}_T^2 \rangle$.

⁽¹⁶⁾ H. W. MEIER: *Nuovo Cimento*, **11**, 308 (1958).

3. - Properties of S -matrix elements.

The purpose of the present section is to derive the properties of S -matrix elements responsible for multiple pion production by using knowledge obtained from the kinematical analysis given in the previous sections. In the kinematical analysis appeared three kinds of important parameters Δ_μ , ξ and ε_0 . These parameters depend on the structure and the properties of S -matrix describing the process.

3'1. General expression for cross-section. - Corresponding to Fig. 1 we introduce just as an assumption that the matrix element of Møller's ⁽¹⁷⁾ invariant collision operator for our process has the following form:

$$(3.1) \quad \langle I | \rangle = \langle p_0^{(1)} | I_1(\Delta) | p_1^{(1)}, k_1^{(1)} \dots \rangle V(\Delta) \langle p_0^{(2)} | I_2(-\Delta) | p_1^{(2)}, k_1^{(2)} \dots \rangle,$$

where $V(\Delta)$ is essentially the matrix element of nuclear force. Then the cross-section of the collision can be written as

$$(3.2) \quad \sigma = \frac{(2\pi)^4}{\vartheta_r E_0} \int d^4\Delta |V(\Delta)|^2 \sum_{n_1} \int \frac{d\mathbf{p}_1}{E_1} \prod_{i=1}^{n_1} \frac{d\mathbf{k}_i}{\varepsilon_i} |\langle I^{(1)} | \rangle|^2 \delta^4(p_0^{(1)} - p^{(1)} - \Sigma k^{(1)} - \Delta) \cdot \\ \cdot \sum_{n_2} \int \frac{d\mathbf{p}_2}{E_2} \prod_{i=1}^{n_2} \frac{d\mathbf{k}_i'}{\varepsilon_i'} |\langle I^{(2)} | \rangle|^2 \delta^4(p_0^{(2)} - p^{(2)} - \Sigma k^{(2)} + \Delta) = \\ = \frac{(2\pi)^4}{\vartheta_r E_0} \int d^4\Delta |V(\Delta)|^2 \sum_{n_1} J_{n_1}^{(1)}(\Delta) \sum_{n_2} J_{n_2}^{(2)}(-\Delta).$$

By introducing new variables Q_μ , $J_n(\Delta)$ can be written as follows

$$(3.3) \quad J_n(\Delta) = \int \frac{d\mathbf{p}_1}{E_1} \int d^4Q \delta^4(p_0 - p - \Delta - Q) \int \prod_{i=1}^n \frac{d\mathbf{k}_i}{\varepsilon_i} |\langle I_1 | \rangle|^2 \delta^4(Q - \Sigma k - \Delta) = \\ = \int \frac{d\mathbf{p}_1}{E_1} \int d^4Q \delta^4(p_0 - p - \Delta - Q) F_n(p_0, \Delta, Q).$$

3'2. Mass spectrum of the fire ball. - Let us now obtain information about the invariant function which in FBS can be written as

$$(3.4) \quad F_n(p_0^*, \Delta^*, \mathcal{M}) = \int \prod_{i=1}^n \frac{d\mathbf{k}_i^*}{\varepsilon_i^*} |\langle p_0^* - \Delta^* | I | p_0^* - \Delta^*, \mathbf{k}_1^* \dots \mathbf{k}_n^* \rangle|^2 \cdot \\ \cdot \delta(\Sigma \mathbf{k}^*) \delta(\mathcal{M} - \Sigma \varepsilon_i^*).$$

⁽¹⁷⁾ C. MØLLER: *Kgl. Dan. Viden. Selsk.*, **23**, no. 1 (1943); **23**, no. 9 (1946).

By using the relation $Q_0 = \sqrt{Q^2 + \mathcal{M}^2}$ the integration over Q_0 can be replaced by integration over \mathcal{M}^2 . Then (3.3) turns out to be

$$(3.5) \quad J_n(\Lambda) = \int \frac{dQ d\mathcal{M}^2}{2\sqrt{Q^2 + \mathcal{M}^2}} \frac{d\mathbf{p}_1}{E_1} \delta^4(p_0 - p - \Lambda - Q) F_n(\mathbf{p}_0, \Lambda, \mathbf{Q}, \mathcal{M}).$$

After integrating over \mathbf{p}_1 , we get

$$(3.6) \quad J_n(\Lambda) = \int d\mathcal{M}^2 \int \frac{dQ}{\sqrt{Q^2 + \mathcal{M}^2}} \delta((p_0 - \Lambda - Q)^2 - M^2) F_n.$$

In IBS (3.6) is written as

$$(3.7) \quad J_n(\Lambda) = \int d\mathcal{M}^2 \int \frac{|\bar{\mathbf{Q}}| d\bar{Q}^2}{\bar{E}_0 - \bar{\Lambda}_0} \delta\left(\bar{Q}^2 + \mathcal{M}^2 - \frac{[\mathcal{M}^2 - M^2 - (\bar{E}_0 - \Lambda_0)^2]^2}{4(\bar{E}_0 - \bar{\Lambda}_0)^2}\right) \cdot 2\pi \int_{-1}^{+1} d(\cos \bar{\theta}) F_n(\mathbf{p}_0, \Lambda, \mathcal{M}, \cos \bar{\theta}).$$

Since we have

$$(3.8) \quad \bar{Q} = \frac{\sqrt{[(\bar{E}_0 - \Lambda_0)^2 + \mathcal{M}^2 - M^2]^2 - 4\mathcal{M}^2(\bar{E}_0 - \Lambda_0)^2}}{2(\bar{E}_0 - \bar{\Lambda}_0)} \simeq \frac{(\bar{E}_0 - \Lambda_0)^2 + \mathcal{M}^2}{2(\bar{E}_0 - \bar{\Lambda}_0)},$$

the result of the $|\bar{\mathbf{Q}}|^2$ integration can be written as

$$(3.9) \quad J_n(\Lambda) = \pi \int_0^{\mathcal{M}_{\max}} d\mathcal{M}^2 \left(1 - \frac{\mathcal{M}^2}{(\bar{E}_0 - \bar{\Lambda}_0)^2}\right) \tilde{F}_n(\mathbf{p}_0, \Lambda, \mathcal{M}),$$

where

$$(3.10) \quad \tilde{F}_n = \int_{-1}^{+1} d(\cos \bar{\theta}) F_n(\mathbf{p}_0, \Lambda, \mathcal{M}, \cos \bar{\theta}).$$

Thus the mass spectrum of the fire ball is obtained:

$$(3.11) \quad \varrho(\mathcal{M}^2) = \sum_n \left(1 - \frac{\mathcal{M}^2}{\mathcal{M}_{\max}^2}\right) \tilde{F}_n(\mathbf{p}_0, \Lambda, \mathcal{M}).$$

Then the parameter $\langle \xi^2 \rangle$ will be calculated by

$$(3.12) \qquad \langle \xi^2 \rangle = \frac{\sum_n \int_0^{\mathcal{M}_{\max}} (\mathcal{M}/\mathcal{M}_{\max})^2 (1 - \mathcal{M}^2/\mathcal{M}_{\max}^2) \, \widetilde{F}_n(\mathbf{p}_0, \Delta, \mathcal{M}) \, d\mathcal{M}^2}{\sum_n \int_0^{\mathcal{M}_{\max}} (1 - \mathcal{M}^2/\mathcal{M}_{\max}^2) \, \widetilde{F}_n(\mathbf{p}_0, \Delta, \mathcal{M}) \, d\mathcal{M}^2} = \\ = \frac{\int_0^1 x(1-x) \, dx \sum_n \widetilde{F}_n(\mathcal{M}_{\max}^2, x)}{\int_0^1 (1-x) \, dx \sum_n \widetilde{F}_n(\mathcal{M}_{\max}^2, x)} .$$

If \widetilde{F}_n is independent of the fire ball mass

$$\langle \xi^2 \rangle \rightarrow \frac{1}{3} = 0.33 .$$

As $\langle \xi^2 \rangle \simeq 0.25$ in the 10^{13} eV region, $\sum_n \widetilde{F}_n$ seems to be a constant or a very slowly decreasing function of \mathcal{M} .

From this phenomenological restriction much important information on the properties of matrix elements $\langle |I| \rangle$ will be deduced in the following subsection.

3'3. n -dependence of the matrix elements. – In the previous subsection, we examined the properties of

$$(3.13) \qquad F_n(\mathbf{p}_0^*, \Delta^*, \mathcal{M}) = \int \prod_{i=1}^n \frac{d\mathbf{k}_i^*}{\varepsilon_i^*} P_n(\mathbf{p}_0^*, \Delta^*, \mathbf{k}_1^*, \dots, \mathbf{k}_n^*) \delta(\Sigma \mathbf{k}^*) \delta(\mathcal{M} - \Sigma \varepsilon^*) ,$$

as a function of \mathcal{M} , where

$$(3.14) \qquad P_n = |\langle \dots | I(\Delta) | \dots \rangle|^2 .$$

Now, let us investigate the n -dependence of $F_n(\mathcal{M})$ for a given value of \mathcal{M} . For this purpose we shall calculate $\langle 1/n \rangle$ and $\langle (1/n^2) - \langle 1/n \rangle^2 \rangle$, which characterize the distribution of F_n .

Consider the following sum:

$$(3.15) \qquad \sum_{n=1}^{\infty} \frac{1}{n} F_n = \frac{1}{\mathcal{M}} \sum_{n=1}^{\infty} \frac{\mathcal{M}}{n} \int \prod_{i=1}^n \frac{d\mathbf{k}_i^*}{\varepsilon_i^*} P_n(\mathbf{p}_0^*, \Delta^*, \mathbf{k}_1^* \dots \mathbf{k}_n^*) \delta(\Sigma \mathbf{k}^*) \delta(\mathcal{M} - \Sigma \varepsilon^*) .$$

This can be written as

$$(3.16) \qquad \frac{1}{\mathcal{M}} \sum_{n=1}^{\infty} \frac{1}{n} \int \prod_{i=1}^n \frac{d\mathbf{k}_i^*}{\varepsilon_i^*} P_n \delta(\Sigma \mathbf{k}^*) \delta(\mathcal{M} - \Sigma \varepsilon^*) \sum_{i=1}^n \varepsilon_i^* .$$

As the integrand is a symmetric function of the k^* 's, this turns out to be

$$(3.17) \quad \frac{1}{\mathcal{M}} \sum_{n=1}^{\infty} \int \varepsilon_1^* \frac{d\mathbf{k}_1^*}{\varepsilon_1^*} \cdots \frac{d\mathbf{k}_n^*}{\varepsilon_n^*} P_n \delta(\Sigma \mathbf{k}^*) \delta(\mathcal{M} - \Sigma \varepsilon^*) = \frac{\langle \varepsilon^* \rangle}{\mathcal{M}} \sum_n F_n.$$

Hence, we get

$$(3.18) \quad \left\langle \frac{1}{n} \right\rangle = \frac{\langle \varepsilon^* \rangle}{\mathcal{M}} = \frac{\varepsilon_0}{\mathcal{M}}.$$

In the same way, we can calculate

$$(3.19) \quad \left\langle \frac{1}{n^2} \right\rangle = \frac{(1/\mathcal{M}) \sum_{n=1}^{\infty} (1/n^2) \int \left(\sum_{i=1}^n \varepsilon_i^* \right)^2 P_n \prod_{i=1}^n (d\mathbf{k}_i^*/\varepsilon_i^*) \delta(\Sigma \mathbf{k}^*) \delta(\mathcal{M} - \Sigma \varepsilon^*)}{\sum_{n=1}^{\infty} F_n}.$$

On account of the symmetry of the integrand, $\left(\sum_{i=1}^n \varepsilon_i^* \right)^2$ can be transformed into:

$$(3.20) \quad \left(\sum_{i=1}^n \varepsilon_i^* \right)^2 \Rightarrow n\varepsilon_1^{*2} + n(n-1)\varepsilon_1^* \varepsilon_2^* = n^2 \varepsilon_1^* \varepsilon_2^* + n(\varepsilon_1^{*2} - \varepsilon_1^* \varepsilon_2^*).$$

Then, we get

$$(3.21) \quad \left\langle \frac{1}{n^2} \right\rangle = \frac{1}{\mathcal{M}^2} \cdot \left[\langle \varepsilon_1^* \varepsilon_2^* \rangle + \frac{(1/\mathcal{M}) \sum_n (\mathcal{M}/n) \int (\varepsilon_1^{*2} - \varepsilon_1^* \varepsilon_2^*) P_n \prod (d\mathbf{k}^*/\varepsilon^*) \delta(\Sigma \mathbf{k}^*) \delta(\mathcal{M} - \Sigma \varepsilon^*)}{\sum_n F_n} \right].$$

In the second term of the right hand side, $\mathcal{M} \rightarrow \sum \varepsilon^*$ can be transformed as follows:

$$(3.22) \quad \sum_{i=1}^n \varepsilon_i^* (\varepsilon_1^{*2} - \varepsilon_1^* \varepsilon_2^*) \Rightarrow n(\varepsilon_1^{*2} - \varepsilon_1^* \varepsilon_2^*) \varepsilon_3^* + (\varepsilon_1^{*3} + 2\varepsilon_1^* \varepsilon_2^* \varepsilon_3^* - 3\varepsilon_1^{*2} \varepsilon_2^*).$$

Then, we get

$$(3.23) \quad \left\langle \frac{1}{n^2} \right\rangle = \frac{\langle \varepsilon_1^* \varepsilon_2^* \rangle}{\mathcal{M}^2} + \frac{\langle (\varepsilon_1^{*2} - \varepsilon_1^* \varepsilon_2^*) \varepsilon_3^* \rangle}{\mathcal{M}^3} + \frac{\langle \varepsilon_1^{*3} + 2\varepsilon_1^* \varepsilon_2^* \varepsilon_3^* - 3\varepsilon_1^{*2} \varepsilon_2^* \rangle}{\mathcal{M}^4} + \dots,$$

by repeating the same procedure.

By using (3.18) and (3.23), we can calculate the fluctuation of $1/n$ in powers of $1/\mathcal{M}$:

$$(3.24) \quad \left\langle \frac{1}{n^2} - \left\langle \frac{1}{n} \right\rangle^2 \right\rangle = \frac{\varepsilon_1^* \varepsilon_2^* - \varepsilon_0^2}{\mathcal{M}^2} + \frac{(\varepsilon_1^{*2} - \varepsilon_1^* \varepsilon_2^*) \varepsilon_3^*}{\mathcal{M}^3} + O\left(\frac{\langle \varepsilon^{*3} \rangle}{\mathcal{M}^4}\right),$$

or

$$(3.25) \quad \frac{\langle (1/n^2) - \langle 1/n \rangle^2 \rangle}{\langle 1/n \rangle^2} = \frac{\langle \varepsilon_1^* \varepsilon_2^* \rangle - \langle \varepsilon_1^* \rangle \langle \varepsilon_2^* \rangle}{\langle \varepsilon_1^* \rangle \langle \varepsilon_2^* \rangle} + O\left(\sqrt{\frac{M}{E_0}}\right).$$

We see that the fluctuation in the $1/n$ distribution at very high energy is expressed by the correlation of the pion energy in the fire ball. It is plausible that the correlation in energy is small when the number of mesons is large and then the first term in (3.25) will be negligible. That is, in very high energy collisions, the width of the distribution F_n over n will be very small compared to the average value. In such cases, we may approximate \tilde{F}_n by

$$(3.26) \quad \tilde{F}_n(\mathbf{p}_0^*, \Delta^*, \mathcal{M}) \simeq \tilde{F}_n(\mathbf{p}_0^*, \Delta^*, n\varepsilon_0) \frac{1}{\varepsilon_0} \delta(\mathcal{M} - n\varepsilon_0).$$

By inserting (3.26) into (3.9), we can calculate the matrix element of « branch (1) »:

$$(3.27) \quad J_n(\Delta) = \pi \int_0^{\mathcal{M}_{\max}} d\mathcal{M}^2 \left(1 - \frac{\mathcal{M}^2}{\mathcal{M}_{\max}^2}\right) \frac{\tilde{F}_n}{\varepsilon_0} \delta(\mathcal{M} - n\varepsilon_0) = \\ = 2\pi \tilde{F}_n(\mathbf{p}_0, \Delta, n\varepsilon_0) n \left(1 - \frac{n^2}{n_{\max}^2}\right).$$

As $\sum_n \tilde{F}_n$ is constant or a very slowly decreasing function of \mathcal{M} ,

$$(3.28) \quad \sum_n \tilde{F}_n(\mathbf{p}_0, \Delta, \mathcal{M}) \simeq \tilde{F}_{\bar{n}}(\mathbf{p}_0, \Delta, \bar{n}\varepsilon_0), \quad \bar{n} = \frac{\mathcal{M}}{\varepsilon_0}.$$

is also a very slowly decreasing function of $\bar{n} = \mathcal{M}/\varepsilon_0$.

By using these knowledge deduced from phenomenological considerations, we can estimate the parameter $\langle (n_1 - n_2)^2 \rangle / \langle (n_2 + n_2)^2 \rangle$. For this purpose, let us calculate

$$(3.29) \quad \sum_{n_1 n_2} J_{n_1}^{(1)}(\Delta) J_{n_2}^{(2)}(-\Delta) (n_1 \pm n_2)^2 \propto \int_0^{n_{1\max}} n_1 dn_1 \left(1 - \frac{n_1^2}{n_{1\max}^2}\right) \cdot \\ \cdot \int_0^{n_{2\max}} n_2 dn_2 \left(1 - \frac{n_2^2}{n_{2\max}^2}\right) (n_1 \pm n_2)^2 = \\ = n_{1\max}^2 n_{2\max}^2 \int_0^1 dx (1 - x^2) \int_0^1 dy (1 - y^2) (n_{1\max} x + n_{2\max} y)^2,$$

by ignoring the slowly decreasing function \tilde{F}_n .

Then, we get

$$(3.30) \quad \frac{\langle (n_1 - n_2)^2 \rangle}{\langle (n_1 + n_2)^2 \rangle} \simeq \frac{1 - \frac{12 \times 16}{15 \times 15} \frac{2n_{1\max} n_{2\max}}{n_{1\max}^2 + n_{2\max}^2}}{1 + \frac{12 \times 16}{15 \times 15} \frac{2n_{1\max} n_{2\max}}{n_{1\max}^2 + n_{2\max}^2}}.$$

When $\Delta_0 = 0$, that is, when $n_{1\max} = n_{2\max}$

$$(3.31) \quad \left(\frac{\langle (n_1 - n_2)^2 \rangle}{\langle (n_1 + n_2)^2 \rangle} \right)^{\frac{1}{2}} \simeq \frac{1}{3.5}.$$

For example, in a collision of $n_1 + n_2 = 35$, the probable difference $\langle (n_1 - n_2)^2 \rangle^{\frac{1}{2}}$ will be 10, that is to say a large asymmetry like $n_1 = 22$, $n_2 = 13$ occurs rather frequently even due to statistical fluctuation alone.

3'4. *Analysis of matrix elements and approximate universality of fire balls.* — In order to get more detailed information, we shall analyse the collision operator,

$$(3.32) \quad \langle I(\Delta) | \rangle = \sqrt{E'} \bar{u}_e(p) M'_{e\sigma}(p_0, p, \Delta, k_1 \dots k_n) u_\sigma(p_0) \sqrt{E_0}.$$

As this matrix depends on n -vertices of $\pi\mathcal{N}$ interaction, we shall put

$$(3.33) \quad M'_{e\sigma} = (M_n \gamma_5^n)_{e\sigma} \left(\frac{g}{\mu} \right)^n.$$

Then, $M_{e\sigma}$ does not depend explicitly on γ_5 any more.

Now let us expand $M_{n e\sigma}$ into γ -algebra. By using the possible 4-vectors, the most general form of the expansion will be

$$(3.34) \quad M_n = A_n'' + B_n'' \gamma \cdot (\alpha p_0 + \beta p + \lambda \Delta + \sum_i c_i k_i) + \\ + C_n'' \gamma \cdot (\alpha' p_0 + \beta' p + \dots) \gamma (\alpha'' p_0 + \beta'' p + \dots),$$

where A_n'' , B_n'' , α , β , ..., etc., are coefficients of expansion. Since M_n is a symmetric function of the k 's, all C_i must be equal. Then there appears $\sum_i k_i$, but this sum is expressed by another vector as $\sum_i k_i = p_0 - p - \Delta$. Among the remaining vectors, $\gamma \cdot p_0$ and $\gamma \cdot p$ are replaced by M . Therefore, the only remaining γ -dependence is $\gamma \cdot \Delta$. Now, M_n will be

$$(3.35) \quad M_n = A_n' + B_n' (\gamma \cdot \Delta) + C_n' (\gamma \cdot \Delta)^2 + \dots = A_n + B_n \frac{i\gamma \cdot \Delta}{M},$$

where A_n and B_n are linear functions of M_n given by

$$(3.36) \quad A_n = \frac{1}{4} \text{Tr} (M_n) ; \quad -\frac{\Delta^2}{M^2} B_n = \frac{1}{4} \text{Tr} \frac{i\gamma \cdot \Delta}{M} M_n .$$

Next, let us expand A_n and B_n into series of orthonormal wave functions Ψ_r of the fire ball:

$$(3.37) \quad A_n(p_0^* p^* \Delta^* k_1^* \dots k_n^*) = \sum_r a_n^r(p_0^* p^* \Delta^*) \Psi_r(k_1^* \dots k_n^*) ,$$

where r is a set of quantum numbers describing the states of the fire ball:

$$r = (J, J_3, \zeta) .$$

Here, J and J_3 are total angular momentum quantum numbers of the fire ball and ζ denotes the set of remaining quantum numbers, such as quantum numbers describing charge states or states of subsystems, etc.

We shall assume that the fire balls are spherically symmetric and that they have no angular momentum: $J = J_3 = 0$. We shall thus neglect the terms with $J \neq 0$. Then, M_n can be written as

$$(3.38) \quad M_n = \sum_{\zeta} \left(a_n^{\zeta} + i \frac{\gamma \cdot \Delta}{M} b_n^{\zeta} \right) \Psi_{n\zeta}(k_1^* \dots k_n^*) .$$

As the total angular momentum is zero, the wave function $\Psi_{n\zeta}$ is scalar. Therefore, this decomposition of M_n into $\Psi_{n\zeta}$ and $a_n^{\zeta} + i(\gamma \cdot \Delta/M)b_n^{\zeta}$ is an invariant procedure.

Inserting (3.38) into (3.32), squaring and integrating we get

$$(3.39) \quad F_n = \sum_{\zeta} \sum_{\text{spin}} \frac{E_0 E}{2} \cdot \left| \bar{u} \left(a_n^{\zeta} + i \frac{\gamma \cdot \Delta}{M} b_n^{\zeta} \right) \gamma_5^* u_0 \right|^2 \left(\frac{g^2}{\mu^2} \right)^n \int |\Psi_{n\zeta}|^2 \prod_{i=1}^n \frac{d\mathbf{k}_i^*}{\varepsilon_i^*} \delta(\Sigma \mathbf{k}^*) \delta(\mathcal{M} - \Sigma \varepsilon^*) .$$

By averaging over all possible ζ ,

$$(3.40) \quad F_n = \sum_{\text{spin}} \frac{E_0 E}{2} \left| \bar{u} \left(a_n + i \frac{\gamma \cdot \Delta}{M} b_n \right) \gamma_5^* u_0 \right|^2 g_{\zeta} \left(\frac{g}{\mu} \right)^{2n} \cdot \int |\Psi_n|^2 \prod_{i=1}^n \frac{d\mathbf{k}_i^*}{\varepsilon_i^*} \delta(\Sigma \mathbf{k}^*) \delta(\mathcal{M} - \Sigma \varepsilon^*) ,$$

where g_{ζ} is the statistical weight. It is easily shown that γ_5^* , in (3.39), (3.40) disappears when $|\mathbf{p}_0| \gg M$.

Now, \tilde{F}_n consists of two parts:

$$(3.41) \quad \tilde{F}_n(\mathbf{p}_0^*, \Delta^* \mathcal{M}) = G_n(\mathbf{p}_0^*, \Delta^* \mathcal{M}) Z_n(\mathcal{M}),$$

where

$$(3.42) \quad Z_n(\mathcal{M}) = \left(\frac{g}{\mu}\right)^{z_n} \int |\Psi_n(\mathbf{k}_1^* \dots \mathbf{k}_n^*)|^2 \prod_{i=1}^n \frac{d\mathbf{k}_i^*}{\varepsilon_i^*} \delta(\Sigma \mathbf{k}_i^*) \delta(\mathcal{M} - \Sigma \varepsilon_i^*)$$

may be called the « partition function » of the fire ball. By inserting (3.41) into (3.9) and (3.10) we get

$$(3.43) \quad J_n(\Delta) = \pi \int_0^{\mathcal{M}_{\max}} d\mathcal{M}^2 \left(1 - \frac{\mathcal{M}^2}{\mathcal{M}_{\max}^2}\right) G_n(\mathbf{p}_0, \Delta, \mathcal{M}) Z_n(\mathcal{M}).$$

With these preparations, let us now investigate the main problem of this sub-section. Consider the mean value of n :

$$(3.44) \quad \langle n \rangle_{\mathbf{p}_0, \Delta, \mathcal{M}} = \frac{\sum_n n G_n(\mathbf{p}_0^*, \Delta^*, \mathcal{M}) Z_n(\mathcal{M})}{\sum_n G_n(\mathbf{p}_0^*, \Delta^*, \mathcal{M}) Z_n(\mathcal{M})}.$$

which is equal to $\mathcal{M}/\varepsilon_0$ and so it does not depend explicitly on \mathbf{p}_0^* and Δ^* but only on \mathcal{M} . The right hand side of (3.44) may, in general depend on \mathbf{p}_0^* and Δ^* . Now, our problem is « What is the condition by which $\langle n \rangle_{\mathbf{p}_0, \Delta, \mathcal{M}}$ will be independent of \mathbf{p}_0^* and Δ^* ? »

The simplest solution is to assume that G_n is independent of n or, at least, up to a universal function $z_n(\mathcal{M})$ of \mathcal{M} and n

$$(3.45) \quad G_n(\mathbf{p}_0^*, \Delta^*, \mathcal{M}) = G(\mathbf{p}_0^*, \Delta^*, \mathcal{M}) z_n(\mathcal{M}).$$

Then, (3.44) reduces to

$$(3.46) \quad \langle n \rangle = \frac{\sum_n n z_n Z_n}{\sum_n z_n Z_n},$$

which depends only upon \mathcal{M} .

Physically, (3.45) means that:

1) The probability of the production of the fire ball $G(\mathbf{p}_0^*, \Delta^*, \mathcal{M})$ does not depend on the details (for example, on n) of the fire ball. It depends only upon the mass \mathcal{M} and total momentum \mathbf{Q} of the fire ball. This means that the fire ball is produced as if it were an elementary particle.

2) The properties of the fire ball do not depend on the details of the collision by which it is produced. In this sense the properties of the fire ball are « universal »; and multiplicity is essentially determined by the properties of the fire ball. This situation is very similar to the virtual production of a $(\frac{3}{2}, \frac{3}{2})$ isobar in π - N or γ - N collision. This universality is much more general. The properties of the isobar do not depend on the mechanisms of production.

The same situation seems to appear in the case of the fire ball. The fire ball with the same properties seems to appear in the final state of N - \bar{N} annihilation. This point will be discussed in the next section.

4. - Similarity of multiple productions in high energy N - N collision and in N - \bar{N} annihilation.

Now, let us suppose that our process of multiple production in N - N collision proceeds in the following two steps.

1) Formation of an excited nucleon (« isobar ») by the collision of an incident nucleon and pions surrounding the other nucleon.

2) Decay of the excited nucleon into a nucleon and a fire ball.

In FBS, the last step of our process can be characterized by the following scheme:

Isobar \rightarrow Nucleon + Fire ball

Momentum $\mathbf{P}^* \rightarrow \mathbf{P}^* \quad 0$

Energy $E^* + \mathcal{M} \rightarrow E^* \quad \mathcal{M}$



Fig. 7.

That is, the momentum of the « nucleon » does not change, the only change happens in its mass. The change of the mass energy will be deposited at the point of decay, and a fire ball will be formed around this point. This decay process seems to be similar to the N - \bar{N} annihilation process. Let us examine this similarity in more detail. For that purpose we shall examine the velocities of the relevant particles. On account of the Lorentz invariance of $Q_\mu P_\mu$, E^* is expressed by quantities in IBS:

$$(4.1) \quad E^* = \frac{\bar{E}\bar{Q}_0 - \mathbf{Q} \cdot \bar{\mathbf{P}}}{\mathcal{M}} = \frac{\sqrt{\bar{\mathbf{P}}^2 + M^2} \sqrt{\bar{\mathbf{P}}^2 + \mathcal{M}^2} + \bar{\mathbf{P}}^2}{\mathcal{M}} \simeq \mathcal{M} \frac{\bar{\mathbf{P}}^2}{\mathcal{M}^2} \left(1 + \sqrt{1 + \frac{\mathcal{M}^2}{\bar{\mathbf{P}}^2}} \right).$$

Therefore, the Lorentz factor of the nucleon γ_N^* will be

$$(4.2) \quad \gamma_N^* = \frac{E^*}{M} \simeq \frac{\mathcal{M}}{M} \frac{\bar{\mathbf{P}}^2}{\mathcal{M}^2} \left(1 + \sqrt{1 + \frac{\mathcal{M}^2}{\bar{\mathbf{P}}^2}} \right) \sim \sqrt{\frac{E_0}{M}}.$$

On the other hand, the Lorentz factor of pions in the fire ball is

$$(4.3) \quad \gamma_{\pi}^* = \frac{\varepsilon^*}{\mu} \simeq \frac{\varepsilon_0}{\mu} \simeq 3 \text{ or } 4.$$

Therefore, $\gamma_{N'}^* \gg \gamma_{\pi}^*$ holds in very high energy collisions. This means that the nucleon will go out from the fire ball in very short time after the decay. Hence, the structure of the fire ball will not be affected by the presence of the nucleon. This situation of pion cloud is very similar to the final state of the $N\bar{N}$ annihilation.

Next, we shall calculate the Lorentz factor of the hypothetical isobar γ^* . This is simply expressed by the quantities in IBS:

$$(4.4) \quad \gamma^* = \frac{E^* + M}{\sqrt{(E^* + M)^2 - \mathbf{P}^{*2}}} = \sqrt{1 + \frac{\mathbf{P}^2}{M^2}}.$$

In the case of equipartition, $\gamma^* = 1.4$. That is, the isobar is nearly at rest in the fire ball system, and Lorentz contraction of the volume of decay interaction is negligible. This is also a point similar to $N\bar{N}$ annihilation.

There exists much experimental evidence supporting this analogy. According to recent measurements⁽¹⁸⁾ of k_T in relatively low energy collisions:

$$(4.5a) \quad \langle k_T \rangle = (308 \pm 23) \text{ MeV/c} = (2.2 \pm 0.2)\mu,$$

which is very close to the mean value of the pion momenta emitted in $N\bar{N}$ annihilation⁽¹⁹⁾

$$(4.5b) \quad \langle k \rangle = 316 \text{ MeV/c}.$$

This similarity suggests the formation of fire balls with similar structures in both processes.

Another evidence is a regularity discovered by KANEKO and OKAZAKI⁽²⁰⁾. These authors plotted reduced multiplicity N^{\pm}/K (number of charged particles divided by inelasticity K) as a function of the incident energy E_0 in the C.M.S. in log scale (see Fig. 8). Then, all experimental points seem to line up on the same line. They also plotted the multiplicity of the $N\bar{N}$ annihilation by assuming that this process corresponds to the high energy collision in which the energy available for pion production is $2M$. (In the laboratory system, this corresponds

⁽¹⁸⁾ L. F. HANSEN and W. B. FRETTER: *Phys. Rev.*, **113**, 812 (1960).

⁽¹⁹⁾ W. H. BARKAS *et al.*: *Phys. Rev.*, **105**, 1037 (1957).

⁽²⁰⁾ S. KANEKO and M. OKAZAKI: *Nuovo Cimento*, **8**, 521 (1958); D. ITO, S. MINAMI and H. TANAKA: *Nuovo Cimento*, **9**, 208 (1958).

to a 6.5 GeV $N\bar{N}$ collision.) Then, this point also comes on the same line (see Fig. 8).

This regularity also supports our point of view. If we assume that the collision is symmetric, then two fire balls with equal masses will be formed by a 5.6 GeV collision. Moreover, if we assume that the properties of fire balls are independent of the mechanism of its formation (for example, $\langle k_T \rangle = \langle k \rangle$), then the multiplicity of the 6.5 GeV collision will be

$$(4.6a) \quad \langle N \rangle_{\text{coll}} = 2 \langle n \rangle = \frac{2M}{\sqrt{\langle k_T \rangle^2 + \mu^2}},$$

which should be compared with the multiplicity in $N\bar{N}$ annihilation

$$(4.6b) \quad \langle N \rangle_{\text{ann}} = \frac{2M}{\sqrt{\langle k \rangle^2 + \mu^2}}.$$

Of course, these two values must be the same.

As is well known, a simple statistical theory of multiple production can not correctly predict the multiplicity in $N\bar{N}$ annihilation, and the predicted average pion momentum $\langle k \rangle$ is too large. Therefore, the presence of some cut-off mechanism was anticipated. This situation does not change for jets, where $\langle k_T \rangle$ does not increase with the energy E_0 as predicted by the statistical theory. k^* seems to be cut-off. It seems therefore, natural to assume that the mechanism of this cut-off is the same and independent of the creation processes.

As the only particles existing in the final state of $N\bar{N}$ annihilation are pions, the density of which is very large, and as their relative momenta are of the order of several hundred MeV, it seems then that the pions are in favourable condition for pion-pion interaction. Therefore many attempts ⁽²¹⁾ have been made to interpret the possible cut-off by introducing pion-pion interaction.

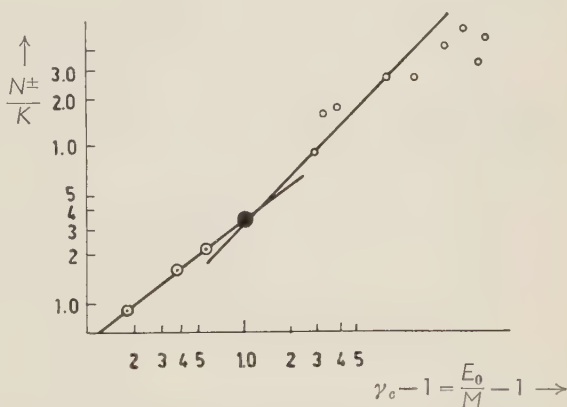


Fig. 8. - Variation of reduced multiplicity N^\pm/K with $\gamma_c - 1$; from Ito *et al.* ⁽²¹⁾. \circ cosmic ray data; \odot GeV p-p collision; \bullet p- \bar{p} annihilation.

⁽²¹⁾ D. ITO and S. MINAMI: *Soryusiron Kenkyu* (1957); F. CERULUS: *Nuovo Cimento*, **14**, 827 (1959).

Now, if pion-pion interaction plays an important role in $N\text{-}\bar{N}$ annihilation, then it will also be important in the fire ball formation in high energy collisions.

5. - Concluding remarks.

We shall summarize and discuss the main conclusions obtained in the preceding sections.

1) One of the difficulties in the problem of multiple production consists in its tremendous degrees of freedom. But after the discovery of two centered production of particles, it was recognized that the actual number of degrees of freedom is not so large. And if we take advantage of this fact, then there appears a possibility of characterizing the S -matrix by a relatively small number of parameters.

2) As we have shown in Sections 3 and 4, the properties of the fire ball are universal and it is produced as if it were an elementary particle. Perhaps, pion-pion interaction has an important role in the formation of fire balls. But even if this is true, a theoretical analysis will be very difficult because the fire ball system is essentially a many body system. Its properties are described by a partition function $Z_n(\mathcal{M})$ and one of the tasks of phenomenological analysis is to investigate the properties of this partition function.

3) On account of the possibility of treating the fire ball as if it were an elementary particle, the degrees of freedom of the collision will be reduced and it will be equivalent to the $N\text{-}N$ collision in which two new particles with indefinite masses are produced, the mass spectrum of which is the partition function Z_n .

4) By introducing the momentum transfer 1 and dividing the process into two parts, it proceeds in two steps such as,

$$\pi + N \rightarrow N + \mathcal{M}; \quad \mathcal{M} = \text{fire ball.}$$

In the center of mass system of this collisions (IBS) there are three kinds of degree of freedom: 1 , 0 and \mathcal{M} (or the parameter ξ which describes the partition of energy between the translational and the internal degrees of freedom.)

5) In this paper, we have tried to characterize the S -matrix by the average and some higher momenta of the distribution of the S -matrix in these degrees of freedom, and fixed some of the parameters by comparing with ex-

periments. By using these results the other properties of the process are predicted.

a) In Section 2, we have assumed $\langle |\Delta| \rangle \simeq M$. This may be connected with the structure of the nucleon but we have made no analysis on this point. Nevertheless, many important conclusions are derived from this assumption which were compared with experiments. For example, the maximum of the multiplicity will be proportional to $\sqrt{E_0}$ and the fluctuation of n partly comes from that of Δ_0 , which will be characterized by the second momentum of the distribution of the S -matrix.

b) The angular distribution $S(\theta)$ is not fully discussed. From the analogy with π - N scattering, $\langle \theta \rangle$ may be small. But this angular distribution will be clear by the analysis of the asymmetric production (angular distribution) of the fire ball.

c) In this paper, our main efforts are concentrated on the phenomenological analysis of the ξ -distribution. The mean values $\langle \xi \rangle$ and $\langle \xi^2 \rangle$ are responsible for multiplicity, the lower limit of inelasticity, their fluctuation, etc. From the value of $\langle \xi \rangle$ fixed by experiments, we can conclude that an approximate equipartition holds in IBS (see Sections 2 and 3). We get also some information on the n -distribution of the S -matrix.

6) The main purpose of the present paper is to propose the method of analysing the high energy multiple production in terms of the S -matrix and to give illustrative examples, showing the usefulness of this method. Therefore, the analysis could not cover all the phenomena. A more comprehensive analysis along this line will be published soon.

In order to understand the high energy multiple production in more detail, the next step will be to develop a dynamical theory starting from first principles. We have to explain why the assumptions 1 and 2 hold in high energy collisions. The total cross-sections may be of great interest too. We shall come back to these problems in the near future.

* * *

We would like to express our sincere thanks to Professor G. WATAGHIN for his illuminating discussions during his stay in São Paulo and to Professor M. MIESOWICZ for his kind informations regarding the two-center model. Two of the present authors (D.I. and T.M.) deeply appreciate the hospitality extended to them by Dr. J. H. LEAL FERREIRA, President of Instituto de Física Teórica, São Paulo.

RIASSUNTO (*)

Facciamo un tentativo di analizzare, con considerazioni fenomenologiche basate sul modello a due centri, la struttura degli elementi della matrice S per la produzione multipla. Partiamo da due ipotesi: 1) le distribuzioni della quantità di moto dei pioni emessi nel cono anteriore e posteriore sono isotropiche in ogni sistema rispetto al centro di massa (il sistema di riposo della sfera di fuoco) e i valori medi ε_0 delle energie dei pioni in quei sistemi non dipendono dai dettagli delle collisioni; 2) il valore medio del trasferimento d'impulso Δ è sempre dell'ordine della massa M del nucleone. Da queste ipotesi deduciamo nella Sez. 2 i seguenti risultati: 1) la molteplicità è data da $n \simeq \xi \sqrt{2E_0 |\Delta| / \varepsilon_0}$, in cui ξ è il rapporto M / M_{\max} fra la massa M della sfera di fuoco ed il suo valore massimo M_{\max} . Sperimentalmente $\xi \simeq 0.5$ a 10^{13} eV; 2) il limite inferiore dell'anelasticità è dato da $K \geq \xi^2$. Discutiamo la relazione fra molteplicità ed anelasticità; 3) nel sistema del centro di massa della sfera di fuoco e del nucleone di rinculo (« sistema isobaro », IBS) anche il rapporto $|\mathbf{p}|/M$ fra il momento \mathbf{p} del nucleone e la massa M della sfera di fuoco è espresso dal parametro ξ nella forma $|\mathbf{p}|/M = (1 - \xi^2)/2\xi$. A 10^{13} eV abbiamo $|\mathbf{p}|/M \simeq 1$. Questo significa che l'equazione dell'energia è approssimativamente valida per i tre gradi di libertà possibili: il moto del nucleone di rinculo, il moto di traslazione e quello interno della sfera di fuoco. $|\mathbf{p}| \ll M$ è escluso, a meno che K sia uno, in contrasto con gli esperimenti; 4) quando vale l'equipartizione, il valore medio dell'impulso trasversale è costante ed il suo valore è dell'ordine di ε_0 . Nella Sez. 3 discutiamo la dipendenza della matrice S da M e da n . E, usando i corrispondenti risultati, stimiamo l'asimmetria dei numeri di particelle n_1 ed n_2 emesse nei coni anteriore e posteriore. Il parametro $[\langle (n_1 - n_2)^2 \rangle / \langle (n_1 + n_2)^2 \rangle]^{1/2}$, misura dell'asimmetria, diventa $\frac{1}{3}$ a causa della sola fluttuazione statistica. Diventa maggiore se il trasferimento di energia Δ_0 non è nullo. Discutiamo anche le condizioni alle quali il valore medio ε_0 dell'energia dei pioni nella sfera di fuoco è costante. Le proprietà della sfera di fuoco sembrano essere indipendenti dal meccanismo con il quale si produce. Estendendo questo modo di vedere, nella Sez. 4 discutiamo la similarità fra la produzione multipla nelle collisioni $N-N$ e nelle annichilazioni $N-\bar{N}$. Nella Sez. 5 esponiamo le conclusioni.

(*) Traduzione a cura della Redazione.

(n, α) and (n, p) Reactions in CsI Crystal with 14 MeV Neutrons.

G. M. MARCAZZAN, E. MENICHELLA SAETTA and F. TONOLINI

Laboratori C.I.S.E. - Milano

(ricevuto il 1° Febbraio 1961)

Summary. — This paper will present the energy spectra of α and of protons emitted in (n, α) and (n, p) reactions with 14 MeV neutrons on a CsI(Tl) crystal. These spectra were obtained by employing a new method of mass discrimination to distinguish different particles in the CsI(Tl) crystal. Total cross-section value for (n, α) reactions has been also obtained.

Introduction.

The number of data accumulated from recent experiments on n, p reactions produced by 14 MeV neutrons, on various elements, especially light and medium, have furnished the possibility of a good comparison with the previsions of the statistical theory ^(1,2) and an estimate of the contribution of direct effects ⁽³⁾.

Experimental data on the reactions (n, α) can give further interesting information on the mechanism of the nuclear reactions at medium energies and, in the case of evaporative processes, on the densities of the energy levels of the nuclei.

While the cross-section values for a certain number of elements are known, though inconsistent sometimes, the angular and energy distributions of emitted particles have been observed only in some cases ⁽⁴⁾. For nuclei with $Z > 50$,

⁽¹⁾ U. FACCHINI, I. IORI and E. MENICHELLA: *Nuovo Cimento*, **16**, 1109 (1960).

⁽²⁾ D. L. ALLAN: *Nucl. Phys.*, to be published.

⁽³⁾ L. COLLI: *Suppl. Nuovo Cimento*, **16**, 67 (1960).

⁽⁴⁾ I. KUMABE, E. TAKEKOSHI, H. OGATA, Y. TSUNEOKA and S. ŌKI: *Phys. Rev.*, **106**, 155 (1957); *Journ. Phys. Soc. of Japan*, **13**, no. 2 (1958).

however, the spectra of the emitted particles are not known, and this is due to the difficulty of creating an adequate technique that will obtain the desired information with good statistics, since the cross-section for reactions (n, α) is very small in these cases ⁽⁵⁾.

The present work describes a measurement of the spectrum of α -particles emitted in reaction (n, α) and produced in a CsI(Tl) crystal. The identification of the α -particles among the various other particles (electrons, protons, deuterons) produced by the irradiation of neutrons in the crystal, was made possible by a discrimination technique based on the different shape of scintillation pulses in the CsI(Tl) crystals.

Parallel to the α -particle measurement a spectrum of protons from (n, p) reaction has been obtained.

1. - Experimental layout.

The 14 MeV neutrons are obtained from a $^3\text{H}(d, n)^4\text{He}$ reaction, with a beam of deuterons produced by a 150 kV accelerator.

Deuteron currents of a few μA are sufficient for the measurements discussed here.

A CsI(Tl) crystal, 4.3 cm thick and 3.8 cm in diameter, acts simultaneously as target and detector for the reaction under study. It is directly coupled, by means of a silicone oil optical contact, with a Dumont 6292 photomultiplier. A thin layer of aluminium (0.18 mg/cm^2) serves as a light reflector. The crystal is placed at a few cm distance from the tritium target and is directly bombarded by the neutron beam.

The neutrons generate a great number of pulses in the crystal, a great part of which is due to secondary electrons of γ -rays, or to β radioactivity, and another part is made up of protons, deuterons and α -particles produced in the various nuclear reactions. The method used for separating the various particles, described in the next section enables us to separate the various types of pulses, particularly those due to α -particles.

Once separated, these pulses are sent to a 100-channel analyser by means of which the energy spectrum of the examined particles is obtained. (Fig. 1 shows a block diagram of the electronic apparatuses).

Measurements have been done on the α -particles spectrum and on the proton and deuteron spectrum. Deuterons have not been separated from protons because of their small number.

A scaler performs counting over a prefixed threshold; it is possible to

⁽⁵⁾ R. F. COLEMAN, B. E. HAWKER, L. P. O'CONNOR and J. L. PERKIN: *Proc. Phys. Soc.*, **73**, 215 (1959).

obtain, the flux of neutrons being known, the value of the average cross-section of (n, α) reaction on the crystal.

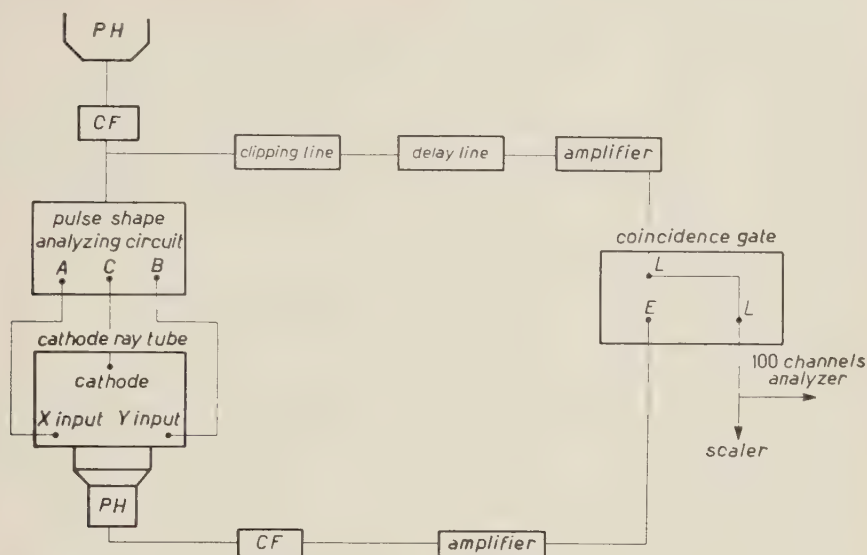


Fig. 1. - Block diagram of the electronic chain set up for energy analysis of α particles and protons.

The flux of neutrons is measured with a spectrometer, of the recoil proton type, which uses a thin sheet of polythene as radiator and a CsI(Tl) crystal as detector. Because it gives a well-defined peak of 14 MeV neutrons, this type of monitor is particularly stable in time, and does not undergo small changes whether of gain in the amplification chain or of the discriminator level.

2. - Separation method.

A certain number of recent studies has shown ⁽⁶⁻⁹⁾ how the temporal shape of the luminous emission of many scintillators depends on the specific ioni-

⁽⁶⁾ F. D. BROOKS: *Prog. Nucl. Phys.*, **5**, 284 (1956); *New Instruments and Methods*, **4**, 151 (1958).

⁽⁷⁾ G. P. WRIGHT: *Proc. Phys. Soc.*, **69 B**, 358 (1956).

⁽⁸⁾ R. B. OWEN: *Proc. of Scintillation Counter Symposium* (Washington, 1958); *Proc. IRR*, NS **5**, 3-4 (1958).

⁽⁹⁾ R. S. STOREY, W. JACK and A. WARD: *Proc. Phys. Soc.*, **72**, 1 (1958).

zation of the ionizing particle. In recent years, various methods (^{6,8,10-12}) have been developed which permit the separation of scintillation pulses due to particles of different mass.

In the case of CsI(Tl) STOREY and co-workers (⁹) have found that the fluorescence decay due to an ionized particle can be described with a good approximation in terms of two exponential components: one fast (responsible for the greater part of the luminous emission) and another slower.

The former depends on the specific ionization of the particles and has, for instance, a half-life of $(0.425 \pm 0.025) \mu\text{s}$ for 4.8 MeV α -particles and $(0.7 \pm 0.025) \mu\text{s}$ for 0.66 MeV electrons respectively, while the latter proves to be independent of the density of ionization.

On the basis of this difference in the temporal shape of the pulses, a device to analyse them has recently been developed in our laboratories by L. VARGA (*).

We discuss here simply the lines of this method.

The signal S that distinguishes the various particles is obtained by a suitable combination between a pulse representing the total light emitted in the scintillation and one corresponding to the fraction of light collected from zero time to a prefixed time.

For simplicity, reference will be made to two particles only: protons and deuterons for instance. $X_p(t)$ and $X_d(t)$ represent the average rate of photoelectrons emitted from the photocathode as a function of time and corresponding to the law of emission of light from the crystal.

Let us consider that two particles (proton and deuteron) have such energies as to give the same number of total photoelectrons, we have

$$(1) \quad \int_0^{\infty} X_p(t) dt = \int_0^{\infty} X_d(t) dt = N,$$

N is the total number of photoelectrons emitted by the photocathode.

Let us now consider separately the number of photoelectrons emitted by the photocathode in an interval of time from 0 to a given time τ , and subsequently from τ to ∞ : let

$$(2) \quad \left\{ \begin{array}{ll} \int_0^{\tau} X_p(t) dt = P & \int_{\tau}^{\infty} X_p(t) dt = p, \\ \int_0^{\tau} X_d(t) dt = D & \int_{\tau}^{\infty} X_d(t) dt = d, \end{array} \right.$$

(¹⁰) M. FORTE: A/CONF/15/P/1514 (Geneva, 1958).

(¹¹) J. C. ROBERTSON and A. WARD: *Proc. Phys. Soc.*, **73**, 523 (1959).

(¹²) V. M. BORMANN, G. ANDERSSON LINDSTRÖM, H. NEUERT and H. POLLEHN: *Zeits. f. Naturf.*, **14 a**, 681 (1959).

(*) To be published in *Nuclear Instruments*.

where P and p , D and d depend on the shape of the pulse, while it follows from (1) that $P + p = D + d$. For τ , the time is chosen in which the two normalized time distributions $X_p(t)$ and $X_d(t)$ intersect. Such time is of the order of $(0.7 \div 0.8) \mu\text{s}$ and depends slightly on the couple of particles under study. The identification signal of the particle furnished by our circuit, which will be indicated with S_p for protons and S_d for deuterons, is given, as has been said, by a suitable linear combination of P and p , and respectively of D and d , and can be indicated with

$$(3) \quad \begin{cases} S_p = P - (1 - C)(P + p), \\ S_d = D - (1 - C)(D + d), \end{cases}$$

where C is a constant of value $0 < C < 1$. We note that both these signals are proportional to the total number of photoelectrons N , that is to the energy of the particles under study.

To study the discriminating effect, we will consider the difference between the two signals given by

$$(4) \quad \varepsilon = (S_p - S_d) = P - D = d - p \neq 0,$$

ε is affected by the statistical fluctuations of P , p , D , d . Supposing that such factors have fluctuations according to the statistics of Poisson we have

$$(5) \quad \Delta\varepsilon = \sqrt{(\Delta S_p)^2 + (\Delta S_d)^2},$$

in which

$$\Delta S_p = \sqrt{C^2 P + (1 - C)^2 p};$$

similarly

$$\Delta S_d = \sqrt{C^2 D + (1 - C)^2 d}.$$

The ratio between the signal and the noise correlated to the same signal depends, therefore, on the value of the constant C . This constant can be chosen in such a way that the ratio $\varepsilon/\Delta\varepsilon$ is maximum⁽¹³⁾.

Such value of C (C optimum) turns out to be

$$(6) \quad C = 1 - \frac{P + D}{2}.$$

⁽¹³⁾ E. GATTI: *Rendiconti Seminario Matematico-Fisico*, vol. XXXI (1960), p. 1.

The type of circuit that produces the signal S , is particularly simple (Fig. 2: outlet B of the circuit). The scintillation is collected at the anode of a photomultiplier Du Mont 6292, and the current pulse integrated on the parasite capacity and with an anodic resistance of $R = 1.5 \text{ M}\Omega$, after a cathode follower, is shaped with a first delay line of 2500Ω of characteristic

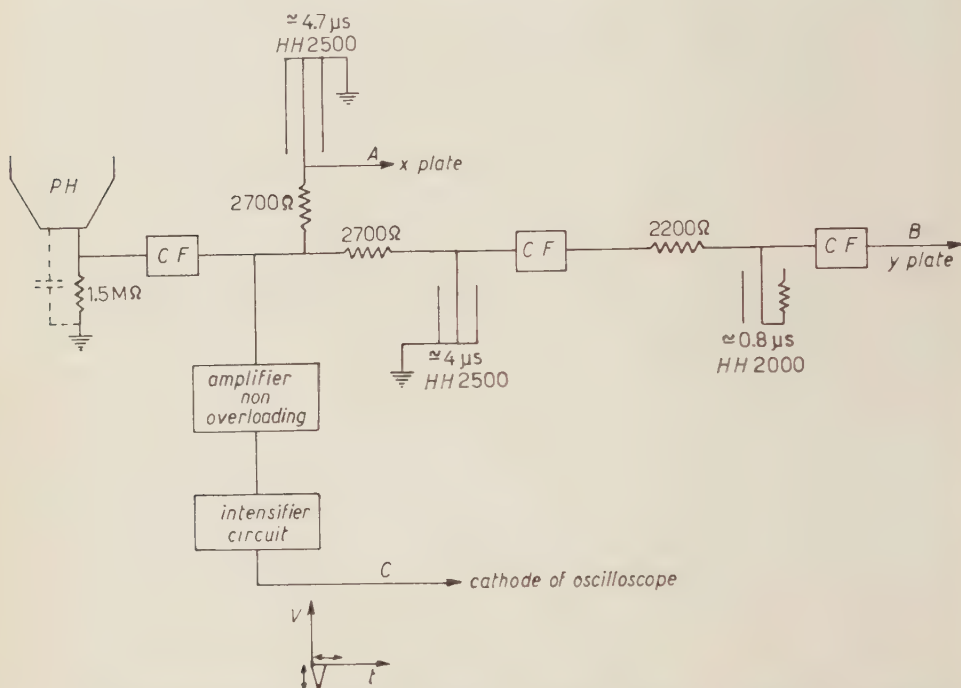


Fig. 2. - Pulse shape discriminating circuit, outlets: A) energy; B) final wave shape; C) intensifier pulse for the oscilloscope cathode.

impedance and delay time t_0 of the order of $4 \mu\text{s}$; and then with a second and shorter delay line of 2000Ω characteristic impedance and delay time τ closed over a variable resistance R_0 .

Time t_0 of the first line is chosen in such a way that the integrated current pulse has reached the maximum for the various types of particles.

The shape of the final wave supplied by the circuit is therefore obtained by adding to the integrated and shaped current pulse of the phototube the same pulse inverted and delayed by the time τ , and reduced in amplitude by a factor C . The shape of the resulting pulse is shown in Fig. 3. From the examination of the pulse, it is easy to see that the signal S considered is given by the value of the amplitude of the resulting pulse at time $t_0 + \tau$.

The value of C depends on the value of the resistance on which the second delay line is closed. It can be seen from the formula, therefore, that with the



Plate I. - Distribution on the cathode ray tube screen of the S pulses as function of energy for electrons, protons, deuterons, α (bottom to top).



Plate II. - Distribution on the cathode ray tube screen of the S pulses as function of the energy, for secondary electrons from γ rays of ^{60}Co and for α particles from ^{210}Po .



Plate III. - Distribution on the cathode ray tube screen of the particles produced by 14 MeV neutrons in CsI(Tl) crystal. The protons and deuterons are not well separated. Clearly visible are the α -particles of high energies produced in the (n, α) reaction.

optimum value of C the amplitude values of pulses S corresponding to two different particles under examination are equal and of opposite sign. Since there are usually more than two types of particles involved, it is necessary to compare directly the signals S with a signal that gives the energy of the particles, that we call E signal (Fig. 2: outlet A of the circuit).

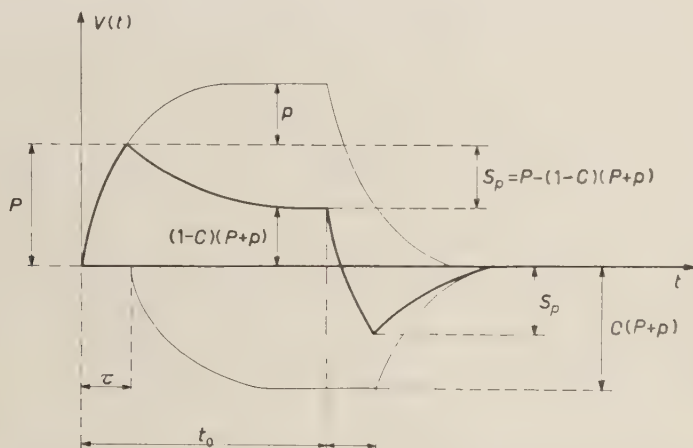


Fig. 3. - Wave shape of the signal leaving the discriminating circuit at B , in the case of protons.

Such comparison is made by sending the E signal corresponding to the energy of the particle and the S signal respectively to the axes X and Y of a cathode ray tube. The luminousness of the cathode ray tube, kept faint normally, is suitably intensified at the time $t_0 + \tau$. The pulses produce bright points which are distributed over almost-straight lines leading out of the zero, each of which has a value of S for ordinate and the particle energy for abscissa.

The cathode of the oscillograph is commanded by the energy signal appropriately amplified by a non-overloading amplifier and converted into a fast standard pulse (of ≈ 100 ns duration) of adjustable amplitude, that can be delayed by a time $t_0 + \tau$.

The complete schema of the pulse shape-discriminating circuit is shown in Fig. 2.

An example of the results is given in Plate I, obtained by irradiating with 14 MeV neutrons a target of paraffin and deuterated paraffin, placed in direct contact with the crystal.

The parameters of the circuit ($\tau = 0.8 \mu\text{s}$, $R_c = 1000 \Omega$) have been so determined as to produce the maximum separation between protons and deuterons.

Plate II on the other hand shows the separation obtained between the secondary electrons of rays from a ^{60}Co source and α -particles of ^{210}Po .

3. - Measurements and results.

Plate III gives a panorama of the distribution of the various luminous points on the cathode ray tube screen produced in the CsI(Tl) crystal described in Section 1 when irradiated with a flux of neutrons of 10^7 n/s. From bottom to top are recognized the regions of electrons, protons and deuterons, and finally, well apart, the region of α -particles.

To maintain a good and stable separation between the α -particles and the proton-deuteron group it was not advisable to increase the flux of neutrons.

Numerous preliminary tests were performed in order to reach a good degree of separation of the particles and a reasonable energy resolution, and to obtain a calibration of the energy scale, both for protons and α -particles.

The energy of the α -particles was calibrated, using a source of ^{210}Po ($E_\alpha = 5.3$ MeV) and one of ^{214}Po (RaC') ($E_\alpha = 7.68$ MeV).

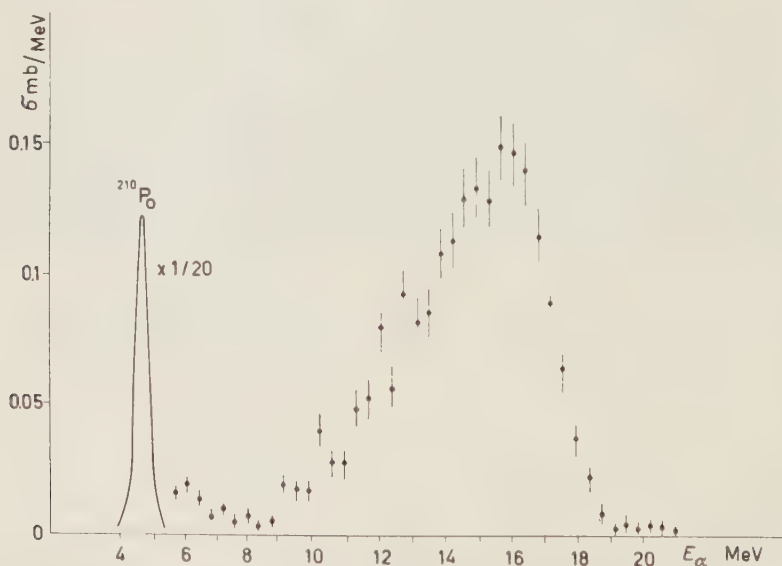


Fig. 4. - Spectrum of the α -particles emitted in the (n, α) reaction on CsI(Tl) .

The points are compared and normalized to the Quinton curve ⁽¹⁴⁾ which gives the response of a CsI(Tl) crystal as function of the energy of α -particles. The curve so obtained was later used to obtain the response of the crystal

⁽¹⁴⁾ A. R. QUINTON, C. E. ANDERSON and W. J. KNOX: *Phys. Rev.*, **115**, 886 (1959).

at higher energies than 10 MeV, as sources of particles at these energies were not available, and to obtain the proton energy scale.

In view of the non-linearity in the response of the crystal and the rather indirect method of calibration used, the uncertainty in the values of the energy scale is about 10%.

The energy resolution for the line of ^{214}Po turned out to be 8%. It was assumed that the behaviour of a thick crystal was identical to that of a thin one, and from comparative measurements this assumption was substantiated to within 5%.

With the technique and the apparatus described in the previous section, it was possible to obtain the spectra of the reaction (n, α) and (n, p) in the crystal. Fig. 4 and 5 give these distributions.

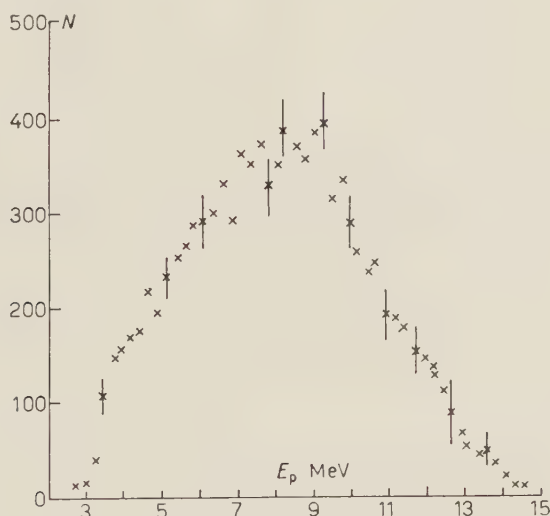


Fig. 5. - Spectrum of the protons emitted in the (n, p) reaction on CsI(Tl).

In the portion of lower energy, the spectrum of the protons contains a contribution of reactions of the type (n, np) and (n, d). In the spectrum (n, α) the line of ^{210}Po was simultaneously analysed.

The value of the total cross-section of the reaction (n, α) turned out to be (0.8 ± 0.2) mb.

4. - Discussion.

With the technique described it has been possible to obtain an energy distribution of the emitted particles over the whole solid angle, with good

On the Effect of n-p Tensor Forces in ${}^3\text{H}_\Lambda$ - I (*).

B. BARSELLA and S. ROSATI

Istituto di Fisica dell'Università - Pisa

Istituto Nazionale di Fisica Nucleare - Sezione di Pisa

(ricevuto il 2 Febbraio 1960)

Summary. — Calculations have been done on the hypertriton with a hamiltonian containing a neutron-proton potential with a tensor part. The integral volume of $\Lambda\text{-}N$ interaction and the wave function parameters are modified to a certain extent with respect to the results of preceding calculations, performed with a purely central potential. It is concluded that a more refined calculation will be necessary to get a definite answer to the question of the importance of n-p tensor corrections in ${}^3\text{H}_\Lambda$.

1. - Introduction.

This paper contains some preliminary results of a work on the effect of tensor forces among nucleons in Λ -hyperfragments. We have done a calculation on the simplest system containing a Λ^0 , that is the hypertriton. The reason for this choice is that the hypertriton is the hyperfragment with the simplest structure and does not require drastic approximations for its description. The preceding calculations ⁽¹⁾ have been performed using a central neutron-proton potential. The parameters of the potential were determined by the prescription to fit the p-p low energy scattering data and the deuteron binding energy. We have introduced into the hamiltonian a neutron-proton tensor term: the aim of this work is to see if the introduction of these corrections influences in some way the prediction of integral volumes of the Λ -nucleon

(*) This work has been presented at the XLVI Congress of the Italian Physical Society, Naples, 29 September - 5 October 1960.

(1) R. H. DALITZ and B. W. DOWNS: *Phys. Rev.*, **110**, 958 (1958) (this work will be indicated by D.D.I); R. H. DALITZ and B. W. DOWNS: *Phys. Rev.*, **114**, 593 (1959).

potential. At the same time we want to see if there are modifications in the wave function which could influence the calculation of decay probabilities and branching ratios for the various decay channels. Such a calculation will be done in a subsequent paper.

In this work we have restricted ourselves to a preliminary calculation, which has been done in the simplest way compatible with tensor corrections.

2. - Construction of trial wave functions.

The possible values of the spin of hypertriton are $\frac{1}{2}$ and $\frac{3}{2}$. We must therefore construct trial functions corresponding to such spin values. To discuss this we shall use the following notation (*):

$$\begin{aligned} \mathbf{L} &= \mathbf{l}_1 + \mathbf{l}_2, & \mathbf{s} &= \frac{1}{2}(\boldsymbol{\sigma}_p + \boldsymbol{\sigma}_n), & \mathbf{S} &= \mathbf{s} + \frac{1}{2}\boldsymbol{\sigma}_\Lambda, \\ \mathbf{L} + \mathbf{s} &= \mathbf{j}, & \mathbf{L} + \mathbf{S} &= \mathbf{J}, \end{aligned}$$

where \mathbf{l}_1 is the neutron-proton relative angular momentum,

\mathbf{l}_2 is the angular momentum of the Λ with respect to neutron-proton center of mass,

$\boldsymbol{\sigma}_p, \boldsymbol{\sigma}_n, \boldsymbol{\sigma}_\Lambda$ are the Pauli spin vectors for the proton, neutron and Λ , respectively.

The selection of trial wave functions is strongly determined by the following consideration: suppose that we are performing a variational calculation for the binding energy of some system and that we would like to use a trial function which is a linear combination of the functions Ψ and Ψ' . Suppose further that the matrix element of the hamiltonian between Ψ and Ψ' is zero: then the mean value of the hamiltonian will reach its minimum in correspondence of the choice of only Ψ or only Ψ' . In our case this is equivalent to say that we must choose as trial wave functions only those composed of parts which are linked by the neutron-proton central potential plus tensor part. Let us now limit our discussion to the case of spin $\frac{1}{2}$; then the maximum value of L is two. Let us list the spin functions which may constitute our trial function; these are the following (**):

$$\begin{array}{lll} S_1) & L = 0 & s = 0 \quad l_1 = l_2 = 0 \\ S_2) & L = 0 & s = 1 \quad l_1 = l_2 = 0 \end{array}$$

(*) We have chosen units such that $\hbar=c=1$.

(**) We have omitted the functions $S_{3,4}$: $L=0, s=0, 1, l_1=l_2=1$ because they are excluded on the same grounds of D_3 . Note also that the symbol P represents three functions which correspond to different values of S and s .

$P)$	$L = 1$	$l_1 = l_2 = 1$		
$D_1)$	$L = 2$	$S = \frac{3}{2}$	$l_1 = 2$	$l_2 = 0$
$D_2)$	$L = 2$	$S = \frac{3}{2}$	$l_1 = 0$	$l_2 = 2$
$D_3)$	$L = 2$	$S = \frac{3}{2}$	$l_1 = l_2 = 1$	

Preceding calculations ⁽¹⁾ have used S_2 . We have chosen a linear combination of S_2 and D_1 and have excluded the others for the following reasons:

- S_1 can be excluded because neither central forces nor tensor forces link spin 1 to spin 0 states.
- P and D_3 states are excluded by the fact that neutron-proton forces do not mix proton-neutron states with different orbital parity.
- D_2 is excluded by the fact that we assume the $\Lambda\mathcal{N}$ potential does not contain tensor terms.

In the case of spin $\frac{3}{2}$ for the hypertriton, the preceding considerations must be partially modified. It is permitted to consider also the value $L = 3$. On the other side this value is excluded for it would require $l_1 = l_2 = 2$ and such a state would not be linked with the others by the potentials. State S_1 cannot be constructed for spin requirements. State D_1 is splitted in two states according to the fact that S can assume both the values $\frac{1}{2}$ and $\frac{3}{2}$. We shall call these states D_1' and D_1'' .

The trial wave functions for spin $\frac{1}{2}$ and $\frac{3}{2}$ are therefore given by:

$$(1) \quad \begin{cases} \Psi_{\frac{1}{2}} \propto f(r, s, t) \Phi_{s_3} + x g(s, r, t) \Phi_{D_1}, \\ \Psi_{\frac{3}{2}} \propto f(r, s, t) \Phi_{s'_1} + x g(r, s, t) \Phi_{D'_1} + y h(r, s, t) \Phi_{D''_1}, \end{cases}$$

where f, g, h are normalized functions of the triangular co-ordinates r, s, t (r is the neutron-proton distance, $s(t)$ the Λ -proton (neutron) distance); x and y are coefficients whose square gives the percentage of D states. The symbols Φ represent the normalized spin functions corresponding to the states defined by their subscripts. The complete form of functions (1) is given in Appendix A.

For the radial functions f, g, h we have chosen simple exponentials of the form

$$f \propto \exp [-\alpha(s+t) - \beta r], \quad g \text{ and } h \propto r^2 \exp [-\gamma(s+t) - \delta r],$$

symmetrical in s and t according to charge symmetry of Λ -nucleon forces. To simplify the calculations we have also chosen $g = h$ in $\Psi_{\frac{3}{2}}$. This is not strictly necessary but results in a considerable reduction of variational parameters.

3. - Variational calculation.

The hamiltonian which we shall use in the variational calculation is the following

$$H = K + V[A] + V_c[np] + V_t[np],$$

where K is the three-body kinetic energy and

$$V[A] = - (U_1 + U_2 \boldsymbol{\sigma}_p \cdot \boldsymbol{\sigma}_\Lambda) \frac{\exp[-\lambda s]}{s^n} - (U_1 + U_2 \boldsymbol{\sigma}_n \cdot \boldsymbol{\sigma}_\Lambda) \frac{\exp[-\lambda t]}{t^n}$$

($n = 0$, exponential shape; $n = 1$, Yukawa shape),

$$(2) \quad V_c[np] = - (W_1 + W_2 \boldsymbol{\sigma}_n \cdot \boldsymbol{\sigma}_p) \frac{\exp[-kr]}{r},$$

$$V_t[np] = - W_3 \frac{\exp[-\eta r]}{r} S_{np}(\mathbf{r}), \quad S_{np}(\mathbf{r}) = \frac{1}{r^2} [3(\boldsymbol{\sigma}_n \cdot \mathbf{r})(\mathbf{r} \cdot \boldsymbol{\sigma}_p) - (\boldsymbol{\sigma}_n \cdot \boldsymbol{\sigma}_p)r^2].$$

The variational calculation is then stated in the following way: if Ψ is the trial function then the inequality must hold

$$(3) \quad - (B_d + B_\Lambda) \leq \frac{\langle \Psi | H | \Psi \rangle}{\langle \Psi | \Psi \rangle},$$

B_Λ is defined as the difference between the absolute value of the ${}^3\text{H}_\Lambda$ binding energy and the absolute value of the deuteron binding energy, B_d .

In the case of spin $\frac{1}{2}$ the expression on the right side of (3) can be written

$$(4) \quad \frac{\langle \psi_{\frac{1}{2}} | H | \psi_{\frac{1}{2}} \rangle}{\langle \psi_{\frac{1}{2}} | \psi_{\frac{1}{2}} \rangle} = P + Q(U_1 + U_2) - R(U_1 - 2U_2),$$

P , Q , R are functions of the variational parameters and of the potential parameters. The whole dependence on U_1 and U_2 has been shown explicitly. Now Q is, with respect to P and R , of order x^2 , which is presumed to be smaller than 0.05 (*). This is the reason why we have set in place of $(U_1 + U_2)$ in the right-hand side of (4) the value deduced from the results of DALITZ and

(*) To justify this point one might notice that the ${}^3\text{H}_\Lambda$ can be considered as composed by a deuteron with a Λ bound to it. According to the small value of B_Λ , one can presume that the deuteron is not much deformed by the presence of the Λ and so the D -state percentage in the ${}^3\text{H}_\Lambda$ must be of the order of that in the deuteron.

Downs⁽²⁾. Such an approximation would not change substantially our results. (4) can now be written as

$$\frac{\langle \psi_{\frac{1}{2}} | H | \psi_{\frac{1}{2}} \rangle}{\langle \psi_{\frac{1}{2}} | \psi_{\frac{1}{2}} \rangle} = P' - R' \bar{U}_2 (J = \tfrac{1}{2}),$$

where $\bar{U}_2(J = \tfrac{1}{2})$ is the total integral volume for spin $\tfrac{1}{2}$:

$$\begin{aligned} \bar{U}_2(J = \tfrac{1}{2}) &= \frac{16\pi}{\lambda^3} (2U_2 - U_1), \quad \text{for exponential shape,} \\ &= \frac{8\pi}{\lambda^2} (2U_2 - U_1), \quad \text{for Yukawa shape.} \end{aligned}$$

From (3) one gets

$$(5) \quad \bar{U}_2(J = \tfrac{1}{2}) \leq \frac{1}{R'} [P' - (B_d + B_\Lambda)];$$

(5) can be written, showing the x -dependence of the right side, in the following form:

$$(6) \quad \bar{U}_2(J = \tfrac{1}{2}) \leq G[A + Bx + Cx^2],$$

where G, A, B, C are functions of $\alpha, \beta, \gamma, \delta$ and of the potential parameters, but U_1 and U_2 .

In the case of spin $\tfrac{3}{2}$, the expression on the right side of (3) has the form

$$\frac{\langle \psi_{\frac{3}{2}} | H | \psi_{\frac{3}{2}} \rangle}{\langle \psi_{\frac{3}{2}} | \psi_{\frac{3}{2}} \rangle} = P_1 + Q_1(2U_1 - U_2) - R_1(U_1 + U_2),$$

Q_1 is of order $(x^2 + y^2)$; with the preceding approximation, one can obtain, in conclusion, the analogous of (6) for spin $\tfrac{3}{2}$

$$(7) \quad \bar{U}_2(J = \tfrac{3}{2}) \leq G \left[A + \frac{B}{\sqrt{2}} (x + y) + C(x^2 + y^2) \right],$$

where G, A, B, C are the same functions as before. $\bar{U}_2(J = \tfrac{3}{2})$ is given by

$$\begin{aligned} \bar{U}_2(J = \tfrac{3}{2}) &= \frac{16\pi}{\lambda^3} (U_1 + U_2), \quad \text{for exponential shape,} \\ &= \frac{8\pi}{\lambda^2} (U_1 + U_2). \quad \text{for Yukawa shape.} \end{aligned}$$

⁽²⁾ For exponential shape see: R. H. DALITZ and B. W. DOWNS: *Phys. Rev.*, **111**, 967 (1958). For Yukawa shape see: R. H. DALITZ and B. W. DOWNS: *Phys. Rev.*, **114**, 593 (1959). In the latter case we have used the results for gaussian shape because there is not substantial difference.

The right sides of (6) and (7) are simple functions of the mixing parameters x and y and one could search for the minimum with respect to them. The minimum of the right side of (6) is reached for

$$x = -B/2C,$$

which gives

$$(8) \quad \bar{U}_2(J = \tfrac{1}{2}) \leq G \left[A - \frac{B^2}{4C} \right].$$

In (7) one finds that the minimum is obtained if

$$x = y = -\frac{\sqrt{2}B}{4C},$$

and (7) reduces to

$$\bar{U}_2(J = \tfrac{3}{2}) \leq G[A + \sqrt{2}Bx + 2Cx^2] = G \left[A - \frac{B^2}{4C} \right],$$

which has the same form of (8). Then there is no difference between the spin $\frac{1}{2}$ and $\frac{3}{2}$ cases except on the different dependence of \bar{U}_2 upon U_1 and U_2 . From now on we shall consider only, for definiteness, the case of spin $\frac{1}{2}$. Then (8) represents the basis of our calculations. The detailed form of G , A , B and C is given in Appendix B.

4. - Results and discussion.

The parameters of the neutron-proton potential (2) are not rigorously determined by the experimental data. Then the variational calculation has been done for five sets of parameters (see Table I) selected from Table VI of Feshbach and Schwinger's paper ⁽³⁾; all the sets give a triplet effective range which agrees with the experimental value. It is worth while to notice that these five potentials give the correct deuteron binding energy. We have used the preceding potentials to make a variational calculation on the deuteron for two reasons:

- i) We wanted to have a reasonable starting point for the parameters which describe the deuteron in the wave function of ${}^3\text{H}_\Lambda$.
- ii) We wanted to check the validity of the approximation of our treatment of the deuteron core of hypertriton.

(3) H. FESHBACH and J. SCHWINGER: *Phys. Rev.*, **84**, 194 (1951).

TABLE I. - *Neutron-proton potential parameters.*

Neutron-proton potential parameters	$W_1 + W_2$ (MeV·fermi)	W_3 (MeV·fermi)	k (fermi ⁻¹)	η (fermi ⁻¹)	$ x $
a)	34.46	20.99	0.7402	0.7236	0.205
b)	46.92	16.88	0.8425	0.6524	0.195
c)	49.82	16.92	0.9050	0.6524	0.198
d)	82.46	6.19	1.0341	0.3619	0.145
e)	75.11	9.32	1.0341	0.4708	0.167

The trial function is given in Appendix B. The results of the calculation are listed in Table II. B_d^* represents our estimate of the binding energy of the deuteron.

TABLE II. - *Binding energy B_d^* and wave function parameters of the deuteron for the potentials of Table I.*

Neutron-proton potential	B_d^* (MeV)	β (fermi ⁻¹)	δ (fermi ⁻¹)	x
a)	-1.206	0.51 ₅	2.09	-0.173
b)	-1.246	0.52 ₅	2.00	-0.166
c)	-1.216	0.53 ₅	2.02 ₅	-0.167
d)	-1.364	0.60	1.68 ₅	-0.129
e)	-1.323	0.58 ₅	1.83 ₅	-0.146

The common feature of the results is that the absolute value of the binding energy and of the *S-D* mixing parameter are too small. Such a fact shows that the neutron-proton pair will be poorly described by the ${}^3\text{H}_A$ wave function (1). A better calculation will require an improvement of this part of the ${}^3\text{H}_A$ description: this will be done in a subsequent paper.

As a test of the importance of tensor corrections in hypertriton we have performed a whole set of calculations which could be compared with those

TABLE III. - Λ -nucleon interaction in ${}^3\text{H}_\Lambda$. The intrinsic range 0.8411 fermi corresponds to exchange of a K-meson; the value 1.4843 corresponds to exchange of two pions. The numbers marked with an asterisk are the results of D.D.I.

a) Yukawa potential shapes.												
B_a+B_Λ (MeV)	(i) intrinsic range 0.8411 fermi					B_a+B_Λ (MeV)	(ii) intrinsic range 1.4843 fermi					
	α (fermi ⁻¹)	β (fermi ⁻¹)	γ (fermi ⁻¹)	δ (fermi ⁻¹)	ϵ		α (fermi ⁻¹)	β (fermi ⁻¹)	γ (fermi ⁻¹)	δ (fermi ⁻¹)	ϵ	\bar{U}_2 (MeV·fermi ³)
2.226	0.66 ₅	0.59 ₅	0.64 ₅	2.49 ₅	—0.177	2.226	0.40	0.55	0.38 ₅	2.24	—0.172	833
	0.62*	0.69*	—	—	—		0.36*	0.65*	—	—	—	766*
2.626	0.69	0.60	0.67	2.52 ₅	—0.177	2.626	0.42 ₅	0.55 ₅	0.40 ₅	2.27	—0.172	853
	0.64*	0.71*	—	—	—		0.39*	0.65*	—	—	—	786*
3.226	0.72 ₅	0.61	0.70 ₅	2.57 ₅	—0.176	3.226	0.46	0.56 ₅	0.44	2.31 ₅	—0.172	879
	0.67*	0.71*	—	—	—		0.43*	0.66*	—	—	—	813*
b) Exponential potential shapes.												
B_a+B_Λ (MeV)	(i) intrinsic range 0.8411 fermi					B_a+B_Λ (MeV)	(ii) intrinsic range 1.4843 fermi					
	α (fermi ⁻¹)	β (fermi ⁻¹)	γ (fermi ⁻¹)	δ (fermi ⁻¹)	ϵ		α (fermi ⁻¹)	β (fermi ⁻¹)	γ (fermi ⁻¹)	δ (fermi ⁻¹)	ϵ	\bar{U}_2 (MeV·fermi ³)
2.226	0.60 ₅	0.59	0.57 ₅	2.45	—0.175	2.226	0.37	0.55	0.35 ₅	2.22 ₅	—0.171	818
	0.52*	0.52*	—	—	—		0.29*	0.52*	—	—	—	742*
2.626	0.62 ₅	0.59 ₅	0.57 ₅	2.45	—0.175	2.626	0.39	0.55	0.37	2.24	—0.171	841
	0.55*	0.53*	—	—	—		0.33*	0.52*	—	—	—	772*
3.226	0.65	0.60	0.58	2.46	—0.175	3.226	0.41 ₅	0.56	0.39 ₅	2.30 ₅	—0.171	871
	0.58*	0.53*	—	—	—		0.37*	0.52*	—	—	—	810*

of D.D.I with a central potential. The results are collected in Table III with the corresponding ones of D.D.I. The latter are marked with an asterisk. All these calculations have been done with the potential of type *b*). Such a potential practically coincides in this case with the more general Hall and Powell's one ⁽⁴⁾, which fits the p-p low-energy scattering data.

Comparing the results of the present work with those of D.D.I, one sees that there is some difference between our wave function parameters and integral volumes and the corresponding quantities of D.D.I. Further the integral volumes increases more than one would expect from the difference between our value for B_d^* and the one of D.D.I. It is doubtful, however, that the potential *b*) is the most suitable to describe the n-p interaction. To improve this point we have done a set of calculations with the five potentials of Table I. These have been done for $B_\Lambda = 0.12$ MeV ⁽⁵⁾. Taking account of the fact that the best value of B^* of D.D.I is 1.6 MeV^(*) and that our B_d^* is smaller of some tenth of MeV (see Table II), these results may be compared with the results of D.D.I for $B_\Lambda = 0.4$ MeV. We have restricted ourselves to the case of a Λ -N interaction of Yukawa shape. This results are listed in Table IV.

Inspection of Table IV shows that the best agreement with the results of D.D.I is obtained with the potential of type *d*). However also for this potential the value of the mixing parameter remains low. On the other hand the biggest difference between our integral volumes and the corresponding ones of D.D.I is of about 10%. Moreover there is a certain difference in the corresponding function parameters. These differences might be relevant on the determination of the Λ -nucleon well depths. The variation of function parameters might also influence the prediction of decay ratios, but this point ought to be checked by a calculation.

5. - Conclusion.

The present work shows that a tensor term in the neutron-proton potential might have some influence in $^3\text{H}_\Lambda$. There are differences between our results and those obtained by D.D.I with a purely central neutron-proton potential, both in the integral volumes and the wave function parameters. Our results, however, are dependent upon the choice of the neutron-proton potential among the five equivalent potentials of Table I. In order to get a definite answer about the origin of these differences it is necessary to perform

⁽⁴⁾ H. H. HALL and J. L. POWELL: *Phys. Rev.*, **90**, 912 (1953).

⁽⁵⁾ The value $B_\Lambda = (0.12 \pm 0.26)$ MeV is the one given at the Kiev Meeting of 1959.

^(*) See D.D.I, p. 963.

TABLE IV. - *Results for the various n-p potentials of Table I and Λ -N Yukawa shape.*
 $B_d + B_\Lambda = 2.346$ MeV.

i) intrinsic range 0.8411 fermi						
Neutron-proton potential	α (fermi $^{-1}$)	β (fermi $^{-1}$)	γ (fermi $^{-1}$)	δ (fermi $^{-1}$)	x	\bar{U}_2 (MeV \cdot fermi 3)
a)	0.67 ₅	0.57 ₅	0.66	2.57 ₅	-0.192	528
b)	0.67	0.59 ₅	0.65	2.50	-0.177	523
c)	0.67	0.61	0.65	2.52 ₅	-0.177	520
d)	0.65 ₅	0.70 ₅	0.62 ₅	2.23 ₅	-0.110	497
e)	0.66	0.68	0.63 ₅	2.36 ₅	-0.136	504
ii) intrinsic range 1.4843 fermi						
Neutron-proton potential	α (fermi $^{-1}$)	β (fermi $^{-1}$)	γ (fermi $^{-1}$)	δ (fermi $^{-1}$)	x	\bar{U}_2 (MeV \cdot fermi 3)
a)	0.41	0.53 ₅	0.39 ₅	2.32 ₅	-0.184	848
b)	0.41	0.55	0.39 ₅	2.24 ₅	-0.172	840
c)	0.41 ₅	0.56 ₅	0.40	2.28	-0.173	835
d)	0.40	0.64 ₅	0.38	1.96 ₅	-0.117	797
e)	0.40	0.62 ₅	0.38	2.10	-0.140	808

a detailed calculation with a more flexible wave function. This is necessary to make it possible to decide if the differences we have found can affect the prediction of the Λ -N well depths and of the decay ratios.

* * *

We would like to thank Prof. L. A. RADICATI for his kind interest in this work and Dr. E. FABRI for valuable suggestions. Thanks are also due to the computer staff of STANIC (Leghorn) for kind assistance in the use of the IBM 650 electronic computer, on which numerical calculations have been performed.

APPENDIX A

Spin functions.

The detailed form of the spin functions used in the work is the following:

i) spin $J = \frac{1}{2}$

$$(\Phi_{S_2})^\alpha = \frac{1}{\sqrt{24\pi^2}} \boldsymbol{\sigma}_p \cdot \boldsymbol{\sigma}_\Lambda \varphi^\alpha,$$

$$(\Phi_{D_1})^\alpha = \frac{1}{\sqrt{48\pi^2 r^2}} S_{jk}(\boldsymbol{\sigma}_p)_j (\boldsymbol{\sigma}_\Lambda)_k \varphi^\alpha,$$

ii) spin $J = \frac{3}{2}$

$$(\Phi_{S_2})^\alpha_j = \frac{1}{6\pi} \left(\boldsymbol{\sigma}_p + \frac{i}{2} \boldsymbol{\sigma}_p \times \boldsymbol{\sigma}_\Lambda \right)_j \varphi^\alpha,$$

$$(\Phi_{D_1})^\alpha_j = \frac{1}{12\pi r^2} S_{jk}(\boldsymbol{\sigma}_p - i \boldsymbol{\sigma}_p \times \boldsymbol{\sigma}_\Lambda)_k \varphi^\alpha,$$

$$(\Phi_{D_1'})^\alpha_j = \frac{1}{12\pi r^2} (S_{jk}(\boldsymbol{\sigma}_p)_k - i \varepsilon_{jkl}(\boldsymbol{\sigma}_p)_k S_{lm}(\boldsymbol{\sigma}_\Lambda)_m) \varphi^\alpha,$$

where

$$\mathbf{r} = \mathbf{r}_p - \mathbf{r}_n,$$

and

$$S_{jk} = 3x_j x_k - \delta_{jk} r^2, \quad (x_1 = x, x_2 = y, x_3 = z),$$

is the irreducible tensor of angular momentum 2. ε_{jkl} is the completely antisymmetric tensor of 3rd order. Further

$$\varphi^\alpha = \chi^0 \chi^\alpha(\Lambda), \quad \chi^0 = \frac{1}{\sqrt{2}} [\chi^{\frac{1}{2}}(p) \chi^{-\frac{1}{2}}(n) - \chi^{-\frac{1}{2}}(p) \chi^{\frac{1}{2}}(n)],$$

where $\chi^s(P)$ represents the Pauli spin function for the particle P . χ^0 is the singlet function for the proton-neutron pair. The functions listed before are not, in general, eigenfunctions of the third component of the total spin J .

All the functions are normalized. Those for spin $\frac{3}{2}$ are normalized according to

$$\sum_j (\Phi_j^\alpha)^* \Phi_j^\alpha = 1.$$

APPENDIX B

Complete wave functions.

The trial function used for the variational calculation of B_d^* is the following

$$\Psi_d = \frac{1}{\sqrt{1+x^2}} (C_1 \exp[-\beta r] \sigma_j + x C_2 \exp[-\delta r] S_{jk} \sigma_k) \chi^0,$$

where C_1 and C_2 are normalization constants and σ represents the spin vector of one of the nucleons.

The trial functions used in the calculations for the ${}^3\text{H}_\Lambda$ have the following detailed form:

$$\Psi_{\frac{1}{2}} = \frac{1}{\sqrt{1+x^2}} \left[\frac{1}{\sqrt{I_{111}(2\alpha, 2\alpha, 2\beta)}} \exp[-\alpha(s+t) - \beta r] \Phi_{s_1} + \frac{x}{\sqrt{I_{115}(2\gamma, 2\gamma, 2\delta)}} \exp[-\gamma(s+t) - \delta r] \Phi_{D_1} \right],$$

$$\Psi_{\frac{3}{2}} = \frac{1}{\sqrt{1+x^2+y^2}} \left[\frac{1}{\sqrt{I_{111}(2\alpha, 2\alpha, 2\beta)}} \exp[-\alpha(s+t) - \beta r] \Phi_{s_1} + \frac{x}{\sqrt{I_{115}(2\gamma, 2\gamma, 2\delta)}} \exp[-\gamma(s+t) - \delta r] \Phi_{D_1} + \frac{y}{\sqrt{I_{115}(2\gamma, 2\gamma, 2\delta)}} \exp[-\gamma(s+t) - \delta r] \Phi_{D_1'} \right].$$

The normalized spin functions Φ are given in Appendix A. $I_{abc}(\alpha, \beta, \gamma)$ is defined by

$$I_{abc}(\alpha, \beta, \gamma) = (-)^{a+b+c} \frac{\partial^{a+b+c}}{\partial \alpha^a \partial \beta^b \partial \gamma^c} I_{000}(\alpha, \beta, \gamma),$$

where

$$I_{000}(\alpha, \beta, \gamma) = \int dr ds dt \exp[-\alpha r - \beta s - \gamma t] = \frac{2}{(\alpha + \beta)(\beta + \gamma)(\gamma + \alpha)},$$

I_{abc} is given explicitly by

$$I_{abc}(\alpha, \beta, \gamma) = I_{000}(\alpha, \beta, \gamma) a! b! c! \sum_{i=0}^a \sum_{j=0}^b \sum_{k=0}^c \binom{a-i+j}{j} \binom{b-j+k}{k} \binom{c-k+i}{i} \cdot \frac{1}{(\alpha + \beta)^{a-i+j} (\beta + \gamma)^{b-j+k} (\gamma + \alpha)^{c-k+i}}.$$

The explicit form of the four functions G , A , B , C (which is the same both for spin $\frac{1}{2}$ and spin $\frac{3}{2}$) is

$$A = \frac{\alpha + \beta}{8\alpha^2 + 5\alpha\beta + \beta^2} \left[(16\alpha^3 + 9\alpha^2\beta + 4\alpha\beta^2 + \beta^3) + \frac{m_\Lambda - m}{m_\Lambda + m} \beta(5\alpha^2 + 4\alpha\beta + \beta^2) - \right. \\ \left. - \frac{8m_\Lambda m}{m_\Lambda + m} (W_1 + W_2) \frac{[(2\beta + 4\alpha + k)^2 + 4\alpha^2](\alpha + \beta)^4}{(2\alpha + 2\beta + k)^4} \right] + \frac{2m_\Lambda m}{m_\Lambda + m} (B_d + B_\Lambda),$$

$$B = \frac{2^{10}m_\Lambda m}{m_\Lambda + m} \sqrt{\frac{3}{5}} W_3 \sqrt{\frac{\alpha^3(\alpha + \beta)^5 \gamma^3(\gamma + \delta)^9}{(8\alpha^2 + 5\alpha\beta + \beta^2)(80\gamma^2 + 27\gamma\delta + 3\delta^2)}} \cdot \\ \cdot \frac{35(\alpha + \gamma)^2 + 18(\alpha + \gamma)(\beta + \delta + \eta) + 3(\beta + \delta + \eta)^2}{(\alpha + \gamma)^3(\alpha + \beta + \gamma + \delta + \eta)^6},$$

$$C = \frac{(\gamma + \delta)}{80\gamma^2 + 27\gamma\delta + 3\delta^2} \left[(128\gamma^3 + 79\gamma^2\delta + 24\gamma\delta^2 + 3\delta^3) + \right. \\ \left. + \frac{m_\Lambda - m}{m_\Lambda + m} (32\gamma^3 + 67\gamma^2\delta + 24\gamma\delta^2 + 3\delta^3) - \frac{128m_\Lambda m}{m_\Lambda + m} (W_1 + W_2) \cdot \right. \\ \left. \cdot \frac{(\gamma + \delta)^8 [84\gamma^2 + 16\gamma(2\delta + k) + (2\delta + k)^2]}{(2\gamma + 2\delta + k)^8} - 256M\gamma^3(\gamma + \delta)^8 I_{5n1}(2\delta, 2\gamma + \lambda, 2\gamma) + \right. \\ \left. + 192 \frac{m_\Lambda m}{m_\Lambda + m} W_3 [84\gamma^2 + 16\gamma(2\delta + \eta) + (2\delta + \eta)^2] \left(\frac{\gamma + \delta}{2\gamma + 2\delta + \eta} \right)^8 \right] + \\ + \frac{2m_\Lambda m}{m_\Lambda + m} (B_d + B_\Lambda),$$

where $n = 0$ for Yukawa shape of the Λ - N potential, $n = 1$ for exponential shape. M is a coefficient given in the following table

$$\begin{array}{ll} \text{exponential shape} & \left\{ \begin{array}{ll} \lambda = 2.3858, & M = 0.13396, \\ \lambda = 4.2102, & M = 0.70509, \end{array} \right. \\ \\ \text{Yukawa shape} & \left\{ \begin{array}{ll} \lambda = 1.4280, & M = 0.0493, \\ \lambda = 2.5200, & M = 0.13765. \end{array} \right. \end{array}$$

The function G also depends on the shape of the Λ - N potential. For Yukawa shape it is given by

$$G = \frac{\pi}{16\lambda^2} \frac{m_\Lambda + m}{m_\Lambda m} \frac{(2\alpha + 2\beta + \lambda)^2 (4\alpha + \lambda)^2 (8\alpha^2 + 5\alpha\beta + \beta^2)}{\alpha^3(\alpha + \beta)^2 [(4\alpha + 2\beta + \lambda)^2 + 4\alpha\beta]}.$$

while for exponential shape it is

$$G = \frac{\pi}{16\lambda^3} \frac{m_\Lambda + m}{mm_\Lambda} \frac{(2\alpha + 2\beta + \lambda)^3 (4\alpha + \lambda)^3 (8\alpha^2 + 5\alpha\beta + \beta^2)}{\alpha^3(\alpha + \beta)^2 [(4\alpha + 2\beta + \lambda)^3 + 4\alpha\beta(2\alpha + \lambda)]}.$$

RIASSUNTO

Conti effettuati sul ${}^3\text{H}_\Lambda$ con una hamiltoniana contenente il potenziale neutrone-protone con parte tensoriale mostrano che il volume integrale della interazione Λ -nucleone ed i parametri della funzione d'onda son modificati rispetto ai risultati di conti precedenti basati su un potenziale totalmente centrale. Si conclude che è necessario un conto più raffinato per avere una risposta definitiva sulla importanza delle correzioni tensoriali nell'ipertritone.

Angular Distribution of Protons from the Reaction $^{28}\text{Si}(n, p)^{28}\text{Al}$.

L. COLLI

Laboratori CISE - Milano
Istituto di Fisica dell'Università - Milano

G. M. MARCAZZAN, F. MERZARI, P. G. SONA and P. TOMAŠ (*)

Laboratori CISE - Milano

(ricevuto il 3 Febbraio 1961)

Summary. — In this work we present the angular distribution of protons emitted in the reaction $^{28}\text{Si}(n, p)^{28}\text{Al}$. The energy spectrum of these contains four peaks, which have an anisotropic component superposed to an isotropic part, which is predominant at low proton energy. The analysis of the anisotropic part shows that it can be described with sufficient approximation by means of a direct interaction mechanism; the angular distribution shape can be correlated with the values of the shell model orbits involved in the process of capture and emission of interacting particles.

1. — Introduction.

In order to study the interaction mechanism in the n, p reaction, we have planned a systematic research on a series of nuclei, to see to what extent the direct interaction is effective in n, p reactions.

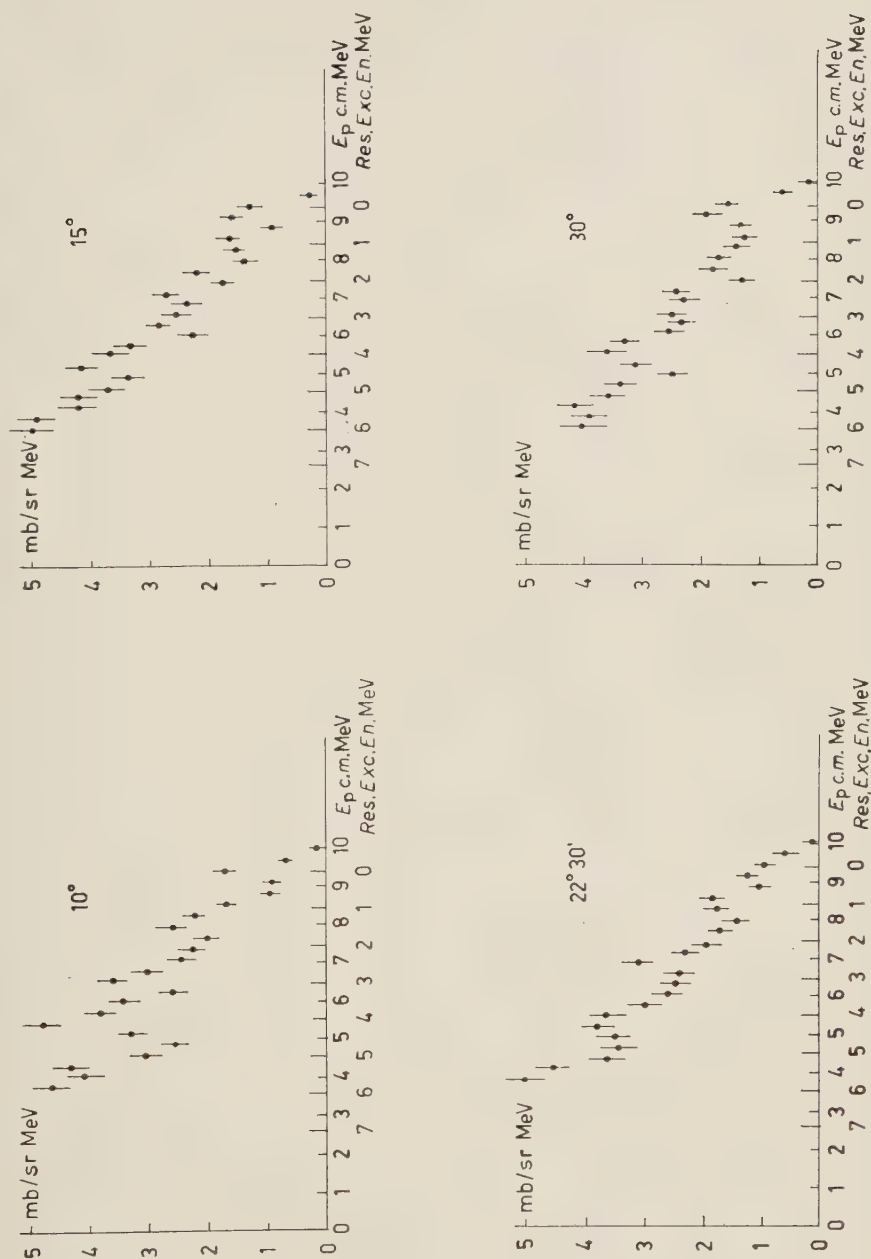
Previous results on ^{24}Mg and ^{32}S ⁽¹⁾ have shown that in these nuclei the direct interaction seems to be very important, and, moreover, that the properties of the emitted protons can be correlated with the quantum numbers of the shell-model orbits in which the proton is found in the target nucleus, and in which the neutron is captured.

These results show the possibility of using the direct n, p reaction to study these shell model orbits.

In the course of this work, we measured the angular distribution of protons

(*) On leave from the Ruder Bosković Institut, Zagreb.

(1) L. COLLI, G. M. MARCAZZAN, F. MERZARI, P. G. SONA and F. TONOLINI: *Nuovo Cimento*, **16**, 991 (1960).


 Fig. 1. — Spectra of protons from $^{28}\text{Si}(n, p)^{28}\text{Al}$ taken at various angles — $E_n = 14.1$ MeV.

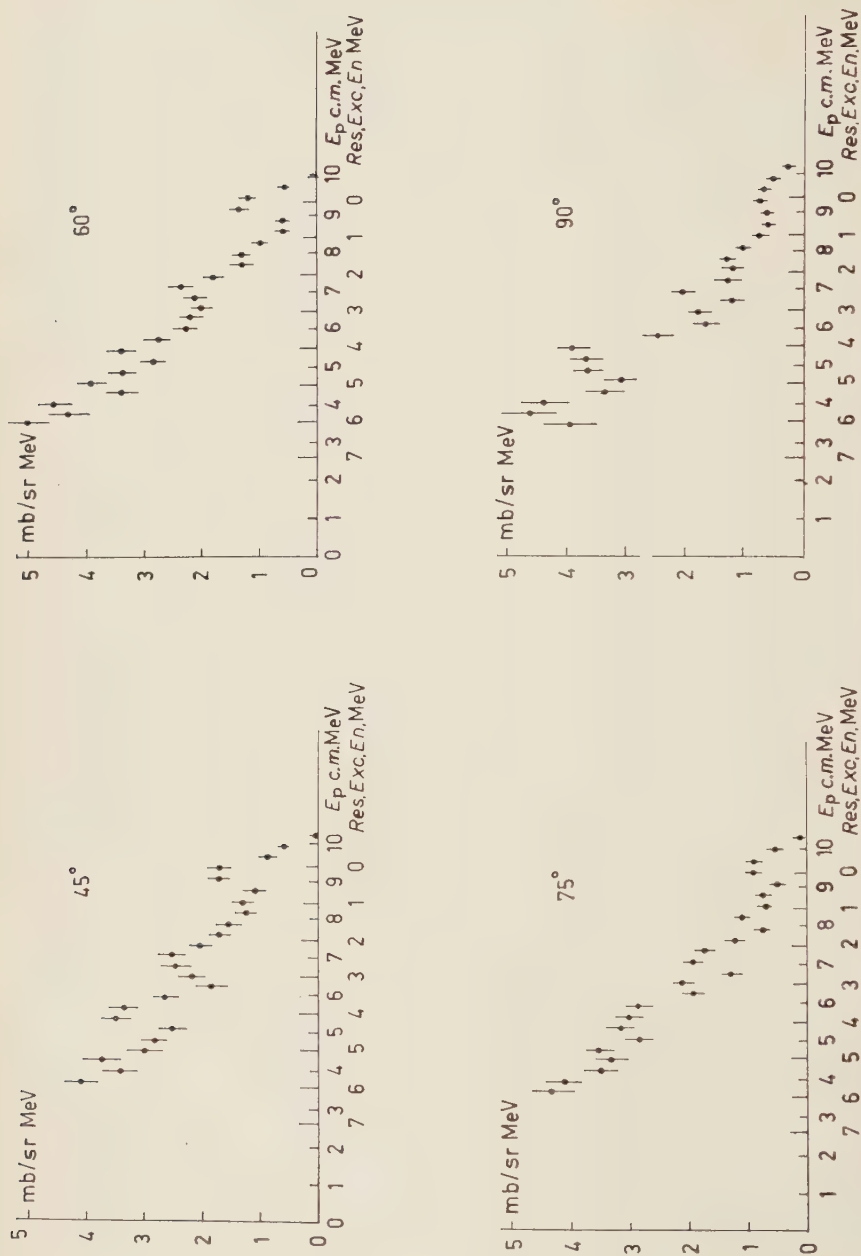


Fig. 2 -- Spectra of protons from $^{28}\text{Si}(n, p)^{28}\text{Al}$ taken at various angles $E_n = 14.1 \text{ MeV}$.

emitted by silicon under bombardment of 14 MeV neutrons. This target was chosen because the proton spectrum from $^{28}\text{Si}(n, p)$ ⁽²⁾, taken in the forward direction with respect to the neutron beam, has shown a characteristic structure, that is four peaks, at the residual nucleus excitation energy of 0; 1.3; 2.4 and 4 MeV, which seemed to give evidence of the presence of surface direct interaction. The knowledge of the angular distribution of the protons included in these peaks can give us information on the direct effect itself and on the shell-model orbits in which the particles involved are found.

2. - Description of experiments.

The proton detector has been described elsewhere ⁽³⁾. It is a telescope, made of two proportional counters and a scintillating counter in coincidence plus a proportional counter in anti-coincidence.

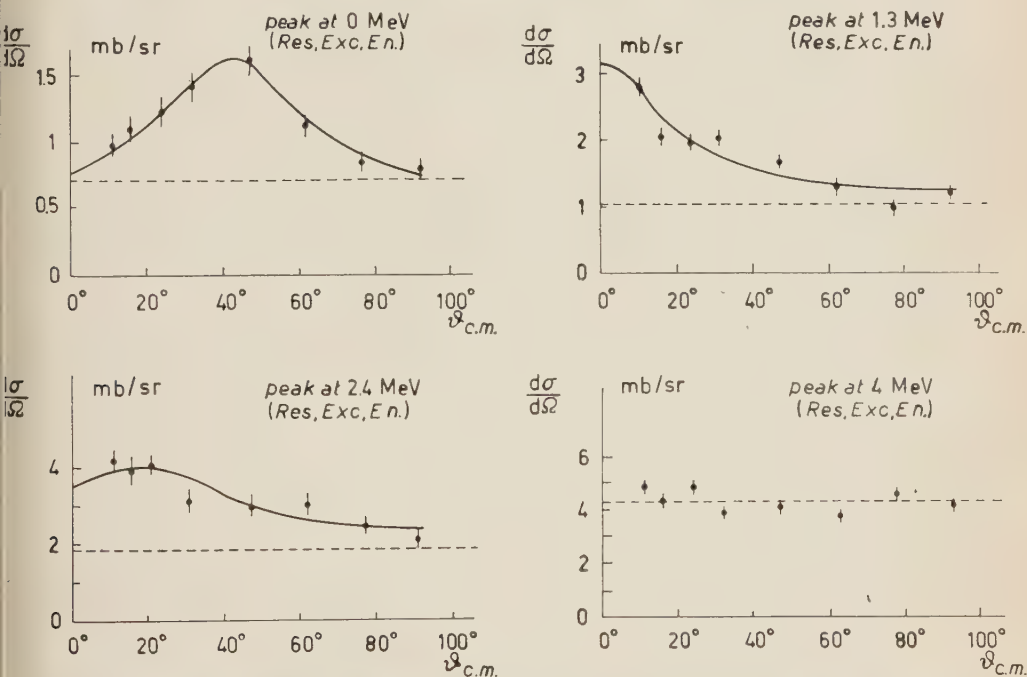


Fig. 3. - Center-of-mass angular distribution of protons in the four peaks of the silicon spectrum. Full lines: curves calculated following formula (1) in the text. Interaction radius $R = 6$ fermi, l -values used: ground state peak: $l = 2$; 1.3 MeV excitation energy peak: $l = 0, 2, 4$; 2.4 MeV excitation energy peak: $l = 1, 3, 5$. Dotted lines represent the isotropic component.

(2) L. COLLI, F. CVELBAR, S. MICHELETTI and M. PIGNANELLI: *Nuovo Cimento*, **14**, 81 (1959).

(3) G. M. MARCAZZAN, M. PIGNANELLI and A. M. SONA: *Nuovo Cimento*, **10**, 155 (1958).

The measurement consists in taking the proton spectrum at 8 different angles, with an angular aperture of about 12° at each angle.

These spectra are displayed in Fig. 1 and 2. Deuterons from the $^{28}\text{Si}(n, d)$ reaction make no contribution because their maximum energy is 3.8 MeV. Once the peaks have been found in the spectra obtained, an energy interval is fixed for each peak, and the sum is made up of all the counts due to protons contained in each peak. Corrections are made as far as concerns the small differences in angular aperture at each angle.

The angular distributions obtained in this way are shown in Fig. 3, where only statistical errors are shown.

3. - Discussion.

These angular distributions with their anisotropy for the first three peaks, certainly show that the reaction goes at least partly through a direct effect. It is interesting to note that an isotropic component is present in all the peaks, and that this isotropic component is dominant in the fourth; this shows that part of the reaction goes through a compound nucleus process. We can construct an «evaporation spectrum» (very approximately) plotting only the isotropic part as function of the excitation energy. The result is a curve with a temperature $\theta \simeq 1.6$ MeV, in good agreement with what one can expect from the consideration of the θ -values for nearby nuclei.

The evaporated part being isotropic, it follows that its total contribution to the reaction is rather important. The various contributions in each peak due to the isotropic and anisotropic parts are given in Table I.

TABLE I. - *Cross-section values for isotropic and anisotropic part of each peak.*

Residual nucleus excitation energy of the peaks (in MeV)	0	1.3	2.4	4
σ_{tot} (in mb)	11.5 ± 1	15.4 ± 2	29.4 ± 3	49.6 ± 5
σ_{anisotr} (in mb)	2.6	2.3	6.8	—
σ_{isotr} (in mb)	8.9	13.1	22.6	49.6 ± 5

Let us now analyse the direct part of the spectrum.

Following the line of discussion we have used in the case of $^{24}\text{Mg}(n, p)$ and $^{32}\text{S}(n, p)$ we will first try to fit our experimental angular distribution with the theoretical curves calculated on the basis of the surface direct interaction.

The underlying idea of this theory is that the interaction goes as follows: the incoming neutron is captured by the target nucleus on a well defined orbit, that is with a definite orbital angular momentum l_n ; then, due to the interaction with the neutron, a proton occupying a well defined orbit with orbital angular momentum l_p of the target nucleus is emitted. Under this hypothesis, a calculation for this reaction was made by BUTLER (4).

In the above description the differential cross-section for this reaction is given by the formula

$$(1) \quad \sigma(\theta) \div \sum_l C_{l_n l_p}^2(l, 0; 0, 0) j_l^2(QR) \left| \left\langle \frac{\mathbf{K}'}{2} | r_{np} | \frac{\mathbf{K}'}{2} - \mathbf{K} \right\rangle \right|^2,$$

where $C_{l_n l_p}(l, 0; 0, 0)$ are Clebsch-Gordan coefficients and j_l the spherical Bessel functions, l being the angular momentum transferred in the reaction, and $Q = |\mathbf{K} - \mathbf{K}'|$, where \mathbf{K} and \mathbf{K}' are the wave vectors for the incident and outgoing particles respectively; the factor

$$\left\langle \frac{\mathbf{K}'}{2} | r_{np} | \frac{\mathbf{K}'}{2} - \mathbf{K} \right\rangle,$$

is the matrix element of the r -matrix which can be determined phenomenologically from two-body scattering measurements; in fact this factor is obtained from the neutron-proton scattering cross-section through the relation

$$\sigma_{np} = \frac{2\pi}{\hbar^2} m^2 \left| \left\langle \frac{\mathbf{K}'}{2} | r_{np} | \frac{\mathbf{K}'}{2} - \mathbf{K} \right\rangle \right|^2.$$

Taking the value of the interaction radius R and the angular momenta l_n, l_p as parameters, we will see if it is possible to find agreement between theory and experiment; we will try to use for the three cases the same value of R , and find the values of l_n and l_p .

This comparison is shown in Fig. 2. Agreement can be found using the same R value of 6 fermi for the three cases and the following values for the angular momenta l_n and l_p :

1) the ground-state transition gives $l = 2$ and this corresponds to $l_p = 2$, $l_n = 0$, or on the contrary, $l_p = 0$, $l_n = 2$.

This indefiniteness in the l_p, l_n value is due to the fact that the three angular momenta l_n, l_p and l are related by the formula

$$l_n + l_p \geq l \geq |l_n - l_p|;$$

(4) S. T. BUTLER: *Nuclear Stripping Reactions* (New York, 1957).

2) the first excited peak gives $l = 0, 2, 4$ (combined according to formula (1), that is, with the appropriate Clebsch-Gordan coefficients) and consequently only $l_n = l_p = 2$ is possible;

3) for the third peak the two sets $l = 1, 3$ or $l = 1, 3, 5$ can both be good, because the contribution from $l = 5$ is expected to be very small. From the formula (1) the l_n and l_p values therefore may be either 1 and 2 or 2 and 3.

The fact that the experimental angular distribution can be fitted with Butler's curves, all with the same R value, is a considerable success. It shows that this comparison gives rather consistent results, allowing the conclusion that Butler's theory gives a good description of the reaction mechanism.

We have now found some possible values for the orbitals of the particles involved in the reaction: let us then see if these orbitals correspond with the ones expected on the basis of the shell-model description of the nucleus.

The l_n and l_p values found have indeed the precise meaning of the orbital angular momentum of captured neutron and emitted proton. The sequence of orbits in which protons and neutrons are found, being known from static properties of nuclei, we can compare our numbers for l_n and l_p with those expected on this basis.

The ground-state transition can be obtained only by taking out from the nucleus the «last» proton, and putting the neutron on the lowest free orbit. In the case of silicon, the last proton is one from the $d_{3/2}$ shell (completely filled) and the first free orbit for the neutron is the $s_{1/2}$. We have in such a way an $l = 2$ transition with $l_p = 2$ and $l_n = 0$, in agreement with the experimental results.

In the next peak the residual nucleus is left with 1.3 MeV excitation energy; it means that either the neutron is captured in an orbit higher than the $s_{1/2}$ or that a proton is taken from an orbit below the $d_{3/2}$.

In the first case, the neutron orbit next to the $s_{1/2}$ is the $d_{3/2}$. Taking out the last proton ($d_{3/2}$) and putting a neutron on the $d_{3/2}$ orbit, we have a transition with $l = 0, 2, 4$ in good agreement with the experimental result.

Agreement is also found for the second excited peak, if the last proton ($d_{3/2}$) is taken and a neutron is put on the next $f_{7/2}$ orbit. That gives allowed l values $= 1, 3, 5$.

The fact that the l_n and l_p values agree well with the prediction of the shell model, considering for the three cases the same l_p values and different l_n values, corresponding to the expected succession $s_{1/2}$, $d_{3/2}$, $f_{7/2}$ seems to show that this agreement between experimental and theoretical values is not a casual one.

On this ground, we must consider the three proton peaks analysed as coming from a direct interaction process in which a proton is taken from the single-particle $d_{3/2}$ orbit and respectively a neutron is captured on a single-particle $s_{1/2}$, $d_{3/2}$ and $f_{7/2}$. Sticking to this description, the distance in energy between these peaks should correspond to the distance in energy between the neutron

orbits involved. The $d_{\frac{3}{2}}$ orbit should be 1.3 MeV above the $s_{\frac{1}{2}}$, and the $f_{\frac{7}{2}}$ would also lay 1.1 MeV above the $d_{\frac{3}{2}}$.

In order to analyse these figures, we must understand which residual nucleus levels contribute to the proton peaks. The ground state peak can possibly include the transition to the very close excited level at 0.031 MeV: the four levels between 1 and 1.6 MeV cannot be distinguished in the second peak, and in the same way, the six levels between 2.14 and 2.66 are the levels in the third group considered.

We can deduce that only few levels contribute, otherwise it would not be possible to have the well defined peaks but rather a smooth shape.

The levels which are brought in evidence in these reactions should be those corresponding to single-particle excited states.

But it is possible that the characteristic of being single-particle level be shared among many levels of the nucleus, so that we may expect rather wide peaks coming from this effect.

Considering our experiments, we must observe that the width of the peaks is of the same order as the energy resolution of our apparatus, so that we cannot guess anything about peak width.

With regard to the energy distance between peaks, we can say that the value 1.3 MeV for the distance between the $s_{\frac{1}{2}}$ and $d_{\frac{3}{2}}$ is not unreasonable, but on the contrary the value 1.1 MeV that we find for the distance $d_{\frac{3}{2}}-f_{\frac{7}{2}}$ seems to be too small compared to what is generally predicted.

We can suppose that the second excited peak corresponds to only a part of the group of levels of the $f_{\frac{7}{2}}$ orbit, in the sense that the center of mass of the group lies at a higher excitation energy, but, due to fluctuations in level density or to some selection rules, a few of these levels appear like a group.

* * *

We cordially thank Prof. U. FACCHINI for many discussions throughout the work.

RIASSUNTO

In questo lavoro viene presentata la distribuzione angolare dei protoni emessi nella reazione $^{28}\text{Si}(\text{n}, \text{p})^{28}\text{Al}$. Lo spettro di energia di questi mostra quattro picchi, i quali hanno una componente anisotropa sovrapposta ad una parte isotropa, che è preponderante per i protoni di energia più bassa. L'analisi della parte anisotropa mostra che essa può essere descritta con sufficiente approssimazione da un meccanismo di interazione diretta e che la forma della distribuzione angolare può essere correlata con i valori dei momenti angolari delle orbite del modello a shell che intervengono nel processo di cattura e di emissione delle particelle interagenti.

Remarks upon the Densitometry of the Tracks of Heavy Nuclei in Nuclear Emulsion.

D. EVANS and R. R. HILLIER

H. H. Wills Physical Laboratory, University of Bristol - Bristol

(ricevuto il 3 Febbraio 1961)

Summary. — An analysis of the structure of tracks of heavy nuclei in nuclear emulsion leads to a method whereby charge scales appropriate to any given parameter which has arisen through measurement upon a track by means of a densitometer may be calculated. As an example, the mean widths of tapers at a residual range of $100\ \mu\text{m}$ are calculated for various values of the charge and good agreement with experimental results is obtained.

1. — Introduction.

The presence of the tracks of heavy cosmic ray nuclei in nuclear emulsion stacks which have been exposed at great altitudes was first recognized by FREIER *et al.* ⁽¹⁾, and since then, numerous attempts have been made to identify the nuclear species represented, for it has become increasingly important to establish as accurately as possible the charge distribution of the primary cosmic radiation in order to understand its origin and accelerating mechanism. Measurable parameters which characterize the tracks and which are functions of mass, charge and velocity of the particles are known and are in common use; nevertheless it has only recently been proved possible to identify charges of relativistic particles unambiguously in the range $3 < Z < 14$ (*e.g.* WALDESKOG and MATHIESEN ⁽²⁾) and at present no accurate method for measuring the charges of heavy, non-relativistic particles is available.

⁽¹⁾ P. FREIER, E. J. LOFGREN, E. P. NEY, F. OPPENHEIMER, H. L. BRADT and B. PETERS: *Phys. Rev.*, **74**, 213 (1948); P. FREIER, E. J. LOFGREN, E. P. NEY and F. OPPENHEIMER: *Phys. Rev.*, **74**, 1818 (1948).

⁽²⁾ B. WALDESKOG and O. MATHIESEN: *Ark. f. Fys.*, **17**, no. 25 (1960).

The source of the difficulty appears to be that although a heavy track contains more information per unit length than a light one, the standard methods of measuring ionization are not suitable for its extraction. In the case of light tracks, either grain counting or blob-gap counting may be used to good effect, and for heavier tracks, δ -ray counting is useful, although it often proves difficult to decide whether a particular collection of grains constitutes a δ -ray with the result that the δ -ray density is a subjective parameter, not readily reproducible when the heaviest tracks are under consideration. Still, the information is there, in the form of the total number of grains per unit length and their distribution about the particle trajectory and the problem is to educe it. A technique which has recommended itself to various workers is that of measuring the obscuration of a beam of light by the track and so obtaining a parameter which depends both upon the number of grains and their distribution. It has been used in one form or another as early as 1952 by CECCARELLI and ZORN ⁽³⁾, by VAN ROSSUM ⁽⁴⁾, ARTOM and GENTILE ⁽⁵⁾, HILLIER ⁽⁶⁾ and by the Lund group ⁽⁷⁾. The purpose of the present paper is to put forward a model of track structure which will enable one to calculate the result of a densitometer measurement on a track of specified charge (Z) and velocity (β): in effect to calculate a charge scale.

The approach is the following. By means of the densitometer, one can measure, in plane projection, the grain distribution of a heavy track of known velocity, say relativistic. One knows from theory the energy distribution of the δ -rays, so that by making an appropriate assumption about the distribution of grains produced by δ -rays one may proceed to a range distribution which, together with the theoretical energy distribution will give a range-energy relation for the δ -rays. Such a range-energy relation permits one to calculate narrow slit profiles, taper half-widths and other densitometer parameters.

2. - The densitometer.

The instrument used in this laboratory consists of a Cooke nuclear research microscope to the head of which a photomultiplier (RCA 931A) has been fitted. A rectangular slit whose dimensions are determined by the parameter which one seeks to measure is fixed below the photocathode and the image of the

⁽³⁾ M. CECCARELLI and G. T. ZORN: *Phil. Mag.*, **43**, 356 (1952).

⁽⁴⁾ L. VAN ROSSUM: *Compt. Rend.*, **266**, 2234 (1953).

⁽⁵⁾ M. ARTOM and C. GENTILE: *Suppl. Nuovo Cimento*, **4**, 254 (1956).

⁽⁶⁾ R. R. HILLIER: *Thesis* (1958), unpublished.

⁽⁷⁾ LUND GROUP: *Ark. f. Fys.* (1957-1960).

track is displaced laterally across it by means of a rotating glass cuboid mounted on a synchronous motor. The signal from the photomultiplier is displayed upon the screen of a cathode ray oscilloscope. The microscope substage illumination system is modified by the introduction of a slit which is focussed in the plane of the emulsion and whose effective width is about $20\text{ }\mu\text{m}$. This

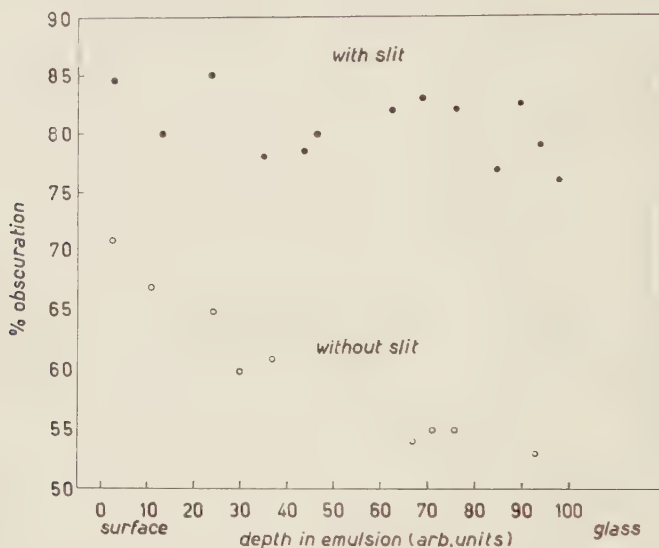


Fig. 1. — The advantage obtained through the use of a slit in the microscope substage condenser system is illustrated by the apparent blackness (obscuration) of a heavy track as a function of depth in the emulsion with the slit in place (black circles) and with it removed (open circles).

serves to suppress the background illumination except in the immediate vicinity of the track and cuts down the amount of light scattered by background grains into the objective directly in front of the track. The result is that tracks appear almost uniformly black throughout the depth of the emulsion. Fig. 1 presents a comparison of the percentage obscuration of a heavy track with this slit in place and with it removed.

3. — The obscuration of light by a heavy track.

It is convenient to propose a simple model for the obscuration of light by a heavy track in order to show what characteristics of its structure determine its blackness. Every track may be regarded as composed of two parts, first the core, which consists of grains produced by the ionization of the pri-

mary particle itself, and secondly the δ -ray grains produced by ionization of electrons scattered by the primary particle in its passage through the emulsion. Light tracks consist mainly of core, and δ -rays play only a minor part in the obscuration of light, whereas the obscuration due to a heavy track is produced largely by the δ -ray grains. In this analysis it will be assumed that the core is completely masked by δ -rays, that a grain is roughly spherical and totally opaque, and that all grains are approximately the same size.

The grains of a track which lies close to the plane of the emulsion exhibit elliptical symmetry about the core as a result of the shrinkage of the emulsion during processing. If however one assumes that the illumination is a parallel beam moving perpendicular to the plane of the emulsion, say in the z -direction, the projection of the grains becomes independent of the distortion of the track in the z -direction, with the result that one may assume the distribution of the grains to be cylindrically symmetric about the core without loss of accuracy. For such a distribution and such a parallel beam of uniform intensity I_0 over the wave front it can be shown (see Appendix) that as a first approximation (neglecting diffraction phenomena and the effects of a small degree of defocussing) the intensity of the attenuated beam at a distance x in the image plane from the track core is given by

$$(1) \quad I(x) = I_0 \exp - 2a \int_x^{r_{\max}} \varrho(r) \frac{dz}{dr} dr,$$

where a is proportional to the projected area of an individual grain, $\varrho(r)$ is the density of grains per unit volume as a function of distance, r , from the particle trajectory, and depends upon the number of grains per unit volume per unit ionization. Since the function $I(x)$ is left unchanged by distortion of the grain distribution in the z -direction, $I(x)$, though calculated for a cylindrically symmetric distribution, applies equally to the elliptical distribution which in fact exists.

Eq. (1) is the plane projection of the track and is called the track profile. One may obtain a profile with the densitometer by making the upper slit sufficiently narrow in relation to the dimensions of the track. A slit whose effective width in the object plane is about $0.5 \mu\text{m}$ has been found to give a satisfactory profile and has been used to measure the profiles of fast, highly charged nuclei ($Z \sim 20, 26$) to determine the form of the function $I(x)$ for relativistic particles. It has been shown by HILLIER⁽⁶⁾ that it is well represented by a particularly simple function, namely

$$(2) \quad I(x) = I_0 \exp \left[- \frac{\text{constant} \cdot \text{ionization}}{x^{0.9}} \right].$$

Fig. 2 exhibits a plot of $\ln(I_0/I(x))$ against x for the tracks of relativistic particles whose charges are estimated as those of iron, argon and neon, plotted

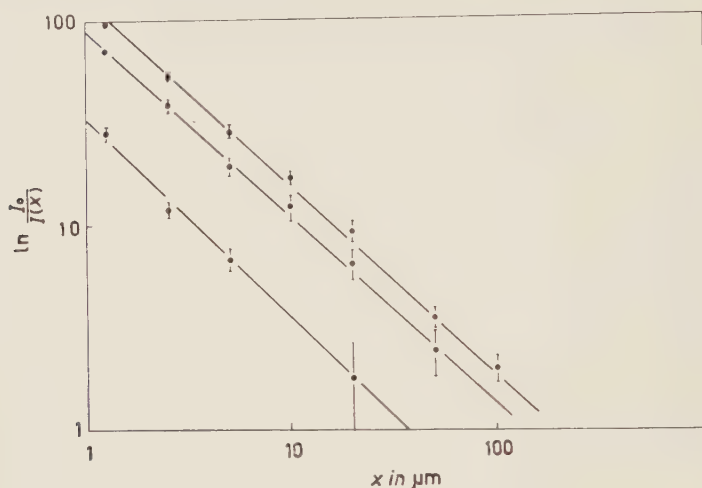


Fig. 2. — The function $\ln(I_0/I(x))$ measured on the profiles of various heavy tracks, plotted on logarithmic scales.

on logarithmic scales. In each case the points lie close to a straight line showing that

$$\ln \ln \frac{I_0}{I(x)} \propto \ln \left(\frac{1}{x} \right).$$

In every case in which relativistic profiles of heavy tracks have been measured this relation has been found to hold; moreover, the constant of proportionality, *i.e.* the slope of the line, appears to be 0.90 ± 0.05 .

4. — The structure of a heavy track.

In view of the foregoing remarks, the structure of a heavy track will be defined by the distribution $q(r)$ of grains due to δ -rays about the particle's trajectory, as a function of the particle's velocity βc and its charge.

It is assumed that the energy spectrum of the δ -ray electrons is adequately described by the formula given by MOTT ⁽⁸⁾ which supposes that only electrostatic forces are important and that the electrons in the medium through which

⁽⁸⁾ N. F. MOTT: *Proc. Roy. Soc.*, **124**, 425 (1929).

the heavy particle passes are unbound and at rest. Where $N(w)dw$ is the number of electrons whose energies lie between w and $w+dw$,

$$(3) \quad N(w)dw = \text{const.} \cdot \frac{Z^2}{\beta^2} \frac{dw}{w^2}.$$

Z and β are as usual charge and velocity of the primary particle. This spectrum has an upper limit given by

$$(4) \quad w_{\max} = 2m_e c^2 \frac{\beta^2}{1 - \beta^2}.$$

Whatever assumption is made about the distribution of grains due to these electrons, it must lead to a projected grain density which will reduce in the relativistic limit to the form of eq. (2). It is possible to make two related and very simple assumptions which do satisfy the relativistic relation and which in other circumstances lead to results which are verified by observation.

The first assumption is that there exists a parameter which may be called the transverse range, and which is defined as the greatest distance, r , transverse to the direction of motion of the primary particle that an electron of energy w reaches. Obviously, this is not well defined for individual electrons, but it is postulated that the transverse range averaged over many electrons of energy w will approach a unique limit, r . Moreover it is assumed that a simple relation of the form $r = kw^\alpha$ exists between r and w , where α is a constant to be determined by the condition that eq. (2) is to be satisfied. One may make an estimate of the size of α through the following consideration. Although due to very large straggling the range-energy relation for electrons is not well defined one may suppose that the exponent in its power law is about the same as that for protons, *i.e.* 1.7. That is, if range measured along the track is denoted by r' , then $r' \propto w^{1.7}$. Now $r < r'$ so that probably $\alpha < 1.7$. On the other hand, electrons of very low energy will execute a random walk for which $r \propto \sqrt{r'}$, and hence α may be expected to exceed (1.7/2). Therefore α may be expected to lie in the interval

$$\frac{1.7}{2} < \alpha < 1.7.$$

Using the Mott formula and the postulated transverse range energy relation one arrives at a range distribution for the δ -rays. The number of δ -ray electrons which have transverse range between r and $r+dr$ is

$$(5) \quad N(r)dr \propto \frac{Z^2}{\beta^2} \frac{dr}{r^{1+1/\alpha}}.$$

The second assumption is that the average number of grains produced at a transverse distance $s < r$ by electrons of transverse range r is constant for all s and r . Note that this implies neither that the electrons are projected perpendicular to the primary track nor that they are projected rectilinearly. Then $\varrho(r)$, the number of grains per unit volume at a distance r from the trajectory is given by

$$\varrho(r) \propto \frac{Z^2}{\beta^2} \cdot \frac{1}{r} \int_{s=r}^{r_{\max}} N(s) ds,$$

where the $1/r$ term before the integral takes account of the cylindrical geometry. By performing the implied integration and substituting the result into eq. (1), and by letting $r \equiv x \sec \theta$, one obtains the result

$$(6) \quad \frac{\ln(I_0/I(x))}{K(Z^2/\beta^2)} = \frac{1}{x^{1/\alpha}} \int_0^{\sec^{-1}(r_{\max}/x)} (\sec \theta)^{1-1/\alpha} d\theta - \frac{1}{r_{\max}^{1/\alpha}} \ln(\sec \theta + \tan \theta),$$

where K is a constant depending upon, amongst other things, grain size a .

For relativistic particles, $r_{\max} \rightarrow \infty$, the second term vanishes and the integral in the first term becomes independent of x . Moreover, it can be shown to converge if $0 \leq 1 - 1/\alpha < 1$, i.e. $\alpha \geq 1$. (SOKOLNIKOFF⁽⁹⁾, p. 350). If this condition is satisfied, then for relativistic tracks

$$(7) \quad \ln \frac{I_0}{I(x)} \propto \frac{1}{x^{1/\alpha}}.$$

It will be seen that this result permits one to fix α experimentally, for by comparison with eq. (2), one obtains $\alpha = 1.1$. The transverse range energy relation for δ -rays must consequently be of the form

$$(8) \quad r = k\omega^{1.1}.$$

In writing the general profile equation, α was in fact set exactly equal to unity. This simplified the form of the resulting function which in any event appears to be somewhat insensitive to the exact value of α . From eq. (6), the general profile equation for the track of a particle of charge Z and velocity β is given by

$$(9) \quad \frac{\ln(I_0/I(x))}{K(Z^2/\beta^2)} = \frac{\theta}{x} - \frac{1}{r_{\max}} \ln(\sec \theta + \tan \theta).$$

(9) I. F. SOKOLNIKOFF: *Advanced Calculus* (New York).

The expression on the right, hereafter referred to as $P(x, r_{\max})$ is independent of the nature of the primary particle. A family of curves $P(x, r_{\max})$ has been computed for various values of r_{\max} and is shown in Fig. 3. These curves may

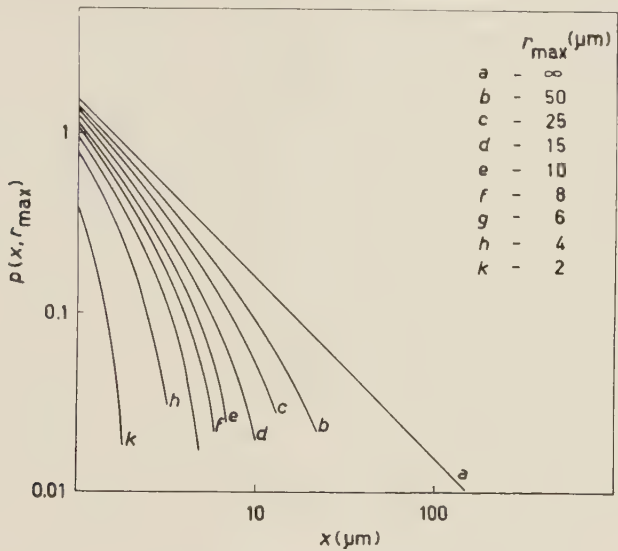


Fig. 3. – The function $P(x, r_{\max})$ for various values of r_{\max} .

be used to calculate the profiles of tracks of any Z and β provided 1) the constant K is known, and 2) the constant k in the transverse range energy relation is known.

1) K depends upon the characteristics of the emulsion being used, in particular upon the average size of grains. It was readily obtained by measuring $I_0/I(x)$ for relativistic tracks of known charge in G-5 emulsion. A group of tracks whose charges must have been of the order of 26 gave the result

$$K = (1.4^{+0.27}_{-0.17}) \cdot 10^{-3} .$$

The error in K corresponds to a possible maximum error in charge identification of ± 2 charges.

2) The constant k ($r = k\omega^{1.1}$) is rather more difficult to determine. At first it was thought feasible to obtain it from measurements on the width of heavy tapers a few microns from their end points. The argument was that near to the core of a heavy track the δ -ray density is so great that all the silver halide grains available are made developable and clogging results. The energy

w_c for which clogging takes place can be calculated (SKJEGGESTAD ⁽¹⁰⁾) and it turns out that as the residual range R diminishes, w_{\max} the maximum δ -ray energy and w_c approach each other, so that for an iron track at about $R \sim 40 \mu\text{m}$, $w_c \sim w_{\max}$. It was therefore expected that a measurement of width on such a track would give r_{\max} and thus k . In fact, at 37.5 microns from the end, the average width of an iron track appears to be about $(2.9 \pm 0.1) \mu\text{m}$ corresponding to $k = 210$, for r in micron, w in MeV. Considerations which will be dealt with in the next section have indicated that this is about 25 % too large, and the cause of the trouble is probably that in this neighbourhood, the transverse range of δ -rays is approaching the dimension of the grains, and the relative error of one grain diameter is becoming intolerably large.

5. - Application to taper width measurements.

The model which has been described in the foregoing sections has been used to calculate the widths of tapers as a function of their residual range and has been compared with measurements made on about 100 tapers of heavy nuclei (^{10}B — ^{56}Fe), chosen for their negligible dip.

The measurements were performed in the following way. By the use of a rotating stage, the track was adjusted parallel to the slit which was $0.5 \mu\text{m}$ wide in the object plane, and the profile was displayed on the screen of the oscilloscope. Because all measurements were made within $200 \mu\text{m}$ of the ends of the tracks, the whole profile of even the heaviest track could be displayed without the need of displacing the track laterally to bring its extreme edges within the field slit. Thus the width at half height called the mean track width (MTW), was read off the screen of the oscilloscope directly, though in arbitrary units. The time base of the oscilloscope is locked to the angular motion of the rotating glass cuboid of the densitometer with the result that the profile abscissa is not rigorously linear; nevertheless no correction was made for this irregularity. It is easy to show that the greatest possible departure from linearity is about 3 %. The MTW scale was calibrated by using the stage movement to shift a feature which could be readily recognized both visually in the emulsion and displayed upon the oscilloscope through a known displacement. The tapers were measured at seven successive $25 \mu\text{m}$ intervals, beginning at a residual range of $37 \mu\text{m}$, and no correction for depth in the emulsion was attempted.

Models for the thin down or taper process have been proposed by various

(¹⁰) O. SKJEGGESTAD: *Nuovo Cimento*, **8**, 927 (1958).

workers, for example LONCHAMP ⁽¹¹⁾, SKJEGGESTAD ⁽¹⁰⁾ and BIZZETI and DELLA CORTE ⁽¹²⁾; these have dealt with nuclei whose charge was in general less than or at most that of oxygen. Amongst the lower charges, the track width is never more than two or three grain diameters, and the question of the probability of the development of individual grains must come under consideration. This has been the approach taken by BIZZETI and DELLA CORTE. Since in our work we are concerned with the heavier nuclei whose track widths, even within 100 μm of the end, may be several grain diameters, we have assumed that approximately correct results could be obtained by extrapolating our essentially continuous theory to these regions, using a range-energy relation for heavy nuclei suitably modified to take account of electron pick-up near the end of their flight. Such range-energy relations for nuclei up to about iron are to be found in POWELL, FOWLER and PERKINS ⁽¹³⁾.

The MTW is the width of the profile where $I(x)/I_0 = \frac{1}{2}$. The function $P(x, r_{\text{max}})$ is used, together with the δ -ray transverse range energy relation, to calculate MTW for various Z and β by locating the point of intersection of the straight line

$$P = \frac{\ln 2}{K} \frac{\beta^2}{Z^2} = 495 \frac{\beta^2}{Z^2},$$

with the curve $P = P(x, \beta^2)$ and reading off from the graph (Fig. 3) the value of x , which is one half the mean track width. This method has been used to obtain a charge scale for mean track widths at 100 μm residual range and this is shown in Fig. 4 superimposed upon the distribution of mean track width at 100 μm obtained by averaging the mean track width at 87.5 μm and 112.5 μm .

In view of the fact that each determination consisted of the average of only two readings, and used at most the information available in a fifty μm length of track, it is remarkable that fair charge resolution has been obtained. Moreover, the theoretical charge scale corresponds satisfactorily with the experimental track widths. It has been considered unwise to try to predict half widths for tracks made by nuclei of charge four and less because the δ -rays on such tracks play a less important role than the core of the track. The mean track width of core alone is illustrated by the very large peak at approximately one μm , which consists of protons measured at one mm residual range.

⁽¹¹⁾ J. P. LONCHAMP: *Annales de Physique*, **10**, 201 (1955).

⁽¹²⁾ P. G. BIZZETI and M. DELLA CORTE: *Particle Photography Conference* (Montreal, 1958), p. 283.

⁽¹³⁾ C. F. POWELL, P. H. FOWLER and D. H. PERKINS: *The Study of Elementary Particles by the Photographic Method* (London, 1959).

To show that the charges of particles represented by peaks in the histogram were not widely different from the values given for them by the charge

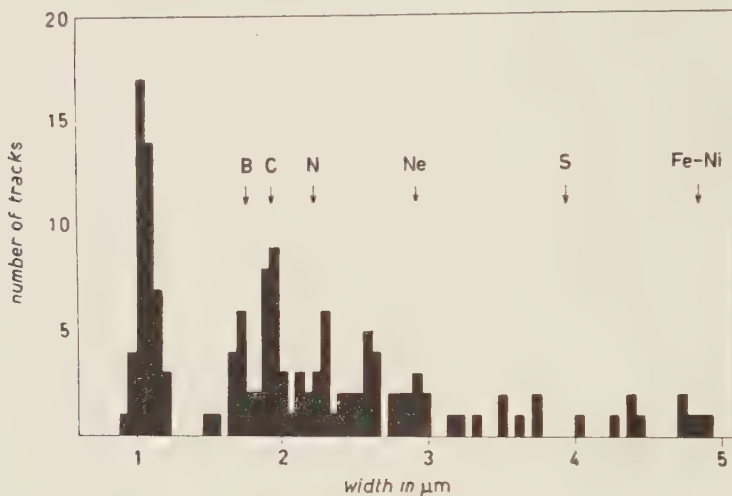
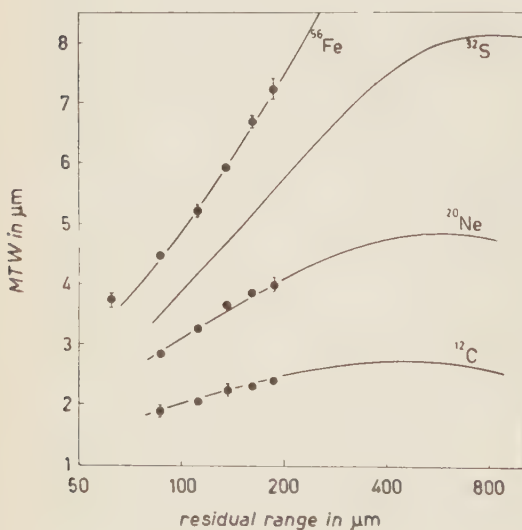


Fig. 4. - Charge spectrum obtained by measuring mean track widths of tapers at 100 μm residual range. The peak at 1 μm is composed of protons measured at 1 mm residual range and serves to illustrate the results of measuring mean track width upon a track bare of δ -rays. The superimposed charge scale has been calculated upon the basis outlined in the text.

scale, a small sample of these were remeasured with a wide slit (2.5 μm) at a residual range of 2 cm. Twenty successive readings, each using the information in 50 μm of track were



taken and averaged to obtain the final parameter which was regarded as a measure of the charge. Formerly, a group of about 100 tracks of particles of all charges down to lithium and including some helium had been dealt with in this way

Fig. 5. - Experimental mean track widths measured between 100 μm and 200 μm residual range (10 carbon, 10 neon, 4 iron) plotted together with theoretical mean track-width curves.

and a charge scale fitted (EVANS⁽¹⁴⁾). Comparison between the present sample and the former spectrum indicates a random discrepancy of plus or minus one charge.

Mean track width *vs.* residual range curves have been calculated for a selection of charges, and MTW's of groups of tracks whose MTW at 100 μm makes them appear to be near the appropriate charges were averaged to obtain points which are displayed together with the calculated curves in Fig. 5. In order to make the iron points fit their curve, it was found necessary to adjust the constant k to 150 *i.e.*

$$r = 150 w^{1.1}.$$

The effect of the adjustment upon the carbon-neon group was negligible.

* * *

The authors wish to thank Professor C. F. POWELL for the hospitality of his laboratory, Dr. C. J. WADDINGTON for helpful discussion and criticism, and the staff of scanners for their valuable assistance.

APPENDIX

Derivation of Equation (1).

Refer to the diagram (Fig. 6) which illustrates the symmetry of the δ -ray grains about the primary particle trajectory. Plane parallel light travels in the $+z$ direction. It is assumed that light is removed from the beam by simple shadowing and diffraction effects are neglected.

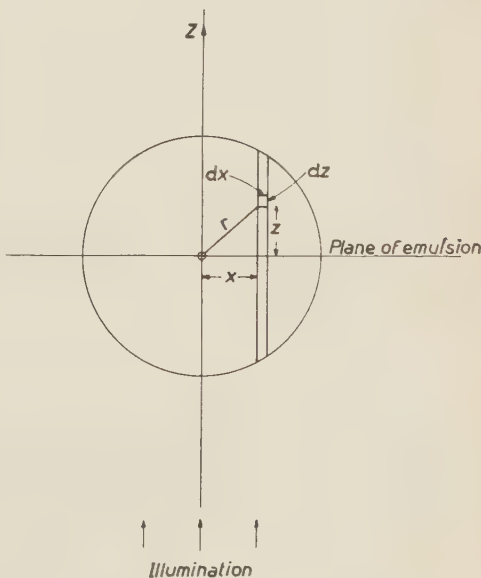


Fig. 6. - Diagram representing the obscuration of light by a track, viewed in cross-section. The particle trajectory is perpendicular to the plane of the diagram and intersects at it the origin.

(14) D. E. EVANS: *Moscow Conf. on Cosmic Rays*, (Moscow, 1960), vol. 3, p. 92.

Consider a beam of light of width dx at x and length into the plane of the diagram one unit. If the intensity in the beam at z is $I(x, z)$, then the loss in intensity consequent upon traversing the element dz is proportional to the ratio

$$\frac{\text{total area of cross-section of grains in volume element}}{\text{area of cross-section of the volume element}}$$

which is

$$a\varrho \frac{dx dz}{dx} = a\varrho dz,$$

where ϱ is the number of grains per unit volume and a the area of cross-section of a single grain; *i.e.*

$$dI(x, z) = -a\varrho I(x, z) dz.$$

From consideration of cylindrical symmetry, ϱ is a function only of r , the radial distance from the primary particle trajectory.

Thus

$$\int_{I_0}^{I(x)} \frac{dI(x, z)}{I(x, z)} = -2a \int_{r=0}^{r_{\max}} \varrho(r) \frac{dz}{dr} dr,$$

which, upon integration, results in

$$I(x) = I_0 \exp \left[-2a \int_{r=0}^{r_{\max}} \varrho(r) \frac{dz}{dr} dr \right].$$

RIASSUNTO (*)

L'analisi della struttura delle tracce dei nuclei pesanti nelle emulsioni nucleari porta ad un metodo per calcolare, con misure sulla traccia con un densitometro, scale di carica appropriate ad ogni dato parametro riscontrato. Come esempio calcoliamo le larghezze medie degli assottigliamenti ad un range residuo di 100 μm , per vari valori della carica, e otteniamo una buona concordanza con i risultati sperimentali.

(*) Traduzione a cura della Redazione.

The Influence of Pressure on the Mobility of Electric Charges in Liquid Helium II.

S. CUNSOLO and P. MAZZOLDI (*)

Istituto di Fisica dell'Università - Padova
Istituto Nazionale di Fisica Nucleare - Sezione di Padova

(ricevuto il 28 Febbraio 1961)

Summary. — The mobility of positive and negative charges in liquid helium II has been measured as a function of the pressure, for pressures ranging from the vapour pressure to the melting point, in the temperature range 1.9 to 1.1 °K. The mobility of the positive charges was found to decrease with the increasing pressure, but this decrease cannot be accounted for in terms of the known change in the roton density. The negative charges behave in a peculiar way which can be easily accounted for by the bubble model. For both charges an unexplained sharp break is found at about 1.3 °K especially at the higher pressures.

1. — Introduction.

Previous measurements of the mobilities of positive and negative electric charges in liquid He (¹⁻⁶) have indicated their dependence on the temperature. The aim of this paper was to investigate further the nature of the electric charges and their behaviour in liquid He II under pressure. To this end we have measured for the positive and negative charges the mobility as a function of the pressure in the range from 1.9 to 1.1 °K.

(*) Attualmente all'Istituto di Fisica dell'Università, Roma.

(¹) G. CARERI, F. SCARAMUZZI and J. O. THOMSON: *Nuovo Cimento*, **13**, 186 (1959).

(²) L. MEYER and F. REIF: *Phys. Rev.*, **110**, 279 (1958).

(³) F. REIF and L. MEYER: *Phys. Rev.*, **119**, 1164 (1960).

(⁴) G. CARERI, S. CUNSOLO and F. DUPRÉ: *Proc. VII International Conference on Low Temperature Physics* (Toronto, August 1960).

(⁵) R. L. WILLIAMS: *Can. Journ. Phys.*, **35**, 134 (1957).

(⁶) A. DAHM, J. LEVINE, J. PENLEY and T. M. SANDERS: *Proc. VII International Conference on Low Temperature Physics* (Toronto, August 1960).

2. - Description of the apparatus.

The method used to measure the mobility is a new time of flight procedure and is thoroughly described elsewhere by one of us ⁽⁷⁾. The electrodes are contained in a stainless steel cell provided with a copper bottom, to maintain good thermal contact with the external bath. The copper plate is sealed to the cell by means of an indium gasket which has been found leak tight below the λ -point even at the highest pressure. The cell is connected to a cylinder containing ^4He at a pressure of 140 atm through a capillary with an inner diameter of 1 mm except on the last section in which it is reduced to 0.2 mm to avoid a large heat input towards the apparatus. The 99% pure He gas from the cylinder is further purified by means of a liquid He trap. The pressure is measured by manometers calibrated to 0.5%. The values which we observed for the melting pressure were in good agreement with those obtained by KEESOM ⁽⁸⁾.

The temperature which was kept constant by an automatic thermoregulator, was monitored by a 10 ohm Allen-Bradley carbon resistance thermometer which was calibrated against the vapour of the liquid helium bath.

3. - Experimental results.

The pressure and temperature range covered by these measurements is shown in Fig. 1 for positive and Fig. 2 for negative ions. The experimental

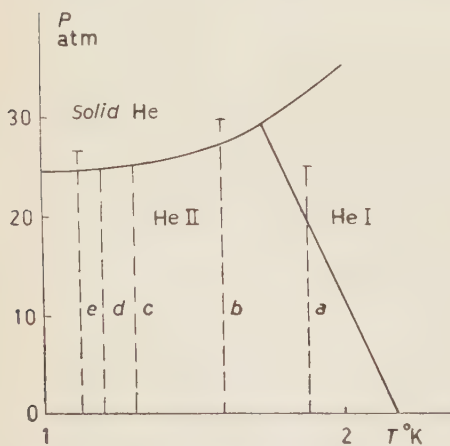


Fig. 1. - The pressure and temperature range covered by these measurements for positive ions.

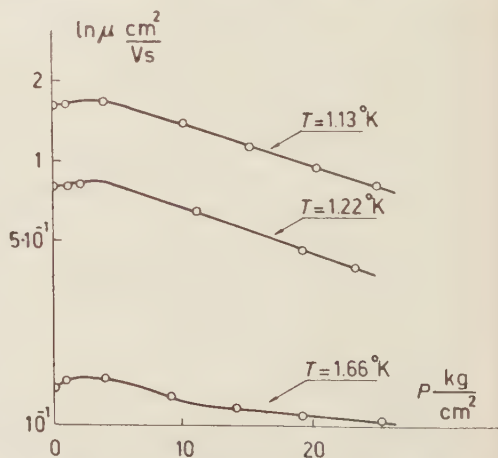


Fig. 2. - Experimental values for the mobility of negative ions as function of the pressure at constant temperature.

⁽⁷⁾ S. CUNSOLO: to be published in *Nuovo Cimento*.

⁽⁸⁾ R. KEESOM: *Helium* (1942), p. 202.

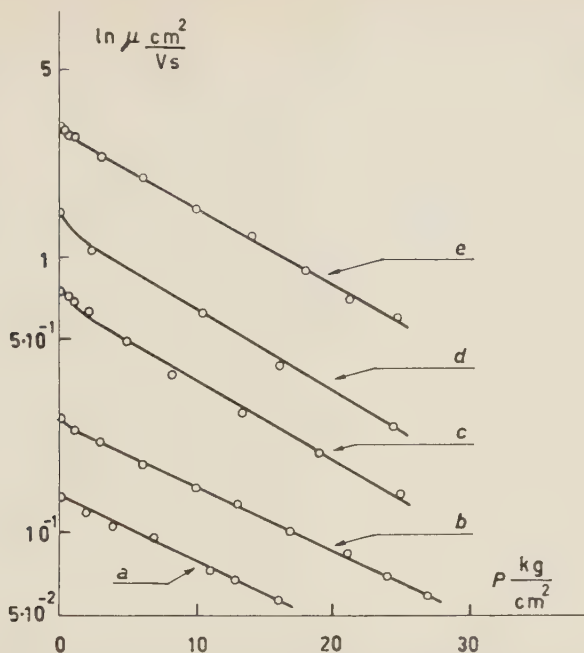


Fig. 3. - Experimental values for the mobility of positive ions as a function of the pressure at constant temperature.

values for the mobility of positive ions have been plotted in the five isotherms of Fig. 3 as a function of the pressure. Similar results for the negative ions are shown in Fig. 2.

Care was taken that the measurements were all made at electric fields low enough to have the mobility independent of the applied field ^(3,4,9). We first explored the change of the mobility when the melting point or the λ -point were reached. In both cases drastic changes were noticed: when we reached the freezing point we found that the

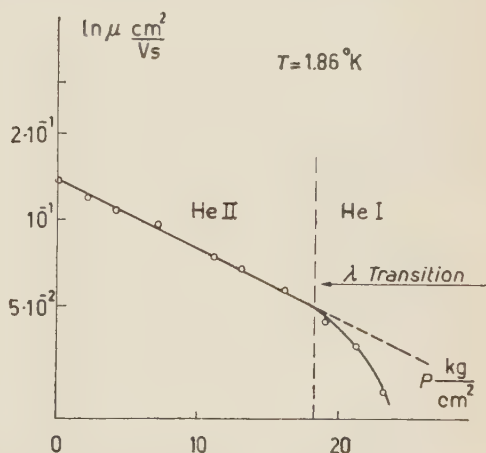


Fig. 4. - Experimental values for the mobility of positive ions at $T=1.86^{\circ}\text{K}$ in He. Note the break at the λ -transition.

⁽⁹⁾ G. CARERI, S. CUNSOLO and P. MAZZOLDI: to be published shortly.

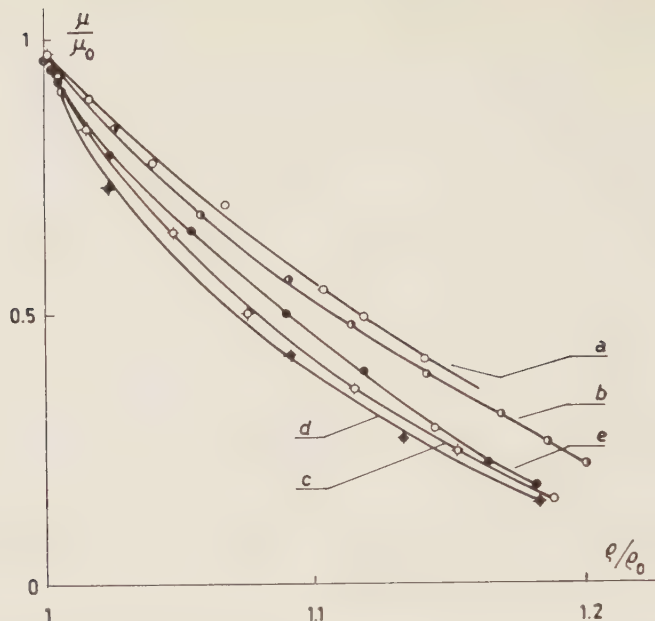
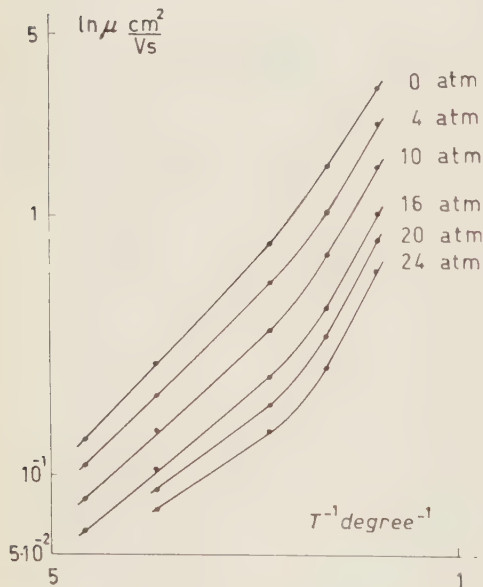


Fig. 5. - The reduced mobility of positive ions μ/μ_0 being the value of the mobility at vapour pressure, vs. the reduced density ρ/ρ_0 of the liquid helium.



currents of both signs disappeared indicating that in the solid neither the positive nor negative charge can move at all⁽¹⁰⁾. The λ -point was crossed at 1.86 °K as shown in Fig. 4. The mobility changes abruptly and reaches at that pressure the value obtained at the λ -point under the vapour pressure.

For a better understanding of the data, we have plotted in Fig. 5

Fig. 6. - The mobility values at constant pressure for positive ions, plotted vs. the reciprocal absolute temperature. These values are interpolated from the data of Fig. 2.

⁽¹⁰⁾ G. CARERI, U. FASOLI and F. GAETA: *Nuovo Cimento*, **15**, 774 (1960). This model is substantiated by recent theoretical work by KUPER, submitted for publication to *Phys. Rev.*

the ratio μ_p/μ_0 (where μ_0 indicates the value of the mobility at vapour pressure) vs. the ratio of the densities ϱ/ϱ_0 , and in Fig. 6 the dependence of the mobility on the temperature at constant pressure.

4. - Discussion.

4.1. *Positive ions.* - Let us start writing the mobility expression

$$(1) \quad \mu = \frac{e\lambda}{m\bar{c}};$$

where e is the electron charge, m the effective mass for the ionic motion, \bar{c} the average velocity and λ the mean free path of the ion. In this temperature range we can consider the rotons as the only scattering agents, and therefore

$$(2) \quad \lambda = \frac{1}{\sigma_{ir}N_r};$$

where σ_{ir} is the ion-roton cross-section and N_r the equilibrium number density of the rotons.

The pressure dependence of the mobility is obviously due to the pressure dependence of m , σ_{ir} and N_r , but before investigating this dependence we must ask ourselves the validity of expression (1). A glance at Fig. 6 shows that the break of $\log \mu$ vs. $1/T$ curve at 1.3 °K is more and more noticeable when the pressure increases. At first one might think this break to be due to the change in the roton energy gap Δ at this temperature, because of the incipient non-ideality of the roton gas which affects (1) by the change in N_r . This change in Δ is also detectable in neutron experiments ⁽¹¹⁾, but these experiments show also that a much more pronounced change in Δ should occur close to the λ temperature, while the mobility curve is then insensitive. Therefore one should considerably doubt of the applicability of eq. (1) to the temperature range below 1.3 °K, where a different kind of expression should be used. This range therefore will not be considered any further, due also to the lack of knowledge of the pressure dependence of Δ and p_0 .

Next we will consider the range of temperature below 1.3 °K, and apply expression (1) with the further hypothesis

$$(3) \quad \left(\frac{\partial m}{\partial \varrho}\right)_T = \left(\frac{\partial \sigma_{ir}}{\partial \varrho}\right)_T = 0,$$

⁽¹¹⁾ D. C. HENSHAW and A. D. B. WOODS: *Proc. VII International Conference on Low Temperature Physics* (Toronto, August 1960).

and calculate the mobility with the resulting assumption that the pressure makes itself felt only through N_τ . The value of μ/μ_0 calculated at this value of the maximum ratio $\varrho/\varrho_0 = 1.15$, is about 30 % lower than our experimental results. Furthermore the relative position of the curves e and d of Fig. 4 is also unexplained. We conclude that the assumption (3) must be wrong, as one could have anticipated. We may hope that a theory will be worked out to account for the correct dependence of m and σ_{ir} from the pressure, but at the present this analysis cannot be pushed any further.

Finally we would like to comment that our measurements below 1.3 have not been extended at too low temperatures because the mobility in this range starts to be voltage dependent (⁹), and the entire matter is still a subject of investigation in this laboratory. But from the very few data here reported at 1.3 °K, 1.2 °K, 1.12 °K, it seems that the slope of the $\log \mu - 1/T$ curve is independent from the pressure. This is in contrast with the known (¹¹) dependence of Δ from the pressure, and this seems therefore one more indication that in the mobility expression also the effect in m and σ_{ir} must be taken into account.

4.2. Negative ion. — The behaviour of the negative ion seems curious at first sight, its mobility first increasing and then decreasing with the increasing pressure. A qualitative explanation however is possible if we assume for the negative ion the « bubble model », already proposed by CARERI, FASOLI and GAETA (¹⁰) to explain its behaviour in other experimental situations.

According to these authors, the negative ion is essentially a free electron trapped in a cage or bubble, by the opposing action of its zero point energy and the polarization forces. It is then quite conceivable that under the action of the external pressure the bubble size will first decrease, reducing in this way its cross-section and augmenting the mobility accordingly. A further increase of the pressure will now decrease the mobility for reasons similar to the ones outlined above for the positive ion.

* * *

Thanks are due to Prof. G. CARERI for many useful discussions and suggestions concerning this work and to Dr. U. FASOLI for kind co-operation for the construction of the high pressure apparatus.

Note added in proof.

While this work was at the printer we received the preprint of a paper by MEYER and REIF on the same argument. These authors have made their measurements in a temperature range somewhat lower than the one which we have investigated in the present work.

In the temperature range where they overlap, their results for positive ions agree with ours.

For negative ions the comparison of the isotherms shows that there is agreement from the vapour pressure up to the pressure at which the mobilities of the positive and negative ions become equal. For higher pressure we find that the mobility of negative ions is always higher than that of the positive ions, while the data of Meyer and Reif show equal mobilities for all the pressures above 7 atm.

RIASSUNTO

È stata misurata la mobilità di cariche elettriche positive e negative in elio liquido II in funzione della pressione, per pressioni che vanno dalla tensione di vapore al punto di solidificazione e nell'intervallo di temperatura compreso tra 1.9 °K e 1.1 °K. Abbiamo trovato che la mobilità delle cariche positive decresce col crescere della pressione, ma questo calo non può essere spiegato in termini della nota variazione della densità dei rotoni. Il comportamento delle cariche negative può essere facilmente spiegato col modello a « bolla ». Per le cariche dei due segni è stato riscontrato un cambiamento di pendenza della mobilità in funzione della temperatura a circa 1.3 °K, specialmente alle più alte pressioni.

A Discussion of the Noyes and Wong Equation for Potential Scattering.

V. DE ALFARO and T. REGGE

Istituto di Fisica dell'Università - Torino
Istituto Nazionale di Fisica Nucleare - Sezione di Torino

(ricevuto il 2 Marzo 1961)

Summary. — A discussion is outlined on the Martin form of the Noyes and Wong equation in potential theory. A theorem is given about the connection between zeros of the discontinuity of the S -function and the resonant states.

1. — Introduction.

In a recent paper MARTIN ⁽¹⁾ has proposed a new form of the well known Noyes and Wong N/D equation. The discussion of this equation is particularly simple for the case of potential scattering although it can be readily extended to fit into more involved situations.

We shall limit here ourselves to S -waves. As MARTIN has pointed out, for finite range potentials the following representation of $S(k) \exp[2i\delta]$ can be written, where $k^2 = E$ (we adopt natural units, $\hbar = c = 2m = 1$):

$$(1) \quad S(k) = \frac{1 + \int_{\mu/2}^{\infty} \frac{w(x) dx}{x + ik}}{1 + \int_{\mu/2}^{\infty} \frac{w(x) dx}{x - ik}}.$$

⁽¹⁾ A. MARTIN: *S-matrix, left hand cut discontinuity and potential*, CERN preprint.

The problem is that of constructing the function $S(k)$ from the knowledge of its discontinuity along the imaginary axis of k . It should be pointed out that in the current literature the so-called Noyes and Wong equation refers to the upper plane of k only and it is written with the energy E as variable. From (1) we see that $S(k)$ is clearly unitary and that the discontinuity is given by

$$(2) \quad \frac{S(i\xi - \varepsilon) - S(i\xi + \varepsilon)}{2\pi i} = \frac{w(\xi)}{1 + \int_{\mu/2}^{\infty} \frac{w(x) dx}{x + \xi}} = D(\xi).$$

This formula is at the same time an equation for the weight function $w(\xi)$ and, if solved, yields $w(\xi)$ and therefore $S(k)$ in terms of $D(\xi)$. Let $w(\xi) = D(\xi)F(\xi)$. We have

$$(3) \quad F(\xi) = 1 + \int_{\mu/2}^{\infty} \frac{D(x)F(x) dx}{x + \xi}.$$

This is an integral equation for $F(\xi)$ of the Fredholm type. $S(k)$ is related to F as follows:

$$S(k) = \frac{F(ik)}{F(-ik)} = \frac{f(k)}{f(-k)}.$$

$F(ik)$ is better known as the Jost function $f(k)$. Eq. (3) can be solved according to the standard methods of analysis. The solution is formally given by

$$(4) \quad F(x) = 1 + \frac{\Delta(x)}{\Delta},$$

where

$$(5) \quad \Delta = \sum_{n=0}^{\infty} \frac{(-1)^n}{n!} \int_{\mu/2}^{\infty} \dots \int_{\mu/2}^{\infty} d\xi_1 \dots d\xi_n D(\xi_1) \dots D(\xi_n) \det_{p,q \leq n} \left| \frac{1}{\xi_p + \xi_q} \right|,$$

$$\Delta(x) = \sum_{n=1}^{\infty} \frac{(-1)^{n-1}}{(n-1)!} \int_{\mu/2}^{\infty} \dots \int_{\mu/2}^{\infty} D(\xi_1) \dots D(\xi_n) d\xi_1 \dots d\xi_n \det_{q' p \leq n} \left| \frac{1}{\xi_p + \xi_{q'}} \right|,$$

where $\xi'_q = \xi_q$ if $q < n$, and $\xi'_n = x$.

2. - Discussion of the integral equation.

The condition under which this expansion converges can be found with the help of Hadamard's lemma which places an upper bound on the determinants. A more refined result can be derived by finding first an explicit form for the determinant as follows. The determinant

$$\det_n = \det_{q, p \leq n} \left| \frac{1}{\xi_p + \xi_q} \right| = \begin{vmatrix} \frac{1}{2\xi_1} & \frac{1}{\xi_1 + \xi_2} & \cdots & \frac{1}{\xi_1 + \xi_n} \\ \vdots & & & \\ \frac{1}{\xi_n + \xi_1} & \cdots & & \frac{1}{2\xi_n} \end{vmatrix},$$

is obviously a homogeneous rational function of the ξ_p 's of degree $-n$; i.e. it is the ratio of two homogeneous polynomials in these variables: $\det_n = \mathcal{N}/\mathcal{D}$. The lower polynomial \mathcal{D} can be taken to be the product $\prod_{p < q} (\xi_p + \xi_q)$ which is of degree n^2 . The upper polynomial \mathcal{N} is clearly of degree $n(n-1)$. It is invariant under any permutation of the indexes $1 \dots n$, because any such permutation leaves the denominator unchanged and displaces in the same way both rows and columns of the determinant. On the other hand the numerator has to vanish whenever two ξ_p 's coincide; \mathcal{N} has to be of the form $\mathcal{P} \prod_{p < q} (\xi_p - \xi_q)^2$, where \mathcal{P} is of degree zero since $\prod_{p < q} (\xi_p - \xi_q)^2$ is already of degree $n(n-1)$. \mathcal{P} is therefore a constant, $\mathcal{P} = P_n$. It follows

$$(6) \quad \det_n = P_n \frac{1}{2^n} \frac{1}{\xi_1 \dots \xi_n} \prod_{p < q} \frac{(\xi_p - \xi_q)^2}{(\xi_p + \xi_q)^2}.$$

But by taking the limit $\xi_p \rightarrow \infty$ we easily see that

$$\lim_{\xi_n \rightarrow \infty} 2\xi_n \det_n = \det_{n-1}.$$

From this limit it follows that $P_n = P_{n-1}$. But $P_0 = 1$; hence we have $P_n = 1$. From (6) we have the upper and lower bound:

$$(7) \quad 0 \leq \det_n \leq \prod_{p=1}^n \frac{1}{2\xi_p}.$$

From this bound we find for Δ :

$$|\Delta - 1| < e\Delta - 1,$$

where

$$A = \frac{1}{2} \int_{\mu/2}^{\infty} \frac{|D(x)|}{x} dx.$$

If $A < \ln 2$, Δ cannot vanish and we have certainly a solution of the Fredholm equation.

If the integral for A does not converge we have so far no way of saying anything about the solution.

With the same procedure sketched above for \det_n , we find;

$$\det \left| \frac{1}{\xi_p + \xi_q'} \right| = \frac{1}{2^{n-1}} \frac{1}{\xi_1 \dots \xi_{n-1}} \prod_{p < q}^{n-1} \frac{(\xi_p - \xi_q)^2}{(\xi_p + \xi_q)^2} \frac{1}{\xi_n + x} \prod_{q < n} \frac{(\xi_q - \xi_n)(\xi_n - x)}{(\xi_q + \xi_n)(\xi_q + x)}.$$

It follows

$$\left| \det \frac{1}{\xi_p + \xi_q'} \right| \leq \prod_{p=1}^{n-1} \frac{1}{2\xi_p} \frac{1}{\xi_n + x},$$

and

$$\Delta(x) \leq e^A \int_{\mu/2}^{\infty} \frac{|D(\xi)| d\xi}{x + \xi}.$$

If $D(x) < 0$, Δ is certainly positive and the equation admits a solution if $A < \infty$. In his work MARTIN has shown that $D(x)$ determines uniquely the potential. This is also evident from the fact that $f(k)$ is also completely determined by $D(x)$. Now GEL'FAND and LEVITAN have shown how to derive $V(x)$ from $f(k)$ and the result is again unique.

Some doubt could exist as to whether $S(k)$ determines $V(x)$ uniquely. In fact in Gel'fand and Levitan's theory there is room for phase equivalent potentials, *id est* potentials with the same phase shifts and different bound states. It is worth noticing that all these potentials have different $f(k)$ but the same $S(k)$.

But one works here with finite range potentials, which give singularities of $f(k)$ only for $|k| > \mu/2$, $\arg k = \pi/2$. In this case the potential is uniquely determined, once the S -matrix is known. Let us suppose that $\delta(k)$ be the phase-shift corresponding to a finite range potential, which, for sake of simplicity, has no bound states, and let $f(k)$ be the corresponding Jost function. $f(k)$ is easily obtained from $\delta(k)$, writing down a dispersion relation for $\ln f(k)$:

$$\operatorname{Re} \ln f(k) = \frac{P}{\pi} \int_0^{\infty} \frac{\delta(\xi) d\xi^2}{\xi^2 - k^2}.$$

Here clearly we have taken the determination of $\delta(k)$ such that $\delta(\infty) = 0$.

Now we suppose to have another potential with the same phase shift but a bound state in $k = -i\lambda$. The integration has now to be performed along the path shown in Fig. 1. Let us call $f(k)$ the corresponding Jost function. We see that

$$\operatorname{Re} \ln f^1(k) = \frac{P}{\pi} \int_0^\infty \frac{f(\xi) d\xi^2}{\xi^2 - k^2} + \ln \frac{\lambda^2 + k^2}{k^2},$$

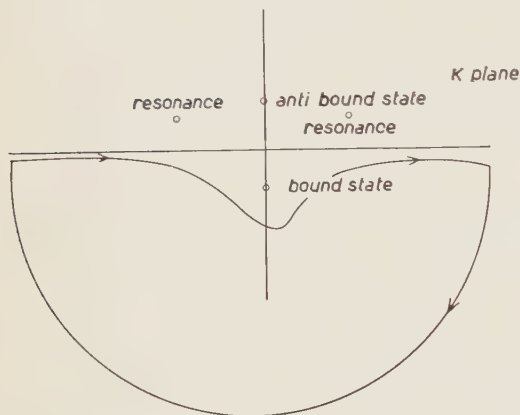


Fig. 1.

from which $f^1(k) = f(k)[(k^2 + \lambda^2)/k^2]$. Besides the bound state there appears a virtual one in $k = i\lambda$, in order not to affect the value of $S(i\lambda)$. A factor k appears also, in order to restate the behaviour at infinity; but this shows a pole at the origin, and the corresponding potential is not a short range one (see BARGMANN'S ⁽²⁾ paper, in which some phase equivalent potentials are given: only one is short ranged).

3. - The sign of $D(x)$ and the number of poles of $S(k)$.

There is a simple and interesting inequality between the number of changes of sign of $D(x)$ in the interval $\mu/2 \dots \infty$, and the number of poles of $S(k)$ with $\operatorname{Im} k > 0$. In order to find it let us consider the Jost function. The zeros of this function with $\operatorname{Im} k < 0$ correspond to bound states, those with $\operatorname{Im} k > 0$ to the resonant and virtual (or antibound) states. Let us suppose that none of the last ones falls on the cut $\mu/2 \dots \infty$.

The function $q(k) = \arg f(k)$ is multivalued in k since each zero of $f(k)$ is a branch point of $\ln f(k)$. In order to make it single-valued we cut the k plane with straight lines connecting each zero of $f(k)$ with $k = i(\mu/2)$. We define $\arg f(k)$ elsewhere in such a way as to have $\lim_{k \rightarrow \infty} \arg f(k) = 0$, $\arg k \neq \pi/2$. We know that $q(-k^*) = -q(k)$. Suppose now that $q((i\mu/2) - \varepsilon) = q_0$. We have $q((i\mu/2) + \varepsilon) = -q_0$. On the other hand one can go from $k = (i\mu/2) - \varepsilon$

(2) V. BARGMANN: *Rev. Mod. Phys.*, **21**, 488 (1949).

to $k = (i\mu/2) + \varepsilon$ through the path P shown in Fig. 2. In so doing we encircle all zeros of $f(k)$ anticlockwise and q must increase by the amount $2m\pi$ where m is the total number of zeros of $f(k)$ enclosed by P , *i.e.* is the number n of bound states plus the total number of resonances and antibound states.

Therefore $q_0 = -m\pi$. On the other hand

$$D(x) = \frac{S(ix - \varepsilon) - S(ix + \varepsilon)}{2\pi i} = \frac{f(ix - \varepsilon) - f(ix + \varepsilon)}{2\pi i f(-ix)}.$$

$f(-ix)$ is analytic for x real > 0 . Putting $f(ix + \varepsilon) = \varrho(0) \exp[-i\Phi(x)]$ we have

$$D(x) = \frac{\varrho(x) \sin \Phi(x)}{\pi f(-ix)}.$$

Let $D(x)$ be at first continuous. If we let x increase from $\mu/2$ to ∞ , and if $\Phi(x)$ is continuous, then Φ must change continuously from the value $m\pi$ to the value 0.

Therefore $\sin \Phi(x)$ must have at least $m-1$ zeros in the interval $\mu/2 < x < \infty$. These are also zeros of $D(x)$ if $f(-ix)$ does not vanish simultaneously with $\sin \Phi(x)$. This may happen only if $k = -ix$ is a bound state and therefore it can happen at most n times. $D(x)$ vanishes at least $m-n-1$ times. If we know the number of zeros of $D(x)$ then we may place an upper limit on $m-n$. In particular if $D(x)$ is of constant sign we have $m-n \leq 1$.

If $D(x)$ is a distribution, for instance a Dirac function, we may proceed by approximating it with a continuous strongly peaked function and then going to the limit.

This theorem obviously recalls the analogous result of Levinson which states that $\delta(0) = n\pi$.

Our results can be easily checked for the simple case where $D(x) = D \cdot \delta(x - x_0)$. Here the solution of eq. (2) is elementary and one has

$$F(\xi) = 1 + \frac{D}{1 - (D/2x_0)} \frac{1}{x_0 + \xi}.$$

This function has one zero only in $\xi = -x_0(2x_0 + D)/(2x_0 - D)$. It can have therefore at most one antibound state and no resonance since these occur in pairs of conjugate zeros. This could be seen as said by approximating the δ -function by some strongly peaked function.

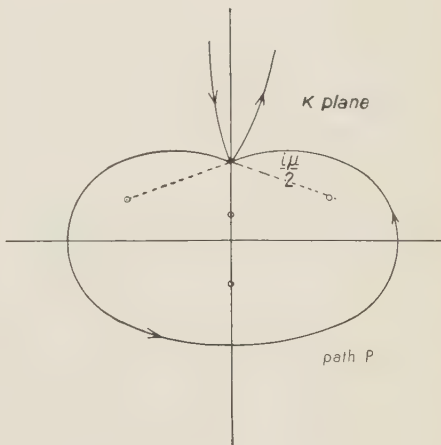


Fig. 2.

We may now examine the case where $f(x)$ has a zero in $k = k_0$, where k_0 is on the discontinuity. We have of course $f(k_0 - \varepsilon) = f(k_0 + \varepsilon)$. This case is quite possible, indeed it appears already in the above example. If $D > 0$ and $2x_0 > D$ the ensuing zero of $F(\xi)$ lies on the support of $D(x)$ beyond the point x_0 . If this antibound states appear, they do not show up in computing the number m of the formula $\varphi_0 = -m\pi$. Yet they act in the sense that $\Phi(x)$ has a discontinuity $\Delta\Phi = \pi$ whenever these zeros appear; $\sin \Phi(x)$ changes its sign and simultaneously $\varrho(x)$ vanishes. The result is that these zeros appear as additional zeros of $D(x)$. Luckily this reinforces our statement regarding the difference $m - n - 1$; we are still able to say that $m - n - 1$ does not exceed the number of zeros of $D(x)$.

If $D(x) = 0$ in some interval $a < x < b$ then $f(k)$ is analytic and real in this interval, and therefore $\Phi = q\pi$, q integer. q may not be a constant in this interval since $f(k)$ may vanish.

The case $D(x) > 0$ is interesting. Since $\varrho(x) > 0$ and $\lim F(x) = 1$, $\sin \Phi(x)$ is asymptotically positive and so is $\Phi(x)$ because Φ is small for large x and $\sin \Phi \sim \Phi$. But Φ must finally approach the value $-m\pi$ where $m > 0$. In so doing $\sin \Phi$ must change its sign at least m times. But these changes take place only by having $f(x) = 0$, or by having m bound states. Therefore there are neither antibound nor resonant states. If we allow $D(x) = 0$ then we could have an antibound state where $D(x) = 0$; the detailed discussion of these and other particular cases would however carry us too far.

We want at last to note that this problem could be treated in an analogous way also out from a potential theory framework, if the approximation of only elastic scattering is done. In this case however we have no prescriptions on the behaviour of $w(x)$ at infinity, so that there could be the need for a subtracted form of $f(k)$; this is a way for introducing arbitrary parameters analogous to the Castillejo-Dalitz-Dyson poles, *i.e.* bound or resonant states which don't vanish with the switching off of the coupling constant.

* * *

We wish to thank Prof. M. CINI for many discussions. This work was done while one of us (V.D.A.) was at the Istituto di Fisica dell'Università di Roma, and he wishes to thank very much the Direction of the Institute and the Theoretical Division for the kind hospitality.

RIASSUNTO

In questo lavoro viene fatta una discussione della equazione di Noyes e Wong in teoria del potenziale nella forma data da Martin. Si dimostra un teorema sulla relazione tra gli zeri della discontinuità della funzione S e il numero di stati risonanti.

Superfluidity and Perturbation Expansion in a Large Fermi System.

A. TOMASINI

Istituto di Fisica dell'Università - Bologna
Istituto Nazionale di Fisica Nucleare - Sezione di Bologna

(ricevuto il 13 Marzo 1961)

Summary. — The Bogoljubov-Valatin canonical transformation is performed, then the perturbation approach for the evaluation of the true states of a large Fermi system is examined. It is shown that the difficulty of the usual perturbation expansions due to the pole in the Brueckner t matrix is in general overcome by this procedure. It is shown that the corrections introduced by the interaction between the quasi-particles in the excitation energy are of the same order of magnitude of the excitation energy itself in the region of its minimum. These corrections appear to be slowly dependent on the strength of the interaction. An approximation is introduced which is an extension of the Brueckner one.

1. — Introduction.

In the theory of some Fermi systems one finds a difficulty in defining the perturbative expansions, due to the pole which appears in the t matrix defined by BRUECKNER ⁽¹⁻³⁾; this pole is strictly connected with the bound states of two particles of opposite momentum and spin near the Fermi surface, discovered by COOPER ⁽⁴⁾.

The existence of the Cooper state gives rise to the superfluidity of the system, since it introduces a gap in the excitation spectrum of the system ⁽⁵⁾.

⁽¹⁾ C. BLOCH: *Comptes rendus du Congrès international de Physique Nucléaire* (1958) (Paris, 1959).

⁽²⁾ V. J. EMERY: *Nucl. Phys.*, **12**, 69 (1958).

⁽³⁾ L. VAN HOVE: *Physica*, **25**, 849 (1959).

⁽⁴⁾ L. N. COOPER: *Phys. Rev.*, **104**, 1189 (1956).

⁽⁵⁾ J. BARDEEN, L. N. COOPER and J. R. SCHRIEFFER: *Phys. Rev.*, **108**, 1175 (1957).

A mathematical clarification of the problem is obtained introducing the Bogoljubov-Valatin ⁽⁶⁻⁸⁾ canonical transformation, which makes the hamiltonian of the system formally identical with that of a system of fermions (called quasi-particles) whose kinetic energy has a minimum value Δ . In such a way we introduce a gap in the energy spectrum.

Since this procedure eliminates the vanishing denominators which were at the origin of the difficulty, it is likely that one overcomes the difficulty itself performing first the canonical transformation and then making the perturbative expansions ⁽³⁻⁹⁾.

If this is verified, one can calculate the real states of the system and see if the gap, which appears in the unperturbed (kinetic) part of the quasi-particle hamiltonian, remains after the introduction of the interaction hamiltonian H_{int} between the quasi-particles.

In this paper H_{int} is examined with the use of diagrams which are the natural extension of those used by HUGENHOLTZ ⁽¹⁰⁾.

The corrections introduced by H_{int} to the energy of excitation in the region of minimum (*i.e.* $k \simeq k_F$) are of the order of magnitude of the excitation energy itself.

A τ matrix is introduced, which is the analogue of the Brueckner t matrix. The absence of poles in the τ matrix is proved directly in the case of separable potentials; it seems that this property is very general.

With the use of the τ matrix an approximation is considered which should have its validity at low density. The approximation could be modified applying a self-consistent method which is an extension of the Brueckner one ⁽¹¹⁾.

2. - The perturbation expansion.

Let us consider a large system of fermions, whose hamiltonian is:

$$(1) \quad H = \sum_{k_s} (\varepsilon_k - \lambda) a_{k_s}^+ a_{k_s} + \frac{1}{4} \sum_{\substack{k_1 k_2 k_4 \\ s_1 s_2 s_3 s_4}} \langle k_1 s_1, k_2 s_2 | V | k_3 s_3, k_4 s_4 \rangle a_{k_1 s_1}^+ a_{k_2 s_2}^+ a_{k_3 s_3} a_{k_4 s_4}.$$

⁽⁶⁾ N. N. BOGOLJUBOV: *Nuovo Cimento*, **7**, 794 (1958).

⁽⁷⁾ N. N. BOGOLJUBOV, V. V. TOLMACHER and D. V. SHIRKOV: *A New Method in the Theory of Superconductivity* (Moscow, 1958).

⁽⁸⁾ J. G. VALATIN: *Nuovo Cimento*, **7**, 843 (1958).

⁽⁹⁾ G. FANO: *Nuovo Cimento*, **15**, 959 (1960).

⁽¹⁰⁾ N. M. HUGENHOLTZ: *Physica*, **23**, 481 (1957).

⁽¹¹⁾ For a short review of the Hartree and Brueckner approximations see: R. J. EDEN: *Nuclear Reactions*, edited by P. M. ENDT and M. DEMEUR (Amsterdam), p. 1.

Let us perform the canonical transformation ⁽⁶⁻⁸⁾:

$$(2) \quad \begin{cases} \alpha_{ks} = u_k a_{ks} - v_{ks} a_{ks}^+ , \\ v_{k\uparrow} = -v_{k\downarrow} = v_k , & u_k^2 + v_k^2 = 1 . \end{cases}$$

With the usual procedure of elimination of the dangerous diagrams (minimization of the expectation value of the hamiltonian) one obtains ⁽⁶⁻⁸⁾:

$$(3) \quad H = U + \sum_{ks} E_k a_{ks}^+ a_{ks} + H_{\text{int}} ,$$

where

$$(4) \quad U = \sum_{ks} \left\{ (\varepsilon - \lambda) + \frac{1}{2} \sum_{k's'} \langle k s, k' s' | V | k' s', k s \rangle v_{k'}^2 \right\} v_k^2 - \sum_k \Delta_k u_k v_k ,$$

$$(5) \quad E_k = \sqrt{\xi_k^2 + \Delta_k^2} ,$$

$$(6) \quad \xi_k = \varepsilon_k - \lambda + \sum_{k's'} v_{k'}^2 \langle k s, k' s' | V | k' s', k s \rangle ,$$

$$(7) \quad v_k^2 = \frac{1}{2} \left(1 - \frac{\xi_k}{E_k} \right) ,$$

and Δ_k is solution of the equation:

$$(8) \quad \Delta_k = -\frac{1}{2} \sum_{k'} \langle k'\uparrow, -k'\downarrow | V | -k\downarrow, k\uparrow \rangle \frac{\Delta_{k'}}{E_{k'}} .$$

The trivial solution of (8)

$$(9) \quad \Delta_k = 0$$

gives the normal state; in this case the energy of the ground state is identical to the energy evaluated with the Hartree approximation ⁽¹²⁾.

H_{int} can be written in the form ⁽¹³⁾:

$$(10) \quad H_{\text{int}} = \frac{1}{4} \sum \langle k_1 s_1, k_2 s_2 | V | k_3 s_3, k_4 s_4 \rangle N(a_{k_1 s_1}^+ a_{k_2 s_2}^+ a_{k_3 s_3} a_{k_4 s_4}) ,$$

$$(11) \quad a_{ks} = u_k \alpha_{ks} + v_{ks} \alpha_{-k-s}^2 ,$$

where N means normal form.

⁽¹²⁾ The connection of the method with the Hartree-Fock self consistent method is discussed in a paper by VALATIN (to be published).

⁽¹³⁾ For a clear derivation of the various parts of the hamiltonian see ref. ⁽⁹⁾.

We wish now to examine the effect of H_{int} by means of diagrams; therefore we write (10) explicitly. After some manipulations one finds:

$$(12) \quad H_{\text{int}} = H_{04} + H_{13} + H_{22} + H_{31} + H_{40},$$

where

$$(13) \quad H_{04} = \frac{1}{4} \sum \langle -k_1 - s_1, -k_2 - s_2 | V | k_3 s_3, k_4 s_4 \rangle \cdot (v_{-k_1 - s_1} v_{-k_2 - s_2} u_{k_3} u_{k_4}) \cdot \alpha_{k_1 s_1} \alpha_{k_2 s_2} \alpha_{k_3 s_3} \alpha_{k_4 s_4},$$

$$(14) \quad H_{13} = H_{13}^{(1)} + H_{13}^{(2)} = \frac{1}{2} \sum [\langle k_1 s_1, -k_2 - s_2 | V | k_3 s_3, k_4 s_4 \rangle \cdot u_{k_1} v_{-k_2 - s_2} u_{k_3} u_{k_4} + \langle -k_1 - s_2, -k_3 - s_3 | V | -k_1 - s_1, k_4 s_4 \rangle \cdot v_{-k_1 - s_1} v_{-k_2 - s_2} v_{-k_3 - s_3} u_{k_4}] \alpha_{k_1 s_1}^+ \alpha_{k_2 s_2} \alpha_{k_3 s_3} \alpha_{k_4 s_4},$$

$$(15) \quad H_{22} = H_{22}^{(1)} + H_{22}^{(2)} + H_{22}^{(3)} = \sum [\frac{1}{4} \langle k_1 s_1, k_2 s_2 | V | k_3 s_3, k_4 s_4 \rangle \cdot u_{k_1} u_{k_2} u_{k_3} u_{k_4} + \langle k_1 s_1 - k_3 s_3 | V | k_4 s_4, -k_2 - s_2 \rangle u_{k_1} v_{-k_2 - s_2} v_{-k_3 - s_3} u_{k_4} + \frac{1}{4} \langle k_1 s_1, k_2 s_2 | V | k_3 s_3, k_4 s_4 \rangle v_{-k_1 - s_1} v_{-k_2 - s_2} v_{-k_3 - s_3} v_{-k_4 - s_4}] \alpha_{k_1 s_1}^+ \alpha_{k_2 s_2}^+ \alpha_{k_3 s_3} \alpha_{k_4 s_4},$$

$$(16) \quad H_{31} = H_{31}^{(1)} + H_{31}^{(2)} = \frac{1}{2} \sum [\langle k_1 s_1, k_2 s_2 | V | -k_3 - s_2, k_4 s_4 \rangle \cdot u_{k_1} u_{k_2} v_{-k_3 - s_2} u_{k_4} + \langle k_1 s_1, -k_4 - s_4 | V | -k_2 - s_2, -k_3 - s_3 \rangle \cdot u_{k_1} v_{-k_2 - s_2} v_{-k_3 - s_3} v_{-k_4 - s_4}] \alpha_{k_1 s_1}^+ \alpha_{k_2 s_2}^+ \alpha_{k_3 s_3}^+ \alpha_{k_4 s_4},$$

$$(17) \quad H_{40} = \frac{1}{4} \sum \langle k_1 s_1, k_2 s_2 | V | -k_3 - s_3, -k_4 - s_4 \rangle \cdot (u_{k_1} u_{k_2} v_{-k_3 - s_3} v_{-k_4 - s_4}) \alpha_{k_1 s_1}^+ \alpha_{k_2 s_2}^+ \alpha_{k_3 s_3}^+ \alpha_{k_4 s_4}^+.$$

In the case of the normal solution (9) one has:

$$(18) \quad u_k = 0, \quad v_k = 1, \quad k < k_F$$










$$(19) \quad u_k = 1, \quad v_k = 0, \quad k > k_F$$

and a quasi-particle corresponds to a particle for $k > k_F$ and to a hole for $k < k_F$. The various terms of the hamiltonian give rise to the diagrams shown in Table I.

Therefore we see that the canonical transformation with the normal solution (9) is completely equivalent to the use of the single-particle potential which annihilates all the diagrams containing lines with two end points at the same vertex ⁽¹¹⁾.

In the case of the not trivial solution of (8) we can again indicate the various terms of H_{int} with the diagrams of Table I.

TABLE I.

H_{04}	annihilation of two particles and two holes.	
$H_{13}^{(1)}$	annihilation of two particles and one hole, and creation of one particle.	
$H_{13}^{(2)}$	annihilation of one particle and two holes and creation of one hole.	
$H_{22}^{(1)}$	scattering of two particles.	
$H_{22}^{(2)}$	scattering of one particle and one hole.	
$H_{22}^{(3)}$	scattering of two holes.	
$H_{31}^{(1)}$	annihilation of one particle and creation of two particles and one hole.	
$H_{31}^{(2)}$	annihilation of one hole and creation of one particle and two holes.	
H_{40}	creation of two particles and two holes.	

This is equivalent to indicate with an arrow pointing to the left (to the right) a factor u_k (a factor v_k).

Now each internal line must be indicated with two arrows since diagrams can appear which contain a factor $u_k v_k$, which must be represented with an arrow pointing to the left and one pointing to the right. Such lines will be called Δ -lines.

For example both diagrams of Fig. 1 exist, while in the normal case only $1a$ is different from zero, since $u_k v_k = 0$.

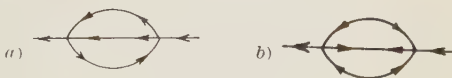


Fig. 1.

In the not trivial case each Δ -line introduces an integration with a factor

$$(20) \quad u_k v_k = \frac{1}{2} \frac{1_k}{E_k},$$

which is different from zero only near $k = k_F$. Therefore in general the contributions of the diagrams containing these lines are very small. However there are cases in which they can give contributions of the same order as the others.

3. - Corrections to the quasi-particle energy.

We will now examine the corrections to the energy of a free quasi-particle given by H_{int} .

Following HUGENHOLTZ⁽¹⁰⁾ we can see that the energy of a system with one quasi-particle is equal to the energy:

$$(21) \quad \hat{E}_k = E_0 + \bar{E}_k,$$

where E_0 is the energy of the vacuum. In order to evaluate \bar{E}_k one must calculate the contribution of all the single-particle self-energy diagrams.

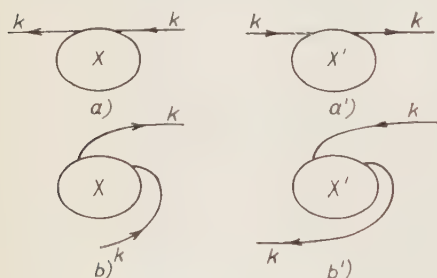


Fig. 2.

We want now to show that the contributions to \bar{E}_k of the diagrams without Δ -lines can be summed in pairs in such a way that for $k = k_F$ they give rise to terms which are of the order of magnitude of the unperturbed energy $\Delta = \Delta_{k_F}$.

Such pairs of diagrams are shown in Fig. 2, where the bubble X (X') means any sort of diagram without Δ -lines.

The diagrams $2a$ ($2b'$) are multiplied by a factor u_k^2 while the diagrams $2b$ ($2a'$) are multiplied by a factor v_k^2 .

The denominators of $2a$ ($2a'$) and those of $2b$ ($2b'$) are all positive and differ by a quantity $2E_k$.

Apart from these differences one can reduce the expressions which give the contributions of the diagrams $2a$ ($2a'$) to that of $2b$ ($2b'$) merely with the exchange of one creation and one destruction operator: therefore $2a$ ($2a'$) and $2b$ ($2b'$) have opposite sign.

If we put $k = k_F$ ($u_k^2 = v_k^2$) the sum of $2a$ ($2a'$) and $2b$ ($2b'$) is at least of the first order in Δ .

As an example consider the contribution to \bar{E}_k of the diagram of Fig. 1a and of the other one of Fig. 3.

The contribution of 1a is

$$(22) \quad \frac{1}{2} \sum_{\substack{k_1 k_2 k_3 \\ s_1 s_2 s_3}} \frac{|\langle ks, k_1 s_1 | V | k_2 s_2, k_3 s_3 \rangle|^2 u_k^2 v_{k_1}^2 u_{k_2}^2 u_{k_3}^2}{E_{k_1} + E_{k_2} + E_{k_3} - E_k},$$

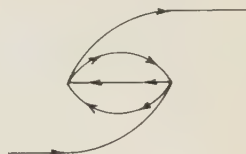


Fig. 3.

and the contribution of 2:

$$(23) \quad - \frac{1}{2} \sum_{\substack{k_1 k_2 k_3 \\ s_1 s_2 s_3}} \frac{|\langle ks, k_1 s_1 | V | k_2 s_2, k_3 s_3 \rangle|^2 v_k^2 v_{k_1}^2 u_{k_2}^2 u_{k_3}^2}{E_{k_1} + E_{k_2} + E_{k_3} + E_k}.$$

If $k \simeq k_F$ the importance of the two diagrams is comparable; putting $k = k_F$ the sum of (22) and (23) gives:

$$(24) \quad \frac{1}{2} \Delta \sum_{\substack{k_1 k_2 k_3 \\ s_1 s_2 s_3}} \frac{|\langle ks, k_1 s_1 | V | k_2 s_2, k_3 s_3 \rangle|^2 v_k^2 u_{k_1}^2 u_{k_2}^2 u_{k_3}^2}{(E_{k_1} + E_{k_2} + E_{k_3})^2 - \Delta^2}.$$

Let us consider the particular case of an interaction:

$$(25) \quad \langle k_1 s_1, k_2 s_2 | V | k_3 s_3, k_4 s_4 \rangle = -V^2 \delta(k_1 + k_2 - k_3 - k_4),$$

if k_1, k_2, k_3, k_4 are in the range $k_F - k_0 < k < k_F + k_0$, with $k_0 \ll k_F$, $s_4 = -s_3$, $s_2 = -s_1$; and zero otherwise.

In this case (24) becomes:

$$(26) \quad \Delta \sum_{k_1 k_2 k_3} \frac{V^4 v_{k_1}^2 u_{k_2}^2 u_{k_3}^2 \cdot \delta(k_1 + k_2 - k_3 - k_4)}{(E_{k_1} + E_{k_2} + E_{k_3})^2 - \Delta^2} < \Delta \sum_{k, k_2 k_3} \frac{V^4 v_{k_1}^2 u_{k_2}^2 u_{k_3}^2 \cdot \delta(k_1 + k_2 - k_3 - k_4)}{E_{k_2} - E_{k_3}} \simeq \\ \simeq \Delta \left(\frac{V^2}{2} \sum_k \frac{u_k^2}{E_k} \right) \simeq \frac{\Delta}{4} \left(\frac{V^2}{2} \sum_k \frac{1}{E_k} \right)^2.$$

From (8) one obtains:

$$(27) \quad 1 = \frac{1}{2} V^2 \sum_k \frac{1}{E_k},$$

therefore the expression (24) is $\leq \Delta/2$. (All the sums are inside the range $k_F - k_0 \rightarrow k_F + k_0$).

This result (2) is independent of the strength of the interaction; it seems also to be quite independent of the particular form of the interaction, in the sense that it depends essentially on the definition of E_k given by (8).

So we expect that in general the corrections to Δ from the considered diagrams depend quite slowly on the strength of the interaction.

Let us now consider the contributions to \bar{E}_k of the two diagrams with one Δ -line shown in Fig. 4:

The contribution of 4a is:

$$(28) \quad u_k v_{-k-s} \sum_{\substack{k_1 k_2 k_3 \\ s_1 s_2 s_3}} \langle k_3 s_3, -k_2 - s_2 | V | -k - s, k_1 s_1 \rangle \langle k_1 s_1, k_2 s_2 | V | k_3 s_3, k s \rangle \cdot \\ \cdot \frac{u_{k_1}^2 v_{k_3}^2 u_{k_2} v_{-k_2-s_2}}{E_{k_1} + E_{k_2} + E_{k_3} - E_k}.$$

and the contribution of 4b:

$$(29) \quad -u_k v_{-k-s} \sum_{\substack{k_1 k_2 k_3 \\ s_1 s_2 s_3}} \langle k_3 s_3, -k_2 - s_2 | V | -k - s, k_1 s_1 \rangle \langle k_1 s_1, k_2 s_2 | V | k_3 s_3, k s \rangle \cdot \\ \cdot \frac{u_{k_1}^2 v_{k_3}^2 u_{k_2} v_{+k_2 s_2}}{E_{k_1} + E_{k_2} + E_{k_3} + E_k}.$$

As was already pointed out, we see that each term is of the order of Δ due to the factor $u_{k_2} v_{k_2}$. Since $v_{-k_2-s_2} = -v_{k_2 s_2}$ we see that the sum of (28) and (29) gives a term of the order of Δ for $k = k_F$. Therefore in this problem one cannot neglect the contributions of the diagrams with one Δ -line.

Also for these diagrams the definition (8) makes the contributions to \bar{E}_k slowly dependent on the strength of the interaction.

The compensations described above occur only for $|\xi_k| \ll 1$. If $|\xi_k|$ is of the order of 1 the corrections to E_k become much larger than E_k itself, since u_k^2 is very different from v_k^2 .

However this is not a trouble: a state with one quasi-particle is not an excited state of the ground state Φ_0 (vacuum of quasi-particles), since it has a number of particles different from Φ_0 . We are interested in the possible existence of a gap in the excitation spectrum; therefore we must consider states with a number of particles equal to that of Φ_0 .

In order to construct such states one needs (at least) two quasi-particles with momenta k and k' such that:

$$(30) \quad u_k^2 = v_{k'}^2, \quad (u_{k'}^2 = v_k^2).$$

Now we will see that the corrections to the unperturbed energy $E_k + E_{k'}$ of such states are of the order of $E_k + E_{k'}$ if $|k - k_F|, |k' - k_F| \ll k_0$, where k_0 is the range of the forces in momentum space.

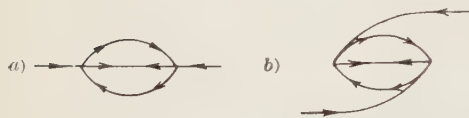


Fig. 4.

The contributions of the diagrams with one Δ -line are of the order of $E_k + E_{k'}$ for $k = k' = k_F$, and go to zero just as k and k' become different from k_F .

Let us now consider the diagrams without Δ -lines of Fig. 1a and of Fig. 2. Since $|k - k_F|, |k' - k_F| \ll k_0$ the matrix elements appearing in (22) and (23) are slowly varying, and we can put k_F in place of k and k' in the matrix elements.

Moreover from (30) we have $u_k v_k = u_{k'} v_{k'}$, i.e. $\Delta_k/E_k = \Delta_{k'}/E_{k'}$; since the range of variation of k is essentially k_0 we can put $\Delta_k = \Delta_{k'} = \Delta_{k_F}$, i.e. $E_k = E_{k'}$. In this way we obtain for the excitation energy:

$$(31) \quad \bar{E}_k + \bar{E}_{k'} = 2E_k - E_k \sum_{k_1 k_2 k_3} \frac{|\langle k_F s, k_1 s_1 | V | k_2 s_2, k_3 s_3 \rangle| v_{k_1}^2 u_{k_2}^2 u_{k_3}^2}{(E_{k_1} + E_{k_2} + E_{k_3})^2 - E_k^2}.$$

One could extend these considerations to the diagrams of any order.

Also in this case one can see that the corrections are not strongly dependent on the strength of the interaction, due to (8).

From these considerations it appears that the existence of a not trivial solution of (8) is not a sufficient condition for the superfluidity of the system. Also for a very weak interaction one should examine the corrections to the gap introduced by H_{int} .

We have completely neglected the possibility that the two quasi-particles bind each other giving rise to new excited states of lower energy which are generally called collective excitations.

This problem will not be examined here.

4. - Low density approximation.

The energy of the ground state is given by:

$$(32) \quad E_0 = U + \langle \Phi_0 | V(H_0 - U)^{-1} V + \dots | \Phi_0 \rangle,$$

where Φ_0 is the vacuum of quasi-particles.

Let us now assume that the system has low density, i.e. that k_F is smaller than the range of the forces in momentum space.

Since $v_k \simeq 0$ for $k < k_F$, in this case the most important diagrams are those with the minimum number of v_k factors⁽¹⁴⁾. In the evaluation of (32) these diagrams are of the type shown in Fig. 5.



Fig. 5.

⁽¹⁴⁾ N. M. HUGENHOLTZ: *Physica*, **23**, 533 (1957).

Let us define

$$(33) \quad \langle k_1 s_1, k_2 s_2 | \tau | k_3 s_3, k_4 s_4 \rangle = \frac{1}{2} \langle k_1 s_1, k_2 s_2 | V | k_3 s_3, k_4 s_4 \rangle - \\ - \frac{1}{2} \sum_{\substack{k' k'' \\ s' s''}} \frac{\langle k_1 s_1, k_2 s_2 | V | k' s', k'' s'' \rangle \langle k'' s'', k' s' | \tau | k_3 s_3, k_4 s_4 \rangle}{E_{k'} + E_{k''} + E_{k_3} + E_{k_4}} u_{k'}^2 u_{k''}^2.$$

All the diagrams of the type of Fig. 5 can be summed; the contribution of this sum to (32) is:

$$(34) \quad \frac{1}{2} \sum_{\substack{k_1 k_2 k' k'' \\ s_1 s_2 s' s''}} \frac{\langle k_1 s_1, k_2 s_2 | V | k' s', k'' s'' \rangle \langle k'' s'', k' s' | \tau | k_2 s_2, k_1 s_1 \rangle u_{k_1}^2 u_{k_2}^2 u_{k'}^2 u_{k''}^2}{E_{k'} + E_{k''} + E_{k_1} + E_{k_2}}.$$

The τ matrix here defined is the analogue of the t matrix of Brueckner. Clearly in such a way one cannot eliminate the difficulty introduced by an infinitely repulsive core. However the case of a really infinite core is not physical and the expression (34) can be calculated for any large but finite potential.

We investigate now the possibility that the τ matrix previously defined shows a pole analogous to the pole of the Brueckner t matrix. In the t matrix the pole can appear because of the vanishing denominators.

It appears likely that in the τ matrix these poles can disappear, since now the denominators do not vanish.

We will examine here a case in which it has been demonstrated that the pole in the t matrix exists.

Let us consider pairs of particles of total momentum zero and opposite spin, and assume that the interaction is of the type

$$(35) \quad \langle ks, -k-s | V | -k'-s', k's' \rangle = -V(k)V(k'),$$

with $V(k) > 0$.

In this case:

$$(36) \quad \sum_s \langle ks, -k-s | \tau | -k'-s', k's' \rangle = \\ = -V(k)V(k') - \frac{1}{2} V(k)V(k') \sum_{k''} \frac{[V(k'')] u_{k''}^4}{E_{k''} + E_{k'}} + \dots,$$

the series (36) can be summed, giving:

$$(37) \quad \sum_s \langle ks, -k-s | \tau | -k'-s', k's' \rangle = - \frac{V(k)V(k')}{1 - \frac{1}{2} \sum_{k''} ([V(k'')]^2 / (E_{k''} + E_{k'})) u_{k''}^4}.$$

From the eq. (8) one obtains

$$(38) \quad 1 = \frac{1}{2} \sum_{k''} \frac{[V(k'')]^2}{E_{k''}},$$

and since

$$(39) \quad \frac{u_{k''}^4}{E_{k''} + E_{k'}} < \frac{1}{E_{k'}},$$

one has that

$$(40) \quad \frac{1}{2} \sum_{k''} \frac{[V(k'')]^2}{E_{k''} + E_{k'}} u_{k''}^4 < 1,$$

and for any k' (37) does not show any pole.

Let us now consider the case of a general interaction, but again of pairs of particles of zero total momentum and opposite spin. Now:

$$(41) \quad \sum_s \langle ks, -k-s | \tau | -k'-s', k's' \rangle = \langle ks', -k-s' | V | -k'-s', k's' \rangle - \\ - \frac{1}{2} \sum_{k''s''} \frac{\langle ks'', -k-s'' | V | -k''-s'', k''s'' \rangle \langle k''s'', -k''-s'' | \tau | -k'-s', k's' \rangle}{E_{k''} + E_{k'}} u_{k''}^4;$$

(41) has no solutions if the homogeneous eq. (42) has a solution

$$(42) \quad \langle ks, -k-s | \bar{\tau} | -k'-s, k's \rangle = \\ = - \frac{1}{2} \sum_{k''} u_{k''}^4 \frac{\langle ks, -k-s | V | -k''-s, k''s \rangle \langle k''s, -k''-s | \bar{\tau} | -k'-s, k's \rangle}{E_{k''} + E_{k'}}.$$

Let us assume that the eq. (28) has only solutions such that the maximum value of Δ_k is much smaller than the Fermi energy ε_{k_F} . In this case one can substitute in the denominators of (8) and (42).

$$(43) \quad E_k \rightarrow E_k^A = \sqrt{\varepsilon_k^2 + \Delta^2},$$

where $\Delta = \Delta_{k_F}$. In the definition of the τ matrix let us use the largest of the solution Δ_k of (8).

Then it follows that (42) can be written (with \tilde{O}_k we indicate an operator which is diagonal in k space with eigenvalues O_k):

$$(44) \quad \left(\frac{\tilde{E}_k^A + E_k}{\tilde{u}_k^4} \right) |\varphi\rangle + \frac{1}{2} V |\varphi\rangle = 0,$$

from (44) one derives:

$$(45) \quad \tilde{E}_k^A |\varphi\rangle + \frac{1}{2} V |\varphi\rangle = -\delta |\varphi\rangle,$$

with $\delta > 0$. For a large class of potentials from (45) it follows that it exists a

$$(46) \quad \Delta' > \Delta$$

such that:

$$(47) \quad \tilde{E}_k' | \chi / + \frac{1}{2} V | \chi \rangle = 0$$

and since we have used the largest Δ_k solution of (8) we see that a Δ' satisfying (45) cannot be found and (44) has no solutions.

In the same approximation in which the energy of the ground state has been written, one can evaluate the energy of a state with one quasi-particle.

In this approximation one must take account of the contribution to E_k of the diagrams of Fig. 6.

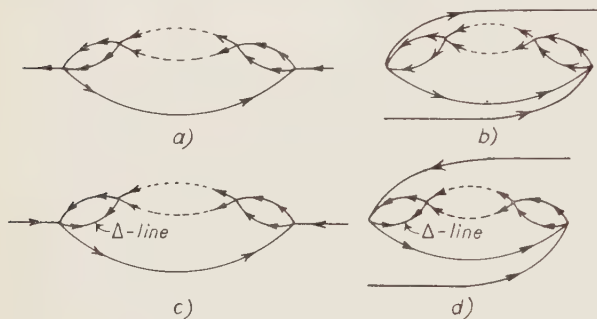


Fig. 6.

The diagrams obtained from 6c and 6d putting the Δ -line at the right in place of the left give a contribution equal to that of 6c and respectively 6d. In this approximation the energy \bar{E}_k is given by:

$$(48) \quad \bar{E}_k = E_k - \frac{u_k^2}{2} \sum_{\substack{k_1 k_2 k_3 \\ s_1 s_2 s_3}} \frac{\langle ks, k_1 s_1 | V | k_2 s_2, k_3 s_3 \rangle \langle k_3 s_3, k_2 s_2 | \tau' | k_1 s_1, ks \rangle}{E_{k_1} + E_{k_2} + E_{k_3} - E_k} v_{k_1}^2 u_{k_2}^2 u_{k_3}^2 +$$

$$+ \frac{v_k^2}{2} \sum_{\substack{k_1 k_2 k_3 \\ s_1 s_2 s_3}} \frac{\langle ks, k_1 s_1 | V | k_2 s_2, k_3 s_3 \rangle \langle k_3 s_3, k_2 s_2 | \tau | k_1 s_1, ks \rangle}{E_{k_1} + E_{k_2} + E_{k_3} + E_k} v_{k_1}^2 u_{k_2}^2 u_{k_3}^2 -$$

$$- 2u_k v_{-k-s} \left| \sum_{\substack{k_1 k_2 k_3 \\ s_1 s_2 s_3}} \frac{\langle k_3 s_3, -k_2 - s_2 | V | -k - s, k_1 s_1 \rangle \langle k_1 s_1, k_2 s_2 | \tau' | k_3 s_3, ks \rangle}{E_{k_1} + E_{k_2} + E_{k_3} - E_k} u_{k_1}^2 v_{k_2}^2 u_{k_3}^2 v_{-k_2 - s_2} + \right.$$

$$\left. + \sum_{\substack{k_1 k_2 k_3 \\ s_1 s_2 s_3}} \frac{\langle k_3 s_3, -k_2 - s_2 | V | -k - s, k_1 s_1 \rangle \langle k_1 s_1, k_2 s_2 | \tau | k_3 s_3, ks \rangle}{E_{k_1} + E_{k_2} + E_{k_3} + E_k} u_{k_1}^2 v_{k_2}^2 u_{k_3}^2 v_{-k_2 - s_2} \right|,$$

where:

$$(49) \quad \langle k_2 s_2, k_3 s_3 | \tau' | ks, k_1 s_1 \rangle = \frac{1}{2} \langle k_2 s_2, k_3 s_3 | V | ks, k_1 s_1 \rangle -$$

$$- \frac{1}{2} \sum_{\substack{k' k'' \\ s' s''}} \frac{\langle k_2 s_2, k_3 s_3 | V | k' s', k'' s'' \rangle \langle k'' s'', k' s' | \tau' | ks, k_1 s_1 \rangle}{E_{k'} + E_{k''} + E_{k_1} - E_k} u_{k'}^2 u_{k''}^2.$$

So far in the denominators we have used the unperturbed energy. However it is possible to define the τ and τ' matrices self-consistently, developing a method which is very similar to the Brueckner one.

In this approximation the single quasi-particle energy is given by an expression similar to (48), where in the denominators there is the perturbed energy \bar{E}_k in place of the unperturbed one, and the τ , τ' matrices are defined by expressions similar to (49) where again the perturbed energy \bar{E}_k is used. Therefore in this case (48) and (49) must be solved self-consistently by iteration.

The ground state energy, neglecting terms of the order of Δ , is given by the expression:

$$(50) \quad E_0 = U - \frac{1}{2} \sum_{\substack{k k_1 k_2 k_3 \\ s s_1 s_2 s_3}} \frac{\langle k s, k_1 s_1 | V | k_2 s_2, k_3 s_3 \rangle \langle k_3 s_3, k_2 s_2 | \tau | k_1 s_1, k s \rangle}{\bar{E}_k + \bar{E}_{k_1} + \bar{E}_{k_2} + \bar{E}_{k_3}} v_k^2 v_{k_1}^2 v_{k_2}^2 v_{k_3}^2.$$

5. - Conclusions.

In Section 4 we have defined the τ matrix which is the analogue of the usual Brueckner t matrix. In general the τ matrix has no poles if all the solutions Δ_k of the eq. (8) are much smaller than the Fermi energy ε_{k_F} . At present this condition does not seem to be very strong in the case of physical systems⁽¹⁵⁾.

If there are several solutions of (8) ($\ll \varepsilon_{k_F}$) one should choose the largest one.

The corrections introduced by H_{int} on the excitation energy in the region of minimum ($k \simeq k_F$) are of the order of magnitude of the excitation energy itself.

The contributions to the excitation energy of the diagrams containing one Δ -line are very important.

In fact let us consider the case of the approximation outlined in Section 4, in which self-consistency is used, and neglect the last two terms of (48) which are the contribution of the diagrams with one Δ -line. Let us consider one state with two quasi-particles satisfying the condition (30), i.e. of an excited state corresponding to the ground state Φ_0 . In this case the excitation energy is given by:

$$(51) \quad \bar{E}_k + \bar{E}_{k'} = E_k + E_{k'} - (\bar{E}_k + \bar{E}_{k'})g,$$

⁽¹⁵⁾ See, f.i., for ^3He and nuclear matter: V. J. EMERY and A. M. SESSLER: *Phys. Rev.*, **119**, 43, 248 (1960); G. FANO and A. TOMASINI: *Nuovo Cimento*, **18**, 1247 (1960).

where g is a positive constant. In (51) it has been assumed $k, k \simeq k_F$: terms of higher order in E_k and $E_{k'}$ are neglected, and we have put k_F in place of k and k' in the matrix elements. Then

$$(52) \quad \bar{E}_k + \bar{E}_{k'} = \frac{E_k + E_{k'}}{1 + g},$$

and the excitation energy is merely reduced by a factor $(1+g)$.

The contribution of the two last terms is proportional to the unperturbed gap Δ and not to the excited energy; therefore it is determining to find whether the energy gap exists in the excitation spectrum of the interacting quasi-particles.

* * *

The author is greatly indebted to Prof. B. FERRETTI and Dr. G. FANO for discussions on the argument of this paper.

RIASSUNTO

Si esamina il metodo perturbativo, per la valutazione degli stati di un largo sistema di fermioni, che si ottiene facendo preventivamente la trasformazione canonica di Bogoljubov-Valatin. Si mostra che la difficoltà dei normali sviluppi perturbativi, dovuta al polo nella matrice di Brueckner, è in generale eliminata da questo procedimento. Si mostra che le correzioni introdotte dall'interazione tra le quasi particelle nell'energia di eccitazione sono dell'ordine di grandezza dell'energia di eccitazione stessa, nella regione in cui questa è minima. Queste correzioni appaiono dipendere poco dall'intensità dell'interazione. Si introduce una approssimazione, estensione di quella di Brueckner.

Production of δ -Electrons in Distant Collisions by Charged Ultrarelativistic Particles.

V. BORTOLANI

Istituto di Fisica dell'Università - Bologna
Istituto Nazionale di Fisica Nucleare - Sezione di Bologna

(ricevuto il 14 Marzo 1961)

Summary. — In this paper a method is discussed to determine the connection between the number of δ -electrons, extracted by distant collision of an ultrarelativistic particle with the electrons of a medium, and the $\gamma = 1/\sqrt{1 - (v/c)^2}$ of the particle. The Weizsäcker-Williams method is used to reduce the problem to a photoelectric effect. Hydrogen atom type eigenfunctions are used to describe the metallic electrons. Errors due to this approximation are estimated.

1. — Introduction.

It is well known that with the present experimental techniques it is very difficult to distinguish between the masses, or the velocities, of the ultrarelativistic particles. In this note, we discuss a method, based upon the relativistic increase of the number of δ -electrons produced by *distant* collision of a particle with the electrons of a medium, to determine the ratio $\gamma = 1/\sqrt{1 - \beta^2}$ between the energy and the rest energy of the particle. We consider only the effect of distant collisions because they are more sensitive to the increase of velocity than near collisions. In order to select this kind of collisions one considers the particle travelling near a metallic surface at a distance of the order of a few μm .

The larger the velocity of the particle, the more intense is the particle's electro-magnetic field inside the metal and the bigger is the number of δ -electrons that are able to escape from the metallic surface. Our main aim will be to determine the connection between the number of δ -electrons which leave the metallic surface (in the following it will be indicated by \mathcal{N}) and the γ of the incident particle:

2. - Relation between \mathcal{N} and γ .

The problem may be divided in two steps:

- i) determine the probability of a given excitation of an electron in the metal by the electro-magnetic field;
- ii) calculate the probability that such an excited electron escapes from the metal.

The incident particle being ultrarelativistic we can apply the Weizsäcker-Williams' method ⁽¹⁾ and decompose the particle's field in a continuous spectrum of virtual photons with energy ω . In this manner we are led to a study of the photoelectric effect.

The photoeffect in metals consists ⁽²⁾ of a surface effect and a volume effect. The first being important near the threshold and the second at higher energy. Studying the first effect we may consider the electrons as free and inside a potential well (of depth W).

We obtain then

$$\mathcal{N} = \int_{\omega_0}^{\infty} d\omega J(\omega, b, \gamma) A(\omega) B(\omega),$$

where

$$J(\omega, b, \gamma) = \frac{\pi}{2} \frac{Z_1^2 e^2 \omega^2}{c^3 \hbar^2} \{K_1^2(x) + \gamma^{-2} K(x)\} \quad \text{with } x = \frac{\omega b}{\gamma c \hbar},$$

is the Weizsäcker-Williams spectrum ⁽³⁾; the K are the Hänkel functions; Ze is the charge of the moving particle; ω_0 is the ionization energy;

$$A(\omega) = \frac{8e^2}{\hbar c} \frac{(\omega - \omega_0)}{\omega^3} \frac{W \sqrt{W - \omega}}{W + \sqrt{\frac{1}{3}(\omega - \omega_0)}}, \quad \text{for } \omega \leq 9.5 \text{ eV},$$

$$A(\omega) = \frac{4e^2}{\hbar c} \frac{\tau^2}{\omega^3} \frac{\sqrt{\frac{1}{2}\tau}}{\sqrt{\tau + 2W} + \sqrt{\tau + 2(\omega - W)}}, \quad \text{for } \omega \geq 9.5 \text{ eV}$$

is the number of electrons leaving the surface per incident quantum ⁽⁴⁾, with $\tau = W - \omega_0$; $B(u) \simeq 10^{-8} \text{ cm}$, is the mean free path of a photon in the metal.

⁽¹⁾ E. J. WILLIAMS: *Proc. Roy. Soc.*, A **139**, 163 (1935); *Kgl. Dan. Vid. Selsk.*, **13**, no. 4 (1935); C. F. VON WEIZSÄCKER: *Zeits. Phys.*, **88**, 612 (1934).

⁽²⁾ IG. TAMM and S. SCHUBIN: *Zeits. Phys.*, **68**, 97 (1931).

⁽³⁾ P. BUDINI: *Nuovo Cimento*, **7**, 835 (1950).

⁽⁴⁾ A. SOMMERFELD and H. BETHE: *Handb. d. Phys.*, **24**, 471 (1933).

Performing the calculation for Cu we obtain for $\gamma = 100$ that the result is not much greater than 5.

This number as we shall see is of a smaller order of magnitude than the number of electrons escaping due to the volume effect and will therefore be neglected.

In order to estimate the volume effect we should consider the Bloch's eigenfunctions for the electrons, *i.e.* $\psi_{\mathbf{k}}(\mathbf{r}) = u_{\mathbf{k}}(\mathbf{r}) \exp[i\mathbf{k}\mathbf{r}]$, where $u_{\mathbf{k}}(\mathbf{r})$ can be obtained within the Wigner-Seitz approximation ⁽⁵⁾ (r is the electron's distance from the cell center).

As a first approximation, however we shall use hydrogen atom type eigenfunctions to describe the electron inside the metal.

This hypothesis is not as bad as it may seem. In fact the $u_{\mathbf{k}}(\mathbf{r})$ obtained with the W-S approximation are very similar to hydrogen atom type eigenfunctions over almost all of the cell's volume. For $r < 1$ Bohr radius, the eigenfunctions in the two cases are very different, but the probability that the electron is in this region, is very small and therefore the contribution coming from this region should not change the order of magnitude of the effect. With this assumption the photoelectric cross-section, for an electron with the orbital quantum number n becomes ⁽⁶⁾

$$\varphi(\omega) = \frac{\varphi_0 x^3 m^3 c^6 Z^4}{4\sqrt{3} \pi^3 \hbar^3} \frac{\hbar^3}{\omega^3 n^3}$$

where: φ_0 = Thompson cross-section,

$$\alpha = \frac{e^2}{\hbar c}.$$

The spectrum of virtual photons has a cylindrical symmetry. Therefore it is convenient to study the case in which the particle goes along the axis of a cylindrical hole made in the solid. Then by means of a graphic integration we shall obtain the result for the case in which the particle travels near a plane surface.

In the case of a cylindrical hole of radius b_0 we obtain

$$\mathcal{N} = N \int_0^\infty d\mathbf{x} \int_{\omega_0}^\infty d\omega J(\omega, \gamma, b_0, x) \exp\left[-\frac{x}{A \cos \theta}\right] \frac{2\pi b}{\omega}, \quad \text{with } x = \frac{\omega_0 b_0}{\gamma c \hbar}.$$

In the case of Cu only the electrons of the most external orbit may be ionized because the mean energy of the photoelectrons is ~ 10 eV.

⁽⁵⁾ E. WIGNER and F. SEITZ: *Phys. Rev.*, **45**, 794 (1933); **46**, 509 (1934).

⁽⁶⁾ H. A. BETHE and E. E. SALPETER: *Handb. d. Phys.*, **35**, 394 (1957).

The number of photons at a distance x from the surface, may be expressed as

$$J(\omega, \gamma, b_0, x) = J(\omega, \gamma, b_0) \exp \left[-\frac{x}{\lambda \cos \theta} \right],$$

where λ is the mean free path of a photon in the medium, and Λ the mean free path of the photoelectrons produced in the solid.

Noticing that $\lambda > \Lambda$ we may put $\exp[-x/\lambda] = 1$.

In order to determine Λ we shall follow Van der Ziel's procedure ⁽⁷⁾.

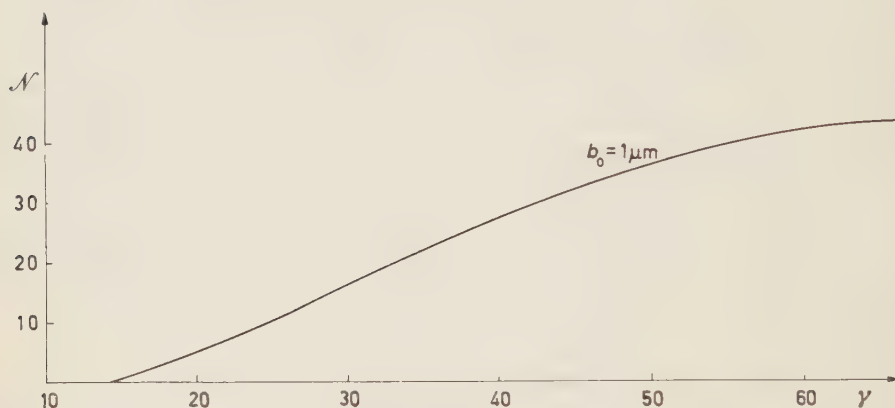


Fig. 1. - The variation of \mathcal{N} as a function of γ in the case of a cylindrical hole.

In his work the final eigenfunctions are not antisymmetrized because the energy of the incident electron is large (~ 150 eV) compared to that of the lattice electrons. As one can easily verify the error made by neglecting the antisymmetrization is in this case very small (0.01 %).

Our case is not so favorable because the energy of the photoelectrons is not much greater than the energy of the electrons in the lattice. On the

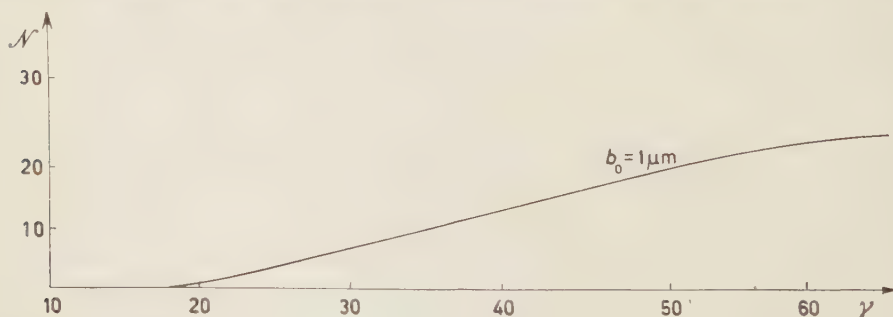


Fig. 2. - The function $\mathcal{N}(\gamma)$ for the case in which the particle travels near a plane surface.

(7) A. VAN DER ZIEL: *Phys. Rev.*, **92**, 35 (1953).

other hand neglecting the collisions in which the two energies are just about the same, one sees that λ increases roughly as the first power of the photoelectrons ($\sim E/20 \cdot 10^{-7}$ cm).

Since the energy of these electrons is about 10 eV and varies in a range of few eV, we shall take as mean value $\lambda \simeq 10^{-7}$ cm.

The weaker part of this calculation is due, as already mentioned, to the fact that in our case the energy of the photoelectrons is not much greater than the energy of the lattice electrons.

In order to check the errors, which are due to the asymptotic eigenfunction we have used (*i.e.* plane waves), we will use the Kronig's one-dimensional model, supposing the lattice potential separable in the three co-ordinates. The results of this model may easily be extended to our potential.

In the one-dimensional model ⁽⁸⁾ one finds

$$u_K(r) = \sum_{-\infty}^{+\infty} c_n(k) \exp \left[i \frac{nr}{a} \right], \quad c_0 = 0.8, \quad c_{-1} = 0.07, \quad c_1 = 0.006 \dots$$

In this way we can see that the use of plane waves (which amounts to put $c_0 = 1$), does not modify more than by a factor two the term introduced by the antisymmetrization.

We wish to add that for high values of γ , $\mathcal{N}(\gamma)$ is roughly constant due to the effect of the polarization of the medium. This effect has been neglected in our calculation. This is not a serious drawback because for large γ we can increase $b_0(\mathcal{N} = f(\gamma/b_0))$. We can make use of the last consideration by sending the particle at a given angle to a thin metal foil. Then the larger is γ the larger is the distance b_0 at which the electrons begin to escape from the metal and consequently the larger the useful particle's path. It is

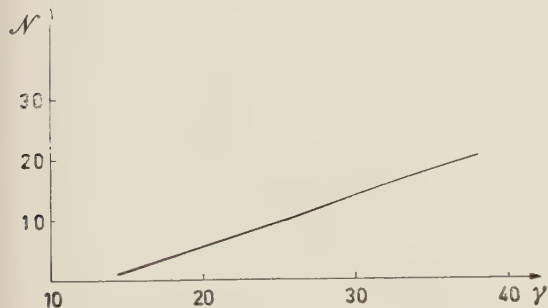


Fig. 3. - The function $\mathcal{N}(\gamma)$ in the case in which the particle travels toward the plane surface at a given angle ($(1/100)^\circ$).

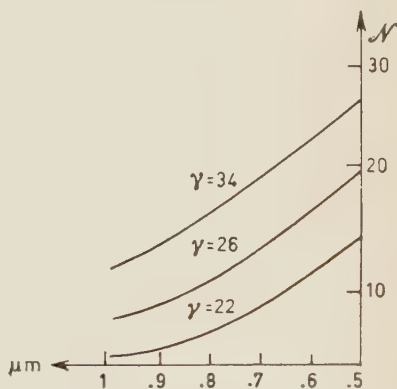


Fig. 4. - The connection between γ and the length of the useful path travelled by the particle.

⁽⁸⁾ A. SOMMERFELD and H. BETHE: *Handb. d. Phys.*, **24**, 383 (1933).

therefore possible to establish a connection between γ and the length of the useful path travelled by the particle (see Fig. 4).

Summarizing we can say that the number of δ -electrons escaping from the metal is enough sensitive to γ the ratio E/mc^2 . Therefore it will be possible to measure the γ of the heavy particles of energies of about 10 GeV and of electrons of energy of about 50 MeV.

* * *

I wish to thank Prof. B. FERRETTI, who has suggested this problem, and for his constant and useful advice throughout this work, and also Prof. A. TOMASINI and Drs. L. BERTOCCHI and J. CHAHOTD for many discussions.

RIASSUNTO

In questo lavoro si discute un metodo per determinare la connessione fra il numero di elettroni δ estratti da una particella ultrarelativistica per collisione cogli elettroni di un mezzo materiale e il $\gamma = 1/\sqrt{1 - (v/c)^2}$ della particella stessa. Si usa il metodo di Weizsäcker-Williams per ridurre il problema allo studio di un effetto fotoelettrico. Per descrivere gli elettroni metallici si usano autofunzioni tipo atomo di idrogeno e si valutano anche gli errori dovuti a questa approssimazione.

On Some Consequences of Charge Independence for K^+ -Nucleon Interactions.

V. DE SANTIS

Istituto Nazionale di Fisica Nucleare - Sezione di Padova

(ricevuto il 29 Marzo 1961)

Summary. — In the present work an attempt to find consistent relations between the three K^+ - N cross sections assuming the validity of charge independence is made. It is seen that, in this spirit, the K^+ - n elastic cross section should be much greater than previously deduced from counter and emulsion experiments. These experiments are then analysed and the possibility of increasing the value deduced from them for this cross section, bringing it in the limits required by charge independence, is shown to be consistent with reasonable changes of the parameters of the nuclear model used in the analysis of this interaction. Finally, a Tamm-Dancoff calculation in terms of pseudoscalar KN^*Y coupling, taking into account the recoils, is made; a somewhat good fit with the experimental data is found, with values of the two coupling constants g_Σ and g_Λ of the same order of magnitude as the π - N one.

Introduction.

In these last years a considerable amount of work has been done concerning both the phenomenological analysis of the low energy K -nucleon scattering data ⁽¹⁻⁴⁾ and their theoretical interpretation through the lowest order approx-

⁽¹⁾ D. KEEFE, A. KERNAN, A. MONTWILL, M. GRILLI, L. GUERRIERO and G. A. SALANDIN: *Nuovo Cimento*, **12**, 241 (1959) and further references quoted in this paper,

⁽²⁾ J. E. LANNUTTI, S. GOLDBABER, G. GOLDBABER, W. W. CHUPP, S. GIAMBUZZI, C. MARCHI, G. QUARENI and A. WATAGHIN: *Phys. Rev.*, **109**, 2121 (1958).

⁽³⁾ B. SECHI-ZORN and G. T. ZORN: to be published.

⁽⁴⁾ L. T. KERTH, T. F. KYCIA and R. G. BAENDER: *Phys. Rev.*, **118**, 553 (1960).

imation diagrams (⁵⁻⁹). However, up to now no clear understanding of this process may be said to have been reached. The reasons for this situation are twofold:

a) most of the data so far analysed, come from platework which has allowed to give directly only the K^+p and less directly, the K^+n charge exchange cross-sections, both with still large statistical errors, while rather elaborate and delicate manipulation of the rough experimental data is necessary to obtain the elastic K^+n cross-section; and in fact, the results obtained for it by different authors are extremely variable in shape and magnitude. Quite recently bubble chamber work (¹⁰) has yielded both the total and angular K^+p and charge exchange cross-sections with much greater accuracy; however no information on K^+n scattering from this experiment has yet been published.

b) From the theoretical point of view, dispersion relation approaches (⁸) have been so far mostly used, only to try to determine the relative parity of the KY pairs, as no sufficient information on high energy data and on K^- nucleon scattering are yet available for more detailed predictions. Quantitative calculations have generally been made only according to the Tamm-Dancoff approximation for lower order diagrams based on the direct KNY interactions (^{5,6}). However, the results obtained in this way, did not appear suitable to fit the most accepted interpretation of the data. And this fact has recently induced some authors to focus their attention on a quite different possible explanation of the process, mainly through a strong $KK\pi\pi$ interaction (⁹).

Nevertheless, before giving definitely up the conventional interpretation, we think that some points should be reconsidered more carefully. In fact, two main reasons may be responsible for the failure of finding an agreement between the data and their interpretation.

(⁵) C. CEOLIN and L. TAFFARA: *Nuovo Cimento*, **5**, 435 (1957); **6**, 425 (1957); H. P. STAPP: *Phys. Rev.*, **106**, 134 (1957); D. AMATI and B. VITALE: *Nuovo Cimento*, **5**, 1533 (1957).

(⁶) C. CEOLIN, V. DE SANTIS and L. TAFFARA: *Nuovo Cimento*, **12**, 502 (1959).

(⁷) D. AMATI and B. VITALE: *Nuovo Cimento*, **6**, 1273, 1013 (1957); **7**, 190 (1958).

(⁸) C. GOEBEL: *Phys. Rev.*, **110**, 572 (1958); P. T. MATTHEWS and A. SALAM: *Phys. Rev.*, **110**, 565, 569 (1958); K. IGI: *Progr. Theor. Phys.*, **19**, 238 (1958); S. BARSHAY: *Phys. Rev. Lett.*, **1**, 97, 177 (1958).

(⁹) S. BARSHAY: *Phys. Rev.*, **110**, 743 (1958); Y. YAMAGOUCHI: *Report Padua-Venice Conf.*, **V**, 42 (1957); C. CEOLIN, N. DALLAPORTA and L. TAFFARA: *Nuovo Cimento*, **9**, 353 (1958); F. FERRARI, G. FRY and M. PUSTERLA: *Phys. Rev. Lett.*, **12**, 526 (1960); UCRL-9421 (1960) to be published in *Phys. Rev.*; UCRL-9434 (1960).

(¹⁰) W. CHINOWSKY, G. GOLDBABER, S. GOLDBABER, W. LEE, T. O'HALLORAN, T. STUBBS, W. E. SLATER, D. H. STORK and H. K. TICHO: *Rochester Conference* (1960).

1) As already stressed, the only reliable data being the K^+ -proton and the charge exchange cross-sections, the theoretical prediction must mainly be adapted to fit them. Disagreement concerning the K^+ -neutron scattering cross section, could mostly be due to errors introduced by the indirect procedure of obtaining it from the data; an useful step in understanding the whole experimental picture might therefore be achieved by critically reconsidering the different steps and assumptions used to deduce this cross-section.

2) The lack of agreement between calculations and data may, of course, be attributed to the unreliability of the Tamm-Dancoff approximation which has been mostly used throughout. An attempt to improve the situation could then be: *a*) to clearly separate the results implied by general properties or symmetries of the system from those depending on the method of calculation; confusion on this point might in fact confer undue credit to uncertain results or, conversely, undervalue conclusions which could be true under wider assumptions, than those explicitly implied in the particular case considered; *b*) to modify some of the assumptions of the Tamm-Dancoff calculation in order to test the dependence from them of the results deduced.

The present work tries to reconsider the whole question in the spirit of these previous remarks. It divides, therefore, into the three following main parts:

A) By assuming only:

- 1) the full validity of charge independence for K -nucleon interactions;
- 2) the presence of only S and P waves at low energies;
- 3) the correctness within the errors of the experimental behaviour of the total K proton and charge exchange cross-sections:

the possible limits of the values for the K^+ -neutron cross-section compatible with these assumptions, are deduced.

B) The experimental procedures for obtaining the K^+ -neutron cross-section used by the different authors and the reasons for the large discrepancies in their results are discussed. The results of this discussion are then compared with the deductions obtained in part A).

C) Finally, as a quantitative test for the sensitivity of the Tamm-Dancoff results on the approximations used in the procedure, a new calculation taking into account the recoil, is presented and compared with the previous one in which the effect of recoils was not considered.

The whole discussion on these three points will be mainly based on the total cross-sections only. This is because, up to now, sufficiently reliable data were not available for the angular distribution. The comparison of the experimental angular distributions as soon as they will be completely available, with the results obtained from the present discussion will act as a test for them.

A) Phenomenological Analysis.

1. - Experimental data and charge independence.

Let us define:

$$(1) \quad \begin{cases} \sigma_p = \sigma(K^+p \rightarrow K^+p) \\ \sigma_{ce} = \sigma(K^+n \rightarrow K^0p) \\ \sigma_n = \sigma(K^+n \rightarrow K^+n) . \end{cases}$$

The experimental information concerning σ_p and σ_{ce} can be summarized as follows:

a) Up to 300 MeV, σ_p (Fig. 1) is substantially flat around 16 mb; this already known fact, is underlined by the more recent data; in particular the angular distribution ⁽¹⁰⁾ is strictly consistent with *S* wave only, and zero or very little contribution of *P* wave scattering;

b) σ_{ce} instead (Fig. 2) is monotonically increasing from

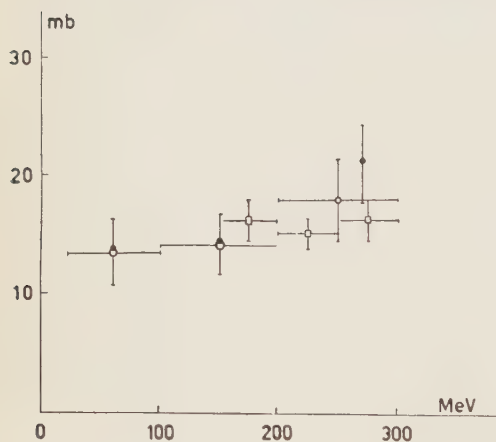
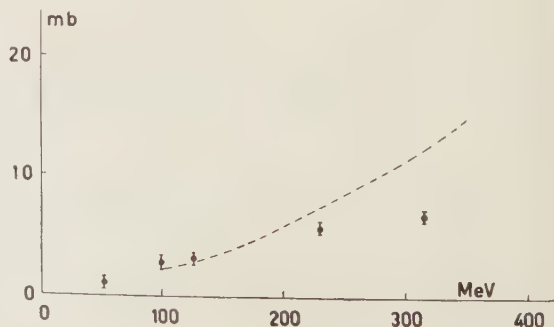


Fig. 1. - K^+p experimental cross-section. The recent plate compilation of STORK and PROWSE reported by KYCIA *et al.* ⁽⁴⁾ together with their counter data, is compared with the compilation of KEEFE *et al.* ⁽¹⁾ (their own, plus the data reported at the Geneva Conference) showing the flattening of σ_n . ● Keefe *et al.* compilation; ○ Stork-Prowse compilation; □ Kycia *et al.* counter.

Fig. 2. - $K^+n \rightarrow K^0p$ experimental cross-section. The curve calculated by KEEFE *et al.* ⁽¹⁾ from plate data (continuous line) compared with the points obtained in deuterium bubble chamber (Rochester Conference). σ_{ce} appears to be something lowered by these last data, but the behavior remains fundamentally the same.



about zero at threshold, to a value oscillating in the neighborhood of 300 MeV around 10 mb, (plate-work) or 7 mb (K^+ -D bubble chamber data.) These data, in agreement with the assumptions generally made up to now, are consistent with a substantial P wave charge exchange.

The information on the K^+ -n elastic cross-section as deduced by the different authors from both counter and plate-work, has the following general common feature:

c) $\sigma_n < \sigma_p$; its behaviour, at least for energy larger than about 100 MeV, has generally been found as decreasing with the energy.

Our program now, is to examine the consistency of the point c) with the data a) and b), according to the assumptions already stated, that charge independence holds and that S and P waves only are present up to about 300 MeV. In these hypothesis the cross-sections (1) can be expressed as follows:

$$(2) \quad \begin{cases} \sigma_p = \sigma_1, \\ \sigma_{ce} = \frac{4\pi^2}{k^2} \left[\frac{1}{4} \sin^2 (\delta_{10} - \delta_{00}) + \frac{1}{4} \sin^2 (\delta_{11} - \delta_{01}) + \frac{1}{2} \sin^2 (\delta_{13} - \delta_{03}) \right], \\ \sigma_n = \frac{1}{2} (\sigma_1 + \sigma_0) - \sigma_{ce}, \end{cases}$$

in which

$$(3) \quad \begin{cases} \sigma_1 = \frac{4\pi}{k^2} (\sin^2 \delta_{10} + \sin^2 \delta_{11} + 2 \sin^2 \delta_{13}), & (T=1), \\ \sigma_0 = \frac{4\pi}{k^2} (\sin^2 \delta_{00} + \sin^2 \delta_{01} + 2 \sin^2 \delta_{03}). & (T=0). \end{cases}$$

(The first index of the phases refers to isotopic spin, the second to angular momentum.)

We can introduce the results of the points a) and b) into (2) and (3) in the form

$$(4) \quad \begin{cases} \delta_{11} = \delta_{13} = 0 \\ \delta_{10} = \delta_{00}, \end{cases}$$

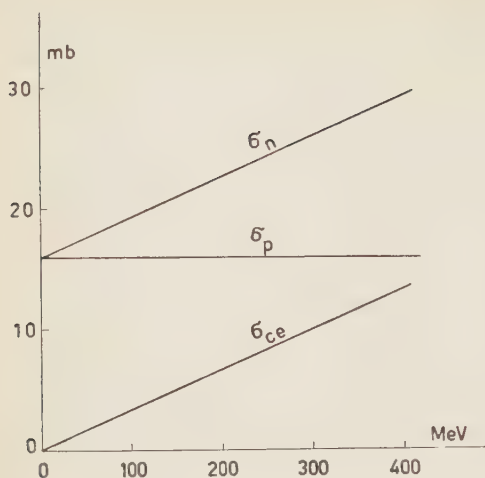
then it is easily seen that

$$(5) \quad \sigma_0 = \sigma_1 + 4\sigma_{ce}$$

and

$$(6) \quad \sigma_n = \sigma_1 + \sigma_{ce}.$$

In (5) and (6) the first term is evidently the S wave contribution, while the



second one is the P wave contribution.

If we represent in a rough approximation σ_p and σ_{ce} as straight lines, we have clearly the situation of Fig. 3 in which σ_n appears to be substantially higher than σ_p and increasing with energy: it is impossible for σ_n to have the behavior summarized in c) if (4) strictly holds.

Fig. 3. - Behaviour of the cross sections in the hypothesis $\delta_{11} = \delta_{13} = 0$; $\delta_{10} = \delta_{00}$.

2. - Modified hypothesis.

We may now modify, as far as possible, consistently with σ_p and σ_{ce} data, the conditions (4) trying to see how much σ_n can be decreased. As a first possibility, we consider what may happen if we suppose $\delta_{00} \neq \delta_{10}$; obviously, the two phases cannot be of opposite sign, because if so, σ_{ce} should start higher than $\frac{1}{4}\sigma_p \simeq 4$ mb, which is already too high; we must also eliminate values of $\delta_{00} > \delta_{10}$, because this would still increase σ_0 . We remain merely with the possibility δ_{00} of the same sign and smaller than δ_{10} . In this case, for what refers only to the S wave contribution, σ_0 would be smaller than σ_1 , and therefore, also σ_n could be smaller. For the P wave contribution the situation remains unchanged. Then, (5) and (6) becomes

$$(7) \quad \sigma_0 = (\sigma_0)_S + 4(\sigma_{ce})_P,$$

$$(8) \quad \sigma_n = \left[\sigma_1 + \frac{(\sigma_0)_S}{2} - (\sigma_{ce})_S \right] + (\sigma_{ce})_P,$$

where the S and P contributions are clearly separated. In Fig. 4 the dotted lines indicate the S wave contributions and the full lines the total

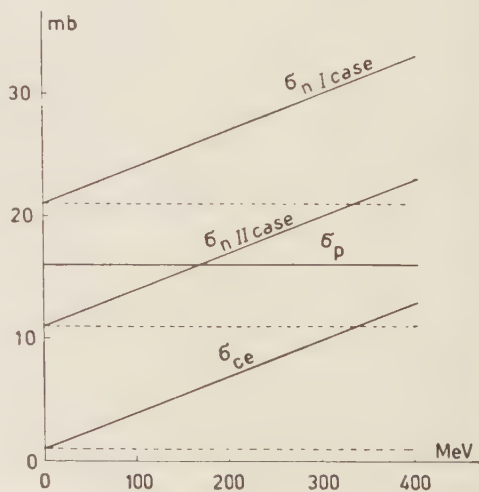


Fig. 4. - First modification: $\delta_{10} \neq \delta_{00}$: I case: $\delta_{00} > \delta_{10}$; II case: $\delta_{00} < \delta_{10}$. --- S contribution; — total cross-section.

cross-sections. We may see that the S term of σ_n can be somewhat reduced, but the behaviour remains strongly increasing with energy. Anyway, although experimental discrimination for the threshold behaviour of σ_{ce} is difficult, the most recent data for it agree better with the previous (only P wave) than with the present case (appreciable S wave).

We have now to investigate if the situation may change by modifying the first of the conditions (4). For instance, we put $\delta_{11} \neq 0$, $\delta_{13} = 0$ (a similar discussion would follow if we had $\delta_{11} = 0$, $\delta_{13} \neq 0$). Nothing changes for S and $P_{\frac{1}{2}}$ terms and particularly the $P_{\frac{3}{2}}$ contribution is equal for σ_{ce} and for σ_n . The dotted lines of Fig. 5 show a possible behaviour of the sum of S and $P_{\frac{3}{2}}$ contributions for the three cross-sections.

Analysing the $P_{\frac{1}{2}}$ contribution, we have from (2) and (3)

$$(3') \quad \begin{cases} (\sigma_1)_{P_{\frac{1}{2}}} = \frac{4\pi}{k^2} \sin^2 \delta_{11}, \\ (\sigma_0)_{P_{\frac{1}{2}}} = \frac{4\pi}{k^2} \sin^2 \delta_{01}, \end{cases}$$

and

$$(2') \quad \begin{cases} (\sigma_p)_{P_{\frac{1}{2}}} = (\sigma_1)_{P_{\frac{1}{2}}}, \\ (\sigma_{ce})_{P_{\frac{1}{2}}} = \frac{4\pi}{k^2} \cdot \frac{1}{4} \sin^2 (\delta_{11} - \delta_{01}), \\ (\sigma_n)_{P_{\frac{1}{2}}} = \frac{1}{2} [(\sigma_1)_{P_{\frac{1}{2}}} + (\sigma_0)_{P_{\frac{1}{2}}}] - (\sigma_{ce})_{P_{\frac{1}{2}}}, \end{cases}$$

from which we get

$$(9) \quad (\sigma_n)_{P_{\frac{1}{2}}} = \frac{4\pi}{k^2} \left[\frac{1}{2} \sin^2 \delta_{11} + \frac{1}{2} \sin^2 \delta_{01} - \frac{1}{4} \sin^2 (\delta_{11} - \delta_{01}) \right] = \frac{4\pi}{k^2} f(\delta_{11}, \delta_{01}).$$

This contribution could remarkably increase σ_n ; we limit ourselves to show that it cannot be but positive. This is evident if δ_{11} and δ_{01} are of the same

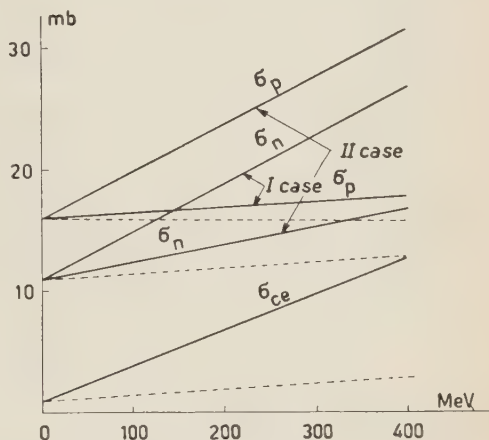


Fig. 5. - Second modification: $\delta_{00} < \delta_{10}$ and $\delta_{11} \neq 0$. I case: δ_{11} and δ_{01} of the same sign: σ_p is flat but σ_n increases strongly; II case: $\delta_{11} \simeq -\delta_{01}$: maximum lowering for σ_n , but σ_p increases unacceptably. --- $S + P_{\frac{3}{2}}$ contribution; — total cross-section.

sign, because in any case

$$\sin^2(\delta_{11} - \delta_{01}) \ll \sin^2 \delta_{11} + \sin^2 \delta_{01}$$

that is

$$(10) \quad f(\delta_{11}, \delta_{01}) \gg \frac{1}{4} \sin^2 \delta_{11} + \frac{1}{4} \sin^2 \delta_{01} \gg 0.$$

If now δ_{11} and δ_{01} are of opposite sign, we have

$$\sin^2(\delta_{11} - \delta_{01}) < \sin^2 \delta_{11} + \sin^2 \delta_{01} + 2 \sin |\delta_{11}| \sin |\delta_{01}|$$

and

$$f(\delta_{11}, \delta_{01}) = \frac{1}{4} \sin^2 \delta_{11} + \frac{1}{4} \sin^2 \delta_{01} + \frac{1}{4} \{ \sin^2 \delta_{11} + \sin^2 \delta_{01} - \sin^2(\delta_{11} - \delta_{01}) \},$$

i.e.

$$(11) \quad f(\delta_{11}, \delta_{01}) > (\frac{1}{2} \sin |\delta_{11}| - \frac{1}{2} \sin |\delta_{01}|)^2 \geq 0.$$

From (11) we see that the considered contribution is always positive. When $\delta_{01} \simeq -\delta_{11}$ we obtain the lowest contribution, but in this case σ_p increases up to values unacceptably higher than the experimental ones (if for instance, the $P_{\frac{1}{2}}$ wave predominates on $P_{\frac{3}{2}}$, some rough calculations show that at about 300 MeV we have approximately $0.35 \leq |\delta_{11}| \simeq |\delta_{01}| \leq 0.60$).

Summarizing, we can say for the $P_{\frac{1}{2}}$ wave that if $\delta_{11} = 0$ the contribution to σ_n and to σ_{ce} is the same; if instead, $\delta_{11} \neq 0$, the contribution to σ_n could be smaller than the contribution to σ_{ce} ; but in this case, the contribution to σ_p would unacceptably increase. It then appears that, according to the assumptions we have made, σ_n is in any case increasing with energy up to 300 MeV and that, at least from 200 to 300 MeV it must be greater and perhaps appreciably greater than σ_p .

This conclusion, although roughly qualitative, is in contrast with those reached according to the analysis of the counter and plate-work data (point c)). Thus, if we insist on the reliability of charge independence, it is necessary to re-examine critically the analysis of the data, to see whether errors in the deduction of the K^+n elastic cross-section may have crept in it.

B) Scattering K^+n - K^+n .

3. - The medium cross-section per nucleon.

The elementary cross-section is generally obtained from the formula

$$(12) \quad \bar{\sigma} = \alpha \sigma_p + \beta (\sigma_n + \sigma_{ce}),$$

where $\bar{\sigma}$ is the medium cross-section of K^+ on a free nucleon of the emulsion, α and β being the average percentage of protons and respectively neutrons in the emulsion nuclei. If σ_p and σ_n are known, σ_n can then be obtained directly from $\bar{\sigma}$. The methods used to determine experimentally $\bar{\sigma}$ in previous works, may be divided in two main types. For brevity we shall not discuss here the detailed corrections common to the two methods, namely those due to the Coulomb and nuclear potential effects and to the cut-off due to the Pauli principle on small transfer interactions.

In the first method, mostly used in the old works, the medium cross-section per nucleon is deduced ⁽¹¹⁾ from the measured mean free path in emulsion and from the nuclear radii generally defined as $R_i = r_0 A_i^{\frac{1}{3}}$.

The value obtained for it is strongly dependent on r_0 , as has already been emphasized by different authors who have used this method. (See especially KEEFE *et al.* ⁽¹⁾).

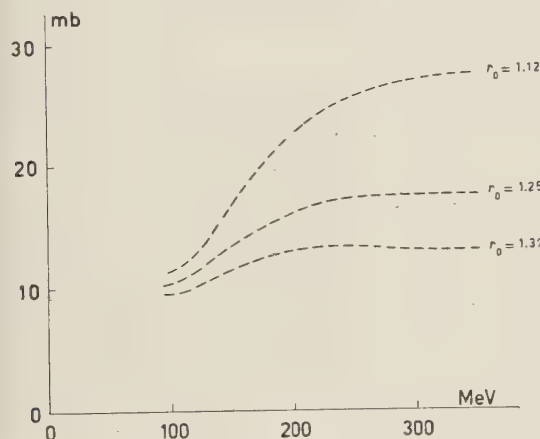


Fig. 6. - Medium cross section K^+-N for different values of r_0 .

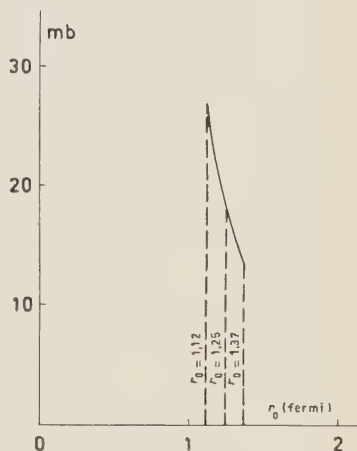


Fig. 7. - Medium cross section K^+-N at 300 MeV as a function of r_0 .

In Fig. 6, we report from this work, the $\bar{\sigma}$ as calculated by these authors according to a world summary of the experimental data available, for different values of r_0 . The value of $\bar{\sigma}$ at 300 MeV as a function of r_0 has been plotted in Fig. 7 and clearly indicates the strong dependence of it on r_0 ; it is seen that $\bar{\sigma}$ may conspicuously increase by diminishing this parameter even by a very little amount. Therefore, one of the main points to be revised for our problem is the direct experimental evidence that we have now on the r_0 value.

⁽¹¹⁾ K. BRÜCKNER, R. SERBER and K. M. WATSON: *Phys. Rev.*, **84**, 258 (1951).

Before 1953 experiments of different kinds for the determination of r_0 gave a value ranging from $(2 \div 2.8)$ fermi ⁽¹²⁾ to 1.45 fermi ⁽¹³⁾. Much more reliable results, mainly based on the scattering of high energy electrons by nuclei have continuously reduced this quantity to smaller and smaller values down to 1.07 fermi ⁽¹⁴⁾; in the last experiments of HOFSTADTER *et al.* ⁽¹⁵⁾ a value $r_0 = 0.8$ fermi has been deduced.

This general trend of our information on r_0 explains most of the apparently disagreeing results on the K^+n cross-section. In the oldest papers, rather high values $(1.25 \div 1.40)$ fermi of r_0 are assumed: among these, *e.g.* KEEFE *et al.* ⁽¹⁾ (to which we mainly refer for our comparison), have adopted $r_0 = 1.25$ fermi; but in the light of the more recent results we should consider that this value is not yet sufficiently small and that we should rather put $r_0 = 1.12$ or 1.07 fermi. For the first of these values we obtain the higher $\bar{\sigma}$ in Fig. 6 (still lower values of r_0 would further increase $\bar{\sigma}$); it is apparent that a decrease of r_0 of some percent implies as a consequence a corresponding increase of $\bar{\sigma}$ of the order of 100 %. The same conclusions may be derived from the counter experiments of KYCIA *et al.* ⁽⁴⁾. The small value of $\bar{\sigma}$ they have obtained is in connection with their large value of r_0 (1.41 fermi).

In more recent works, $\bar{\sigma}$ has been calculated with a method in principle, somewhat more refined than the first one, according to the optical model of the nucleus. This model depends on four parameters: the real and the imaginary potential depth V and W , the nuclear radius $R = r_0 A^{\frac{1}{3}}$, and the surface thickness a ; in general the imaginary potential depth W is chosen in order to fit the reaction cross-section K -nucleus for a set of values of V , r_0 and a . W being so obtained, $\bar{\sigma}$ is given as a function of W .

However, the choice of W in relation with the experimental data is actually performed for few values of the energy of the incident K and is not very precisely defined, owing to the low statistics for each energy interval. Moreover the results of this analysis still leave a considerable amount of ambiguity because a fairly wide range of the geometrical parameters r_0 and a , gives acceptable fits to the experimental data and W results to be strongly dependent on little changes of r_0 ; a decrease of some percent of r_0 makes W increasing by

⁽¹²⁾ M. E. ROSE: *Phys. Rev.*, **73**, 279 (1948).

⁽¹³⁾ L. K. ACHESON: *Phys. Rev.*, **82**, 488 (1951); E. M. LYMAN, A. O. HANSON and M. B. SCOTT: *Phys. Rev.*, **84**, 627 (1951); R. HOFSTADTER, H. R. FECHTER and J. A. MCINTIRE: *Phys. Rev.*, **92**, 979 (1953).

⁽¹⁴⁾ R. HOFSTADTER, B. HAHN, A. W. KUNDSEN and J. A. MCINTYRE: *Phys. Rev.*, **95**, 512 (1954); V. L. FITCH and I. RAINWATER: *Phys. Rev.*, **92**, 789 (1953); R. W. PIDD, C. L. HAMMER and E. C. RAKA: *Phys. Rev.*, **92**, 436 (1953); B. HAHN, D. G. RAVENHALL and R. HOFSTADTER: *Phys. Rev.*, **101**, 1131 (1956).

⁽¹⁵⁾ R. HOFSTADTER, F. BUMILLER and M. R. YEARIAN: *Rev. Mod. Phys.*, **30**, 482 (1958).

about 100% (e.g. ZORN ⁽³⁾ reports that calculations made by the UCLA group show that if r_0 changes from 1.20 to 1.07, the value of W goes from 11.7 ± 1.5 to 19.3 ± 2).

Obviously, this introduces a large error in the determination of $\bar{\sigma}$. For instance LANNUTTI *et al.* ⁽²⁾ (by using $r_0 = 1.20$ fermi) give in this way $\bar{\sigma} = 22_{-9}^{+10}$ mb in the interval $(180 \div 220)$ MeV.

Generally, the value obtained for $\bar{\sigma}$ oscillates around 20 mb with values of r_0 between $(1.15 \div 1.25)$ fermi. It is obvious therefore, that also in this case, by still decreasing the values of r_0 according to the more recent data, and taking into account the large experimental uncertainty for the choice of W , it is not impossible to reach a value of $\bar{\sigma}$ of about 25 mb or higher.

4. - K^+n elastic cross-section.

Having so indicated that $\bar{\sigma}$ may be actually higher than so far found, we may now see the effect of the increase of it on the behaviour of σ_n with energy (Fig. 8). In plate-work, this point was somewhat difficult to determine, because only σ_p was measured independently from hydrogen events, while experimental data on interactions with nuclei yielded only the ratio of the charge exchange events to all other ones. In the present work, however, now that the direct bubble chamber data on charge exchange are available, we can take both σ_p and σ_{ce} as independently given, and thus deduce as only unknown σ_n . We report the σ_n calculated from Fig. 6 using $r_0 = 1.12$ fermi together with those by KEEFE *et al.* ⁽¹⁾ (with $\alpha = 0.46, \beta = 0.54$) for constant and slightly increasing σ_p . It is immediately seen

that σ_n is completely different not only in magnitude but also in shape. Low values of $\bar{\sigma}$ give a σ_n decreasing with energy, at least for ranges higher than 200 MeV and this, in fact, was found by different authors who took $r_0 \approx 1.25$ fermi. If instead, we adopt the upper $\bar{\sigma}$ of Fig. 6 we get a σ_n increasing with energy and reaching values of the order of 30 mb; we should assume an unacceptable

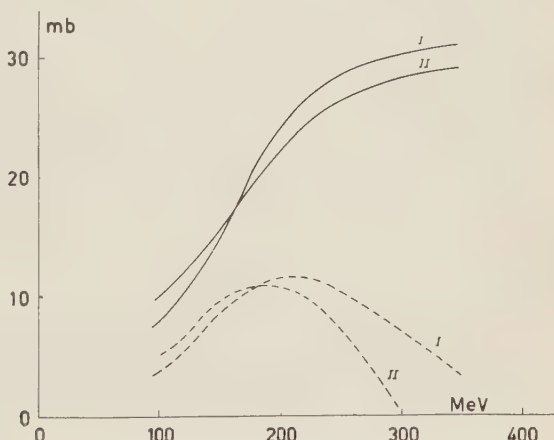


Fig. 8. - K^+n - K^+n : Keefe's curves ($r_0 = 1.25$) and the same with $r_0 = 1.12$ (I) for constant and (II) slightly increasing σ_p . --- Keefe *et al.* calculation; — present calculation.

slope for σ_p with respect to the experimental one if we insisted on obtaining a σ_n decreasing with energy.

If one accepts the previous interpretation of the work done on σ_n we should conclude that the values firstly deduced from the experimental data (counter and plate-work) up to about 300 MeV can be modified and much increased. The effect of this increase will bring σ_n within the region required for charge independence to be valid, while the previous lower values of σ_n could hardly be reconciled with it. Therefore, the increase of σ_n which we stress in this paper, could greatly simplify the interpretation of the whole K-nucleon scattering process.

Such a possibility has already been outlined by the recent data ⁽¹⁰⁾, on the bubble chamber K-D scattering, which indeed gives an indication that the elastic K⁺-n cross-section from a similar analysis as done here, increases up to about 25 mb.

(C) Tamm-Dancoff Calculation.

5. - Integral equations.

According to our program, we shall calculate now the three cross-sections in a Tamm-Dancoff approximation, taking into account the recoil and the Σ - Λ mass difference and compare them with the previous calculation ⁽⁶⁾ indicated as CDT in the following in which both these effects were neglected.

We refer to similar formulae as in CDT. We have:

$$(13) \quad (E - H_0) |NK\rangle = H_{\text{int}} |NK\rangle,$$

$$(14) \quad |NK\rangle = \sum c_{\lambda} |l; m; n; p; q; r\rangle,$$

$$(15) \quad H_{\text{int}} = \sum_{pq} \frac{1}{\sqrt{2\omega(k)\Omega}} \left\{ G_{\Sigma} \sum_{i=1}^3 [\psi_{\Sigma}^{*i} \gamma_5 a^*(k) \tau_i \psi_N + \psi_N^* \tau_i \gamma_5 a(k) \psi_{\Sigma}^i] \right. \\ \left. + G_{\Lambda} [\psi_{\Lambda}^* \gamma_5 a^*(k) \psi_N + \psi_N^* \gamma_5 a(k) \psi_{\Lambda}] \right\};$$

with some meaning for the used symbols as in CDT.

To separate the total isotopic spin and the total angular momentum states, we adapt to the K-N scattering the method described for π -N scattering by DYSON *et al.* ⁽¹⁶⁾ so obtaining the following set of integral equations:

$$(16) \quad (E - E_p - \omega_p) c_N^{\tau\mu}(p) = \int \mathcal{L}^{\tau\mu}(k, p, q) c_N^{\tau\mu}(q) dq,$$

⁽¹⁶⁾ F. J. DYSON, M. ROSS, E. E. SALPETER, S. S. SCHWEBER, M. K. SUNDARESAN, W. M. VISSCHER and H. A. BETHE: *Phys. Rev.*, **95**, 1644 (1954).

in which

$$(17) \quad E = E_0 + \omega_0 ,$$

$$(18) \quad \mathcal{L}^{x\mu}(k, p, q) = \frac{1}{2\pi} \frac{q^2}{\sqrt{\omega_p \omega_q} D_p D_q (M_N + E_p)} Q^{x\mu}(k, p, q) ,$$

$$(19) \quad D_p = \sqrt{\frac{2E_p}{M_N + E_p}} ,$$

and $Q^{x\mu}(k, p, q)$ are complicated kernels depending on the interaction constants, the expressions of which are not explicitly given here for brevity, which take into account the nucleon recoil, and the Σ - Λ mass difference. Solving (16) with the Fredholm method, we obtain the phase shifts

$$(20) \quad \text{tg } \delta^{x\mu} = a(k) \frac{Q^{x\mu}(k, k, k)}{1 - I^{x\mu}(k)} ,$$

with

$$(21) \quad \begin{cases} a(k) = -\frac{k}{4(E_k + \omega_k)} , \\ I^{x\mu}(k) = \frac{1}{4\pi} \int \frac{p^2 dp}{\omega_p E_p (E_k + \omega_k - E_p - \omega_p)} Q^{x\mu}(k, p, p) . \end{cases}$$

Putting then

$$(22) \quad \begin{cases} S = g_\Sigma + g_\Lambda^2 , \\ R = g_\Sigma^2 / g_\Lambda^2 , \end{cases}$$

we have, for the two isospin states, $T=1$ and $T=0$

$$(23) \quad \begin{cases} \text{tg } \delta^{1\mu} = a(k) \frac{[S/(R+1)](RQ_\Sigma^\mu + Q_\Lambda^\mu)}{1 - [S/(R+1)](RI_\Sigma^\mu + I_\Lambda^\mu)} , \\ \text{tg } \delta^{0\mu} = a(k) \frac{[S/(R+1)](3RQ_\Sigma^\mu - Q_\Lambda^\mu)}{1 - [S/(R+1)](3RI_\Sigma^\mu - I_\Lambda^\mu)} , \end{cases}$$

in which μ is the angular momentum index, as in CDT, Q_Σ^μ and Q_Λ^μ are the Σ and Λ Kernels differing only for the Σ - Λ mass difference. I_Σ^μ and I_Λ^μ are the Σ and Λ integrals (form. (21)) with the same difference.

6. - Numerical calculations.

The numerical calculations have been performed with the IBM 650 computer of Bologna. Initially the integrals I_Σ^μ and I_Λ^μ have been calculated for various values of the cut-off in order to test if the dependence of the integrals on the

cut-off is strong or not. It has been then found that over a certain value they become practically independent from it: changing the laboratory cut-off from 8.4 GeV to about 33 GeV the variation in the integrals was about 20% and to obtain a further variation of the same order, it was necessary to increase the cut-off to $\sim 1.3 \cdot 10^5$ GeV.

The effect of such variations of the integral on the phase shifts may be compensated by a variation in the opposite sense of the parameters and mainly of S , of the order of some percent. For these reasons, the cut-off has been fixed to 17 mk. In a second time, the three cross-sections have been calculated for various values of S and R . For comparison with the corresponding data of CDT, they have been calculated also for a cut-off about 5.2 mk (corresponding to c.m. cut-off momentum of 2 mk). Other calculations, which we do not report, have been performed with higher cut-offs supporting that the variation in the cross-sections become practically negligible when the cut-off increases over 17 mk.

7. - Results.

The K^+p cross-section is in a pure $T=1$ state, so that it depends mainly on S and little on R (putting $m_\Sigma = m_\Lambda$ the dependence from R vanishes).

In Fig. 9 we report the calculated cross-section for $S=18$ and $R=2$ with cut-off 17 mk and 5.2 mk together with the data in CDT with $S=3.05$.

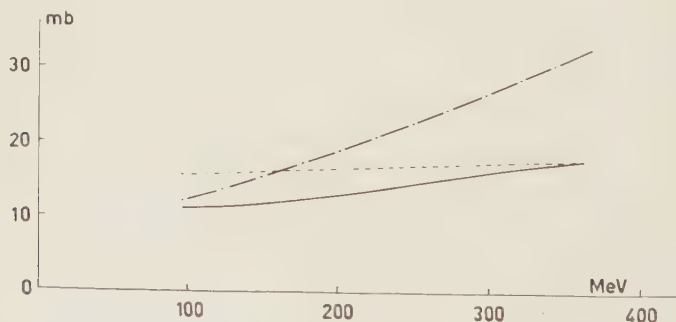


Fig. 9. - K^+p cross-section. Comparison between present and CDT calculation shows that very different values of S are necessary to obtain the same order of magnitude for σ_p .
 - - - C.D.T. calculation: cut-off momentum c.m. $2m_k$, $S=3.05$; - · - · - present calculation: same cut-off, $S=18$; — present calculation: actually chosen cut-off, $S=18$.

From the comparison of the present curves with the old one, we can see that a much higher value of S is necessary in order to obtain a cross-section of the same order of magnitude; the main effect of the recoil is to lower and

to flatten strongly the cross-sections. In Fig. 10 the behaviour of the K^+p scattering cross-section for $R=2$ and various values of S , is plotted together

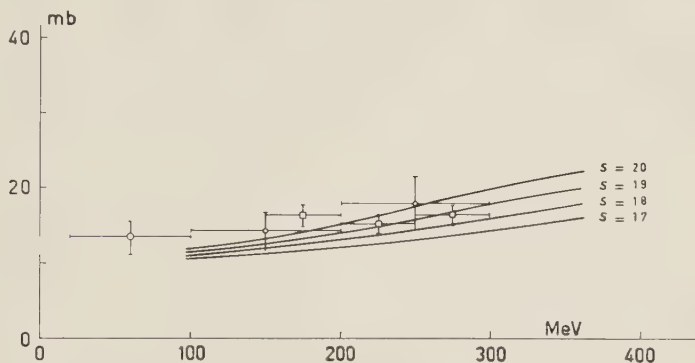


Fig. 10. — K^+p cross-section calculated for different values of S ; plate-work data (Stork-Prowse compilation) and counter data of Fig. 1 are plotted for comparison.

with the experimental data and their errors. The best fit is then to be obtained with

$$18 \leq S \leq 19.$$

In Fig. 11 the behaviour of the three $T=1$ calculated phase shifts is reported.

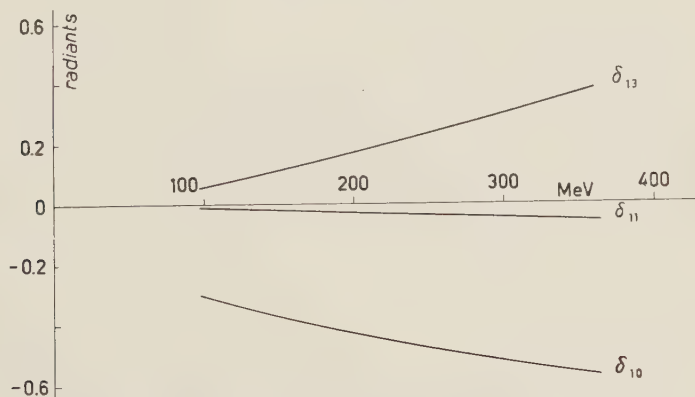


Fig. 11. — Phase shifts for $T=1$ states.

The charge exchange cross-section instead, for a fixed S depends strongly on the value of the ratio R as for the $T=0$ shifts. In a first approach, we have found that there are only two bands of variability of R by which the

calculated cross-section has almost the same behaviour than the experimental one. They are:

$$R \leq 0.05 \quad \text{and} \quad R > 1.$$

For the first band, a more detailed analysis shows that at least a qualitative fit of the experiments, requires $R < 0.01$. But for many reasons, it is highly improbable that R should assume such low values. We then remain only with

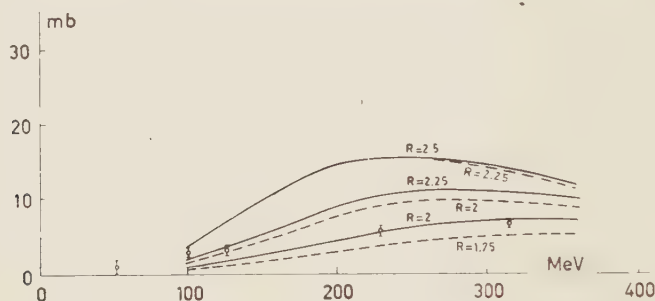


Fig. 12. - K^+n charge exchange cross-section for different values of S and R . Experimental data from K^+D scattering are reported for comparison. — $S=18$; --- $S=19$.

the other band $R > 1$ which gives a better possibility of fitting the data. Fig. 12 shows the behaviour of σ_{cx} for $S=18$ and $S=19$ and various values of R .

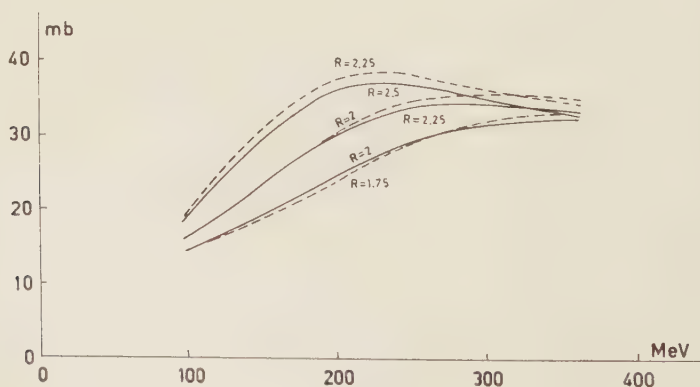


Fig. 13. - K^+n elastic cross-section for different values of S and R . — $S=18$; --- $S=19$.

If $S=18$, we obtain the best agreement with $R \simeq 2$; if S increases up to 19, R decreases a little ($1.75 < R < 2$). A comparison with the CDT result

considering that in CDT the ratio Q was defined as $g_{\Lambda}^2/g_{\Sigma}^2 = 1/R$, shows that the recoil makes steeper the behaviour of σ_{ce} thus improving the fit with the experimental data, particularly with the later ones (Rochester Conference), which seem to be something lower that was previously assumed.

Finally, Fig. 13 shows the behaviour of σ_n calculated with $S=18$ and $S=19$ and various values of R .

8. — Concluding remarks.

The comparison of our curves with those obtained by CDT shows that, if one takes into account the recoil, the results are completely changed.

First, the slope of the curves is in all cases modified in a sense that improves the possibility of coherently fitting the experimental data on σ_p and σ_{ce} . Second, in all cases much higher values than in CDT for the sum of the coupling constants $S = g_{\Sigma}^2 + g_{\Lambda}^2$ are required in order to fit the data. Although we cannot draw from this any definite conclusion on their true values, owing to our derivation method, we should like to point out at least, that the present result may create some doubts on the reliability of the well known conclusion, mostly based on previous perturbation or Tamm-Dancoff calculations, that the $K-N'$ interactions are decidedly weaker than the $\pi-N'$ ones.

On the other side, the values found for σ_n are greater than those of σ_p and its slope, for each choice of values of R and S , is very similar to that of σ_{ce} , in good agreement with the charge independence considerations of part A).

Finally, if we accept the conclusions reached in part B) and assume the order of magnitude and the slope of σ_n to be given by the upper Fig. 8, then the results of our calculations turn out to be in a quite surprising agreement with the experimental data. The best fit is obtained with $S \simeq 18$ and $R = 2$.

As already stressed, a better knowledge of the experimental angular distribution should be highly desirable as a more sensitive test to be compared with the considerations of the present approach.

* * *

The author is greatly indebted with Prof. N. DALLAPORTA for his interest in the work and for many discussions. Many thanks are due to Proff. M. BALDO CEOLIN, M. GRILLI and G. A. SALANDIN, for information on the experimental situation, and to Proff. D. AMATI and B. VITALE for an enlightening discussion. He wishes to thank also Dr. CHIARINI and Messrs. MAGANZANI and DEL BONO for the kind assistance at the IBM Bologna computer, and finally C.N.R. for financial support.

RIASSUNTO

In questo lavoro si fa un tentativo di trovare relazioni compatibili tra le tre sezioni d'urto K^+N assumendo la validità dell'indipendenza di carica. Si vede che, in questo spirito, la sezione d'urto elastica K^+n dovrebbe essere molto maggiore di quanto dedotto finora dagli esperimenti con lastre e contatori. Questi sono quindi rianalizzati: si pone in evidenza la possibilità di aumentare il valore da questi dedotto per tale sezione d'urto, portandola nei limiti richiesti dalla indipendenza di carica, con ragionevoli cambiamenti dei parametri del modello nucleare usato nelle analisi di tale interazione. Infine si fa un calcolo con l'approssimazione di Tamm-Dancoff in termini di accoppiamento pseudoscalare $KN\bar{Y}$, tenendo conto dei rinculi: si trova un accordo abbastanza buono coi dati sperimentali, con valori delle due costanti di accoppiamento g_Σ e g_Λ dello stesso ordine di grandezza della costante di accoppiamento $\pi N\bar{N}$.

Unitarity Conditions in Terms of Propagation Kernels (*).

E. R. CAIANIELLO and H. UMEZAWA (**)

Appendix by B. PREZIOSI

Istituto di Fisica Teorica dell'Università - Napoli

(ricevuto il 19 Aprile 1961)

Summary. — It is shown that, if the group property (macroscopic causality) of the U -matrix is postulated, the proof of its unitarity reduces to a most simple verification on the propagation kernels of the theory. The Appendix gives an explicit proof of that property for electro- and meso-dynamics by means of perturbative expansions, which may be easily generalized.

We propose to show that the proof of the unitarity of the S -matrix, which usually involves rather awkward handling of bilinear expressions, becomes a straightforward operation if it is performed, rather than directly on the elements of the S -matrix, on the kernels (propagation kernels, Green's functions), from which those elements are easily obtained by means of standard and unambiguous operations ⁽¹⁾. Things become indeed as simple as with the reaction matrix: the reason is, as is shown in detail below, that the same kernel serves to calculate both a given process and its inverse, while the elements of the S -matrix depend also upon the special states of the particles involved.

We expect this result to be useful especially in connection with the questions that arise in the study of renormalization by means of finite-part integrals ⁽²⁾. The demonstration given in the Appendix may show that the

(*) Visiting Professor from the University of Tokyo.

(**) Research reported in this document has been sponsored in part by the European Office of the A.R.D.C. United States Air Force, with Contract No. AF 61(052)-434.

⁽¹⁾ E. R. CAIANIELLO: *Nuovo Cimento*, **11**, 497 (1954) (referred to in the text as II).

⁽²⁾ E. R. CAIANIELLO: *Nuovo Cimento*, **13**, 637; **14**, 185 (1959); E. R. CAIANIELLO, A. CAMPOLATTARO and B. PREZIOSI: *Nuovo Cimento*, **18**, 505 (1960)

computation of bilinear, or multilinear, expressions offers no special difficulties if appropriate techniques are used.

Notation and formalism are those adopted in II. Rather than to the S -matrix, we shall refer in fact to the U -matrix, that is to the S -matrix computed between finite initial and final times: there is a significant difference, because unitarity needs to hold, as is well known, only for the latter. The S -matrix, obtains when such times tend to infinity; this is actually a good way to eliminate ambiguities that might otherwise arise in the definition of its elements. (This limiting process may cause the appearance of sharp bound states, about which we do not have to worry so long as we deal with the U -matrix.)

We denote the element $M_{FI}(t_2, t_1)$ of the matrix $U(t_2, t_1)$ relative to the transition from state $|I\rangle$ with Schrödinger wave function Φ_I at time t_1 to state $|F\rangle$ with Schrödinger wave function Φ_F at time t_2 , with $|F\rangle = K_{t_1}^{t_2}|I\rangle$; it is given (II-31) by:

$$(1) \quad M_{FI}(t_2, t_1) = \langle F | K_{t_1}^{t_2} | I \rangle = C_{FI} \int \hat{\Phi}_F K_{t_1}^{t_2} \left(\begin{matrix} x_1 \dots x_{N_0} \\ y_1 \dots y_{N_0} \end{matrix} \middle| t_1, \dots, t_{P_0} \right) \Phi_I.$$

where: C_{FI} is a (real) normalization coefficient, specified by (II-32);

$K_{t_1}^{t_2} \left(\begin{matrix} x_1 \dots x_{N_0} \\ y_1 \dots y_{N_0} \end{matrix} \middle| t_1 \dots t_{P_0} \right)$ is the propagation kernel from t_1 to t_2 defined in II (written here, as already in II, with reference to electro- or meso-dynamics solely for the sake of concreteness; our discussion may easily be extended to more general cases);

\int denotes integration over all space co-ordinates and average over all times $< t_1$ for initial, $> t_2$ for final particles (cf. (II, 2'3)).

Unitarity requires that

$$(2) \quad [U(t_2, t_1)]^+ = [U(t_2, t_1)]^{-1}$$

a relation which is quite unwieldy to prove in terms of M_{FI} .

Besides the unitarity condition, the U -matrix is always required to satisfy the group property:

$$(3) \quad U(t_3, t_2)U(t_2, t_1) = U(t_3, t_1)$$

and in particular:

$$(4) \quad U(t_2, t_1)U(t_1, t_2) = 1.$$

We assume now that (3), or at least (4), is satisfied by a theory in which the U -matrix elements M_{FI} are computed, by means of kernels, with for-

mula (1). This assumption needs here explicit proof, because easy objections might be raised against our using it otherwise; such proof is given in the Appendix by means of perturbative expansions.

Then, from (2) and (4):

$$(5) \quad [U(t_2, t_1)]^+ = U(t_1, t_2)$$

or, in terms of the elements (1):

$$(6) \quad \langle F | K_{t_1}^{t_2} | I \rangle^+ = \langle I | K_{t_2}^{t_1} | F \rangle.$$

It follows from (6) that, under our hypotheses, the unitarity condition (2) is satisfied if, and only if:

$$(7) \quad K_{t_1}^{t_2} \left(\begin{matrix} x_1 \dots x_{N_0} \\ y_1 \dots y_{N_0} \end{matrix} \middle| t_1 \dots t_{P_0} \right) = (II\gamma^4) K_{t_2}^{t_1+} \left(\begin{matrix} y_1 \dots y_{N_0} \\ x_1 \dots x_{N_0} \end{matrix} \middle| t_1 \dots t_{P_0} \right) (II\gamma^4).$$

The products of γ^4 (one for each spinor field) at r.h.s. of (7) originate from the normalization ($\bar{\psi} = \psi^+ \gamma^4$) adopted in II. The definition of $K_{t_2}^{t_1}$ implies of course, besides reversal of times, also that all terms $+i\varepsilon$ denoting causality in the free propagators wherefrom $K_{t_1}^{t_2}$ is constructed (causality from past to future) be replaced with $-i\varepsilon$ in $K_{t_2}^{t_1}$ (causality from future to past). Thus, for example, considering first for simplicity the case of spin zero and vanishing mass, we have in our notation for a free boson propagator:

$$(8) \quad [xy]_{m_0=0} \Big|_{t_1}^{t_2} = \frac{1}{(2\pi)^4} \frac{1}{(x_1 - y_1)^2 + (x_2 - y_2)^2 + (x_3 - y_3)^2 - (x_0 - y_0)^2 + i\varepsilon} = \\ = ([xy]_{t_2}^{t_1})^+ = [yx]_{t_2}^{+t_1},$$

which is clearly true also if $m_0 \neq 0$; for a free fermion propagator:

$$(9) \quad (xy)_{t_1}^{t_2} = (\gamma \partial_x - m_f) [xy]_{m_f t_1}^{t_2} = \gamma^4 ((\gamma \partial_y - m_f) [yx]_{t_2}^{t_1})^+ \gamma^4 = \gamma^4 [(yx)_{t_2}^{t_1}]^+ \gamma^4$$

it would then be a simple exercise to verify that (7) is satisfied also by the general perturbative expansions and by the branching equations among kernels described in II.

We notice that our proof separates steps which are in fact logically distinct: the proof of the group property, which may hold also if the Hamiltonian is not hermitian (*e.g.* if the electric charge is imaginary), and the proof of unitarity, where hermiticity becomes essential. (3) is of course a convenient way of expressing macroscopic causality, or better, determinism.

The concept of «time reversal» used here is not to be mistaken with the familiar ones due to WIGNER and PAULI. In the present context, the time-inverse process is that which carries the final into the initial state of the direct process, going actually from the future towards the past: our relations formulate, thus, a reciprocity both for processes and for the direction of time, and no selection rules can arise from them (but the Hamiltonian must be hermitian). In inversions of the Wigner or Pauli type, the time direction is not altered (only $K_{t_1}^2$ intervenes) and a reciprocity is formulated by stating that, for a given direct process, also inverse processes (of the Wigner or Pauli type) are allowed: this poses more stringent requirements on the interaction and leads to well known consequences.

APPENDIX

We prove here that U satisfies the group property (3). We suppose to have an initial state $|I\rangle$ at time t_0 with n electrons, m positrons, a photons (τ_1 photons in state 1, τ_2 in state 2, ..., τ_α in state α ($\tau_1 + \dots + \tau_\alpha = a$)); a final state $|F\rangle$ at time t_1 with p electrons, $(m + p - n)$ positrons, b photons (σ_1 in state 1', ..., $\sigma_{\beta'}$ in state β' ($\sigma_1 + \dots + \sigma_{\beta'} = b$)); an intermediate state $|i\rangle$ at time t with s electrons, $(m + s - n)$ positrons, c photons (ϱ_1 in state 1'', ..., $\varrho_{\gamma''}$ in state γ'' ($\varrho_1 + \dots + \varrho_{\gamma''} = c$)). The expression for the matrix element $M_{FI}(t_1, t_0)$ is given by (II.2); we have likewise, for $M_{Fi}(t_1, t)$ and $M_{iI}(t, t_0)$,

$$\begin{aligned}
 M_{iI}(t, t_0) &= \frac{(-1)^{s(m+n)+\binom{m}{2}-\binom{s}{2}}}{\sqrt{\varrho_1! \dots \varrho_{\gamma''}! \tau_1! \dots \tau_\alpha!}} \sum_{N'(\alpha+c)} \frac{\lambda_{N'}}{N'!} \int_{t_0}^t \dots \int_{t_0}^t d\xi_1' \dots d\xi_{N'}' \sum \gamma_{\alpha_1 \beta_1}^{\mu_1'} \dots \gamma_{\alpha_N' \beta_N'}^{\mu_N'} \cdot \\
 &\quad \cdot [\xi_1' \dots \xi_{N'}' \tilde{z}^{(1)} \dots \tilde{z}^{(a)} \tilde{z}^{(1'*)} \dots \tilde{z}^{(c'*)}] \left(\xi_1' \dots \xi_{N'}' v^{(1)} \dots v^{(m)} \bar{u}^{(1'')} \dots \bar{u}^{(s'')} \right) \\
 (A.1) \quad M_{Fi}(t_1, t) &= \\
 &= \frac{(-1)^{p(m+2s-n)+\binom{s}{2}-\binom{p}{2}}}{\sqrt{\sigma_1! \dots \sigma_{\beta'}! \varrho_1! \dots \varrho_{\gamma''}!}} \sum_{N''(b+c)} \frac{\lambda_{N''}}{N''!} \int_t^{t_1} \dots \int_t^{t_1} d\xi_1'' \dots d\xi_{N''}'' \sum \gamma_{\alpha_1 \beta_1}^{\mu_1''} \dots \gamma_{\alpha_{N''} \beta_{N''}}^{\mu_{N''}''} \cdot \\
 &\quad \cdot [\xi_1'' \dots \xi_{N''}'' \tilde{z}^{(1'')} \dots \tilde{z}^{(c'')} \tilde{z}^{(1'*)} \dots \tilde{z}^{(b'*)}] \left(\xi_1'' \dots \xi_{N''}'' u^{(1'')} \dots u^{(s'')} \bar{v}^{(1'')} \dots \bar{v}^{(m+p-n'')} \right)
 \end{aligned}$$

where

$$\int_t^{t_1} d\xi = \int_t^{t_1} d^3\xi \int d\xi_0.$$

The group property is proved if it is shown that

$$\sum_{(i)} M_{Fi}(t_1, t) M_{iI}(t, t_0) = M_{FI}(t_1, t_0),$$

where the sum is extended to all intermediate states $|i\rangle$. It will suffice to give our proof only in the case that $t_1 > t > t_0$; it would be a straightforward matter to verify then that the same is true for any other time sequence because of the definition ((II.3), (II.5)) of the free propagators. For given c and s , if we divide by the statistical weights $c!/(c_1! \dots c_{\gamma'}!)$ and $s!(s+m-n)!$ of the corresponding intermediate states, we can sum over all states. Then we sum over c and s . $N' + N''$ has the same parity as N (which appears in M_{FI}). For a fixed N' , we can sum only over the values of c which have the same parity as $N' + a$ (or as $N'' + b$). We may fix arbitrarily also N'' , with the condition that the parity of $N' + N''$ be the same as $a + b$. Then we sum over c with this condition over $N' + N''$. We conclude that

$$\begin{aligned} (A.2) \quad \sum_{(i)} M_{Fi} M_{iI} &= \frac{(-1)^{\binom{n}{2} - \binom{p}{2} + p(m-n)}}{\sqrt{\sigma_1! \dots \sigma_{\beta'}! \tau_1! \dots \tau_{\alpha'}!}} \cdot \\ &\cdot \sum_{N'+N''(a+b)} \frac{\lambda^{N'+N''}}{N'! N''!} \int_{t_0}^t \dots \int_{t_0}^t d\xi_1' \dots d\xi_{N'}' \int_{t_0}^{t_1} \dots \int_{t_0}^{t_1} d\xi_1'' \dots d\xi_{N''}'' \sum \gamma_{\alpha_1' \beta_1'}^{\mu_1'} \dots \gamma_{\alpha_{N'}' \beta_{N'}'}^{\mu_{N'}'} \gamma_{\alpha_1'' \beta_1''}^{\mu_1''} \dots \gamma_{\alpha_{N''}'' \beta_{N''}''}^{\mu_{N''}''} \cdot \\ &\cdot \sum_s \frac{(-1)^{s(m+n)}}{s!(s+m-n)!} \sum_{s,f} \left(\xi_1' \dots \xi_{N'}' v^{(1)} \dots v^{(m)} \bar{u}^{(1'')} \dots \bar{u}^{(s'')} \right) \cdot \\ &\cdot \left(\xi_1'' \dots \xi_{N''}'' u^{(1'')} \dots u^{(s'')} \bar{v}^{(1')} \dots \bar{v}^{(m+n')} \right) \frac{1}{c_1! \dots c_{\gamma'}!} \sum_c \frac{1}{c!/(c_1! \dots c_{\gamma'}!)} \cdot \\ &\cdot \sum_{b,s} [\xi_1' \dots \xi_{N'}' z^{(1)} \dots z^{(a)} z^{(1')*} \dots z^{(a')*}] [\xi_1'' \dots \xi_{N''}'' z^{(1'')} \dots z^{(b'')} z^{(1'')*} \dots z^{(b'')*}] , \end{aligned}$$

where $\sum_{f.s.}$ and $\sum_{b.s.}$ mean respectively sum over all the fermionic states and sum over all the bosonic states.

Now

$$(A.3) \quad \sum_{c(N'+a)} \frac{1}{c!} \sum_{b,s} [\xi_1' \dots \xi_{N'}' z^{(1)} \dots z^{(a)} z^{(1')*} \dots z^{(a')*}] [\xi_1'' \dots \xi_{N''}'' z^{(1'')} \dots z^{(b'')} z^{(1'')*} \dots z^{(b'')*}] ,$$

may be written in the simpler form

$$(A.4) \quad \sum_{c(N'+a)} \frac{1}{c!} \sum_{b,s} [l_1 \dots l_{N'+a} z^{(1'')*} \dots z^{(a'')*}] [l_1 \dots l_{N''+b} z^{(1'')} \dots z^{(b'')}] ,$$

where $l_r = \xi_r'$ for $r \leq N'$, $l_r = z^{(r-N')}$ for $r > N'$, $l_r = \xi_r''$ for $r \leq N''$, $l_r = z^{(r-N'')*}$ for $r > N''$.

A generalization of (II.4) and (II.9) gives

$$(A.5) \quad \sum_{b,s} [l_k \tilde{z}^{(r')*}] [l'_h \tilde{z}^{(r'')}] = [l_k l'_h],$$

which means that a photon is created in l'_h and destroyed in l_k . By using (A.5), (A.4) becomes

$$(A.6) \quad \sum_{c(N'+a)} \frac{1}{c!} \left\{ \sum_{k_1}^{1, \dots, N'+a} \sum_{h_1}^{1, \dots, N''+b} \sum_{k_2 \neq k_1}^{1, \dots, N'+a} \sum_{h_2 \neq h_1}^{1, \dots, N''+b} \dots \sum_{k_c \neq k_1, \dots, k_{c-1}}^{1, \dots, N'+a} \sum_{h_c \neq h_1, \dots, h_{c-1}}^{1, \dots, N''+b} \cdot \right. \\ \left. \cdot [l_{k_1} l'_{h_1}] [l_{k_2} l'_{h_2}] \dots [l_{k_c} l'_{h_c}] [l_{i_1} \dots l_{i_{N'+a-c}}] [l'_{j_1} \dots l'_{j_{N''+b-c}}] \right\},$$

where $i_1, \dots, i_{N'+a-c}$, k_1, \dots, k_c is a permutation of $1, \dots, N'+a$ and $j_1, \dots, j_{N''+b-c}$, h_1, \dots, h_c is a permutation of $1, \dots, N''+b$. Now every term of

$$(A.7) \quad [l_1 \dots l_{N'+a} l'_1 \dots l'_{N''+b}],$$

appears in $\{ \}$ in (A.6) $c!$ times and the number of terms of (6) is equal to

$$\sum_{a(N'+a)} \frac{(N'+a)! (N''+b)!}{e! (N'+a-c)!! (N''+b-c)!!},$$

which is equal to $(N'+N''+a+b-1)!!$ and is also the number of terms of (A.7). It follows that (A.3) is equal to

$$(A.7') \quad [\xi'_1 \dots \xi'_{N'} \xi''_1 \dots \xi''_{N''} \tilde{z}^{(1)} \dots \tilde{z}^{(a)} \tilde{z}^{(1')*} \dots \tilde{z}^{(b')*}].$$

Let us consider now the quantity

$$(A.3') \quad \sum_s \sum_{f,s} \frac{(-1)^{s(m+n)}}{s!(m+s-n)!} \cdot \left(\xi'_1 \dots \xi'_{N'} v^{(1)} \dots v^{(m)} \bar{u}^{(1^*)} \dots \bar{u}^{(s^*)} \right) \left(\xi''_1 \dots \xi''_{N''} v^{(1^*)} \dots v^{(m+s-n)^*} \bar{u}^{(1')} \dots \bar{u}^{(p')} \right) \\ \cdot \left(\xi'_1 \dots \xi'_{N'} u^{(1)} \dots u^{(n)} \bar{v}^{(1^*)} \dots \bar{v}^{(m+s-n)^*} \right) \left(\xi''_1 \dots \xi''_{N''} u^{(1^*)} \dots u^{(s^*)} \bar{v}^{(1')} \dots \bar{v}^{(m+p-n)'} \right).$$

By putting $l_i = \xi'_i$ for $i \leq N'$, $l_i = v^{(i-N')}$ for $i > N'$, $l'_i = \xi'_i$ for $i \leq N'$, $l'_i = u^{(i-N')}$ for $i > N'$, $k_i = \xi''_i$ for $i \leq N''$, $k_i = \bar{v}^{(i-N'')'}$ for $i > N''$, $k'_i = \xi''_i$ for $i \leq N''$, $k'_i = \bar{v}^{(i-N'')'}$ for $i > N''$, (A.3') may be written, after a permutation of terms, in the form

$$(A.8) \quad \sum_s \sum_{f,s} \frac{(-1)^{s(m+n)}}{s!(m+s-n)!} \cdot \left(l_1 \dots l_{N'+m} \bar{u}^{(1^*)} \dots \bar{u}^{(s^*)} \right) \left(k_1 \dots k_{N''+p} v^{(1^*)} \dots v^{(m+s-n)^*} \right) \\ \cdot \left(l'_1 \dots l'_{N'+n} \bar{v}^{(1^*)} \dots \bar{v}^{(m+s-n)^*} \right) \left(k'_1 \dots k'_{N''+m+p-n} u^{(1^*)} \dots u^{(s^*)} \right).$$

A generalization of (II.6) and (II.13) gives

$$(A.15') \quad (v^{(i'')} u^{(j'')}) = (\bar{u}^{(i'')} \bar{v}^{(j'')}) = 0; \quad \sum_{f,s} (u_e l_h) (\bar{u}_e l_k) = - (l_h l_k); \quad \sum_{f,s} (v_e l_k) (\bar{v}_e l_h) = (l_h l_k),$$

with a meaning analogous to that given for (5).

By using these formulae, we prove now that (8) is equal to

$$(A.9) \quad (-1)^{N''(m-n)} \begin{pmatrix} l_1 \dots l_{N'+m} & k_1 \dots k_{N''+p} \\ l'_1 \dots l'_{N'+n} & k'_1 \dots k'_{N''+m+p-n} \end{pmatrix}.$$

If $j_1, \dots, j_s, r_1, \dots, r_{N'+n-s}$ is a permutation of $1, \dots, N'+n$; $j'_1, \dots, j'_s, r'_1, \dots, r'_{N''+p-s}$ is a permutation of $1, \dots, N''+p$; $i_1, \dots, i_{m+s-n}, t_1, \dots, t_{N'+n-s}$ is a permutation of $1, \dots, N'+m$; $i'_1, \dots, i'_{m+s-n}, t'_1, \dots, t'_{N''+p-s}$ is a permutation of $1, \dots, N''+m+p-n$, with $j_d < j_e$ for $d < e$, and likewise for j', i, i', r, r', t, t' , we can expand (8) in the form

$$(A.10) \quad \sum_s \sum_{f,s} \frac{(-1)^{p(m-n)}}{s!(m+s-n)!} \sum_{c(j)} \sum_{c(i')} \sum_{c(i)} \sum_{c(j')} (-1)^A \begin{pmatrix} l_{t_1} \dots l_{t_{N'+n-s}} \\ l'_{r_1} \dots l'_{r_{N''+n-s}} \end{pmatrix} \cdot \begin{pmatrix} l_{i_1} \dots l_{i_{m+s-n}} \\ \bar{v}^{(1'')} \dots \bar{v}^{((m+s-n)'')} \end{pmatrix} \begin{pmatrix} \bar{u}^{(1'')} \dots \bar{u}^{(s'')} \\ l'_{t_1} \dots l'_{j_s} \end{pmatrix} \begin{pmatrix} k_{t'_1} \dots k_{t'_{N''+p-s}} \\ k'_{r'_1} \dots k'_{r'_{N''+m+p-n-s}} \end{pmatrix} \begin{pmatrix} k_{j'_1} \dots k_{j'_s} \\ u^{(1'')} \dots u^{(s'')} \end{pmatrix} \begin{pmatrix} v^{(1'')} \dots v^{((m+s-n)'')} \\ k'_{i'_1} \dots k'_{i'_{m+s-n}} \end{pmatrix},$$

where $\sum_{c(j)}$ means sum over all the possible combinations of j_1, \dots, j_s extracted from $1, \dots, N'+n$, and similarly for the other sums, and

$$A = (N' + m)s + (N'' + p)(m + s - n) + (N'' + p - s)s + \\ + (N' + n - s)(m + s - n) + (m + s - n)(m + s - n + 1) + \\ + s(s + 1) + j_1 + \dots + j_s + i'_1 + \dots + i'_{m+s-n} + i_1 + \dots + i_{m+s-n} + j'_1 + \dots + j'_s.$$

By taking into account (A.5') it is easy to see that

$$(A.11) \quad \frac{1}{s!} \sum_{f,s} \begin{pmatrix} \bar{u}^{(1'')} \dots \bar{u}^{(s'')} \\ l'_{j_1} \dots l'_{j_s} \end{pmatrix} \begin{pmatrix} k_{j'_1} \dots k_{j'_s} \\ u^{(1'')} \dots u^{(s'')} \end{pmatrix} = (-1)^s \begin{pmatrix} k_{j'_1} \dots k_{j'_s} \\ l'_{j_1} \dots l'_{j_s} \end{pmatrix},$$

and that

$$(A.12) \quad \frac{1}{(m + s - n)!} \sum_{f,s} \begin{pmatrix} l_{t_1} \dots l_{t_{m+s-n}} \\ \bar{v}^{(1'')} \dots \bar{v}^{((m+s-n)'')} \end{pmatrix} \begin{pmatrix} v^{(1'')} \dots v^{((m+s-n)'')} \\ k'_{i'_1} \dots k'_{i'_{m+s-n}} \end{pmatrix} = \begin{pmatrix} l_{i_1} \dots l_{i_{m+s-n}} \\ k'_{i'_1} \dots k'_{i'_{m+s-n}} \end{pmatrix}.$$

Then (10) becomes

$$(A.13) \quad \sum_s (-1)^{p(m-n)} \sum_{c(j)} \sum_{c(i')} \sum_{c(i)} \sum_{c(j')} (-1)^{A+s} \begin{pmatrix} l_{t_1} \dots l_{t_{N'+n-s}} \\ l'_{r_1} \dots l'_{r_{N'+n-s}} \end{pmatrix} \begin{pmatrix} k_{t'_1} \dots k_{t'_{N''+p-s}} \\ k'_{r'_1} \dots k'_{r'_{N''+p-s}} \end{pmatrix} \\ \cdot \begin{pmatrix} k_{j'_1} \dots k_{j'_s} \\ l'_{j_1} \dots l'_{j_s} \end{pmatrix} \begin{pmatrix} l_{i_1} \dots l_{i_{m+s-n}} \\ k'_{i'_1} \dots k'_{i'_{m+s-n}} \end{pmatrix}.$$

On the other hand the expansion of (9) gives

$$(A.14) \quad (-1)^{N''(m+n)} \sum_s \sum_{c(j)} \sum_{c(i')} (-1)^B \cdot \begin{pmatrix} k_1 & \dots & k_{N''+p} \\ l'_{j_1} \dots l'_{j_s} & k'_{i'_1} \dots k'_{i'_{N''+p-s}} \end{pmatrix} \begin{pmatrix} l_1 & \dots & l_{N'+m} \\ l'_{r_1} \dots l'_{r_{N'+m-s}} & k'_{i'_1} \dots k'_{i'_{m+s-n}} \end{pmatrix},$$

where

$$B = (N' + m)(N'' + p) + \frac{1}{2}(N'' + p)(N'' + p + 1) + (N' + n)(N'' + m + p - n) + \\ + (\frac{1}{2}N'' + m + p - n)(N'' + m + p - n + 1) - \\ - (N' + n)(m + s - n) + i'_1 + \dots + i'_{m+s-n} + j_1 + \dots + j_s.$$

But (A.14) is equal to

$$(A.15) \quad (-1)^{N''(m+n)} \sum_s \sum_{c(j)} \sum_{c(i')} \sum_{c(j')} \sum_{c(i)} (-1)^{B+B'} \cdot \begin{pmatrix} l_{t_1} \dots l_{t_{N'+n-s}} \\ l'_{r_1} \dots l'_{r_{N'+n-s}} \end{pmatrix} \begin{pmatrix} k_{t'_1} \dots k_{t'_{N''+p-s}} \\ k'_{r'_1} \dots k'_{r'_{N''+p-s}} \end{pmatrix} \begin{pmatrix} k_{j'_1} \dots k_{j'_s} \\ l'_{j_1} \dots l'_{j_s} \end{pmatrix} \begin{pmatrix} l_{i_1} \dots l_{i_{m+s-n}} \\ k'_{i'_1} \dots k'_{i'_{m+s-n}} \end{pmatrix},$$

where

$$B' = \frac{1}{2}s(s+1) + (N' + n - s)(m + s - n) - \\ - \frac{1}{2}(m + s - n)(m + s - n + 1) + i_1 + \dots + i_{m+s-n} + j'_1 + \dots + j'_s.$$

Then, since $p(m-n) + A + s$ has the same parity as $N''(m+n) + B + B'$, it follows that (A.13) and (A.15) are equal. Thus (A.8) and (A.9) are equal, and we can write,

$$(A.16) \quad \sum_{(i)} M_{Fi}(t_1, t) M_{iI}(t, t_0) = \frac{(-1)^{\binom{n}{2} - \binom{p}{2} + p(m+n)}}{\sqrt{\sigma_1! \dots \sigma_{\beta'}! \tau_1! \dots \tau_\alpha!}} \cdot \\ \cdot \sum_{N'+N''(a+b)} \frac{\lambda^{N'+N''}}{N'! N''!} \int_{t_0}^t \dots \int_{t_0}^t d\xi_1^I \dots d\xi_{N'}^I \dots \int_{t_0}^{t_1} d\xi_1'' \dots d\xi_{N''}'' \left\{ \sum \gamma_{\alpha'_1 \beta'_1}^{\mu'_1} \dots \gamma_{\alpha'_{N'} \beta'_{N'}}^{\mu'_{N'}} \gamma_{\alpha_1 \beta_1}^{\mu''_1} \dots \gamma_{\alpha_{N''} \beta_{N''}}^{\mu''_{N''}} \cdot \right. \\ \cdot \left. \begin{pmatrix} \xi_1^I \dots \xi_{N'}^I & \xi_1'' \dots \xi_{N''}'' & v^{(1)} \dots v^{(m)} & \bar{u}^{(1')} \dots \bar{u}^{(p')} \\ \xi_1^I \dots \xi_{N'}^I & \xi_1'' \dots \xi_{N''}'' & u^{(1)} \dots u^{(n)} & \bar{v}^{(1')} \dots \bar{v}^{(m+p-n)} \end{pmatrix} \cdot \right. \\ \cdot \left. [\xi_1^I \dots \xi_{N'}^I \xi_1'' \dots \xi_{N''}'' z^{(1)} \dots z^{(\alpha)} z^{(1')*} \dots z^{(\beta')*}] \right\},$$

by taking into account that (3) is equal to (A.7') and that, from the equality of (A.8) and (A.9), it follows that (A.3') is equal to the determinant which appears in (A.16).

Omitting now for short the integrand of (16), which is symmetric in all the variables of integration, we have:

$$\begin{aligned} & \sum_{N'+N''(a+b)} \frac{\lambda^{N'+N''}}{N'!N''!} \int_{t_0}^t \dots \int_{t_0}^t d\xi'_1 \dots d\xi'_{N'} \int_t^{t_1} \dots \int_t^{t_1} d\xi''_1 \dots d\xi''_{N''} = \\ &= \sum_{N(a+b)} \frac{\lambda^N}{N!} \sum_{N'=0}^N \binom{N}{N'} \int_{t_0}^t \dots \int_{t_0}^t d\xi'_1 \dots d\xi'_{N'} \int_t^{t_1} \dots \int_t^{t_1} d\xi''_1 \dots d\xi''_{N-N'} = \sum_{N(a+b)} \frac{\lambda^N}{N!} \int_{t_0}^{t_1} \dots \int_{t_0}^{t_1} d\xi_1 \dots d\xi_N, \end{aligned}$$

with a change of the names of the variables. Then clearly (16) is equal to (II.2): q.e.d.

RIASSUNTO

Si mostra che se si suppone che U verifichi la proprietà gruppale la sua unitarietà si riconduce ad una più semplice verifica sui nuclei di propagazione della teoria. In Appendice viene dimostrata la proprietà gruppale di U per l'elettrodinamica e la mesodinamica, mediante lo sviluppo perturbativo.

LETTERE ALLA REDAZIONE

(La responsabilità scientifica degli scritti inseriti in questa rubrica è completamente lasciata dalla Direzione del periodico ai singoli autori)

Uniqueness of the Orbital Angular Momentum Operators.

J. R. SHEWELL

Auburn University - Auburn, Ala.

(ricevuto il 2 Gennaio 1961)

The authors of a recent paper with the above title ⁽¹⁾ claim to prove the following theorem:

If, in a separable Hilbert space in which the three cartesian coordinates form a complete set of commuting variables, the two self-adjoint operators \mathbf{L} and $\bar{\mathbf{L}}$ satisfy the commutation relations

$$(1) \quad [q_j, L_j] = 0,$$

$$(2) \quad [q_1, L_2] = -[q_2, L_1] = iq_3 \text{ (cycl.)},$$

$$(3) \quad \mathbf{L} \times \mathbf{L} = i\mathbf{L},$$

$$(4) \quad [q_j, \bar{L}_j] = 0,$$

$$(5) \quad [q_1, \bar{L}_2] = -[q_2, \bar{L}_1] = iq_3 \text{ (cycl.)},$$

$$(6) \quad \bar{\mathbf{L}} \times \bar{\mathbf{L}} = i\bar{\mathbf{L}},$$

then there is a unitary operator U which commutes with \mathbf{q} and which transforms $\bar{\mathbf{L}}$ into \mathbf{L}

$$(7) \quad U\bar{\mathbf{L}}U^{-1} = \mathbf{L}.$$

The purpose of this letter is to show, first, that their proof of this theorem is faulty; and, second, that the theorem is false.

The proof of the theorem depends heavily on the statement that every solution of the equation

$$(8) \quad (\mathbf{x} \times \nabla) \times \mathbf{f}(\mathbf{x}) = -\mathbf{f}(\mathbf{x}),$$

must have the form

$$(9) \quad \mathbf{f}(\mathbf{x}) = (\mathbf{x} \times \nabla) \varphi(\mathbf{x}),$$

where $\varphi(\mathbf{x})$ is an arbitrary scalar field. Now, according to (9),

$$(10) \quad \begin{aligned} \nabla \cdot \mathbf{f}(\mathbf{x}) &= \\ &= (\nabla \varphi) \cdot (\nabla \times \mathbf{x}) - \mathbf{x} \cdot (\nabla \times \nabla \varphi) \equiv 0. \end{aligned}$$

But the vector field

$$(11) \quad \mathbf{f}_1(\mathbf{x}) = r(x\mathbf{i} + y\mathbf{j})/(x^2 + y^2),$$

where

$$(12) \quad r^2 = x^2 + y^2 + z^2,$$

satisfies (8) and its divergence is

$$(13) \quad \nabla \cdot \mathbf{f}_1(\mathbf{x}) = r^{-1} \neq 0.$$

⁽¹⁾ J. S. LOMONT and H. E. MOSES: *Nuovo Cimento*, **16**, 96 (1960).

Therefore, the statement that every solution of (8) must have the form (9) is false and the proof of the theorem is faulty.

It might happen that a proof is faulty, but the theorem is still true. This, however, is not the case for this theorem. For, consider the self-adjoint operator

$$(14) \quad \bar{\mathbf{L}} = \alpha \mathbf{f}_1(\mathbf{q}) + \mathbf{L},$$

where

$$(15) \quad \mathbf{L} = \mathbf{q} \times \mathbf{p},$$

and α is an arbitrary real non-zero number. If the theorem is true then there exists a U such that

$$(16) \quad \mathbf{L} = U^{-1} \bar{\mathbf{L}} U,$$

and which has the property of preserving the form of all equations. In particular, if $\bar{L}_+ = \bar{L}_1 + i\bar{L}_2$, $\bar{L}_- = \bar{L}_1 - i\bar{L}_2$ are the raising and lowering operators, respectively, for functions characteristic of \bar{L}_3 , and if $\eta_0^0 = U^{-1} Y_0^0(\theta, \varphi)$, then we should have

$$(17) \quad \bar{L}_+ \eta_0^0 = 0,$$

and

$$(18) \quad \bar{L} \eta_0^0 = 0.$$

If one transforms to spherical polar coordinates it is easily seen that

$$(19) \quad \bar{L}_+ = \alpha \exp[+i\varphi] \operatorname{cosec} \theta + L_+,$$

$$(20) \quad \bar{L}_- = \alpha \exp[-i\varphi] \operatorname{cosec} \theta + L_-.$$

Solving (17), we get

$$(21) \quad \eta_0^0 = (\operatorname{tg} \frac{1}{2}\theta)^{-\alpha/\hbar}.$$

The substitution of this function into (18) yields

$$(22) \quad \bar{L}_- \eta_0^0 = 2\alpha \exp[-i\varphi] (\operatorname{cosec} \theta) \eta_0^0 \neq 0.$$

Since (18) is not satisfied we conclude that there exists no unitary transformation relating $\bar{\mathbf{L}}$ and \mathbf{L} , and this counter-example proves the theorem to be false.

This counter-example was constructed during the course of a study on generalizations of the angular momentum operators.

Nuclear Excitation and Multiple Production in Proton-Nucleon Collisions at CERN-PS Energies.

G. CVIJANOVICH, B. DAYTON, P. EGLI, B. KLAIBER, W. KOCH, M. NIKOLIĆ,
R. SCHNEEBERGER and H. WINZELER

Physikalisches Institut der Universität - Bern

J. C. COMBE, W. M. GIBSON, W. O. LOCK, M. SCHNEEBERGER
and G. VANDERHAEGHE

CERN - Geneva

(ricevuto il 2 Febbraio 1961)

The external beam ⁽¹⁾ of elastically scattered protons from the CERN Proton Synchrotron was allowed to enter two stacks of Ilford G5 emulsions 15×20 cm². The momentum distribution of these protons, obtained from a magnetic analysis ^(*), is shown in Fig. 1. The average momentum was 23.5 GeV/c.

Individual tracks have been examined and 1241 stars found in a total length searched of 454.4 m. The mean free path for production of these stars is thus $\lambda = (36.6 \pm 1.1)$ cm. Within the limits of error this value is the same as those obtained at 6.2 GeV ⁽²⁾ $((38.2 \pm 1.5)$ cm),

at 9 GeV ⁽³⁾ $((37.1 \pm 1.0)$ cm) and at 250 GeV ⁽⁴⁾ $((41 \pm 10)$ cm.

In Table I we show the main features of the 1241 stars. 10.8% are « white » ones, *i.e.* they show no tracks with $\beta \leq 0.7$ ^(**) ($N_h = 0$). All events with one secondary track with $\beta > 0.7$ only are called « scatterings » and have not been counted as stars. The cut-off angle for detection of these events with no visible excitation energy was about 20'; they occur with a frequency of about 10% of the number of stars. In Fig. 2 we show the distribution of the projected angles on the emulsion plane for these scatterings.

(*) We used the beam arrangement kindly provided by COCCONI, DIDDENS and WETHERELL.

⁽¹⁾ B. DAYTON, W. KOCH, M. NIKOLIĆ, H. WINZELER, J. C. COMBE, W. M. GIBSON, W. O. LOCK, M. SCHNEEBERGER and G. VANDERHAEGHE: *Helv. Phys. Acta*, **33**, 544 (1960).

⁽²⁾ H. WINZELER, B. KLAIBER, W. KOCH, M. NIKOLIĆ and M. SCHNEEBERGER: *Nuovo Cimento*, **17**, 8 (1960).

(**) Selected by visual estimation.

⁽³⁾ N. P. BOGACHEV, S. A. BUNJATOV, T. P. MERKOV and V. M. SIDOROV: *Dokl. Akad. Nauk. SSSR*, **121**, 615 (1958).

⁽⁴⁾ We thank Prof. M. TEUCHER and Dr. E. LOHRMANN for communication of these results prior to publication.

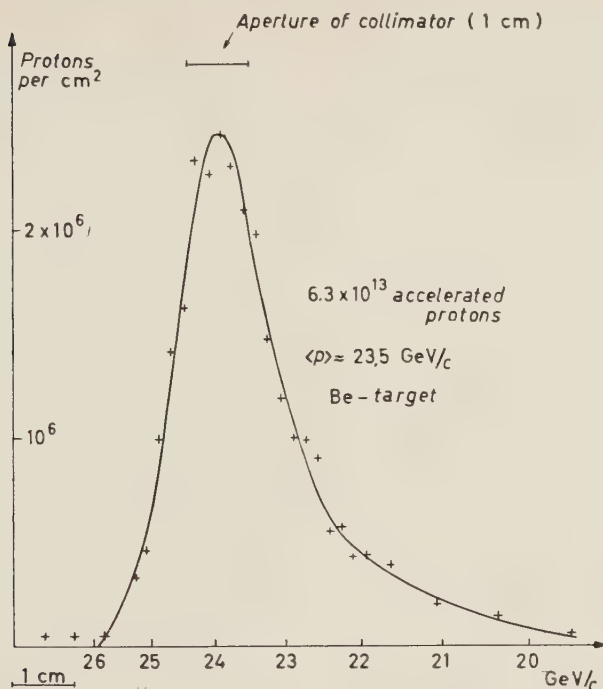


Fig. 1. — Momentum analysis of beam 19 m behind collimator, 13 m behind magnet.

TABLE I. — *Compilation of observed values.*

Total path	454.391 m
Number of observed stars (excluding scatterings)	1241
Mean free path for star production	$(36.6 \pm \pm 1.0)$ cm
Stars with $N_h=0$	134
Stars with $N_h=1$	119
Stars with $2 \leq N_h \leq 6$	454
Stars with $N_h \geq 7$	526
Number of elastic p-free-p scatterings	8
Scatterings	118

We estimated the number of interactions on hydrogen nuclei by using the statistical analysis whose principle was described by WINZELER *et al.* ⁽²⁾. In this analysis kinematical criteria are used to distinguish stars which might have resulted from interactions with hydrogen nuclei. The distribution of electrons and blobs in different types of star is then used to estimate statistically how many of these pre-selected stars are in fact due to interactions with hydrogen nuclei.

This analysis indicates that about 53 of our 1241 stars were due to inelastic proton-free-proton collisions, and a further 8 to elastic proton-free-proton collisions. These results give the following cross-sections

$$\sigma(\text{p-f-p}) \text{ inelastic} = (37 \pm 11) \text{ mb},$$

$$\sigma(\text{p-f-p}) \text{ elastic} = (5.5^{+2.7}_{-1.9}) \text{ mb}.$$

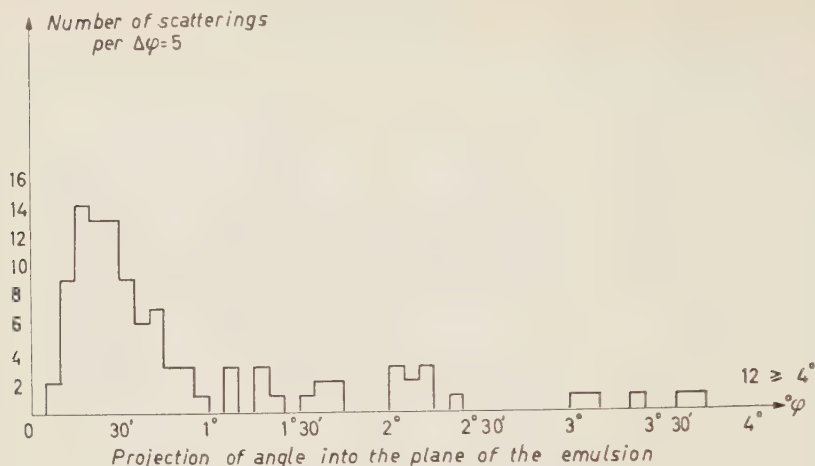


Fig. 2. — Angular distribution of the scattering.

About $\frac{1}{3}$ (*) of the inelastic p-free-p events are still accompanied by a heavy track ($\beta < 0.7$). 40% of the white even-prong stars and also 40% of the even-prong stars with $N_h=1$ are due to collisions with free protons. One cannot identify individually the inelastic interactions with hydrogen nuclei, but the best sample one can obtain from photographic emulsions is given by taking the stars which have $N_h=0$ or 1, have an even number of secondary prongs, and which are « clean », *i.e.* have neither electron track nor blob. About 70% of such a sample in fact results from genuine inelastic collisions with hydrogen nuclei.

The average multiplicity for charged secondary particles of the 53 proton-free-proton interactions was calculated to be

$$\bar{n}(\text{p-f-p inelast.}) = 4.1 \pm 0.6.$$

According to our statistical analysis the multiplicities of the 53 events were distributed as follows:

Multiplicity	2	4	6	8	10
No. of events	20	17.5	10.5	4	1.

These numbers apply to the 53 events as described above; it is possible that a

TABLE II. — Frequency distribution of 660 stars as a function of N_h and the corresponding thin track statistics.

N_h	Number of stars with $n_s=1$	Total number of stars	Average number of thin tracks per star
0	—	63	4.9
1	16	74	3.6
2	9	54	3.8
3/4	12	98	4.6
5/6	2	85	5.2
7/8	4	56	5.7
9/10	6	42	5.1
11/12	0	32	7.1
13/14	—	36	6.0
15/16	—	31	6.3
17/18	—	24	6.7
19/20	—	21	8.8
21/22	—	16	6.9
23/24	—	10	7.4
25/30	—	12	8.0
31/40	—	6	10.0

(*) This value might slightly be overestimated, see discussion below.

\bar{N}_h (excluding stars with $N_h=0$) = 8.4.
 \bar{N}_h (from stars with $n_s=1$, without scatterings) = 3.7.

sample of genuine collisions with hydrogen nuclei would contain a smaller proportion of events with multiplicity 2, since our sample may include some quasi-elastic collisions with bound nucleons.

Finally, we transformed the laboratory system angles of the secondary particles in the events in the best sample into c.m. system angles. For the shower particles we used the simplified trans-

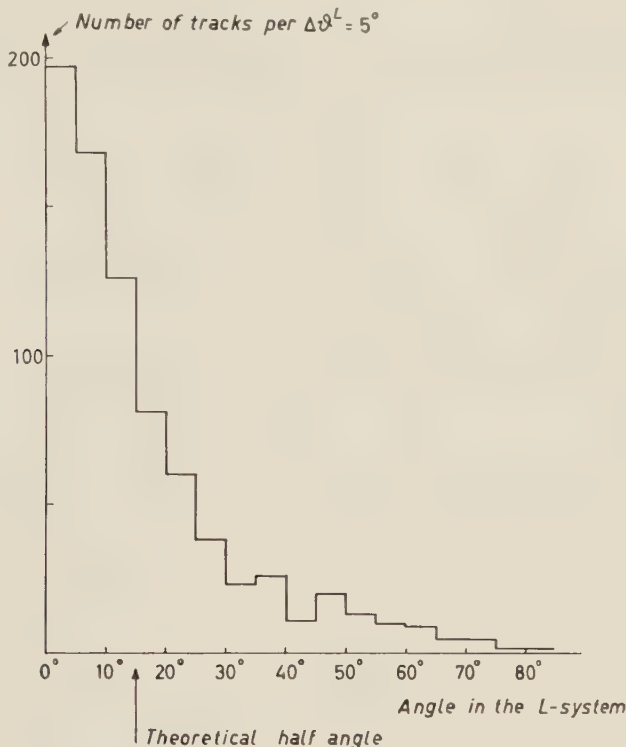


Fig. 3. - L -angular distribution of the shower tracks of all stars with $N_h = 0$ and $N_h = 1$.

In Table II we show the average number of shower particle tracks, \bar{n}_s , as a function of N_h . The apparent correlation between N_h and \bar{n}_s is presumably due to secondary interactions. The stars with large N_h have twice as many shower particle tracks as the proton-free-proton events.

Fig. 3 shows the angular distribution in the laboratory system for the shower particles of 202 stars with $N_h = 0$ and 1. About 25% of these events are due to proton-free-proton collisions, the rest to collisions with bound protons or neutrons.

formation formula

$$\operatorname{tg} \Theta^L = \frac{1}{\gamma_L^{\text{cm}}} \operatorname{tg} \frac{\Theta^{\text{cm}}}{2},$$

valid for $\beta_{\text{cm}}^L = \beta_{\text{particle}}^{\text{cm}}$.

Grey tracks due to protons were followed to the end of their range, their energy determined, and the precise transformation formula was employed in these cases. The distribution thus obtained for the 2, 4 and 6 prong events, in the best sample, is shown in Fig. 4.

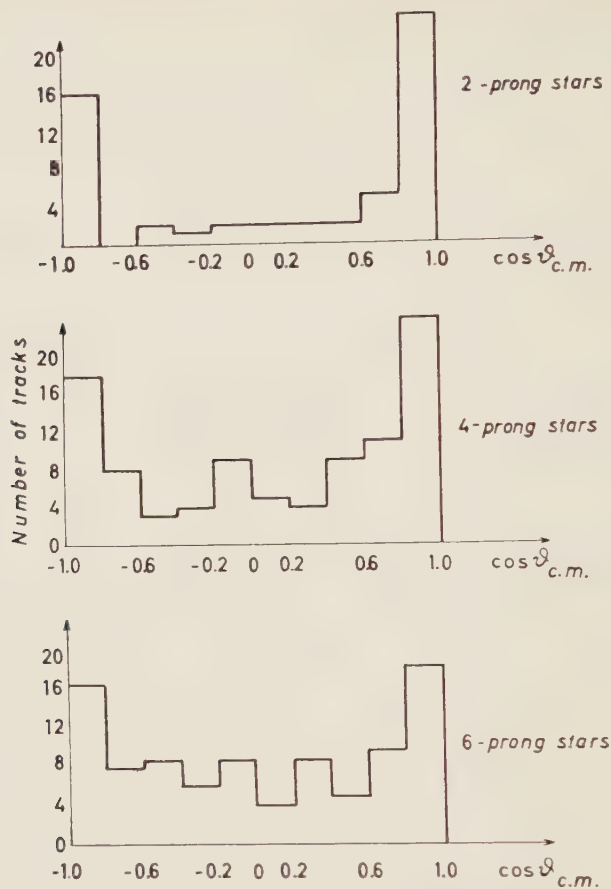


Fig. 4. — Angular distribution of the «best» sample in the c.m. system.

We wish to thank the P.S. Machine Group, under Dr. P. GERMAIN, for their efficient operation of the machine;

Prof. G. COCCONI and his group for their help and co-operation in various stages of the experiment; and the microscopists in Bern and in CERN for their careful and painstaking work.

Interaction of High Energy Protons from the CERN Proton Synchrotron with Photographic Emulsion Nuclei.

C. BRICMAN (*), M. CSEJTHEY-BARTH (**), J. P. LAGNAUX (**) and J. SACTON (**)

Université Libre de Bruxelles - Bruxelles

(ricevuto il 16 Febbraio 1961)

We report here some results on interactions of protons of about 14 GeV with photographic emulsion nuclei (*).

1. - Exposure and experimental method.

A stack of 70 Ilford G-5 emulsion pellicles, each $20\text{ cm} \times 10\text{ cm} \times 500\text{ }\mu\text{m}$ was exposed to an external beam of elastically scattered protons from the CERN proton synchrotron⁽²⁾. The energy of the circulating protons when

they struck the target was 14.9 GeV (*).

The plates were searched by the usual « along the track » method using a $\times 50$ objective and $\times 15$ eyepieces. The tracks were followed over a range of 15 cm or to the point where the proton interacted or left the plate. Great attention was paid to avoid systematic biases against detection of small stars with a shower particle emitted approximately in the beam direction. For this purpose, whenever a slight deviation of the track was observed the exact point of deflection was found and carefully scrutinized.

(*) Assistant à l'Université Libre de Bruxelles.

(**) Chercheur agréé à l'Institut Interuniversitaire des Sciences Nucléaires, Belgique.

(**) Interactions of protons of about 24 GeV are studied in a paper by the CERN and Bern groups⁽¹⁾.

(1) G. CYLIANOVICH, B. DAYTON, P. EGLI, B. KLAIBER, W. KOCH, M. NIKOLIĆ, R. SCHNEEBERGER, H. WINZELER, J. C. COMBE, W. M. GIBSON, W. O. LOCK, M. SCHNEEBERGER and G. VANDERHAEGHE: *Nuovo Cimento*, **20**, 1012 (1961).

(2) B. DAYTON, W. KOCH, M. NIKOLIĆ, H. WINZELER, J. COMBE, W. M. GIBSON, W. O. LOCK, M. SCHNEEBERGER and G. VANDERHAEGHE: *Helv. Phys. Acta*, **33**, 544 (1960).

(*) At the moment of the exposure, the beam was thought to be almost monoenergetic. But later, a magnetic analysis made by COCONI, DIDDENS and WETHERALL of the 24 GeV proton beam obtained in similar conditions showed that the energies were spread over a few Gev. To check this in our stack, we performed some scattering measurements on primary protons. The results show that the measured energies are rather symmetrically distributed from 9 to 20 GeV, with a maximum at 14 GeV. The high energy tail extending up to 20 GeV is obviously due to the inaccuracy of the measurements and the symmetrical low energy tail is thought to have the same origin. It is quite clear that there is no significant contribution below 10 GeV.

All track deflections greater than 2° in the plane of the emulsion sheet or greater than 5° in the perpendicular plane were recorded.

2. - Interaction mean free path.

A total path of 145 m has been followed and 504 interactions were found. In this figure are included:

a) 7 possible elastic proton-free proton collisions;

b) 3 events with one emitted relativistic particle and a short nuclear recoil only;

c) 2 large angle deflections of respectively 4° and 10° .

The mean free path for the production of these interactions by 14 GeV protons is, thus: (28.8 ± 1.3) cm.

were divided in two classes according to their specific ionization:

a) shower particles ($g < 1.5 g_{\text{plateau}}$);

b) heavy particles ($g > 1.5 g_{\text{plateau}}$).

This limit corresponds to a velocity $\beta = 0.63$.

In Fig. 1 is plotted the distribution of the stars with respect to the shower particle number, n_s . The average number of shower particles emitted in one event is $\bar{n}_s = (4.9 \pm 0.1)$. Data on the variation of \bar{n}_s with increasing incident proton energy have been collected by N. P. BOGACHEV *et al.* ⁽³⁾. In Fig. 2, we add to these data our value and the one recently obtained by H. WINZELER *et al.* ⁽⁴⁾ at 6.2 GeV. In our experiment the maximum observed value for n_s is 17. Some 26% of the stars contain more than 6 shower particles. This result is to be compared with the figures

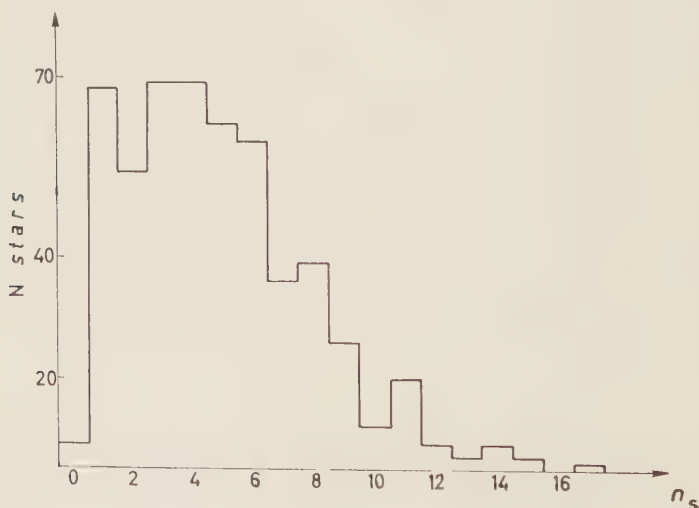


Fig. 1. - Distribution in n_s for all the events.

3. - General analysis of stars.

A general analysis of 481 interactions lying at a distance greater than $40 \mu\text{m}$ from either surfaces of the unprocessed emulsion has been carried out. The particles emitted from these interactions

⁽³⁾ N. P. BOGACHEV, VAN SHU FEN, I. M. GRAMENITSKII, L. F. KIRILOVA, R. M. LEBEDEV, V. B. LIUBIMOV, P. K. MARKOV, I. P. P. MERKOV, M. I. PODGORETSKII, V. M. SIDOROV, K. D. TOLSTOV and M. G. SHAFRANOVA: *The Sov. Journ. of Atomic Energy*, **4**, 373 (1958).

⁽⁴⁾ H. WINZELER, B. KLAIBER, W. KOCH, M. NIKOLIĆ and M. SCHNEEBERGER: *Nuovo Cimento*, **17**, 10 (1960).

reported at 9 and 6.2 GeV, i.e., 13% and 2%. $n_h > 6$ and $n_h > 20$ are equal to 47% and 10%. As can be seen from Table I

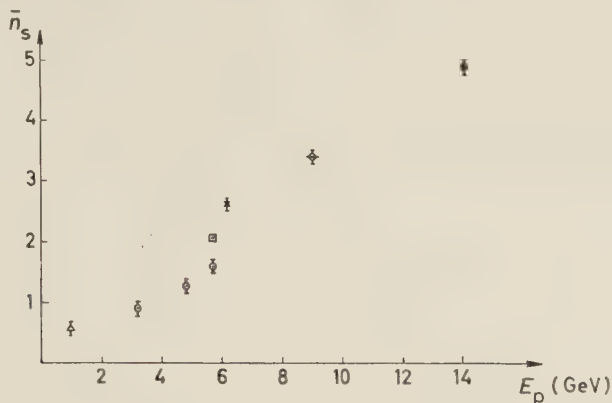


Fig. 2. — Plot of \bar{n}_s versus incident proton energy. Δ Data of W. O. LOCK *et al.* ⁽⁶⁾. \circ Data of W. R. JOHNSON ⁽⁶⁾. \square Data of R. E. CAVANAUGH *et al.* ⁽⁷⁾. \times Data of H. WINZELER *et al.* ⁽⁴⁾. \odot Data of N. P. BOGACHEV *et al.* ⁽⁸⁾. \bullet Present work.

The mean value of n_h per event is 8.4. The fractions of stars characterized by these last three quantities seem to be constant with increasing primary energy

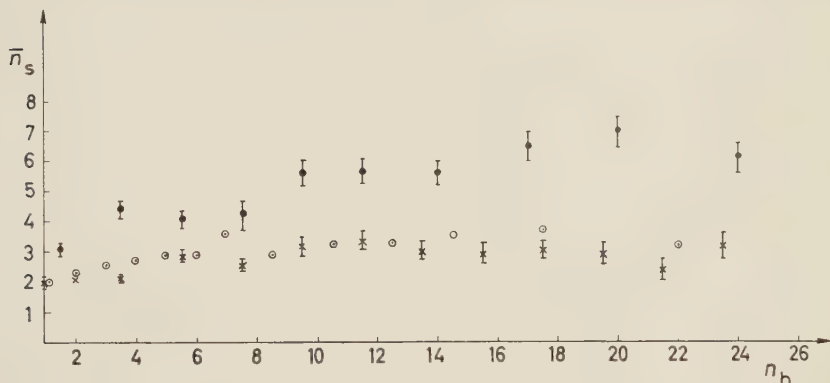


Fig. 3. — Plot of \bar{n}_s versus n_h : \times Data of H. WINZELER *et al.* ⁽⁴⁾. \circ Data of R. R. DANIEL *et al.* ⁽⁸⁾. \bullet Present work.

TABLE I.

Proton energy (GeV)	\bar{n}_h	% of stars with	
		$n_h > 6$	$n_h > 20$
6.2	8.8	48	10
9	8.3	50	11
14	8.4	47	10

⁽⁶⁾ W. O. LOCK, P. V. MARCH, H. MUIRHEAD and W. G. V. ROSSER: *Proc. Roy. Soc.*, A **230**, 215 (1955).

⁽⁶⁾ W. R. JOHNSON: *Phys. Rev.*, **99**, 1049 (1955).

⁽⁷⁾ R. E. CAVANAUGH, D. M. HASKIN and M. SCHEIN: *Phys. Rev.*, **100**, 1263 (1953).

⁽⁸⁾ R. R. DANIEL, N. KAMESWARA RAO, P. K. MALHOTRA and Y. TSUZUKI: *Nuovo Cimento*, **16**, 1 (1960).

at least in the energy range from 6.2 to 14 GeV.

In Table II we give the values of \bar{n}_s (for events with $n_h < 7$ and $n_h > 6$ (at 6.2, 9 and 14 GeV). In Fig. 3 we plot the variation of \bar{n}_s with n_h at 6.2 and 14 GeV. A consideration of the results given in Tables I and II and in Fig. 3

TABLE II.

Proton energy (GeV)	\bar{n}_s for stars with	
	$n_h < 7$	$n_h > 6$
6.2	2.3	3.0
9	3.4	3.5
14	3.8	6.0

suggests that the number of heavy ionizing prongs emitted from heavy nuclei does not increase with the number

distribution of these stars with respect to their number of prongs is given in

TABLE III.

Number of prongs	Number of events	
	even white stars	odd white stars
2	10	—
3	—	8
4	10	—
5	—	6
6	5	—
7	—	4
8	—	—
9	—	—
10	1	—
Total	26	18

Table III. No elastic proton-free proton scattering was found among the two-

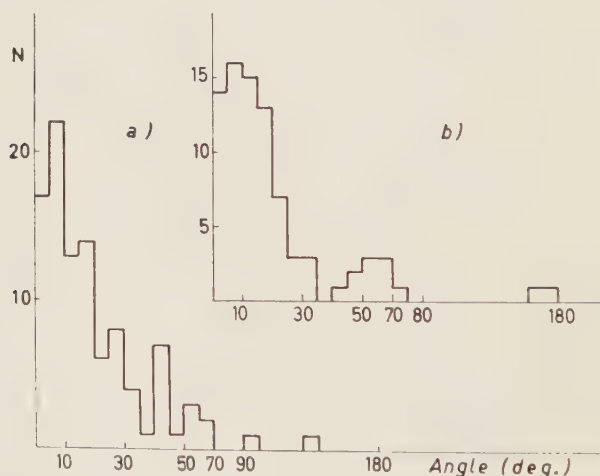


Fig. 4. — Laboratory angular distribution of shower particle tracks with respect to the incident proton direction for white stars with (a) an even number of prongs and (b) an odd number of prongs.

of pions produced (directly or via secondary interactions).

9.3% of the events are «white» stars i.e. stars with only shower tracks. The

pronged white stars. The angular distribution of the prongs with respect to the direction of motion of the primary proton are plotted in Fig. 4a

for the even prong events and in Fig. 4b
for the odd prong events.

* * *

We are greatly indebted to the CERN
P. S. Machine Group under Dr. P. GER-

MAIN for use of the facilities of the
Proton Synchrotron and to the CERN
Emulsion Group for the set up of the
beam. Our further thanks are due to
our scanning team: Mrs. M. FRANCOU,
Mrs. F. JOHNSON, Mrs. F. VANDER-
HOEVEN, Miss J. LEONARD and Miss
CH. STOFFEN for their painstaking work.

Some Remarks on Sakurai's Theory of Strong Interactions.

A. P. BALACHANDRAN (*)

Department of Physics, University of Madras - Madras

AND

N. G. DESHPANDE

(ricevuto il 19 Febbraio 1961)

Recently, SAKURAI⁽¹⁾ has proposed a theory of strong interactions along lines originally suggested by YANG and MILLS⁽²⁾ and subsequently discussed by several authors⁽³⁾. We would like to make a few remarks concerning this theory.

It may be easily seen (for example from eq. (9)–(11) of reference⁽¹⁾) that in such a theory any single baryon or spinless meson field always occurs bilinearly. The Lagrangian is consequently invariant under a change of sign of any one of these fields, the other fields being left unaltered (where, as in what follows, components of isotopic multiplets are regarded as belonging to the same field). A direct consequence of

this is that reactions such as $K^- + p \rightarrow \Sigma^\pm + \pi^\mp$ or $B_\mu \rightarrow$ odd number of pions (where B_μ denotes any vector field) are forbidden. In general, any reaction in which the final state is different from the initial state is not allowed (provided, of course, it is not of some such form as for example $p + \bar{p} \rightarrow \pi^+ + \pi^-$ or $A + B \rightarrow A + B + B_\mu$).

Another consequence of the bilinearity of the Lagrangian in the baryon or spinless meson fields is that it cannot give rise to an effective interaction of the form $ig\bar{\psi}\gamma_5\tau\psi\phi$ or any other interaction which is linear in any one of these fields since such interactions do not possess the symmetries of the actual Lagrangian. This Lagrangian also does not define any of the relative parities between these fields (reactions such as $\pi^- + D \rightarrow n + n$ ⁽⁴⁾ being forbidden).

The above discussion assumes that all the fields are elementary. It was

(*) Atomic Energy Commission Senior Research Fellow.

⁽¹⁾ J. J. SAKURAI: *Ann. Phys.*, **11**, 1 (1960).

⁽²⁾ C. N. YANG and R. L. MILLS: *Phys. Rev.*, **96**, 191 (1954).

⁽³⁾ T. D. LEE and C. N. YANG: *Phys. Rev.*, **98**, 1501 (1955); Y. FUJII: *Frog. Theor. Phys. (Kyoto)*, **21**, 232 (1959).

⁽⁴⁾ W. K. H. PANOFSKY, R. L. AAMODT and J. HADLEY: *Phys. Rev.*, **81**, 565 (1951).

pointed out by DALLAPORTA ⁽⁵⁾ that such difficulties are removed for Σ^- production in \bar{K} -n collisions (for instance) if π and K are regarded as suitable compound particles. This by itself is insufficient and it is necessary to regard all the baryon or spinless meson fields as made up of two basic fields if we are to avoid such difficulties in other reactions. This is at variance with Sakurai's point of view ⁽¹⁾ that it does not matter whether elementary particles are really « elementary » or not in his theory.

The theory also does not explain

why there is no bound system of an \bar{n} and a Σ^+ ⁽⁶⁾.

* * *

We wish to thank Professor N. DALLAPORTA for critical comments and Professor ALLADI RAMAKRISHNAN, Mr. N. R. RANGANATHAN and Mr. K. VENKATESAN for stimulating discussions. One of us (A.P.B.) is grateful to the Atomic Energy Commission for providing him with a Fellowship which enabled him to participate in this work.

⁽⁶⁾ We are grateful to Professor N. DALLAPORTA for pointing out this difficulty.

⁽⁵⁾ Private communication.

Y^* and K^* in Strong Interactions (*)

J. FRANKLIN and S. F. TUAN

Department of Physics, Brown University - Providence, R.I.

(ricevuto il 4 Marzo 1961)

Recent experimental evidence ⁽¹⁾ suggests that a spin of the $I=1$ excited hyperon Y^* of $J=\frac{1}{2}$ with strong decay $Y^* \rightarrow \pi + \Lambda$ through the S -state (*i.e.* (Y^* , Λ) parity is odd) is possible. This supports the attractive hypothesis ⁽²⁾ that the Y^* (pion-hyperon resonance) is induced by the S -wave association of the K^-p system or a « bound state » of the \bar{K} -nucleon system first discussed in some detail two years ago ^(3,4).

It may be of some interest to discuss this « bound-state resonance » Y^* as a third pole (in addition to Λ and Σ) in the unphysical region for $\bar{K}N$ dispersion relations, *i.e.* allow Y^* to assume a particlelike interpretation—exact in the absence of strong decay $Y^* \rightarrow \pi + \Lambda(\Sigma)$. In terms of the physical model proposed, the contribution from this resonance pole to the dispersion equation is to be understood in terms of the analytic continuation of the $\bar{K}N$ scattering amplitude for scattering length solution ($a-$) ⁽⁵⁾. Using an unsubtracted form for the K^-p dispersion relation ⁽⁶⁾, we expect

$$(1) \quad (G_{KY^*}^2/4\pi) \frac{(M_p)}{(M_{Y^*})} \frac{1}{[(M_p - M_{Y^*})^2 - M_K^2]} \sim \frac{1}{\pi} \int \frac{\text{Im } T(\omega') d\omega'}{\omega'^2 - M_K^2}$$

Here $G_{KY^*}^2/4\pi$ is the renormalized coupling constant for the $(\bar{K}N Y^*)$ vertex, $M_{Y^*} \sim 1385$ MeV, and the imaginary part of the K^-p scattering amplitude $T(\omega)$ is evaluated over an energy interval for which the ($a-$) solution gives a resonance to $T(\omega)$. In Fig. 1, we have plotted $\text{Im } T(\omega)$ in the unphysical region below K^-p

(*) This work was supported by the U.S. Atomic Energy Commission.

(1) M. M. BLOCK: private communication on the work of $K^-4\text{He}$.

(2) S. F. TUAN: *Nuovo Cimento*, **18**, 1301 (1960); M. ROSS and G. SHAW: *Phys. Rev. Lett.*, **5**, 579 (1960).

(3) R. H. DALITZ and S. F. TUAN: *Phys. Rev. Lett.*, **2**, 425 (1959); *Ann. Phys.*, **10**, 307 (1960).

(4) R. KARPLUS, L. KERTH and T. KYCIA: *Phys. Rev. Lett.*, **2**, 510 (1959). See also R. H. DALITZ: UCLL-9543, *Phys. Rev. Lett.* (to be published) (1961).

(5) R. H. DALITZ and S. F. TUAN: *Ann. Phys.*, **8**, 100 (1959).

(6) S. F. TUAN: *Phys. Rev.*, **113**, 1375 (1959).

threshold, using the more recently determined scattering parameters for (a) (7).

$$(2) \quad \begin{cases} A_0 = -0.25 + 1.65i = a_0 + ib_0, \\ A_1 = -1.09 + 0.20i = a_1 + ib_1. \end{cases}$$

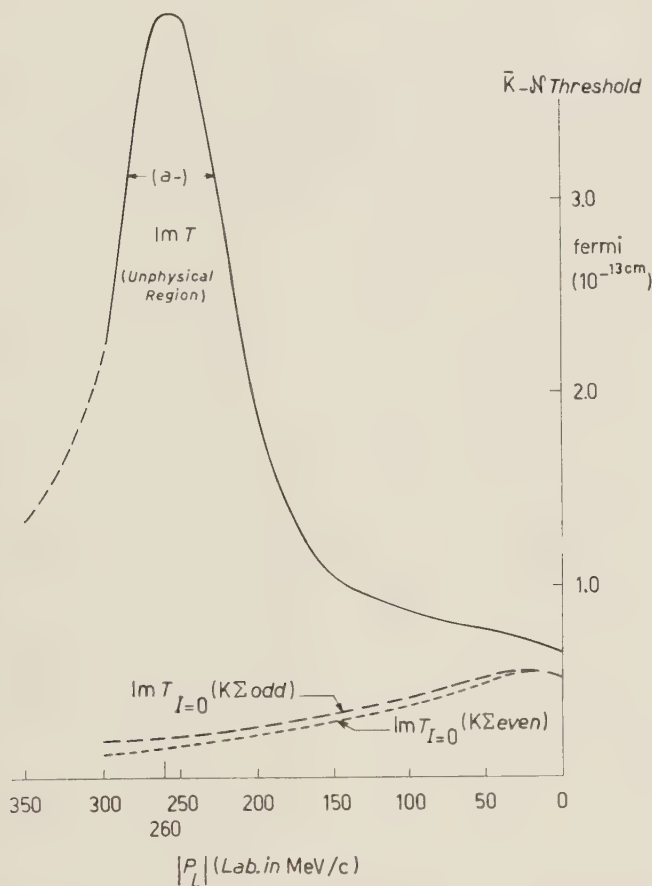


Fig. 1. — $\text{Im } T$ and $\text{Im } T_{I=0}$ as functions of laboratory momentum $|p_L|$ in MeV/c for the region of unphysical K^-p energies for solution (a—). The curves $\text{Im } T_{I=0}$ for the two parity assignments $(K\Sigma)$ odd and even are normalized to $q = q_0$ at the K^-p threshold; q and q_0 are, respectively, the c.m. momentum for the $\pi\Sigma$ system and its value at this threshold.

It is of interest to note that these new scattering lengths solutions do predict a binding energy for the $Y^* \sim -48$ MeV and a half width $\Gamma/2 \sim 17$ MeV on the basis of zero range theory—both consistent with experimental data. In fact the

(7) R. H. DALITZ: *Rev. Mod. Phys.*, to be published (1961). For the purpose of our theoretical discussion here, we ignore the errors on the scattering lengths, eq. (2). They do not influence the qualitative features of our remarks.

introduction of an effective range term to the K^-p analysis will give a larger value for the Y^* binding energy than experiments would indicate⁽⁸⁾.

Evaluating the right-hand side of (1) over an energy range corresponding to the full width (at half maximum), we have

$$(3) \quad \frac{G_{KY^*}^2}{4\pi} \sim 0.4.$$

For a scalar coupling⁽⁹⁾, this is to be regarded as quite substantial, comparable with $(K\Lambda N)$ and $(K\Sigma N)$ scalar couplings⁽¹⁰⁾ ($G_{KY}^2/4\pi \sim 0.7$) ($Y = \Lambda, \Sigma$).

GELL-MANN⁽¹¹⁾ has proposed that the existence of non degenerate parity doublets (K', K) , (Σ', Σ) , (Λ', Λ) will prove very useful concepts in weak interactions for the case of even (Σ, Λ) parity. If we make his identification of particles on the basis of equality of quantum numbers,

$$Y^* = \Sigma' (I=1, J=\frac{1}{2}), \quad K' = K^* (I=\frac{1}{2}, K^* \leftrightarrow (K = \pi)_{S\text{-state}}) \quad (12).$$

then $\Lambda' = \Lambda^* (I=0, J=\frac{1}{2})$ — a particle or $I=0$ ($\pi\Sigma$) resonance yet to be discovered. It is interesting to note that SAKURAI⁽¹³⁾ also predicts the existence of a Λ^* (as a bound state of the S -wave (K^-p) system) corresponding to a much greater binding energy than the Y^* , because of the strong attraction in the $I=0$ state ($J=\frac{1}{2}$). In Fig. 1, we have plotted $\text{Im } T_{I=0}$ for solution (a —) over an energy range up to 65 MeV. ($(\pi\Sigma)Q$ -value ~ 35 MeV) below the $\bar{K}N$ threshold. Even allowing that the strong cross-channel interactions $\bar{K}N \rightarrow \pi\Sigma$ (large b_0 in eq. (2)) in the $I=0$ state may smooth out any structure for S -wave $\pi\Sigma$ scattering in this I spin state, the marked decline of $\text{Im } T_{I=0}$ below the K^-p threshold does not lend support that Λ^* (or S -wave $(\pi\Sigma)$ -resonance) exists above $(\pi\Sigma)Q$ -value ~ 35 MeV — if it is derived from the S -wave K^-p system⁽¹⁴⁾.

The tighter binding in the $I=0$ state is consistent with the existence of a Λ^* below $(\pi\Sigma)$ threshold; selection rules then forbid any strong decay of Λ^* ($\Lambda^* \rightarrow \pi + \Lambda$ is ruled out by L -spin conservation), though the electromagnetic decay $\Lambda^* \rightarrow \Lambda + \gamma$ is possible. Purely heuristically, if we set the mass difference equal for the fermion doublets, then $m_{\Lambda^*} = m_{Y^*} - m_{\Sigma} + m_{\Lambda} \sim 1305$ MeV ($\pi\Sigma$ threshold ~ 1330 MeV).

We would like to add that for (Λ, Σ) parity odd, the doublet scheme breaks down, in particular (Σ, Y^*) have the same parity. In terms of the bound state model, the lack of structure for $\text{Im } T_{I=0}$ ($K\Sigma$ parity even) again suggests little evidence for an $I=0$ $\pi\Sigma(p_{\frac{1}{2}})$ resonance for the same energy range, though a Λ^* below $\pi\Sigma$ threshold remains a distinct possibility⁽¹⁴⁾.

(8) Private communication from Dr. G. SHAW.

(9) Unlike parity determination, coupling constant estimates are relatively insensitive to the form of dispersion relation employed. The use of information from an essentially unsubtracted equation suffices for the purpose at hand.

(10) P. T. MATTHEWS and A. SALAM: *Phys. Rev.*, **110**, 569 (1958).

(11) M. GELL-MANN: *Proc. of the Conference on Strong Interactions* (Berkeley, 1960). Also private communication.

(12) The experimental status for K^* is discussed for instance by M. H. ALSTON: *Rev. Mod. Phys.*, to be published (1961).

(13) J. J. SAKURAI: private communication; see also *Ann. Phys.*, **11**, 1 (1960).

(14) For $(K\Sigma)$ parity odd (even), we cannot rule out the possibility of an $I=0$ $\pi\Sigma p_{\frac{1}{2}}(S_{\frac{1}{2}})$ resonance at energies of the order of K^-p threshold. However such resonances will have no relation to the S -wave K^-p bound state we discuss.

Experimentally such a Λ^* should be seen from the associated production process $\pi + p \rightarrow K^0 + \Lambda^*$ for incident pion kinetic energy greater than 1.1 GeV (lab.), assuming that Λ^* is substantially heavier than Σ . If $M_{\Lambda^*} \sim M_{\Sigma}$ we cannot exclude the possibility that such events have been ambiguously identified with Σ^0 which shares the same electromagnetic decay to $\Lambda^0 + \gamma$; such Λ^* events would have a marked effect on triangular inequalities⁽¹⁵⁾ for associated production.

In the spirit of our theoretical discussion about Y^* , the excited K^* state⁽¹²⁾ would appear as a pole term in the $\bar{K}N$ dispersion relations, the much tighter binding energy involved here would preclude any attempt to simulate the effective range approach adopted for eq. (1). Such a « particle » would be scalar if considered as the parity doublet companion of the K -meson, and could be vector if it were an excited state in a composite model⁽¹⁶⁾ or a « fundamental » ($I = \frac{1}{2}$, $J = 1$) vector boson⁽¹⁷⁾. It is interesting to note that dynamic calculations along the Mandelstam program for the $(K\pi)$ interaction have been unable to produce a S -wave resonance (the K^*) irrespective of the presence or absence of strong pion-pion correlation, though the situation for the P -wave is uncertain⁽¹⁸⁾.

Coupling constants can be calculated from the observed widths for the decays $Y^* \rightarrow \Lambda + \pi$ ($\Gamma \sim 30$ MeV) and $K^* \rightarrow K + \pi$ ⁽¹⁹⁾ ($\Gamma \sim 30$ MeV). These are

$$\frac{G_{Y^*\Lambda\pi}^2}{4\pi M_{Y^*}^2} \sim 0.08; \quad \frac{G_{K^*K\pi}^2}{4\pi (M_{K^*})^2} = \frac{f^2}{4\pi} = 0.2 \text{ (K}^* \text{ scalar)}^{(20)}; \quad \frac{G_{K^*K\pi}}{4\pi} \sim 0.5 \text{ (K}^* \text{ vector)}.$$

The calculations are made on the basis of the experimental width, and thus should be considered as upper limits should the experimental width be broader than the natural width.

We should add that contributions from K^* to low energy $\bar{K}N$ scattering can occur through intermediate state diagrams like Fig. 2. The threshold $K^* + N$ for this intermediate state is some 390 MeV above the $\bar{K}N$ threshold in energy. In a dispersion theoretic framework the contribution from such « distant singularities » — even if substantial, are unlikely to affect greatly the energy dependence of a simple scattering length analysis. The situation with long range pion forces from the exchange of two and three pions say, is less easy to assess. Current experimental

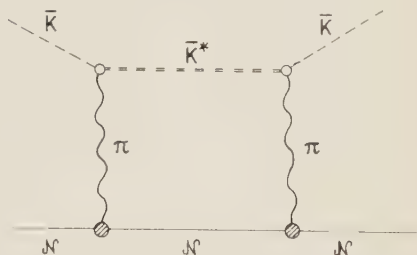


Fig. 2. — \bar{K}^* contribution in intermediate state to $\bar{K}N$ low energy scattering.

⁽¹⁵⁾ F. S. CRAWFORD, R. L. DOUGLAS, M. L. GOOD, G. R. KALBFLEISCH, M. L. STEVENSON and H. K. TICHQ: *Phys. Rev. Lett.*, **3**, 394 (1959).

⁽¹⁶⁾ For example the Sakata model of \bar{K} as a ΛN bound state would permit an excited state which could be identified with the \bar{K}^* . S. SAKATA: *Progr. Theor. Phys.*, **16**, 686 (1956).

⁽¹⁷⁾ M. GELL-MANN (private communication to S. GLASHOW). We wish to thank Dr. GLASHOW for informing us of the recent work done at Cal. Tech. The model proposed however still requires (Λ, Σ) parity to be even.

⁽¹⁸⁾ B. W. LEE: private communication.

⁽¹⁹⁾ M. A. BAQI BEG and P. C. DE CELLES: *Phys. Rev. Lett.*, **6**, 145 (1961); **6**, 428 (1961).

⁽²⁰⁾ This compares with $f^2/4\pi \sim 0.007$ to 0.03 for the $(KK\pi)$ interaction. See A. PAIS: *Phys. Rev.*, **112**, 624 (1958).

evidence ⁽²¹⁾ is consistent with no ($I=1, J=1$) pion-pion resonance at the resonance energy $t_R \sim 12m_\pi^2$ quoted earlier ⁽²²⁾. Theoretical calculations on pion-nucleon scattering ⁽²³⁾ however suggest that such a resonance can exist at a much higher pion-pion energy $t_R \sim 22.4m_\pi^2$; in terms of the $\bar{K}-N$ picture ⁽²⁾ the dominant contribution from this resonance will occur below the $\pi-\Lambda$ threshold and may again be expected to give relatively weak energy dependence to zero range theory. We are on less sure grounds if the $I=0, J=1$ three pion bound state ω_0 ($\sim 2.3m_\pi$) should exist ⁽¹¹⁾, this state can contribute to $\bar{K}-N$ scattering at energies of the order of only 40 MeV below threshold. In fact DALITZ ⁽⁴⁾ has pointed out that some energy dependence for the parameters a_I, b_I are to be expected over and above phase space and centrifugal considerations to account for the very small $(\Sigma/\Lambda)_{I=1}$ ratio at the Y^* resonance ($\lesssim 10\%$). We feel that some understanding on a dynamic basis of the contribution from intermediate vector bosons in the $I=1$ and $I=0$ (the ω_0 particle?) channel may be necessary for a satisfactory clarification of energy dependence in low energy $\bar{K}-N$ scattering.

Much attention has been given recently to global symmetry ⁽²⁴⁾ concepts on the assumption that Y^* is indeed $I=1$ and $J=\frac{3}{2}$. Global symmetry as we understand it today does *not* require K-meson interactions to be weak, in fact virtual K-mesons in intermediate states can be incorporated in a pion-baryon framework ⁽²⁵⁾. However aside from possible experimental difficulties ⁽¹⁾, such a model is unable to accommodate in a dynamic way, the *real* and nearby $\bar{K}-N$ channel, such as is provided by effective range theory ^(3,5) through simple considerations of unitarity and analyticity.

In conclusion, we wish to emphasize the importance of a convincing determination for (Σ, Λ) relative parity from say the observation of correlations of polarizations in the process $\Sigma^0 \rightarrow \Lambda^0 + \gamma$ ⁽¹⁶⁾. Theoretical models like global symmetry ⁽²⁴⁾ or the «fundamental» vector boson theory ⁽¹⁷⁾ depend sensitively on the assumption that (Λ, Σ) parity is even, though the Sakurai theory ⁽¹³⁾ is apparently independent of this assumption. Whereas the effective range approach can be made more consistent with experimental observation for $(\Sigma/\Lambda)_{I=1}$ decay ratio for Y^* on the assumption that (Λ, Σ) parity is odd ⁽⁸⁾, the determination of the scattering length parameters will be to a certain degree ambiguous until such time as we have a reliable experimental estimate for the Σ^0 and Λ^0 separation at $p_K = (150 \pm 2.0)$ MeV/c (lab.) above K^-p threshold ⁽⁵⁾.

* * *

One of us (S.F.T.) would like to thank Professors M. GELL-MANN and J. J. SAKURAI for very helpful and stimulating discussions.

We have received a manuscript from Professor M. GELL-MANN after completion of this letter in which some of the points mentioned here are also discussed, especially the possible existence of a Λ^* hyperon.

⁽²¹⁾ *Proceedings of the Conference on Strong Interactions* (Berkeley, 1960).

⁽²²⁾ W. R. FRAZER and J. R. FULCO: *Phys. Rev.*, **117**, 1603, 1609 (1960). See also J. S. BALL and D. Y. WONG: *Phys. Rev. Lett.*, **6**, 29 (1961).

⁽²³⁾ S. C. FRAUTSCHI (private communication); see also S. FUBINI: *Rev. Mod. Phys.*, to be published (1961).

⁽²⁴⁾ T. D. LEE and C. N. YANG: *Some considerations on global symmetry*, to be published in the *Phys. Rev.* (1961). References to previous works are given in this article.

⁽²⁵⁾ We would like to thank Professor A. PAIS for several helpful comments.

⁽²⁶⁾ N. BYERS and G. H. BURKHARDT: *Phys. Rev.*, **121**, 281 (1961). J. SUCHER and G. A. SNOW: *Nuovo Cimento*, **18**, 195 (1960).

Note added in proof.

The final scattering length solution for $(a-)$ has settled (cf. reference (7)) to the following value:

$$(a-) \quad \begin{cases} A_0 = 0.75({}_{-0.45}^{+0.35}) + i 2.0 (\pm 0.35), \\ A_1 = -0.85(\pm 0.15) + i 0.21(\pm 0.04). \end{cases}$$

This yields a resonance in the $I=1$ channel, some (80 ± 30) MeV below the K^-p threshold according to zero range theory, which is not in disagreement with the observed location of the Y^* resonance.

A Note on the Final State Interaction in $K_{2\pi}^-$ Decay.

K. KAWARABAYASHI

Department of Physics, University of Tokyo - Tokyo

(ricevuto il 13 Marzo 1961)

One of the possible explanations of the $K_{2\pi}^+$ decay has been suggested by GOOD and HOLLADAY ⁽¹⁾ under the assumption that it decays through a strict $\Delta I = \frac{1}{2}$ weak interaction, modified by radiative corrections, with an enhancement by a strong pion-pion interaction in the state of $I=2$ and $J=0$. According to their analysis, it is necessary to assume a_{20} , the scattering length of the pion-pion scattering in the state of $I=2$ and $J=0$, to be positive and of the order of one pion Compton wave-length, while their interaction radius is small and of the order of $1/2M$, in order to obtain an enhancement factor of the desired order of magnitude (≈ 10).

Recent investigation of the energy spectrum of the τ decay ⁽²⁾, however, seems to support a negative value of the scattering length a_{20} . Moreover, if the strength of the interaction is estimated with a square well potential using the above scattering length and interaction radius, the potential depth V_0 is required to be of the order of 30 GeV, which seems too strong to accept.

In this note, therefore, we estimate the final state interaction more field-theoretically by making use of the technique of dispersion relations, which is somewhat different from Watson's treatment of the final state interaction ⁽³⁾ and suggest an alternative possibility for the explanation of the $K_{2\pi}^+$ decay rate.

The decay amplitude can be expressed as follows,

$$(1) \quad \langle \pi^+ \pi_{in}^0 | K^+ \rangle = -i \delta^4(p - q^+ - q^0) \left[\frac{1}{(2\pi)^2} \right]^3 \left[\frac{1}{8p_0 q_0^+ q_0^0} \right]^{\frac{1}{2}} \mathcal{M}(\xi), \quad (\xi = -p^2),$$

where the four-momenta of the K-meson and the final two pions are denoted by p and q^+ , q^0 , respectively.

⁽¹⁾ M. L. GOOD and W. G. HOLLADAY: *Phys. Rev. Lett.*, **4**, 128 (1960).

⁽²⁾ N. N. KHURI and S. B. TREIMAN: *Phys. Rev.*, **119**, 1115 (1960); R. F. SAWYER and K. C. WALK: *Phys. Rev.*, **119**, 1429 (1960).

⁽³⁾ K. M. WATSON: *Phys. Rev.*, **88**, 1163 (1952).

The invariant amplitude $\mathcal{M}(\xi)$ can be proved to satisfy the following unsubtracted dispersion relation

$$(2) \quad \mathcal{M}(\xi) = \frac{1}{\pi} \int_{4\mu^2}^{\infty} \frac{\text{Im } \mathcal{M}(\xi')}{\xi' - \xi} d\xi'.$$

The proof of eq. (2) is done in essentially the same way as that in case of the analytic property of the pion-nucleon vertex part as a function of a nucleon mass ⁽⁴⁾.

To calculate $\text{Im } \mathcal{M}(\xi)$, we adopt the usual assumption that the dominant contribution comes from the lowest mass configuration. $\text{Im } \mathcal{M}(\xi)$ is then approximated, taking into account the fact that $\mathcal{M}(\xi)$ is induced by radiative corrections, as follows:

$$\begin{aligned} \text{Im } \mathcal{M}(\xi) &= -(2\pi)^{\frac{3}{2}} (2\pi)^4 \frac{1}{2} (2q_0^0)^{\frac{1}{2}} \sum_n \langle \pi^+ | j_{\pi^0} | n \rangle \langle n | j_{K^+} | 0 \rangle \delta^4(p - p_n) \approx \\ &\approx \exp[-i\delta] \sin \delta \mathcal{M}(\xi) + \mathcal{N}(\xi), \end{aligned}$$

where the second term $\mathcal{N}(\xi)$ is given by (Fig. 2)

$$(4) \quad \mathcal{N}(\xi) = -(2\pi)^{\frac{3}{2}} (2\pi)^4 \frac{1}{2} (2q_0^0)^{\frac{1}{2}} \sum' \langle \pi^+ | j_{\pi^0} | \pi^{+'} \pi^{0'} \gamma \rangle \langle \gamma \pi^{0'} \pi^{+'} | j_{K^+} | \epsilon \rangle \delta^4(p - q^{+'} - q^{0'} - k_\gamma).$$



Fig. 1. — The contribution from two-pion state. Solid line represents K^+ -meson; broken lines being pions.



Fig. 2. — The contribution from two-pion and one-photon state. Solid line represents K^+ -meson; broken lines, pions and wavy line, photon.

The first term represents the contribution from the two pion intermediate state (Fig. 1), δ being the phase-shift of the pion-pion scattering in the state of $I=2$ and $J=0$.

Inserting (3) into (2), we obtain the inhomogeneous integral equation of the Omnès-Muskhelishvili type.

$$(5) \quad \mathcal{M}(\xi) = X(\xi) + \frac{1}{\pi} \int_{4\mu^2}^{\infty} \frac{\exp[-i\delta] \sin \delta \mathcal{M}(\xi')}{\xi' - \xi} d\xi',$$

⁽⁴⁾ A. BINGER: *Phys. Rev.*, **118**, 855 (1960).

where

$$(6) \quad X(\xi) = \frac{1}{\pi} \int_{\xi - \mu^2}^{\xi} \mathcal{N}(\xi') d\xi'.$$

The general solution of eq. (5) is given by ⁽⁵⁾

$$(7) \quad \mathcal{M}(\xi) = X(\xi) + \frac{1}{\pi} \exp[U(\xi)] \int_{\xi - \mu^2}^{\xi} \frac{X(\xi') \exp[+i\delta] \sin \delta \exp[-U(\xi')]}{\xi' - \xi} d\xi',$$

where

$$(8) \quad U(\xi) = \frac{\xi}{\pi} \int_{\xi - \mu^2}^{\xi} \frac{\delta(\xi')}{\xi'(\xi' - \xi)} d\xi'.$$

Here we have assumed no bound state in the state of $I=2$ and $J=0$ of the pion-pion scattering. (See the foot-note ⁽⁵⁾).

The solution (7) may be expressed in terms of the pion-pion scattering amplitude $f_{\pi\pi}(\xi)$ in the state of $I=2$ and $J=0$, if we approximate the contribution from the left-hand cut of the amplitude with a properly chosen pole as is done by FRAZER and FULCO ⁽⁶⁾. Then

$$(9) \quad \exp[U(\xi)] = \frac{(\xi + \xi_0)f_{\pi\pi}(\xi)}{\xi f_{\pi\pi}(\xi)},$$

where

$$f_{\pi\pi}(\xi) = \sqrt{\frac{\xi}{4\xi - \mu^2}} \exp[i\delta] \sin \delta,$$

— ξ_0 : position of the pole.

Making use of eq. (9), the solution (7) is expressed in terms of $f_{\pi\pi}(\xi)$ as follows,

$$(10) \quad \mathcal{M}(\xi) = X(\xi) \left\{ 1 + \frac{(\xi + \xi_0)f_{\pi\pi}(\xi)}{\pi X(\xi)} \int_{\xi - \mu^2}^{\xi} \frac{X(\xi')}{(\xi' + \xi_0)(\xi' - \xi)} \sqrt{\frac{4\xi' - \mu^2}{\xi'}} d\xi' \right\}.$$

The enhancement factor (E.F.) is given by

$$(11) \quad \text{E.F.} = \left| 1 + \frac{(m_K^2 + \xi_0)}{\pi X(m_K^2)} f_{\pi\pi}(m_K^2) \int_{m_K^2 - \mu^2}^{m_K^2} \frac{X(\xi')}{(\xi' + \xi_0)(\xi' - m_K^2)} \sqrt{\frac{4\xi' - \mu^2}{\xi'}} d\xi' \right|^2.$$

⁽⁵⁾ R. OMNÈS: *Nuovo Cimento*, **8**, 316 (1958).

⁽⁶⁾ W. R. FRAZER and J. R. FULCO: *Phys. Rev.*, **117**, 1609 (1960).

The E.F. (11) can be evaluated if we assumed $X(\xi)$ to be insensitive to its variable and set approximately constant and moreover $k \cot \delta \approx 1/a_{20}$. The result is

$$(12) \quad \text{E.F.} \approx \left| \exp[i\delta] \cos \delta + \frac{1}{\pi} \sqrt{\frac{m_K^2}{m_K^2 - 4\mu^2}} \exp[i\delta] \sin \delta \cdot \right. \\ \left. \cdot \left\{ \frac{\mu^2}{\sqrt{\xi_0(\xi_0 + 4\mu^2)}} \log \frac{\sqrt{\xi_0 + 4\mu^2} + \sqrt{\xi_0}}{\sqrt{\xi_0 + 4\mu^2} - \sqrt{\xi_0}} + \frac{\mu^2}{\sqrt{m_K^2(m_K^2 - 4\mu^2)}} \log \frac{m_K - \sqrt{m_K^2 - 4\mu^2}}{m_K + \sqrt{m_K^2 - 4\mu^2}} \right\} \right|^2 \approx \\ \approx \frac{1}{1 + a_{20}^2(\frac{1}{4}m_K^2 - \mu^2)} \left[1 + \frac{a_{20}m_K}{2\pi} \left\{ \frac{\mu^2}{\sqrt{\xi_0(\xi_0 + 4\mu^2)}} \log \frac{\sqrt{\xi_0 + 4\mu^2} + \sqrt{\xi_0}}{\sqrt{\xi_0 + 4\mu^2} - \sqrt{\xi_0}} + \right. \right. \\ \left. \left. + \frac{\mu^2}{\sqrt{m_K^2(m_K^2 - 4\mu^2)}} \log \frac{m_K - \sqrt{m_K^2 - 4\mu^2}}{m_K + \sqrt{m_K^2 - 4\mu^2}} \right\} \right]^2.$$

Assuming, for example, $|a_{20}| \approx 0.3$, E.F. (12) turns out to be very small independently of the choice of ξ_0 , i.e.,

$$(13) \quad \text{E.F.} \leq \begin{cases} 1.01 & \dots \text{for attractive force } (a_{20} > 0), \\ 1.04 & \dots \text{for repulsive force } (a_{20} < 0); \end{cases}$$

This is because the first and the second term in the curly bracket in (12) have opposite signs.

It will be noted that we have not yet explicitly used the selection rule in the weak interaction. In fact the effect of the selection rule is only included in the evaluation of $X(\xi)$ in this approximation.

From this treatment, we may expect that the enhancement factor alone is not sufficient for explaining the decay rate even if the final state interaction is attractive, though our estimation is based on the assumption that $X(\xi)$ is insensitive to its variable.

It is interesting to note that though the enhancement factor is not large, $X(\xi)$ is expected to be much larger than the usual lowest order nucleon loop calculation with radiative corrections (7) for the following reasons:

- i) the threshold energy is small compared to the nucleon pair state;
- ii) two pions in the intermediate state are mainly in a P -state relative to their c.m. system and a possible P -wave resonance (8) may enhance the decay probability. This is seen in the following way.

We see from (4) that $\mathcal{N}(\xi)$, the imaginary part of $X(\xi)$, consists of two terms; the one is the matrix element of the decay process $K^+ \rightarrow \pi^+ + \pi^0 + \gamma$, while the other is proportional to the matrix element of the double photo-pion production by the

(7) C. ISO: unpublished; R. SUGANO: unpublished; M. KATO and G. TAKEDA: *Suppl. Progr. Theor. Phys.*, no. 7 (1959).

(8) G. F. CHEW and S. MANDELSTAM: *Phys. Rev.*, **119**, 467 (1960).

pion. The general form of the matrix element of the decay process $K^+ \rightarrow \pi^+ + \pi^0 + \gamma$, is written according to gauge invariance,

$$(14) \quad \begin{cases} \langle \pi^+ \pi^0 \gamma | j_{K^+} | 0 \rangle = - \left[\frac{1}{(2\pi)} \right]^3 \left[\frac{1}{8q_0^+ q_0^0 k_0} \right]^{\frac{1}{2}} M, \\ M = \{ (q^+ \varepsilon)(q^0 k) - (q^+ k)(q^0 \varepsilon) \} F, \end{cases}$$

where ε_μ denotes the polarization vector and F is a function of the invariant scalars, p_k^2 , $(q^+ q^0)$ and $(q^+ k)$. Expression (14) shows that two pions are in a P -state relative to each other if F is assumed to be insensitive to the variables. Note also that the magnitude of F is restricted due to the fact that this radiative decay process is rather rare in nature. But this does not necessarily imply the smallness of the contribution to $X(\xi)$ because the « Q -value» is different from the actual decay process. In addition the double photo-pion production by the pion may be enhanced by a possible P -wave pion-pion resonance. In this sense, $X(\xi)$ will be a possible candidate for the explanation of the $K_{2\pi}^+$ decay rate.

* * *

The author would like to express his gratitude to Prof. S. NAKAMURA for his reading the manuscript and helpful discussions. He is also indebted to the Iwanami-Fujukai Fellowship for his financial aid.

Some Remarks About the Photoproduction of Strange Particles.

M. GOURDIN (*)

*Faculté des Sciences - Orsay
Faculté des Sciences - Bordeaux*

(ricevuto il 22 Marzo 1961)

In a previous paper ⁽¹⁾ we have suggested a model to calculate the associated production amplitude for strange particles by the reaction (**):

$$(1) \quad \pi + N \rightarrow K + Y.$$

We essentially retain, in the three channels, the contributions due to the Born terms and some other pole terms in order to simulate the π -K, π -Y and π - N^* resonances.

The same technique, with the same types of arguments can be retained for the photoproduction of strange particles:

$$(2) \quad \gamma + N \rightarrow K + Y.$$

Let us call S the square of the total energy in the c.m. system for the photo-

production channel. Because of the large anomalous cut in the complex plane of S , due to the large unphysical domain for processes (1) and (2):

$$(M_N + \mu)^2 < S < (M_Y + K)^2,$$

the use of dispersion relations and more precisely the determination of the spectral function from the S matrix unitarity condition seems to be hopeless.

Several authors have considered the Born approximation for the strange particle photoproduction, corresponding to the following diagrams ^(2,4).

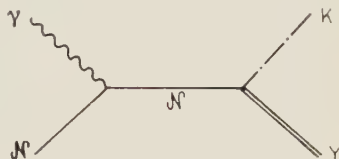


Fig. 1. - Intermediate nucleon.

(*) Postal address: Laboratoire de Physique Théorique et Hautes Energies, B.P. 12, Orsay (Seine et Oise), France.

(1) M. GOURDIN and M. RIMPAULT: *Investigations on the associated production of strange particles*. PTB-6, Bordeaux, February 1961, to be published.

(**) N is a nucleon with mass M_N ; K a K-meson with mass K , Y a hyperon Λ or Σ with mass M_Y and π the pion with mass μ .

(2) M. KAWAGUCHI and M. MORAVCSIK: *Phys. Rev.*, **107**, 563 (1957).

(3) R. CAPPS: *Phys. Rev.*, **114**, 920 (1959).

(4) B. D. McDANIEL, A. SILVERMAN, R. R. WILSON and G. CORTELESSA: *Phys. Rev.*, **115**, 1039 (1959).

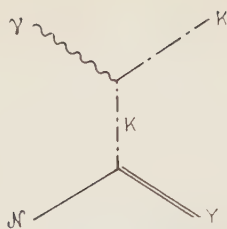


Fig. 2. — Intermediate K-meson.

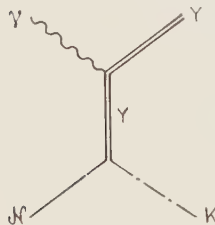


Fig. 3. — Intermediate hyperon.

The values used, for the anomalous magnetic moments of Λ and Σ particles, proceed, in general, from some theoretical speculations⁽⁵⁾. Unfortunately, we have no experimental indications on these values and the situation is very confusing. On the other hand, a dispersion technique approach for the determination of the hyperon magnetic form factors is very difficult because the presence of an anomalous threshold in the dispersion integrals for the Σ^\pm integrals.

If the outgoing hyperon is neutral, the intermediate hyperon of Fig. 3 can be a Λ^0 or a Σ^0 . This introduces a $\Sigma^0\Lambda^0\gamma$ vertex with an unknown transition magnetic moment^(3,4) one can take into account in a consistent treatment but, the experimental data on total and differential cross sections are so poor that one cannot obtain indications on the K, Λ , Σ intrinsic parities with these methods.

By isolating, after extrapolation of the differential cross section, the photo-

electric graph drawn in Fig. 2, MORAVCSIK⁽⁶⁾ tries to determine the $K\Lambda$ relative parity. In the present state of experimental results, it appears as very difficult to give any definite answer to this question. Nevertheless, one has an indication in favour of an odd $K\Lambda$ relative parity.

The aim of this paper is to complete an elementary description of strange particles photoproduction by adding to the Born terms some contributions due to resonances. For Figs. 1 and 3, the situation is exactly the same as for the associated production amplitude. In particular the Y^* resonance corresponds, in the $\cos\theta$ complex plane^(*) to a pole, in the unphysical region $\cos\theta > 1$, but the resonance energy is sufficiently high ($M_{Y^*} \simeq 1380$ MeV) and the width sufficiently small ($\Gamma \simeq 20$ MeV) to permit to consider the corresponding contribution as a correction to the Born term of Fig. 3 and to neglect this in a first approach.

For the Fig. 2, we have the possibility of an intermediate πK state. If we call K' the observed resonance⁽⁷⁾ we replace the cut corresponding to the πK intermediate state by a pole at the resonance energy. By comparing the two $\pi KK'$ and $\gamma KK'$ vertices, it is easy to see that they can vanish by parity conservation. More precisely, the K' particle can give any contribution to the photoproduction amplitude, if the relative KK' parity is even, e.g., if the resonant π -K system is in an *odd* orbital angular momentum state, for instance a P state^(8,9). Isospin and

⁽⁶⁾ M. MORAVCSIK: *Phys. Rev. Lett.*, **2**, 352 (1959).

^(*) We define as θ the c.m. angle in the photoproduction channel between the ingoing photon and the outgoing hyperon.

⁽⁷⁾ M. L. GOOD: *Report at the Rochester Conference* (1960).

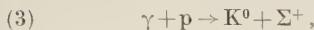
⁽⁸⁾ M. GOURDIN, Y. NOIROT and PH. SALIN: *Nuovo Cimento*, **18**, 651 (1960). B. W. LEE: *Phys. Rev.*, **120**, 325 (1960).

⁽⁹⁾ M. A. BAQI BÉG and P. C. DE CELLES: *Phys. Rev. Lett.*, **6**, 145 (1961).

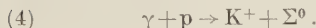
⁽⁵⁾ R. E. MARSHAK, S. OKUBO and E. C. G. SUDARSHAN: *Phys. Rev.*, **106**, 589 (1957).

parity for the π -K resonance are not yet determined.

Such a term gives rise, as the photoelectric term of Fig. 2, to a pole in the unphysical range of the $\cos \theta$ variable ($\cos \theta < -1$) and its principal effect is a backward peaking of the hyperon distribution in the c.m. system. It is possible to isolate this possible K' pole by considering K^0 photoproduction processes in which the photoelectric term cannot occur. The study of the angular distribution, for instance, in the reaction:

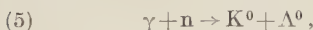


can give some indication for the existence of a P resonant state in π -K scattering; another interest of reaction (3) resides in the fact that no transition magnetic moment occurs and we then have only two Born terms instead of four in the similar process:



At present, only photoproduction of K^+ -mesons has been experimentally studied and we have no information on the reaction (3).

A test for the existence of a π -K resonance in a P state with isospin $I = \frac{1}{2}$ is given by the reaction:



one can, in principle deduce it from experiments with deuteron targets⁽¹⁰⁾ by

⁽¹⁰⁾ F. TURKOT: *Report at the Rochester Conference* (1960).

using impulse approximation. The calculations are straightforward but the interpretation of experimental data, in absence of precise information about the $\gamma + p \rightarrow K^+ + \Lambda^0$ reaction is very difficult.

We adopt, in conclusion, for the strange particles photoproduction the following model:

- a) Born terms;
- b) Isobars for the π - N resonances;
- c) the Y^* resonance as a correction;
- d) the possibility of a π -K resonance in a P state.

The calculations are in progress. We consider the various combinations for the strange particles intrinsic parities as for the associated production problem. Some new parameters must be introduced to describe the coupling between the different isobars and the electromagnetic field. The anomalous magnetic moments and the transition magnetic moment, are considered as parameters related, in principle, to other phenomena as for instance the Compton effect on hyperons. The coupling constants between π -mesons, K-mesons and baryons are not experimentally well-known, one can affect an order of magnitude only for each possible coupling following the assumptions on intrinsic parities.

It seems to be of greatest interest to have more precise and more complete data on total cross sections and angular distributions for the strange particle photoproduction processes.

Interferences Among Feynman Graphs of Different Topology ^(*).

E. R. CAIANIELLO and K. Y. SHEN

Istituto di Fisica Teorica dell'Università - Napoli

(ricevuto il 19 Aprile 1961)

1. — Whenever approximations are made with a theory that describes interactions of fermion fields — that is, when the graphs of a perturbative expansion which do not belong to some summable classes are dropped or, equivalently, the integral equations which become then the substitute for the exact theory are solved — the question arises whether the exclusion principle is being treated correctly. Antisymmetrization of initial and final states does not clearly suffice because the whole dynamical evolution of the process, *i.e.* all that happens in the intermediate states, must violate that principle.

We propose to show here that, even if all the graphs which characterize the chosen approximation procedure are duly antisymmetrized in all the intermediate states, this does not suffice in general to secure that the exclusion principle be rigorously respected (as it is in the exact solution).

The reason is, as is shown in detail below, that a given graph, or partial sum of graphs, although usually regarded for computational purposes as a compact expression, is in fact a sum of contributions arising from all the individual modes of the free fermion fields; these contributions may be partly, or totally, cancelled by others that belong, in the graphical picture, to diagrams which are disregarded by the approximation chosen.

We consider first the case of a fermion field with only a finite number of free modes; the thing is then evident, because there is total cancellation of some graphs by others of different topology. This is, by the way, the ultimate reason why perturbative expansions involving fermion fields are convergent under this assumption (with a finite space-time volume of intergration) ⁽¹⁾. It will then be easy to see that, when the number of fermion modes is infinite, there still remain partial cancellations among graphs of different topology, the more the higher the order of the term in the expansion.

(*) Research reported in this document has been sponsored in part by the European Office of the A.R.D.C., United States Air Force, with Contract no. AF 61(052)-434.

⁽¹⁾ E. R. CAIANIELLO: *Nuovo Cimento*, **3**, 223 (1956); with A. BUCCAFURRI: *Nuovo Cimento*, **8**, 170 (1958).

In the light of this finding, some approximations (especially in questions concerning many-body physics) may turn out to be worse, others, *e.g.* the ladder approximation, better than it might be originally expected.

With bosons the situation is of course entirely similar in principle, but the contributions reinforce rather than cancel one another.

2. — It suffices to restrict our considerations to the simplest case, that of the vacuum-vacuum transition amplitude; they are then true *a fortiori* also for all other matrix elements, as it is evident if these are treated with the same method. We consider, for concreteness' sake, electro- or meso-dynamics; it is however irrelevant to specify the objects with which our fermions interact, because the effect in which we are interested is caused solely by the intervention of the exclusion principle.

It is convenient to use the perturbative expansion without time-ordering ⁽²⁾

$$(1) \quad M_{\epsilon_0} = \sum_{n=0}^{\infty} \lambda^n \int_{T_1}^{T_f} d^4 \xi_1 \dots \int_{T_1}^{\xi_{2n-1}} d^4 \xi_{2n} \sum \gamma^1 \dots \gamma^n [\xi_1 \dots \xi_{2n}] \begin{pmatrix} \xi_1 \dots \xi_{2n} \\ \xi_1 \dots \xi_{2n} \end{pmatrix},$$

where, if the free fermion field contains F modes, the elements of the determinant $\begin{pmatrix} \xi_1 \dots \xi_{2n} \\ \xi_1 \dots \xi_{2n} \end{pmatrix}$ are (cf. ref. ⁽¹⁾, II, form. (13))

$$(2) \quad (\xi_n \xi_k) = \sum_{j=1}^F (\xi_n \xi_k)_j = \begin{cases} \sum_{j=1}^F V_{\alpha_n}(p_j) \bar{V}_{\beta_k}(p_j) \exp[iP_j(\xi_n - \xi_k)] & (\xi_n^0 < \xi_k^0), \\ -\sum_{j=1}^F U_{\beta_k}(p_j) \bar{U}_{\alpha_n}(p_j) \exp[-iP_j(\xi_n - \xi_k)] & (\xi_n^0 > \xi_k^0). \end{cases}$$

Suppose first $F=1$ (only one mode for the particle, and the corresponding mode for the antiparticle). We can expand the fermionic determinant by the elements of the first two rows:

$$(3) \quad \begin{pmatrix} \xi_1 \dots \xi_{2n} \\ \xi_1 \dots \xi_{2n} \end{pmatrix} = \sum_{C_i} (-1)^{p_i} \begin{pmatrix} \xi_1 & \xi_2 \\ \xi_{i_1} & \xi_{i_2} \end{pmatrix} \begin{pmatrix} \xi_3 & \dots & \xi_{2n} \\ \xi_{i_3} & \dots & \xi_{i_{2n}} \end{pmatrix},$$

where p_i is the parity of the combination C_i of the indices $i_1 < i_2; i_3 < \dots < i_{2n}$ (a permutation of $1, 2 \dots 2n$). If F is infinite, all terms for our (3) give non vanishing graphs. With $F=1$ we divide the expansion (3) into two parts:

$$(4) \quad \begin{pmatrix} \xi_1 \dots \xi_{2n} \\ \xi_1 \dots \xi_{2n} \end{pmatrix} = \sum_{C_i(i_1 > 2)} (-1)^{p_i} \begin{pmatrix} \xi_1 & \xi_2 \\ \xi_{i_1} & \xi_{i_2} \end{pmatrix} \begin{pmatrix} \xi_3 & \xi_4 & \dots & \xi_n \\ \xi_1 \xi_2 \xi_{i_3} & \dots & \xi_{i_{2n}} \end{pmatrix} + \dots$$

Because of (2) ($F=1$) and of the time sequence imposed by (1), we find now that

⁽²⁾ E. R. CAIANIELLO: 1) *Nuovo Cimento*, **10**, 1634 (1953), Appendix; 2) **11**, 492 (1954).

all minors $\begin{pmatrix} \xi_1 & \xi_2 \\ \xi_{i_1} & \xi_{i_2} \end{pmatrix}$ with $2 < i_1 < i_2$ are identically vanishing:

$$(5) \quad \begin{pmatrix} \xi_1 & \xi_2 \\ \xi_{i_1} & \xi_{i_2} \end{pmatrix}_{F=1} = \begin{vmatrix} (\xi_1 \xi_{i_1}) & (\xi_1 \xi_{i_2}) \\ (\xi_2 \xi_{i_1}) & (\xi_2 \xi_{i_2}) \end{vmatrix}_{F=1} = 0.$$

(Consider, in particular, the case $n=2$, and neglect boson lines. The terms which vanish in (4) because of (5) (we disregard here additional possible cancellations, because they would not add to our proof reduce to

$$(6) \quad \begin{pmatrix} \xi_1 & \xi_2 \\ \xi_3 & \xi_4 \end{pmatrix} \begin{pmatrix} \xi_3 & \xi_4 \\ \xi_1 & \xi_2 \end{pmatrix} = \begin{pmatrix} \xi_1 & \xi_2 \\ \xi_3 & \xi_4 \end{pmatrix} [(\xi_3 \xi_1) \xi_4 \xi_2 - (\xi_3 \xi_2) \xi_4 \xi_1],$$

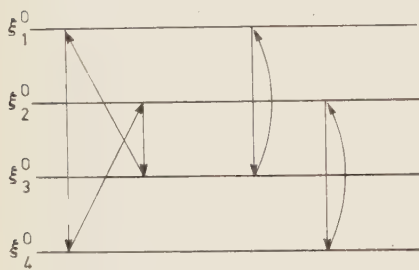


Fig. 1.

is symmetric in both factors (similar facts are true in general); each of the two pieces at the r.h.s. vanishes of its own account; the first corresponds to the two graphs shown in Fig. 1, the second to other two graphs of similar structure.

We see thus that, because of the exclusion principle, for $F=1$, graphs containing two 2-corner loops are cancelled by graphs containing one 4-corner loop. This proves in full our assertion, for $F=1$.

The argument runs entirely in the same manner for arbitrary, but finite F . It suffices to expand (3) by the minors of the first F rows (or columns):

$$(7) \quad \begin{pmatrix} \xi_1 \xi_2 \dots \xi_{2n} \\ \xi_1 \xi_2 \dots \xi_{2n} \end{pmatrix} = \sum_{C_i(i_i > F)} (-1)^{p_i} \begin{pmatrix} \xi_1 \dots \xi_F \\ \xi_{i_1} \dots \xi_{i_F} \end{pmatrix} \begin{pmatrix} \xi_{F+1} \dots \xi_{2F} \xi_{2F+1} \dots \xi_{2n} \\ \xi_1 \dots \xi_F \xi_{i_{2F+1}} \dots \xi_{i_{2n}} \end{pmatrix} + \dots,$$

and again it follows, from (2) and (1), that all the terms of (7) which are explicitly written vanish identically. Total cancellation starts occurring with determinants of order $2F+2$, due to the presence of antiparticles.

3. - When F is infinite we cannot assert any more that some graphs are totally cancelled by others of different structure. It is evident, however, that as soon as the \sum_j in (2) run over the same value of an index in two lines in a minor in an expansion of type (4) or (7), that minor will vanish. There are, thus, more and more cancellations among graphs of different topology as the order of the term increases. It would be easy to see that a minor such as

$$(8) \quad \begin{pmatrix} \xi_1 & \xi_2 & \dots & \xi_N \\ \xi_{i_1} & \xi_{i_2} & \dots & \xi_{i_N} \end{pmatrix} = \sum_{j_1, \dots, j_N} \begin{vmatrix} (\xi_1 \xi_{i_1})_{j_1} & \dots & (\xi_1 \xi_{i_N})_{j_1} \\ \vdots & & \vdots \\ (\xi_N \xi_{i_1})_{j_N} & \dots & (\xi_N \xi_{i_N})_{j_N} \end{vmatrix},$$

$(2N < F' < \infty)$, which gives rise at the r.h.s. to F'^N addends, has only $\binom{F'}{N} \cdot N!$ of them $\neq 0$, because of (2) and (1).

In conclusion, we must reject the view that total antisymmetrization of graphs of special classes may suffice to ensure the validity of the exclusion principle: we have demonstrated that this principle requires cancellations among terms which belong to graphs of different topology.

Reply to Dr. Shewell's Criticism.

J. S. LOMONT

Departement of Mathematics, Polytechnic Institute of Brooklyn - Brooklyn

H. E. MOSES

Department of Physics, Polytechnic Institute of Brooklyn - Brooklyn

(ricevuto il 26 Aprile 1961)

In his letter ⁽¹⁾ Dr. SHEWELL has given what would appear to be a counterexample to a theorem of ours ⁽²⁾. In fact, however, his vector field $\mathbf{f}(\mathbf{q})$ is not a counterexample because it is not continuous, much less differentiable, on the positive z -axis. Hence it does not satisfy the equation

$$\mathbf{L} \times \mathbf{f} = i\mathbf{f},$$

⁽¹⁾ J. R. SHEWELL: *Nuovo Cimento*, **20**, 1010 (1961).

⁽²⁾ J. S. LOMONT and H. E. MOSES: *Nuovo Cimento*, **16**, 96 (1960).

everywhere. A similar situation arises in ordinary vector calculus when one is not careful about singularities ⁽³⁾. For a more detailed discussion of our theorem see references ⁽⁴⁾ and ⁽⁵⁾.

⁽³⁾ Cf., e.g., I. S. SOKOLNIKOFF: *Advanced Calculus*, 1st. ed., Chap. 6 (New York, 1939).

⁽⁴⁾ J. S. LOMONT and H. E. MOSES: *Comm. Pure and App. Math.*, **14**, 69-76 (1961).

⁽⁵⁾ J. B. KELLER: *Comm. Pure and App. Math.*, **14**, 77-80 (1961).

α -Particle Wave Functions and the Muon Capture in ^4He .

A. BIETTI

*Scuola di Perfezionamento in Fisica dell'Università - Roma
Istituto Nazionale di Fisica Nucleare - Sezione di Roma*

(ricevuto il 12 Maggio 1961)

1. - In his paper on the muon capture in ^4He , PRIMAKOFF⁽¹⁾, gives the following formula for the total capture rate $A^{(\mu)}$, calculated with the closure approximation:

$$(1) \quad A^{(\mu)}(^4\text{He}) = 8 \cdot 272 \cdot \mathcal{R}(1 - I) \text{ s}^{-1},$$

where

$$I = \iint \frac{\sin \langle \nu \rangle |\mathbf{r} - \mathbf{r}'|}{\langle \nu \rangle |\mathbf{r} - \mathbf{r}'|} F(\mathbf{r}, \mathbf{r}') d\mathbf{r} d\mathbf{r}'.$$

With

$$F(\mathbf{r}, \mathbf{r}') = \iiint |\varphi(\mathbf{r}_1, \mathbf{r}_2, \mathbf{r}_3, \mathbf{r}_4)|^2 \delta(\mathbf{r}_1 + \mathbf{r}_2 + \mathbf{r}_3 + \mathbf{r}_4) \delta(\mathbf{r} - \mathbf{r}_1) \delta(\mathbf{r}' - \mathbf{r}_2) d\mathbf{r}_1 d\mathbf{r}_2 d\mathbf{r}_3 d\mathbf{r}_4,$$

\mathbf{r}_i are the co-ordinates relative to the nucleus c.m.; φ is the space function of the α -particle, $\langle \nu \rangle$ is the emitted neutrino energy in the closure approximation. PRIMAKOFF gives for ^4He a value $\langle \nu \rangle / m_\mu = 0.75$. \mathcal{R} is a ratio involving the coupling constants (formula (6b) of Primakoff's paper), including the virtual pion effects such as the pseudoscalar term and the weak magnetism term. With all these contributions Primakoff gives $\mathcal{R} \simeq 1.06$ ⁽²⁾.

2. - For the integral I PRIMAKOFF quotes a value of 0.80. The aim of this short note, is a calculation of I with different variational wave functions for ^4He , in order to show the dependence of the results on the wave functions with their variational

⁽¹⁾ H. PRIMAKOFF: *Rev. Mod. Phys.*, **31**, 802 (1959).

⁽²⁾ With Primakoff's data on the coupling constants, omitting the pseudoscalar term only one has $\mathcal{R} \simeq 1.22$; omitting the weak magnetism term only one has $\mathcal{R} \simeq 0.91$; omitting both terms one has $\mathcal{R} \simeq 1.07$.

parameters; particularly when these parameters are fitted in order to obtain the correct r.m.s. radius of the α -particle. Only S wave functions have been considered.

As first wave function was taken a Gaussian

$$(2) \quad \varphi = \sqrt{N} \exp \left[-\alpha \sum_{i>j} r_{ij}^2 \right], \quad \text{with } \mathbf{r}_{ij} = \mathbf{r}_i - \mathbf{r}_j.$$

From this function one obtains for I (3)

$$(3) \quad I_1 = \exp \left(-\frac{\langle v \rangle^2}{16\alpha} \right).$$

As a second step, we have considered the Irving's wave function (4)

$$(4) \quad \varphi = \sqrt{N} \frac{\exp \left[-\alpha \left(\sum_{i>j} r_{ij}^2 \right)^{\frac{1}{2}} \right]}{\left(\sum_{i>j} r_{ij}^2 \right)^n},$$

with $n=0$ and $n=\frac{1}{4}$.

For $n=0$ one has

$$(5) \quad I_2 = \left(\frac{16}{16 + (2\langle r \rangle^2/\alpha^2)} \right)^5,$$

and for $n=\frac{1}{4}$

$$(6) \quad I_3 = \left(\frac{16}{16 + (2\langle v \rangle^2/\alpha^2)} \right)^4.$$

The r.m.s. radius calculated from the wave functions is $\langle r^2 \rangle = 9/64\alpha$ for the (2); $\langle r^2 \rangle = 45/32\alpha^2$ for the (4) with $n=0$, and $\langle r^2 \rangle = 9/8\alpha^2$ for the (4) with $n=\frac{1}{4}$. Now we can introduce for $\langle r^2 \rangle$ the values given from the high energy Hofstadter's electron scattering experiments (5): $\sqrt{\langle r^2 \rangle} = 1.61 \cdot 10^{-13}$ cm, and, if corrected from the charge distribution of the proton $\sqrt{\langle r_p^2 \rangle} = 1.41 \cdot 10^{-13}$ cm. In this way one obtains for the first value of the radius ($1.61 \cdot 10^{-13}$): $I_1 = 0.830$, $I_2 = 0.833$, $I_3 = 0.834$; and for the second one ($1.41 \cdot 10^{-13}$): $I_1 = 0.867$, $I_2 = 0.869$, $I_3 = 0.869$.

It is also possible to adjust the variational parameter α in order to obtain the correct binding energy of the α -particle, but this procedure gives results not very much reliable, because the binding energy does not depend in a simple manner on α , as is the case of the r.m.s. radius, but the dependence is complicated from nuclear parameters such as well depth, range, etc.

For instance, with the function (2), a value $\alpha = 0.0789 \cdot 10^{26} \text{ cm}^{-2}$ gives a binding energy of about 27 MeV (6), and one has $I_1 = 0.88$; and a value $\alpha = 1.134 \cdot 10^{13} \text{ cm}^{-1}$ for the Irving's function (3) with $n=0$, consistent with the binding energy (6), gives $I_2 = 0.92$.

(5) An analogous result was obtained by L. PICASSO and S. ROSATI: private communication.

(6) J. IRVING: *Phil. Mag.*, **42**, 338 (1951); *Proc. Phys. Soc.*, A **66**, 17 (1953).

(7) R. HOFSTADTER: *Ann. Rev. Nucl. Sci.*, **7**, 271 (1957).

(8) B. H. BRANDEN, A. C. DOUGLAS and H. H. ROBERTSON: *Phil. Mag.*, **2**, 1911 (1957).

3. — From these calculations one obtains an interesting result: $A^{(\mu)}$, with a variational parameter adjusted to fit the r.m.s. radius $1.61 \cdot 10^{-13}$ cm, shows a difference between $A_1^{(\mu)}$, $A_2^{(\mu)}$ and $A_3^{(\mu)}$ not more than about 2.5%; and with $\sqrt{\langle r^2 \rangle} = 1.41 \cdot 10^{-13}$ cm a difference not more than about 2%. On the other hand, the difference between the capture rates with the two different values of the radius is of the order of 24%. For this reason it could be interesting to perform an experiment, for instance in a Helium bubble chamber, measuring $A^{(\mu)}$. With this experiment it might be possible: *a*) to obtain a value for the r.m.s. radius which could be compared with those of Hofstadter's experiments; *b*) assuming the Hofstadter's radius as a reliable value, for instance $1.41 \cdot 10^{-13}$ cm, which is also consistent with photodisintegration experiments (⁷), to search any variations of the ratio \mathcal{R} .

* * *

I wish to thank Prof. M. CINI for his helpful advice in these calculations.

(⁷) M. Q. BARTON and J. H. SMITH: *Phys. Rev.*, **110**, 1143 (1958).

LIBRI RICEVUTI E RECENSIONI

Libri ricevuti.

- I. I. GOBDMAN and V. D. KRIVCHENKOV: *Problems in Quantum Mechanics*. Pergamon Press, London, 1961; pp. VIII-275; 56 s.
- A. ABRAGAM: *The Principles of Nuclear Magnetism*. Oxford University Press, 1961; pp. VII-599; Ls. 4. 4 s.
- TAUSIF H. NAQVI: *A Study of the Azimuthal and the Zenithal Distribution of Cosmic Rays at Gulmarg (Kashmir)*. Muslim University, Aligarh, India, 1956, pp. 65.
- S. D. DRELL and F. ZACHARIASEN: *Electromagnetic Structure of Nucleons*. Oxford University Press, 1961; pp. 111; 12 s. 6 d.
- A. ALBERIGI QUARANT and B. RISPOLI: *Elettronica*. Zanichelli Editore, Bologna, 1961; pp. XIII-567; Lire 6000.
- J. F. DENISSE and J. L. DELCROIX: *Théorie des Ondes dans les Plasmas*. Dunod, Paris, 1961; pp. XII-167; 16 NF.
- C. SANCHEZ DEL RIO: *Fundamentos Teóricos de la Física Atómica y Nuclear*. Servicio Publication de la J.E.N., Madrid, 1960; pp. VI-167; 175 pesetas.
- D. M. RITSON: *Techniques of High Energy Physics*, vol. V. Interscience Pub., New York and London, 1961; pp. XII-540; \$ 16.75.
- E. H. PUTLEY: *The Hall Effect and Related Phenomena*. Butterworths, London, 1961; pp. VIII-261; 50 s.
- S. K. FRIEDLANDER and L. TOPPER: *Turbulence*. Interscience Publishers, New York and London, 1961; pp. IX-187; \$ 6.00.
- E. PERUCCA: *Fisica Generale e Sperimentale*, vol. II, parte I e II. U.T.E.T., Torino, 1960; pp. 1228; Lire 16000.

Recensioni.

- N. N. BOGOLIUBOV et D. V. CHIRKOV - *Introduction à la théorie quantique des champs*. Ed. Dunod, Paris, pp. 616; NF 69.

Il volume di Bogoliubov e Chirkov è una esposizione completa ed esauriente della teoria quantistica dei campi.

Il libro è diviso in 9 capitoli: il primo capitolo è dedicato alla teoria classica e mette in particolare rilievo quelle proprietà che saranno utili per lo studio della seconda quantizzazione.

Nel secondo capitolo è discussa la quantizzazione dei campi liberi; essa viene affrontata usando un metodo assai diretto ed elegante che permette di conservare ad ogni stadio l'invarianza relativistica.

Il terzo capitolo discute il calcolo della matrice S di diffusione. Il metodo usato, dovuto originalmente a Stueckelberger, è di grande interesse perché permette di evitare l'uso della rappresentazione d'interazione. Esso mostra che la deduzione della matrice S può

essere fatta usando solo le condizioni di invarianza, di causalità e di unitarietà.

I capitoli quarto e quinto descrivono le ben note difficoltà degli integrali divergenti che compaiono nelle teorie dei campi ed i metodi di rinormalizzazione usati per trattare tali difficoltà.

Il sesto e il settimo capitolo sono dedicati ai metodi di Tomonaga, Schwinger ed a quello dell'approssimazione funzionale e l'ottavo tratta del gruppo di rinormalizzazione.

Finalmente nell'ultimo capitolo, sono esposti con estrema chiarezza e rigore matematico i principi essenziali dei metodi di prolungamento analitico al cui sviluppo gli autori hanno dato contributi di grande importanza.

In conclusione il libro di Bogolioubov e Chirkov rappresenta l'esposizione più completa ed aggiornata della teoria quantistica dei campi. Alcuni capitoli, ad esempio il settimo, l'ottavo ed alcune parti del nono, richiedono dal lettore una notevole preparazione matematica e possono essere saltati in una prima lettura.

S. FUBINI

Proceedings of the International Conference on Nuclear Structure, Kingston, Canada. Edited by D. A. BROMLEY and E. W. VOGT. University of Toronto Press, Toronto and North Holland Publishing Company, Amsterdam, 1960; pp. 990, \$ 60.00.

Questo sommario di lavori presentati alla conferenza di Kingston costituisce un vasto panorama sulle interazioni fondamentali fra le particelle e sulla struttura dei nuclei. Vi è raccolta una quantità veramente eccezionale di dati sperimentali e vi sono discusse molte nuove idee. Scorrendo le sue pagine si può notare che i modelli nucleari fondamentali hanno ora raggiunto un grado di evoluzione notevole,

più intimamente compresi nelle loro basi e perfezionati nella loro veste matematica.

L'interesse dei fisici nucleari, come traspare da queste letture, è ora accentrato su due questioni essenziali. La prima è discussa, tra gli altri, da R. E. PEIERLS e da D. H. WILKINSON: secondo tali autori si può sperare che i calcoli sulla materia nucleare permettano di chiarire la composizione della forza elementare nucleone-nucleone. La seconda questione, anch'essa di notevole interesse, è la determinazione della consistenza interna e delle basi teoriche dei modelli.

Per quanto riguarda il confronto tra predizioni dei modelli e dati sperimentali, l'accordo deve essere considerato « sorprendentemente buono », anche se, logicamente, non si può parlare in tutti i casi di un accordo perfetto dal punto di vista quantitativo.

Una nota decisamente positiva può essere ritrovata nelle parole poste da W. P. LEWIS, presidente della conferenza, nella prefazione:

« Si è riscontrata una nuova tendenza. Vi sono nuovi sforzi tendenti ad analizzare il nucleo nelle sue misteriose distorsioni transienti, quelle che avvengono immediatamente prima della fissione, durante l'intimo contatto temporaneo con un secondo nucleo e negli stadii immediatamente seguenti l'interazione diretta tra nucleoni. »

Il testo è diviso in dieci capitoli, ognuno dedicato ad un problema fondamentale. Riportiamo di seguito i titoli originali di alcuni di essi, poichè nulla potrà dare un panorama più fedele degli argomenti trattati.

- Open problems in nuclear structure.
- Physical foundations of nuclear models.
- Gross properties of nuclear matter.
- Nuclear reaction mechanisms.
- Properties of individual levels.
- Statistics of nuclear levels and giant dipole resonances.
- Fission.

Nella prima sessione, dedicata alla discussione di problemi basilari ancora aperti, sono state tenute due relazioni. La prima di PEIERLS, ha un carattere puramente discorsivo e contiene una vivace discussione sulle ragioni che spingono ancora oggi ad approfondire lo studio della fisica dei nuclei. La seconda, di WILKINSON, è strettamente tecnica e racchiude una gran massa di suggerimenti per i teorici e per gli sperimentali su svariati problemi, come la struttura dei nuclei leggeri, la costituzione della superficie nucleare, l'assorbimento di mesoni K^- , ecc. .

La parte dedicata ai modelli nucleari contiene, tra le altre, relazioni di BRUECKNER, BLOCK e DE SHALIT. Quest'ultima è stata dedicata alla discussione dei « tests » di consistenza dei modelli. Per riassumere tale relazione si può dire che vi è una buona evidenza che i nuclei possono essere approssimati da strati di particelle indipendenti con deboli interazioni residue, o almeno da strati di « quasi-particelle ». Non si sa se le interazioni residue possono essere espresse in termini di semplici funzioni delle coordinate delle « quasi-particelle », ma è molto probabile che nel subspazio

di un piccolo numero di orbite i suoi effetti possano essere simulati da semplici interazioni, ad esempio da forze δ . Inoltre è molto probabile che si possano attribuire alle « quasi-particelle » indipendenti una carica ed un momento intrinseco effettivo in modo da descrivere le proprietà elettromagnetiche dei nuclei.

Da notare la relazione di BROWN e di SAXON sui fondamenti del modello ottico e sulle interazioni dirette, la relazione di ZUCKER sulle reazioni nucleari indotte da ioni pesanti e la relazione di BARTHOLOMEW dedicata ad un'analisi comparativa degli schemi di livelli ottenuti mediante reazioni (n, γ) . Ricordiamo, inoltre, le ultime varianti apportate da A. S. DAVYDOV al suo noto modello nucleare, che contribuiscono a rinfoculare la vecchia polemica con la scuola di Copenaghen sulla esistenza di deformazioni nucleari a simmetria non assiale. Citeremo, infine, la relazione di PEIERLS sulle risonanze giganti di dipolo, che ora si possono considerare ben comprese, e l'efficace sommario di V. F. WEISSKOPF che chiude la rassegna.

D. PROSPERI

PROPRIETÀ LETTERARIA RISERVATA

Direttore responsabile: G. POLVANI

Tipografia Compositori - Bologna

Questo Fascicolo è stato licenziato dai torchi il 29-V-1961